

UNIVERSITY OF ALBERTA

Predicting Capacity of Helical Screw Piles in Alberta Soils

By

Diane Jia Ying Zhang



A thesis submitted to the Faculty of Graduate Studies and Research in partial fulfillment of the requirements for the degree of **Master of Science**

in

Geotechnical Engineering

Department of Civil and Environmental Engineering

**Edmonton, Alberta
Fall, 1999**



National Library
of Canada

Acquisitions and
Bibliographic Services

395 Wellington Street
Ottawa ON K1A 0N4
Canada

Bibliothèque nationale
du Canada

Acquisitions et
services bibliographiques

395, rue Wellington
Ottawa ON K1A 0N4
Canada

Your file Votre référence

Our file Notre référence

The author has granted a non-exclusive licence allowing the National Library of Canada to reproduce, loan, distribute or sell copies of this thesis in microform, paper or electronic formats.

The author retains ownership of the copyright in this thesis. Neither the thesis nor substantial extracts from it may be printed or otherwise reproduced without the author's permission.

L'auteur a accordé une licence non exclusive permettant à la Bibliothèque nationale du Canada de reproduire, prêter, distribuer ou vendre des copies de cette thèse sous la forme de microfiche/film, de reproduction sur papier ou sur format électronique.

L'auteur conserve la propriété du droit d'auteur qui protège cette thèse. Ni la thèse ni des extraits substantiels de celle-ci ne doivent être imprimés ou autrement reproduits sans son autorisation.

0-612-47122-5

Canada

Abstract

Screw piles have been used widely in engineering applications. They can be used to provide structural stability against axial compression, uplift, overturning, and lateral forces. The complexity of Alberta soil, due to past glaciation history, creates uncertainties in adapting many of the design methods proposed by previous studies. Therefore, to properly understand the axial load-carrying behavior of multi-helix screw piles installed in the Alberta soil, a field testing program was carried out. Eighteen pile load tests including axial compression, axial tension and lateral pile load tests were performed on full-scale multi-helix screw piles at the University Farm site (cohesive soil) and the Sand Pit site (cohesionless soil). Thirteen pile load tests were conducted using fully instrumented research piles and the remaining five pile load tests were carried out using regular non-instrumented production piles. The pile load test results and the field measurements provided a detailed understanding of the screw pile axial loading behavior in compression and tension.

Capacity predictions using both direct and indirect methods were performed and the prediction results were compared to the field experiment results. At the end, recommendations and guidance are provided in order to aid in predicting the load carrying capacity of screw piles installed in typical soils of Alberta.

Acknowledgments

I would like to express my sincere gratitude to Dr. D. C. Sego, Dr. P. K. Robertson, and Dr. R. Chalaturnyk for their wisdom and guidance during my research program. I would like to extend a very special thanks to Dr. D. C. Sego for his care and support to his student throughout this thesis. His enthusiasm and encouragement not only contributed to my technical development but also helped me in terms of personal growth.

I am gratefully indebted to the Department of Civil and Environmental Engineering, University of Alberta and ALMITA Manufacturing Ltd. for much appreciated financial support to make this thesis possible.

Sincere thanks to the members of the technical support staff within the department of Civil and Environmental Engineering, University of Alberta. Special thanks are extended to Gerry Cyre for the many hours spent preparing instruments and performing the field pile load tests.

Special gratitude to thank my parents for their love and encouragement, as well as their effort to provide this learning opportunity for me. I would also like to thank Jeremy Lim, without whom completion of this research would not have been possible. Jeremy's love and continual support of my goals were the driving force that supported me through the tough times.

I would also thank my true friends, Hassan El-Ramley, May Ngu, Richard Lim and Li Hoalim for their companionships during my studies and also for their unselfish help given to me when I needed advises.

Table of Contents

CHAPTER 1 – INTRODUCTION

1.1	SCREW PILE (ANCHOR) – GENERAL	1
1.2	OBJECTIVE OF THE THESIS	2
1.3	TEST PROGRAM.....	2
1.4	ORGANIZATION OF THE THESIS	2
1.5	LIMITATIONS OF THE INVESTIGATION	3
1.6	SYMBOLS AND DEFINITION.....	4

CHAPTER 2 – SCREW PILE REVIEW

2.1	INTRODUCTION.....	5
2.2	SCREW PILE AND ITS INSTALLATION.....	6
2.3	BEHAVIOR OF SINGLE PILE UNDER VERTICAL COMPRESSIVE LOADING	7
2.3.1	Ultimate Pile Point Resistance	8
2.3.1.1	The Terzaghi Bearing Capacity Equation	8
2.3.1.2	Skempton and Meyerhof's Bearing Capacity Theory.....	10
2.3.1.3	Other Bearing Capacity Theory	13
2.3.1.4	Other Factors	15
2.3.2	Shaft Skin Friction Capacity	15
2.3.3	Estimate Pile Capacity by Cone Penetrometer.....	20
2.3.3.1	Bustamante and Giasenelli (1982) Method.....	21
2.3.3.2	De Ruiter and Beringen (1979) Method	22
2.3.4	Helical Pile under Compression Condition in Clay ($\phi = 0$).....	23

2.4	BEHAVIOR OF SCREW PILE UNDER VERTICAL UPLIFT	
	LOADING	24
2.4.1	Introduction	24
2.4.2	Theories of Uplift Resistance for Anchors in Sand	24
2.4.3	Anchor in Clay Under Undrained Loading	33
2.4.4	Failure Models of Screw Pile in Soil	35
2.4.4.1	Cylindrical Shear Method	35
2.4.4.1.1	<i>Helical Pile Under Uplift Condition in Sand</i>	<i>36</i>
2.4.4.1.2	<i>Helical Pile Under Uplift Condition in Clay ($\phi = 0$)</i>	<i>39</i>
2.4.4.2	Individual Plate Method	43
2.4.4.3	Empirical Method	45
2.5	THE EFFECTS OF TIME ON PILE RESISTANCE	45
2.6	EFFECT OF INSTALLATION METHOD	48
2.7	COMPRESSION CAPACITY VERSUS TENSION CAPACITY	50
2.8	CYCLIC LOADING	51
2.9	FACTOR OF SAFETY USED FOR DESIGN	52
2.10	REFERENCES	55

CHAPTER 3 – PILE DEVELOPMENT

3.1	SCOPE	113
3.2	PILE GEOMETRY AND INSTRUMENTATION	113
3.3	STRAIN GAUGE AND END LOAD CELL CALIBRATION	115

CHAPTER 4 – SITE INVESTIGATION OF TEST SITES

4.1	INTRODUCTION	126
------------	---------------------------	------------

4.2	SITE GEOLOGY	126
4.2.1	Glacial Lake Edmonton Sediments (University Farm Site).....	126
4.2.2	Sand Dunes (Sand Pit Site)	127
4.2.3	Glacial Till.....	127
4.3	SITE INVESTIGATION.....	128
4.3.1	Site Investigation Program	128
4.3.2	Site Investigation Results	130
4.3.2.1	Stratigraphic Interpretation.....	130
4.3.2.2	Soil Strength Properties	132
4.4	REFERENCES.....	138

CHAPTER 5 – TESTING PROGRAM

5.1	INTRODUCTION.....	169
5.2	TEST SITE LAYOUT	170
5.3	LOADING SYSTEM.....	170
5.4	DISPLACEMENT MEASUREMENT	171
5.5	REACTION SYSTEM	172
5.5.1	Axial Compression and Axial Tension Tests.....	172
5.5.2	Lateral Load Test	173
5.6	PILE LOAD TESTING	174
5.7	REFERENCES.....	175

CHAPTER 6 – PILE LOAD TEST RESULTS

6.1	INTRODUCTION.....	191
6.2	PILE CAPACITY RESULTS	192
6.2.1	Definition of Failure Load	192

6.2.2	Axial Compression and Tension Test Results	192
6.2.3	Lateral Test Results	193
6.2.4	Load Transfer Mechanism	193
6.3	DISCUSSION ON THE PILE LOAD TEST RESULTS	197
6.3.1	Effective Shaft Length, H_{eff}	197
6.3.2	Effect of the Bearing Capacity in Compression Versus in Tension	198
6.3.3	Effect of the Cylindrical Resistance	199
6.3.4	Effect of the Embedment Ratio (H/D)	199
6.3.5	Effect of Space to Diameter Ratio (S/D)	200
6.3.6	Ultimate Capacity in Compression Versus in Tension	201
6.3.7	Lateral Capacity	202
6.4	PILE CAPACITY PREDICTION	202
6.4.1	Prediction of Shaft Resistance	203
6.4.2	Ultimate Pile Bearing Resistance	204
6.4.3	Ultimate Cylindrical Shearing Resistance	207
6.4.4	Ultimate Screw Pile Axial Capacity Prediction Using Both Indirect and Direct Methods	208
6.5	REFERENCES	210

CHAPTER 7 – CONCLUSION AND RECOMMENDATION253

7.1	SUMMARY	253
7.2	CONCLUSIONS	254
7.3	DESIGN RECOMMENDATIONS: INDIRECT APPROACHES	257
7.3.1	Multi-helix Screw Pile	257
7.3.1.1	In Cohesive Soil ($\phi = 0$ condition)	258
7.3.1.2	In Cohesionless Soil	261

7.3.2	Single Helix Screw Pile	264
7.3.2.1	Single Helix in Cohesive soil ($\phi = 0$ condition)	264
7.3.2.2	Single Helix in Cohesionless Soil	265
7.4	DESIGN RECOMMENDATION: DIRECT APPROACH.....	266
7.5	OTHER FACTORS THAT INFLUENCE THE ULTIMATE CAPACITY	268
7.5.1	Compression Capacity Versus Uplift Capacity	268
7.5.2	Torque Method	269
7.6	FUTURE RESEARCH.....	271
7.7	REFERENCES.....	272

List of Table

Table 2.1:	Bearing Capacity Equations by Several Authors (after Bowles 1988)	63
Table 2.2:	Shape, Depth, and Inclination Factors for the Meyerhof Bearing Capacity (after Bowles, 1988).....	64
Table 2.3:	Bearing Capacity Factors for Shallow Foundations for the Meyerhof, Hansen, and Vesic' Theory (after Bowles, 1988).....	64
Table 2.4:	Shape, Depth, Inclination, Ground and Base Factors for Use in Either the Hansen (1970) or Vesic (1973) Bearing Capacity Equations. Factors Apply to Either Method Unless Subscripted with (<i>H</i>) or (<i>V</i>). (after Bowles, 1988)	65
Table 2.5:	Estimates for the Rigidity Index, I_r (after Bowles, 1988)	66
Table 2.6:	Bearing Capacity Factors for Shallow Foundations for the Janbu and Vesic' Theory (after Bowles, 1988).....	66
Table 2.7:	Bearing Capacity Factor N_c Related to the Pile Diameter (after CFEM, 1992)	67
Table 2.8:	Range of N_q Factors (after CFEM, 1992).....	67
Table 2.9:	Adhesion Factors for Drilled Shafts in a Cohesive Soil (after Reese and O'Neill, 1988).....	68
Table 2.10:	Design Value of Adhesion Factors for Piles Driven into Stiff to Very Stiff Cohesive Soils (after Tomlinson, 1994).....	69
Table 2.11:	Values of the Coefficient of Horizontal Soil Stress, K_s (after Kulhawy, 1984)	69
Table 2.12:	Typical Values of K_0 for a Normally Consolidated Sand (after Kulhawy, 1984)	69

Table 2.13:	Values of the Angle of Pile to Soil Friction for Various Interface Conditions (after Kulhawy, 1984)	70
Table 2.14:	Range of β Coefficients (after CFEM, 1992)	70
Table 2.15:	Bearing Capacity Factors, k_c (after Bustamante and Gianeselli, 1982)	71
Table 2.16:	Friction Coefficient, α (after Bustamante and Gianeselli, 1982).....	72
Table 2.17:	Descriptions of Deep Foundations Used in Combination with Figure 2.20 (after Bustamante and Gianeselli, 1983)	73
Table 2.18:	European CPT design method (after de Ruiter and Beringen, 1979).....	73
Table 2.19:	Coefficient m and Maximum Factor, s used in Meyerhof and Adam's Theory (after Meyerhof and Adam, 1968)	74
Table 2.20:	Critical Embedment Ratio, $(H/B)_{cr}$ for Circular Anchor (after Meyerhof and Adam, 1968)	74
Table 2.21:	Recommended Uplift Coefficients, K_u for Helical Anchors (after Mitsch and Clemence, 1985)	74
Table 2.22:	Reduction in Ultimate Capacity with Time (after Tomlinson, 1994)	74
Table 2.23:	Soils – Index Properties Used in Test (after Narasimha Rao et al., 1991).....	75
Table 2. 24:	Measured Ultimate Load Carrying Capacities for Model Piles Tests (after Narasimha Rao et al., 1991)	75
Table 2.25:	Reducing Coefficient, m	76
Table 2.26:	Recommended Factors of Safety for Axial Capacity of Piles from CPT (after Lunne, et al., 1998).....	76

Table 3.1:	Test Pile Properties.....	106
------------	---------------------------	-----

Table 4.1:	Estimate of Unit Weights based on Soil Behavior Type Classification System (see Figure 4.17, after Lunne et al., 1997)	141
Table 4.2:	Corrections for SPT Test (Robertson and Ghionna, 1987).....	142
Table 4.3:	Results of Undrained Triaxial Compression Tests on Undisturbed and Remolded Recomacted Samples of Clay and Till (modified from Bhanot, 1968)	143
Table 4.4:	Empirical Values for ϕ , D_r , and Unit Weight of Normally Consolidated Granular Soils Based on the SPT (after Bowles, 1988)	144
Table 4.5:	Strength Determination of Sand Pit Soil Using SPT Data (after Bowles, 1988)	144
Table 4.6:	Strength Determination of Sand Pit Soil Using SPT Data (after De Mello, 1971 and Gibbs and Holtz, 1957)	144

Table 6.1:	Summary of the Test Pile Geometry and Test Results	214
Table 6.2:	Measured Load at Failure at Each Strain Gauge Level for the University Farm Site.....	215
Table 6.3:	Measured Load at Failure at Each Strain Gauge Level for the Sand Pit Site	216

Table 6.4:	Measured Load Differences between Strain Gauge Levels as Indicated for the University Farm Site	217
Table 6.5:	Measured Load Differences between Strain Gauge Levels as Indicated for the Sand Pit Site.....	218
Table 6.6:	Measured Shaft Resistance, Bearing Capacity and Cylindrical Shearing Resistance at Failure for the Length Indicated for Both Test Sites	219
Table 6.7:	Comparison of Each Load Contribution Components to the Ultimate Load Measured by the Tests for Both Test Sites	220
Table 6.8:	Shaft Adhesion Prediction for the Compression and Tension Tests at the University Farm Site	221
Table 6.9:	Shaft Resistance Prediction for the Compression and Tension Tests at the Sand Pit Site	222
Table 6.10:	Predicting Plate Bearing Capacity for the Compression and Tension Tests at the University Farm Site	223
Table 6.11:	Predicting Plate Bearing Capacity for the Compression and Tension Tests at the Sand Pit Site	224
Table 6.12:	Predicting Cylindrical Shear Resistance for the Compression and Tension Tests at the University Farm Site.....	225
Table 6.13:	Predicting Cylindrical Shear Resistance for the Compression and Tension Tests at the Sand Pit Site	225
Table 6.14:	Summary of Predicted and Measured Axial Pile Capacity for Screw Piles Installed at the University Farm Site.....	227
Table 6.15:	Summary of Predicted and Measured Axial Pile Capacity for Screw Piles Installed at the Sand Pit Site	228

Table 7.1:	Example Calculation using the Proposed Cylindrical Shearing Method to Predict the Compression Capacity of Screw Pile Installed in the Lake Edmonton Clay	274
Table 7.2:	Example Calculation using the Proposed Cylindrical Shearing Method to Predict the Uplift Capacity of Screw Pile Installed in the Lake Edmonton Clay	275
Table 7.3:	The Cylindrical Shearing Method and The Individual Bearing Method Used to Predict the Compression Capacity of Screw Pile Installed in the Sand	276
Table 7.4:	Compression Capacity Prediction Results using the Proposed Design Methods for Cohesionless Soil	277
Table 7.5:	Proposed Cylindrical Shearing Method to Predict the Uplift Capacity of Screw Pile Installed in Sand	278
Table 7.6:	Uplift Capacity Prediction Results using the Proposed Design Methods for Cohesionless Soil	279
Table 7.7:	Flowchart for the LCPC CPT Method (after Robertson and Campanella, 1988)	280
Table 7.8:	Flowchart for the Modified LCPC CPT Method (after Robertson and Campanella, 1988)	281
Table 7.9:	Comparison of Original and Modified Coefficients used in CPT Method for the Research Piles (after Bustamante & Giasenelli, 1982)	282
Table 7.10:	Comparison of Capacity Prediction Results Using the Original and Modified LCPC CPT Method (after Bustamante & Giasenelli, 1982)	283

List of Figures

Figure 2.1:	Configuration of Single and Multiple Helix.....	77
Figure 2.2:	Pile Installation at the University Farm Site.....	78
Figure 2.3:	Leveling of the Pile during Installation.....	78
Figure 2.4:	Stress Around Piles (after Winterkorn and Fang, 1975).....	79
Figure 2.5:	General Development of Pile Capacity (after Bowels, 1988) ...	79
Figure 2.6:	Boundaries of Zone of Plastic Equilibrium after Failure of Soil Beneath a Continuous Footing with Rough Base and Surcharge (after Terzaghi, 1943 and Bowles, 1988)	80
Figure 2.7:	Terzaghi & Meyerhof's Pile Capacity Theories (after Meyerhof, 1982).....	81
Figure 2.8:	Bearing Capacity Factors and the Critical Depth Ratios (after Meyerhof 1976).....	82
Figure 2.9:	Approximate of Limiting Unit Point Resistance Based on the Static Cone Resistance ($1 \text{ tsf} = 95.8 \text{ kN/m}^2$, after Meyerhof 1976).....	83
Figure 2.10:	Bearing Capacity Factors of N_r and N_q for Deep Foundations in Drained Loading: a) Values of N_r b) Values of N_q (after Kulhawy, 1984)	84
Figure 2.11:	Bearing Capacity Factors Versus Angle of Internal Friction According to Various Authors (after Winterkorn and Fang, 1975).....	85
Figure 2.12:	Reduction of Undrained Shear Strength for Anchorage Design (after CFEM, 1992)	85
Figure 2.13:	Limiting Adhesion for Soft to Stiff Clays. (after Tomlinson, 1957)	86
Figure 2.14:	Design Curves for Adhesion Factors for Piles Driven into Clay Soils (after Tomlinson, 1994)	87

Figure 2.15:	Adhesion Factor for Pile Driven in Till (after Weltman and Healy, 1978).....	88
Figure 2.16:	Adhesion Factors for Piles Driven to Deep Penetration into Clays: a) Peak Adhesion Factor Versus Shear Strength/Effective Overburden Pressure; b) Length Factor (After Randolph and Wroth, 1982)	88
Figure 2.17:	Coefficient of Earth Pressure on Shaft of Piles above Critical Depth in Sand (After Meyerhof, 1982).....	89
Figure 2.18:	Lateral Earth Pressure and Friction Angle Factor, β as a Function of Friction Angle Prior to Installation (after ASCE, 1993, Data from Meyerhof, 1976 and Poulos and Davis, 1980).....	89
Figure 2.19:	CPT Method to Determine Equivalent Cone Resistance at Pile Base (after Bustamante and GIANESELLI, 1982).....	90
Figure 2.20:	Pile Capacity Prediction Based on CPT - Curves Used with Table 2.17 (after Bustamante and GIANESELLI, 1983).....	91
Figure 2.21:	Predict Pile Capacity Using CPT – De Ruiter and Beringen Method (after De Ruiter and Beringen, 1979)	92
Figure 2.22:	Correction for Over-Consolidated Sand for De Ruiter and Beringen Method (after De Ruiter and Beringen, 1979).....	92
Figure 2.23:	Screw Pile in Compression and Tension Loading (after Narasimha Rao et al., 1991)	93
Figure 2.24:	Failure of Soil Above a Strip Footing Under Uplift Load (after Meyerhof and Adam, 1968)	94
Figure 2.25:	Previous Uplift Bearing Capacity Theories (after Das, 1990) ...	95
Figure 2.26:	Variation of $F_1 + F_3$ Based on Balla's Theory (after Balla, 1961).....	96
Figure 2.27:	Mariupol'skii's Uplift Capacity Model for Plate Anchor (after Das, 1990)	97

Figure 2.28:	Uplift Coefficient sK_u used in Meyerhof and Adam's Uplift Capacity Theory (after Meyerhof and Adam, 1968)	98
Figure 2.29:	Plot of Breakout Factor, F_q , for Shallow Circular Anchors Based on Meyerhof and Adam's Theory (after Das, 1990).....	98
Figure 2.30:	Plot of Breakout Factor, F_q^* , for Deep Circular Anchors Based on Meyerhof and Adam's Theory (after Das, 1990).....	99
Figure 2.31:	Failure Mechanism for Deep Anchor used in Meyerhof and Adam's Theory (after Das, 1990).....	99
Figure 2.32:	Variation of F_q for Shallow Circular Anchors Based on Vesic's Model (after Das, 1990)	100
Figure 2.33:	Breakout Factor Based on Saeedy's Theory (after Das, 1990).....	100
Figure 2.34:	Breakout Factor, F_q for Shallow Circular Anchors Based on Veesaert and Clemence's Theory (after Das, 1990)	101
Figure 2.35:	Uplift Coefficient N_u Based on Meyerhof and Adam Theory (after Meyerhof and Adam, 1968)	101
Figure 2.36:	Shallow Model Screw Anchor Test with Marker Lines (after Mitsch and Clemence, 1985)	102
Figure 2.37:	Deep Model Screw Anchor Test with Marker Lines (after Mitsch and Clemence, 1985)	102
Figure 2.38:	Failure Surface for Shallow Multihelix Anchor in Sand (after Mitsch and Clemence, 1985)	103
Figure 2.39:	Failure Surface of a Deep Multihelix Anchor in Sand (after Mitsch and Clemence, 1985)	103
Figure 2.40:	Recommended Lateral Stress Values, K_u for Helical Anchors and Foundations in Uplift (after Mitsch and Clemence, 1985).....	104

Figure 2.41:	Uplift Capacity Factor, N_{qu} , Versus Embedment Ratio, H/D Ratio for Helical Anchors in Sand (after Mitsch and Clemence, 1985).....	104
Figure 2.42:	Variation of Breakout Factor with Embedment Depth for Shallow Anchor Condition based on Mitsch and Clemence's Theory (after Das, 1990)	105
Figure 2.43:	Variation of Breakout Factor with Embedment Depth for Deep Anchor Condition based on Mitsch and Clemence's Theory (after Das, 1990)	105
Figure 2.44:	Comparison of Maximum Shear Strain Measured and Proposed Failure Surface for a) Shallow Model Tests in Clay and b) Deep Model Test in Lacustrine Silt (after Mooney et al., 1985)	106
Figure 2.45:	Proposed Failure Mode for Multihelix Anchors in Clay and Silt (after Mooney, et al., 1985)	107
Figure 2.46:	Uplift Capacity Factor, N_{cu} (after Mooney et al., 1985).....	108
Figure 2.47:	Variation of Uplift Capacity Factor N_{cu} with $(H/D)/(H/D)_{cr}$ Ratio (after Das, 1990).....	108
Figure 2.48:	Behavior of Helical Anchor at Various Embedment Ratios: a) Shallow; b) Transitions; c) Deep (after Narasimha Rao and Prasad, 1993).....	109
Figure 2.49:	Individual Bearing Method.....	110
Figure 2.50:	Comparison between Theory and the Results of the Full-Scale Tests of Belled Footings. (after Adams and Radhakrishna, 1971).....	111
Figure 2.51:	Relative Anchor Movement Versus Number of Cycles (after Andreadis et al., 1978).....	111
Figure 2.52:	Relative Cyclic Load Versus Number of Cycles (after Andreadis et al., 1978).....	112

Figure 2.53:	Results of Pile Load Tests: a) Continuous Uplift Tests in Various Soils; b) Uplift Test Under Different Loading Condition in Medium Stiff Clay; c) Uplift Tests Under Different Loading Condition in Saturated Loose Sands (after Trofimenkov and Mariupolskii, 1965)	112
--------------	---	-----

Figure 3.1:	Dimensions of the Research Screw Pile Used in the Compression & Tension Tests Installed to Depth of 5.18 m (Not to Scale)	117
Figure 3.2:	Dimensions of the Research Screw Pile Used in the Compression & Tension Tests Installed to Depth of 3.05 m (Not to Scale)	118
Figure 3.3:	Dimensions of the Research Screw Pile Used in Lateral Tests Installed to Depth of 5.18 m (Not to Scale)	119
Figure 3.4:	Comparison of Short, Long, and Production Piles	120
Figure 3.5:	Wires are Protected by Fiber Glass Insulation Prior to Welding of Sections	121
Figure 3.6:	Pile Assembled at Manufacture's Floor Shop	121
Figure 3.7:	Protecting Strain Gauge during Welding by Water Cooling of Sections being Welded	122
Figure 3.8:	Research Pile after Assembly	122
Figure 3.9:	Pile End Load Cell installed Inside of the Compression Piles	123
Figure 3.10:	Size of Research Piles used in the Test Program	123
Figure 3.11:	Data Acquisition System Used to Collect Test Data	124
Figure 3.12:	Complete Data Collection System Setup	124
Figure 3.13:	Strain Gauge Calibration	125

Figure 4.1:	University Farm Pile Test Location (after Bhanot, 1968)	145
-------------	---	-----

Figure 4.2:	Sand Pit Pile Test Location (after Godfrey, 1993).....	146
Figure 4.3:	Cone Truck used to Perform CPT (Sponsored by ConeTec Investigation Ltd.)	147
Figure 4.4:	Drill Rig used to Perform SPT and CPT	147
Figure 4.5:	CPT Test at the University Farm Site.....	148
Figure 4.6:	Standard CPT Cone.....	148
Figure 4.7:	Comparison of Conventional CPT Cone and DCPT Cone: a) CPT Cone; b) DCPT Cone (after Robertson and Campanella, 1988 and Treen et al., 1992).....	149
Figure 4.8:	Preparation of DCPT Test.....	150
Figure 4.9:	DCPT Cone.....	150
Figure 4.10:	DCPT Performed by Conventional Drill Rig (after Treen et al., 1992)	151
Figure 4.11:	Mobile Auger Performing DCPT at the University Farm Site.....	151
Figure 4.12:	SPT Test Conducted by Mobile Auger at the Sand Pit Site ...	152
Figure 4.13:	Cone Penetration Profile for the University Farm Site (after Robertson and Campanella, 1983b)	153
Figure 4.14:	Cone Penetration Profile for the Sand Pit Site (after Robertson and Campanella, 1983a)	154
Figure 4.15:	Cone Penetration Profile for the Till Site (after Robertson and Campanella, 1983b).....	155
Figure 4.16:	Comparing the CPT and the DCPT Result.....	156
Figure 4.17:	Normalized CPT Soil Behavior Type Chart (Lunne et al., 1997).....	157
Figure 4.18:	Soil Classification Result for the University Farm Site.....	158
Figure 4.19:	Soil Classification Result for the Sand Pit Site	159
Figure 4.20:	Soil Classification Result for the Till Site	160
Figure 4.21:	Undrained Shear Strength Profile for the University Farm Site and the Till Site	161

Figure 4.22:	Normalized C_u/σ'_{vo} Ratio Versus OCR for Use in Estimating OCR (after Schmertmann, 1978a).....	162
Figure 4.23:	Plasticity Chart for Field Soil at the University Farm Site (modified from Bhanot, 1968).....	162
Figure 4.24:	Plots for Soil Composition, Natural Moisture Content, Liquid Limit, Plastic Limit, Degree of Saturation and Bulk Density of Soil (modified from Bhanot, 1968).....	163
Figure 4.25:	Strength Characteristics of Field Soil (modified from Bhanot, 1968)	164
Figure 4.26:	Correlation between Peak Friction Angle ϕ and q_c for the Sand Pit Site (after Robertson and Campanella, 1983)	165
Figure 4.27:	Correlation between Peak Friction Angle ϕ and q_c for the Sand Pit Site (after Durgunoglu and Mitchell, 1975)	165
Figure 4.28:	q_c , σ'_{vo} , D_r Relationship for Ticino Sand in Terms of (a) Normally and (b) Overconsolidated Behavior (after Baldi et al., 1986)	166
Figure 4.29:	Relationship between Standard Penetration Test N -Values and Angle of Shearing Resistance (after Peck, Hanson and Thornburn, 1974)	167
Figure 4.30:	Correlation between Peak Friction Angle ϕ and N_{SPT} for the Sand Pit site (after De Mello, 1971)	168
Figure 4.31:	Correlation between Relative Density D_r and N_{SPT} for the Sand Pit site (after Gibbs and Holtz, 1957)	168
<hr/>		
Figure 5.1:	Site Layout at the University Farm Site	176
Figure 5.2:	Site Layout at the Sand Pit Site	176
Figure 5.3:	The Loading System: a) Hydraulic Jack; b) Hydraulic Pump; c) Pressure Meter	177
Figure 5.4:	The Top Load Cell used to Measure Total Load Applied	178

Figure 5.5:	Load Cell Setting is Used to Ensure No Eccentric Vertical Loading Applied	178
Figure 5.6:	Electronic Displacement Potentiometers and Dial Gauge Used to Measure Displacement	179
Figure 5.7:	Setup for the Electronic Displacement Transducers	179
Figure 5.8:	Reference Beam Location.....	180
Figure 5.9:	Displacement Transducer and Dial Gauge Location for Lateral Load Test	180
Figure 5.10:	Steel Bars Used to Connect the Reaction Beam to the Test Pile	181
Figure 5.11:	Plates used to Connect the Test Piles to the Reaction Beam.....	181
Figure 5.12:	Compression Test Setup at the University Farm Site.....	182
Figure 5.13:	Loading the Test Pile during A Compression Test at the University Farm Site.....	182
Figure 5.14:	Structure C-Channels Used for Making the Reaction Frame.....	183
Figure 5.15:	Reaction Frame and Connection to the Reaction Pile at the University Farm Site.....	183
Figure 5.16:	Tension Setup at the University Farm Site.....	184
Figure 5.17:	Tension Setup at the Sand Pit Site	184
Figure 5.18:	Setting Up the Tension Test at the Sand Pit Site	185
Figure 5.19:	Reaction Setup Using Timber Cribbing for the Tension Test.....	185
Figure 5.20:	A Schematic Layout of the Compression Test	186
Figure 5.21:	A Schematic Layout of the Tension Test.....	187
Figure 5.22:	Reaction Frame Design for the Lateral Pile Load Test.....	188
Figure 5.23:	Steel Wire Rope Used in the Lateral Tests	188
Figure 5.24:	Lateral Pile Load Test at the University Farm Site	189
Figure 5.25:	Lateral Test Setup at the Sand Pit Site	189
Figure 5.26:	A Schematic Layout of the Lateral Test	190

Figure 6.1:	Compression Pile Load Test Results from the U of A Farm Site	229
Figure 6.2:	Compression Pile Load Test Results from the Sand Pit Site.....	230
Figure 6.3:	Tension Pile Load Test Results from the U of A Farm Site.....	231
Figure 6.4:	Tension Pile Load Test Results from the Sand Pit Site.....	232
Figure 6.5:	Lateral Pile Load Test Results from the U of A Farm Site.....	233
Figure 6.6:	Lateral Pile Load Test Results from the Sand Pit Site.....	234
Figure 6.7:	Strain Gauge Locations and Soil Strength versus Depth (CS & TS Tests)	235
Figure 6.8:	Strain Gauge Locations and Soil Strength versus Depth (CL & TL Tests).....	236
Figure 6.9:	Load Distribution Curve for the Compression Tests at the University Farm Site.....	237
Figure 6.10:	Load Distribution Curve for the Tension Test at the University Farm Site.....	238
Figure 6.11:	Load Distribution Curve for the compression Test at the Sand Pit Site.....	239
Figure 6.12:	Load Distribution Curve for the Tension Test at the Sand Pit Site.....	240
Figure 6.13:	Strain Gauge Locations as Indicated in Load Distribution Curves.....	241
Figure 6.14:	Unit Skin Resistance versus Depth Curves Calculated Based on the Strain Gauge Measurements at Indicated Depth	242
Figure 6.15:	Relationship between the Ultimate Capacity and the Embedment Ratio (H/D).....	243

Figure 6.16:	Relationship between the Ultimate Capacity and the Space to Diameter Ratio (S/D).....	244
Figure 6.17:	Comparison of Shaft Resistance Measured with Predicted Values for the CS and TS Tests.....	245
Figure 6.18:	Comparison of Shaft Resistance Measured with Predicted Values for the CL and TL Tests	246
Figure 6.19:	Comparison of Bearing Capacity Measured with Predicted value for the CS and TS Tests	247
Figure 6.20:	Comparison of Bearing Capacity Measured with Predicted Values for the CL and TL Tests	248
Figure 6.21:	Comparison of Cylindrical Resistance Measured with Predicted Value for the CS and TS Tests	249
Figure 6.22:	Comparison of Cylindrical Resistance Measured with Predicted Value for the CL and TL Tests	250
Figure 6.23:	Comparison of Predicted Total Capacity Results with Measured Capacity Results for Screw Piles Installed in the University Farm Site.....	251
Figure 6.24:	Comparison of Predicted Total Capacity Results with Measured Capacity Results for Screw Piles Installed in the Sand Pit Site	252
<hr/>		
Figure 7.1:	Comparison of the Modified and Unmodified CPT Predictions for the Compression Capacities using Bustamante and Giasenelli (1982) method (the University Farm site)	284
Figure 7.2:	Comparison of Modified and Unmodified CPT Predictions for the Tension Capacities using Bustamante and Giasenelli (1982) method (the University Farm Site).....	285

Figure 7.3:	Comparison of Modified and Unmodified CPT Predictions for the Compression Capacities using Bustamante and Giasenelli (1982) method for the Research Piles (Sand Pit Site).....	286
Figure 7.4:	Comparison of Modified and Unmodified CPT Predictions for the Compression Capacities using Bustamante and Giasenelli (1982) method for the Production Piles (the Sand Pit Site)	287
Figure 7.5:	Comparison of Modified and Unmodified CPT Predictions for the Tension Capacities using Bustamante and Giasenelli (1982) method (the Sand Pit Site)	288
Figure 7.6:	The Relationship between the Normalized Installation Torque and the Cone Tip Resistance.....	289

List of Symbols

A_1	area of the top helix, m^2
A_a	area of cross section of the helical plate = $\pi (D^2 - d^2)/4$, m^2
A_p	area of the pile base, m^2
A_s	area of the pile shaft, m^2
A_s'	surface area of cylinder between top and bottom plates = $\pi D L_c$, m^2
B	breadth of the foundation, m
c	unit cohesion of the soil, kPa
C_a	average cohesion of soil along the pile shaft, kPa
C_a'	average cohesion of soil around cylinder of soil between top and bottom helical plates, kPa
C_p	cohesion of soil around pile toe, kPa
C_u	undrained shear strength, kPa
D	diameter of a circular footing or anchor plate, m
d	the diameter of the shaft, m
D_1	diameter of top helix, m
D_a	average helix diameter, m
D_r	relative density of compaction
ER_r	energy that delivered to the drill stem
F	a length factor
f	unit skin resistance along the stem of the anchor used in Macdonald (1963) uplift capacity theory
$F_1(\phi, H/D)$	non-dimensional factors, determined using with Figure 2.26
$F_3(\phi, H/D)$	non-dimensional factors, determined using with Figure 2.26

F_q	the breakout factor for shallow condition screw piles (anchor)
F_q^*	the breakout factor for deep condition screw piles (anchor)
FS	factor of safe
f_s	the average unit skin friction on shaft of area A_s , kPa
h	effective length of anchor stem, m
H	the embedment depth, m
H_1	depth to top helix, m
H_3	depth to bottom helix, m
H_{cr}	limiting embedment depth where the failure mechanism transfers from shallow to deep, m
H_{eff}	effective length of the shaft, m
H_f	depth of foundation to the bottom of the footing, m
$H-H_{cr}$	effective length of the anchor shaft, m
H/D	the embedment ratio
$(H/D)_{cr}$	critical embedment ratio
I_r	the rigidity index
I_{rr}	the reduced rigidity index
k_c	end bearing coefficient used in LCPC CPT method
K_o	the original earth pressure coefficient
K_s	lateral earth pressure coefficient
K_t	empirical factor used in empirical torque method
k_u	nominal uplift coefficient of earth pressure
L	length of the screw pile, m
L_c	the distance between top and bottom helical plates, m
L_c	distance between top and bottom helical plate, m
m	coefficient relating to the embedment depth

n	and empirical coefficient used in Macdonald (1963) uplift capacity model
N	sinusoidal duration cycles
N	the SPT count number
N_k	the cone factor
N_c , N_q , and N_r	dimensionless bearing capacity factors
N_{qu}	uplift capacity factor for cohesionless soils
N_u	uplift bearing capacity factor for cohesive soils
OCR	the overconsolidation ratio
PI	plasticity index
P_p	total passive earth pressure per unit length along the failure surface
P_s	perimeter of the anchor shaft, m
q_b	the unit bearing capacity of pile point of area A_b , kPa
Q_b	end-bearing resistance of the displacement pile, kPa
$Q_{bearing}$	bearing capacity of the top helix (uplift loading) or the bottom helix (compression loading), kPa
q_c	cone tip resistance, term used in CPT profiling, bar
q_c	ultimate unit bearing capacity in compression, kPa
q_{ca}	equivalent average cone resistance, bar
q_l	the limiting unit point resistance, in tons per square foot (100 kN/m ²)
q_o	radial pressure under which the cavity is expanded, kPa
q_s	skin resistance mobilized along the pile shaft for given soil layer, kPa
Q_c	the ultimate pile compression capacity, kN
Q_s	the ultimate skin friction developed along the pile shaft, kN

Q_{shaft}	adhesion developed along the steel shaft, kN
Q_t	the ultimate uplift capacity, kN
Q_{helix}	shearing resistance mobilized along the cylindrical failure surface, kN
$Q_{u(bearing)}$	bearing capacity of the anchor in pullout loading, kN
Q_{allow}	allowable net ultimate capacity used for design, kN
$Q_{ultimate}$	ultimate capacity of the pile, kN
R_f	friction ratio used in CPT
s	shape factor governing the passive earth pressure on a convex cylindrical wall
S_F	spacing ratio factor
S/D	the space to helix diameter ratio
t	wall thickness of the steel shaft, m
T	average installation torque, ft lb
U	suction force below the anchor, kPa
W	weight of soil inside of failure surface, kN
W_a	weight of anchor, kN
ΔL	increment of embedment length (to allow for pile shaft variations and soil stratification (layering), m
$\Delta \lambda$	allowable cyclic relative anchor displacement
Δ_u	ultimate displacement obtained from static pile load test
α	the adhesion factor
α_{LCPC}	friction coefficient for shaft resistance used in LCPC CPT method
α^*	friction coefficient for cylindrical resistance used in LCPC CPT method
δ	soil-shaft effective friction angle, $\leq \phi'$, degrees

ε_v	volumetric strain
ϕ	the angle of internal friction angle, degree
γ'	unit weight of soil above water table or buoyant weight if below water table, kN/m ³
μ	compaction factor
β	a combined shaft factor which is equal to $K_s \tan \delta$
Σ	summation of contributions from several strata or pile segments
ζ_{qd}	a depth factor
ζ_{qs}	a shape factor
$\zeta_{\gamma r}$ and ζ_{qr}	rigidity factors
$\bar{\sigma}'_o$	average effective stress between $Z = 0$ to $Z = H - H_{cr} = \frac{1}{2}\gamma(H - H_{cr})$, kPa
σ_{vo}'	effective overburden pressure, kPa
(Q_c / Q_t)	the ultimate compression to tension capacity ratio
$Q_{sustain}/Q_{ult}$	relative cyclic load
$\Sigma Q_{i(bearing)}$	sum of the bearing capacity of each individual helix, kN

CHAPTER 1 INTRODUCTION

1.1 SCREW PILE (ANCHOR) – GENERAL

Helical piles, also known as screw piles, have been used in various engineering applications for decades. In particular, screw piles are selected for resisting large uplifting forces associated with transmission towers, guyed towers, utility poles, aircraft moorings, and submerged pipelines. They can also provide structural support for excavations, tunnels, and hydraulic structures. Screw piles are primarily designed and constructed for anchoring purposes, hence, they are commonly known as "screw anchors". For this thesis, the term screw pile will be used.

In Alberta, screw piles have been widely used in foundation applications to resist axial compression, tension and lateral loads associated with drill rigs used in hydrocarbon exploration. They have also been used as foundation support for pump jacks, pipelines, and light structures that are subjected to large wind loads. A review of the literature shows that past research has focused on predicting the uplift capacity of screw piles and that limited research has been carried out on predicting the pile capacity in compression and under lateral loading. In addition, the complexity and variability of Alberta sediments, due to its glacial history, creates uncertainties in predicting screw pile capacity in Alberta soil.

With these problems in mind, the Department of Civil and Environmental Engineering of the University of Alberta, at the request of ALMITA Manufacturing LTD, conducted a field testing program including axial compression, axial tension and lateral loading tests on full scale multi-helix screw piles installed in typical Alberta Soil.

1.2 OBJECTIVE OF THE THESIS

The objective of this full-scale field test program was to study the load transfer phenomena in compression, tension and lateral loading conditions for the purpose of developing a reliable design approach to assist in predicting the capacity of screw piles installed in typical local soils. The design method is supported by the interpretation of results from pile load tests, along with the results obtained from an in-situ test apparatus called the Downhole Cone Penetrometer test (DCPT). It is hoped that this thesis will achieve its objective of providing guidelines and recommendation for the design of the screw pile installed in Alberta.

1.3 TEST PROGRAM

A total of 18 full-scale pile load tests, were test-loaded to failure on two sites in the Edmonton area. The soil types were Lake Edmonton Clay at the University Farm site (cohesive material) and sand dunes at the Sand Pit site (cohesionless material). Ten tests including five compression tests, three tension tests and two lateral tests were conducted on the University Farm site in central Edmonton. In addition, eight tests, consisting of three compression, three pull out and two lateral pile load tests, were conducted at a Sand Pit site located at Bruderheim, northeast of Edmonton.

1.4 ORGANIZATION OF THE THESIS

This thesis is organized into a series of 8 chapters. After the introduction (**Chapter 1**), **Chapter 2** describes the literature reviews that has been undertaken on screw piles. Bradka (1997) provided a detailed survey, summarizing recent studies on screw piles. A condensed version of this work appears in **Chapter 2**. The design of the test program, including the test pile properties and design, its instrumentation, and data acquisition system

selected, is highlighted in **Chapter 3**. **Chapter 4** outlines the site investigation adopted in this program, and the results of the site characterization are summarized. **Chapter 5** provides the documentation of the pile load test program. The design of the loading system, as well as the test setup and procedure, are summarized. The results of the full-scale pile load tests and the analysis of these results are presented in **Chapter 6**. Test results obtained during the study, including the ultimate pile load capacities achieved, load-settlement relationships, lateral test results and the axial stress distribution along the pile shaft under static load conditions, are documented. In addition, available design methods for predicting the loading capacity of the screw pile are investigated in **Chapter 6**. The conclusions drawn from the work carried out for this thesis are presented in **Chapter 7**. Based on the site investigation, pile load test results, and the capacity from the literature prediction, design recommendations are provided (see **Chapter 7**) for future design of screw pile installed in Alberta soil.

Appendix A includes information on calibration of the strain gauges, end load cell, and structural properties of the steel pipes used to manufacture the screw pile. **Appendix B** contains the original Cone Penetration test data collected on the University Farm site, the Sand Pit site and the Till site. **Appendix C** presents additional information obtained during the full-scale testing on the University Farm site, and the Sand Pit site.

1.5 LIMITATIONS OF THE INVESTIGATION

The level of detail and the examination of results from this extensive field test program was limited given the scope of a Master of Science thesis. Design, fabrication, calibration of the strain gages and load cells, as well as implementation of the instrumentation of the research piles used in the test program, were all completed in approximately three months. The test piles were installed at the University Farm site at the end of November 1997. Only

three sets of pile load tests could be performed between December 1997 to February 1998 because of the freezing temperature reigning at the site. The top soil, within an area of approximate ten pile diameters of the test pile, had to be thawed before testing. The heat supplied by burning coal ensured that soil to a depth of 2.0 m was sufficiently thawed prior to carrying out the tests. After spring 1998, testing resumed slowly whenever the weather permitted for testing. The field program was finished in late June 1998. A number of strain gauges were damaged because of the site conditions and the method used for thawing of the ground.

1.6 Symbols and Definition

Symbols used in the text are presented in the List of Symbols of this thesis. In general, the terms used herein are those recommended by the American Society of Civil Engineers or by the American Society for Testing and Materials (ASTM: D 653-64). All symbols used are not necessarily those used by their originator, however, they are defined wherever they first occur in the text.

CHAPTER 2 SCREW PILE REVIEW

2.1 INTRODUCTION

The purpose of this chapter is to provide the background information regarding screw piles. A survey of the literature on the behavior of screw piles is presented. The topics reviewed are foundation design in compression, tension, screw pile design in tension, pile capacity prediction using direct method (Cone Penetration test), and geotechnical issues involved in designing screw pile foundations. There has been limited research carried out on predicting capacity of a screw pile in compression, since most of the previous works concentrated on estimating the uplift capacity of the pile. In order to study the load carrying mechanism of a screw pile in compression loading, conventional theories available for obtaining the compression capacity of a deep foundation are reviewed here. These methods will provide a fundamental geotechnical framework for the design of a screw pile in compression. A design procedure can be recommended based on its confirmation by comparing the predicted capacity using these direct or indirect methods to the field test data obtained from this study.

Bradka (1997) provided a review on the pullout capacity of helical screw piles as a part of his Master of Engineering report. The historical background of screw piles provided an overview for this research program. Factors that affect the ultimate capacity of the screw pile including pile geometry, ground characteristics, installation procedure and depth of the pile embedment, were carefully examined. This chapter does not concentrate on these topics, but is focused mainly on design methods that are available for designing a screw pile. Therefore, a summary of theories provided by current researchers on the design of screw pile in tension is presented.

2.2 SCREW PILE AND ITS INSTALLATION

A screw pile consists of a central steel shaft with one or multiple circular plates (helices) affixed to the main shaft. Figure 2.1 shows a sketch of a typical configuration for both single and multi-helix screw pile. There are a wide variety of shaft sizes available for design ranging from 89 to 200 mm diameter shaft for axially loaded piles and up to 273 mm diameter shaft for laterally loaded applications (Hoyt and Clemence, 1985). The pitch and center to center spacing of the helices can be varied so that the upper helices will follow the lower one when advancing into the soil. The helix can be manufactured in single pitch, multi-variable pitch, and multi-equal pitch. They can be welded, riveted, or bolted to the steel shaft, and the helical blades can be knife edged to facilitate their installation and minimize disturbance to the soil during installation (Bradka, 1997).

In Alberta, helical screw piles are typically installed to a shallow depth of less than 6.0 m. A typical set up for installing a screw pile is demonstrated in Figure 2.2. They are installed by applying an axial compressive force to the shaft while rotating it into the ground with a hydraulic torque head mounted on a boom. First, the pile is lifted and secured vertically inside of a detachable steel frame. The pile head is connected to the hydraulic torque head using steel shear pins (2 holes were pre-cut about 150 mm from the pile head allowing connection to the torque head). Then, the pile is lifted to the desire location and rotation commenced. The recommended rate of penetration should be equal to one pitch per revolution in order to avoid shearing of the soil (Bradka, 1997). The rate of penetration is typically monitored manually which required field experiences to control the installation rate. During the installation, a level is used to check and ensure that the piles are installed vertically as shown in Figure 2.3.

Helical screw piles have many advantages. For example, the installation cost is relatively low, with a typical installation requiring only two people per crew. They are fast and easy to install. A 5 m pile installed into Lake Edmonton clay requires

approximately 20 minutes. In addition, they can be easily transported, removed and reused; they allow immediate loading once installed; they can be installed under variable weather and site condition; and most importantly, relatively large capacity can be achieved using these screw piles.

2.3 BEHAVIOR OF SINGLE PILE UNDER VERTICAL COMPRESSIVE LOADING

The mechanism of load transfer from the deep foundation to the surrounding soil medium is complex, and to date, still not well understood by researchers. Methods available for designing deep foundations all contain a certain degree of empirical approximation. Thus, full scale load tests are still required to confirm the prediction of the pile capacity for most projects and to determine the actual pile performance. Nevertheless, if a vertical pile is loaded with an axial compressive force in a homogeneous soil, the load is assumed to be carried partly by skin friction and partly through the pile bearing resistance as shown in Figure 2.4. The general development of pile capacity in soil mass is demonstrated in Figure 2.5. Both components depend on the properties of the soil and the characteristics and method of installing the pile. In general, most of the design theories proposed for estimating the ultimate pile capacity, Q_c , consist of the basic components: the end bearing load (or point resistance), Q_b , and the shaft or skin friction load Q_s . The general form for axially loaded single piles can be expressed as follow:

$$Q_c = Q_b + Q_s = q_b A_b + f_s A_s \quad \text{Equation 2.1}$$

where

Q_c = the ultimate pile compression capacity

Q_b = end-bearing resistance of the displacement pile

Q_s = skin friction developed along the pile shaft

q_b = the unit bearing capacity of pile point of area A_b

f_s = the average unit skin friction on shaft of area A_s

2.3.1 Ultimate Pile Point Resistance

Methods used to obtain the ultimate static pile point capacity are further extensions of the bearing capacity theory developed for shallow foundations. Major work done on shallow foundations by Terzaghi (1943), Skempton (1951) and Meyerhof (1968) have provided the framework for estimating the bearing capacity of a deep foundation. Nevertheless, methods proposed to obtain the ultimate bearing capacity by current researchers still incorporate many uncertainties. Bowles (1988) stated that Vesic (1973) tabulated 15 theoretical solutions since 1940, but there is no single method in current use that Vesic considered as a more outstanding method. The major reason is the high cost involved in performing full scale testing, which directed most of researchers to carry out model tests. Little experimental verification of the methods is available from prototype foundations. Consequently, all the bearing capacity theories proposed involve using empirical factors to take this scale effect into account. Despite all the uncertainties, some major theories proposed in the literature have demonstrated great success in foundation design when these methods are used with local experiences of foundation engineers.

2.3.1.1 The Terzaghi Bearing Capacity Equation

The most important contribution for analyzing the behavior of a shallow foundation using theory of plasticity was proposed by Terzaghi (1943). Terzaghi extended the Prandtl-Reissner theory to analyze strip footings placed on a level ground surface where foundation depth (H) is less than the minimum width (B) (see Figure 2.6). Terzaghi ignored the shear strength of the soil located above the depth of the excavation and assumed the shape of the lines limiting Zone II could be modeled as a logarithmic spiral, and the stress conditions in Zone III corresponded best to Rankine's Passive state. In addition, Terzaghi also assumed that the shear strength was simultaneously mobilized along the entire failure surface. Based on these assumptions, Terzaghi obtained the following

expression for the failure stress that could be transmitted by the foundation where the soil failed in accordance with Coulomb's law:

$$q_c = cN_c + \gamma' H_f N_q + \gamma' \frac{B}{2} N_r \quad \text{Equation 2. 2}$$

where

q_c	= ultimate unit bearing capacity in compression
c	= unit cohesion of the soil
γ'	= unit weight of soil above water table or buoyant weight if below water table
$N_c, N_q, \text{ and } N_r$	= dimensionless bearing capacity factors
H_f	= depth of foundation to the bottom of the footing
B	= breadth of the foundation

As expressed in Equation 2.2, the first term of the bearing capacity equation relates to the cohesion of the soil. The second component takes into account the surcharge effect of the soil above the base of the foundation, and the third part takes into account the weight of the soil and the passive earth pressure block. The terms N_c , N_q , and N_r are the bearing capacity factor in Terzaghi's theory. Terzaghi indicated that these factors are used to characterize the bearing capacity of the soil, and they depend only on the cohesion c , and angle of internal friction, ϕ , of the soil. To correct for the effect of the local shear failure, Terzaghi provided solution by empirically reducing the cohesion and the tangent of the angle of shearing resistance to $2/3$ of their test value. In addition, Terzaghi also provided adjustment for square and circular foundations by applying shape correction factors. Terzaghi's bearing capacity equation was intended for 'shallow' foundation. For deep foundations, Terzaghi extended the analysis for a surface footing plus the effect of shearing forces along the pile surface and on an outer cylindrical shear boundary CE as shown in Figure 2.7. The resulting equation for a circular base deep foundation can be expressed as:

$$q_c = 1.3cN_c + \gamma' H_f N_q + 0.6\gamma' D N_r \quad \text{Equation 2. 3}$$

where

D = diameter of a circular footing

2.3.1.2 Skempton and Meyerhof's Bearing Capacity Theory

Skempton investigated a case where the foundation penetrates the bearing stratum in a purely cohesive soil based on the same framework set by Terzaghi. Terzaghi's approach does not take into account the depth, H , to which the foundation penetrates the bearing stratum. He assumed that N_c is only related to the cohesion of the soil and is independent of the excavation depth. However, cases where the foundation punches through the bearing stratum, the foundation will have a larger shear surface, which results in greater total effect of cohesion, and therefore, should result in a larger N_c value. Skempton carried out experiments to quantify these ideas and found that N_c increased with the depth of the footing. For the bearing capacity of cohesive soils, he proposed an expression similar to Terzaghi's. The difference is that here N_c is not always 5.14, but varies with the embedment relation (H/B), where H is the depth at which the foundation is embedded in the firm stratum and B is the width of the foundation. The formula and coefficients can in principle be applied to shallow foundations and deep foundations in insensitive clay.

Following Skempton's work on the bearing capacity factor N_c , Meyerhof undertook a series of investigation on the bearing capacity factors that were proposed by Terzaghi's theory. Assumptions were made similar to those proposed by Terzaghi. In Meyerhof's model (see Figure 2.7), the solution considers correction factors for eccentricity, load inclination, foundation roughness and foundation depth. N_c , N_q and N_r in the Meyerhof equation are now known as General Bearing Factors which depend upon depth and shape of the foundation as well as the roughness of the base and friction angle of the soil,

ϕ. At shallow depth, Meyerhof's unit bearing capacity, q_c , is not greatly different from the Terzaghi value. The difference is more pronounced at larger embedment ratios. For deep foundations, Meyerhof extended the analysis of Prandtl-Reissner' theory for surface loading to the condition of deep foundations by employing the model shown in Figure 2.7. The semi-empirical bearing capacity factors N_c and N_q for round or square driven piles with 60° points are shown in Figure 2.8.

In Meyerhof's model, the ultimate pile point resistance in homogeneous sand may be represented by:

$$q_c = \gamma' H N_q \quad \text{Equation 2. 4}$$

For piles installed in homogeneous saturated clay, the ultimate unit bearing capacity of a pile or the ultimate unit pile point resistance under drained loading condition may be simplified as:

$$q_c = c N_c + \gamma' H N_q \quad \text{Equation 2. 5}$$

For undrained vertical loading condition in homogenous cohesive soil, equation 2.5 can be expressed as:

$$q_c = c N_c \quad \text{Equation 2. 6}$$

Where

- c = the average unit cohesion of soil near pile point
- N_c = the bearing capacity factor with respect to cohesion
- N_q = the bearing capacity factor with respect to overburden pressure
- γ' = the effective unit weight of the soil
- H = the embedment depth

The relationship between the embedment depth ratio, H_b/D , and the angle of internal friction, ϕ , of the soil is shown in Figure 2.8, where D = pile diameter, H_b = bearing depth, and H_c = critical depth of penetration of pile. Meyerhof (1976) indicated that the factor N_q increases almost linearly with H_b/D and reaches a maximum value at a depth ratio of roughly $\frac{1}{2}$ of the critical depth ratio H_c/D . The conventional bearing capacity theory no longer applies for ratio greater than H_c/D . If piles are driven into homogenous sand to more than the critical depth, the pile point resistance is independent of the overburden pressure and it depends on the value of q_l , the limiting unit point resistance. The relationship between q_l and ϕ may be directly derived from the limiting static cone resistance, q_c as shown in Figure 2.9, or may be represented in the form of:

$$q_l = 0.5 N_q \tan \phi \quad \text{Equation 2. 7}$$

Where

N_q = the bearing capacity factor for pile with H_b/D ratio less than the critical

q_l = the limiting unit point resistance, in tons per square foot (100 kN/m²)

ϕ = the angle of internal friction angle

Meyerhof indicated that the limiting unit point resistance, q_l corresponds only to a limiting effective vertical stress near the pile base at failure, and is independent of the effective overburden pressure and ground water conditions. A typical value shown by tests varies from approximately 0.25 tsf (25 kN/m²) for loose sand to 0.5 tsf (50 kN/m²) for dense sand.

For a pile installed in homogenous saturated clay, theory and laboratory experiments have shown that the value of N_c , under undrained conditions, varies with the sensitivity and deformation characteristics of the clay. It has a typical value of 5 for very sensitive brittle normally consolidated clay to about 10 for insensitive stiff overconsolidated clay (Meyerhof, 1976). A typical value of 9 is often used for estimating bearing capacity of driven and bored piles in clay.

2.3.1.3 Other Bearing Capacity Theory

The works of Terzaghi, Skempton and Meyerhof laid the basis for a great deal of research on pile foundations, and analyses of field test results. Other theories were developed by different investigators, in which the basic form of the equations is maintained. The only difference between the theories is the values of the bearing capacity factors N_c , N_q and N_r . Bowles (1988) summarized some of the major works carried out on bearing capacity (Table 2.1), with computed bearing capacity values presented in Table 2.3. Hansen's bearing capacity method (1970) is a further extension of the earlier Meyerhof (1951) work. Hansen's method simply adopted many of the more complicated situations such as the factor for the footing being tilted from the horizontal surface and other shapes other than square, strip and circular. The Hansen equation implicitly allows any H/D and thus can be used for both shallow (footings) and deep (piles, drilled caissons) bases. Vesic (1975) calculated the bearing capacity factors N_c and N_q based on cavity expansion theory. He indicated that the failure pattern below the base of a pile consists of a highly compressed conical wedge of soil that forms beneath the base as the pile is driven or pushed down into the soil. In a loose soil the wedge pushes down without forming a definable failure surfaces. In a dense soil, the wedge pushes the radial shear zone into the surrounding plastic zone and the failure pattern can be modeled in terms of a spherical cavity expansion theory. Thus, the bearing capacity factors can be calculated based on the internal friction angle of the soil and a reduced rigidity index, I_{rr} as:

$$I_{rr} = \frac{I_r}{1 + \varepsilon_v I_r} \quad \text{Equation 2. 8}$$

where

I_{rr} = the reduced rigidity index

I_r = the rigidity index which can be determined using method outlined in Section 4.3.2.2.

ε_v = volumetric strain

When the soil is failed under the undrained conditions or the soil is in a dense state, the volumetric strain, ε_v , may be taken as zero and I_r can be taken as I_r . Bowles (1988) provided some estimates for I_r as listed in Table 2.5. Janbu (1976) computes N_q based on angle ϕ (see Figure 2.5). Table 2.6 provides selected values of N_c and N_q used in Vesic's and Janbu's equation. Kulhawy (1984) reviewed and extended Vesic's concepts. The rigidity index, shape and depth factors are related to the angle of internal soil friction, ϕ . A simplified equation for square or circular pile embedded in a cohesionless soil under drained loading condition is provided as follow:

$$q_b = 0.3 D \left[\gamma' N_r \zeta_{rr} + \sigma'_{vo} N_q \zeta_{qr} \zeta_{qs} \zeta_{qd} \right] \quad \text{Equation 2.9}$$

where

- q_b = the ultimate unit base resistance
- D = the pile diameter
- σ'_{vo} = effective overburden pressure
- γ' = the density of the soil
- N_r and N_q = bearing capacity factors
- ζ_{rr} and ζ_{qr} = rigidity factors
- ζ_{qs} = a shape factor
- ζ_{qd} = a depth factor

Figure 2.10 presents the bearing capacity factors $N_r^* = 0.3N_r\zeta_{rr}$ and $N_q^* = N_r\zeta_{qr}\zeta_{qs}\zeta_{qd}$ proposed for the design method. As shown in Figure 2.10, the N_q^* values decreases with decreasing values of the rigidity index, and the rigidity index decreases with increasing penetration depth. As a result, the method applies a reduction in the bearing capacity factor with increase in penetration depths. For loose sands, Kulhawy (1984) provided the following equation for determining the rigidity index:

$$I_r = \frac{30}{\sqrt{\sigma'_{vo}} \tan(28^\circ \text{ to } 26^\circ)} \quad \text{Equation 2. 10}$$

Similarly, for dense sands, the rigidity index can be estimated using following equation:

$$I_r = \frac{110}{\sqrt{\sigma'_{vo}} \tan(40^\circ \text{ to } 37^\circ)}$$

Equation 2. 11

where

σ'_{vo} = the effective overburden pressure, is expressed in ton/ft²

For a pile installed with penetration depth greater than five pile diameters, the first term in equation 2.9 is found typically less than 10% of the second term. Therefore, for deep penetrations the first term can be neglected.

Nevertheless, there are substantial differences proposed by different theories in terms of evaluating the bearing capacity factor $N_q^* = N_q S_q$ in which S_q is the shape factor. As demonstrated in Figure 2.11, design curves were proposed by different authors under assumptions of different failure surfaces.

2.3.1.4 Other Factors

In cohesive soil, reduction of the bearing capacity factor, N_c , should be applied with respect to pile toe diameter as suggested by CFEM (1992). Values of N_c are recommended as in Table 2.7. CFEM (1992) provided a summary for typical ranges of values N_q for piles installed in cohesion less soil which is related to installation method of the foundation and property of the material (see Table 2.8).

2.3.2 Shaft Skin Friction Capacity

Shaft resistance develops with relative movement between the soil and the surface of the pile (shaft) once the foundation is loaded. The maximum side resistance is developed after small displacement less than 0.5 in (13 mm), and increases with increasing depth to a maximum, then decreases toward the pile toe. Side friction is hard to estimate accurately, especially for foundations constructed in augered or foundations in stiff, fissured clays where installation of

the foundation can reduce the soil shear resistance to much lower value due to remolding of sensitive clay. Nevertheless, side friction often contributes the most pile capacity in practical situations unless the base is bearing on foundation material that is much stiffer and stronger than the overlying soil (ASCE, 1993). The skin resistance capacity may be estimated by following expression:

$$Q_s = \sum A_s \times q_s \quad \text{Equation 2. 12}$$

where

- Q_s = ultimate capacity contribute from skin friction
- A_s = effective pile surface area on which q_s acts and commonly computed as perimeter x embedment increment ΔL .
- ΔL = increment of embedment length (to allow for pile shaft variations and soil stratification (layering))
- q_s = skin resistance mobilized along the pile shaft for given soil layer
- \sum = summation of contributions from several strata or pile segments

The unit shaft resistance for foundations installed in cohesive soils is often approximated by empirically applying a reduction factor (adhesion factor) to the shear strength of the adjacent soil in which

$$q_{shaft} = \alpha C_u \quad \text{Equation 2. 13}$$

where

- α = adhesion factor
- C_u = undrained shear strength

The difficulty of predicting the shaft resistance in cohesive soils arises from the difficulty of determining the adhesion factor. Often, local experience with existing soils and load test results should be used to predict the appropriate

adhesion factor. Estimates of adhesion were provided by a number of researchers, and following methods are listed for design consideration:

1. Recommendation provided by Reese and O'Neill (1988) for drilled shafts in a cohesive soil (see Table 2.9). Estimation of α may be used accordingly in the absence of load test data and for preliminary design.
2. Recommendation provided by Canadian Foundation Engineering Manual (1992). A chart to reduce the undrained shear strength for anchorage design is provided as shown in Figure 2.12.
3. Recommendation provided by ASCE (1993). Based on the data from Stewart and Kulhawy (1981), ASCE provides an estimation of adhesion factor for drilled shafts constructed dry, by relating α to the plasticity index PI . The method is outlined as follow:

Overconsolidated: $\alpha = 0.7 - 0.01 \times PI$

Slightly overconsolidated ($OCR \leq 2$): $\alpha = 0.9 - 0.01 \times PI$

Normally consolidated: $\alpha = 0.9 - 0.004 \times PI$

4. Recommendations provided by Tomlinson (1957) for special case, where the foundation is driven into stiff to very stiff soil. Tomlinson (1957) showed that the observed adhesion, expressed as a percentage of the undisturbed cohesion of the clay, falls with increasing stiffness of the clay from approximately 100% in very soft clays to 20% in very stiff clays (see Figure 2.13). For firm and stiff clays, the loss of adhesion is not related to loss of strength by remolding, but it is believed to be due to the presence of a partial gap between the pile and the soil formed by installation method. In soft clays, the soil heaved during installation will reconsolidate and close the gap, thus giving 100 percent adhesion, but, firm and stiff clays will only partially re-consolidated. At present, no general law is available to determine such reduction in adhesion. As a guideline, Tomlinson (1994) proposed recommendation listed in Table 2.10. Figure 2.14 provides

charts for estimating shaft resistance for deep foundations driven into stiff and very stiff clay and can be used in combination with Table 2.10.

5. Chart recommended by Weltman and Healy (1978) as shown in Figure 2.15. The results of a number of loading tests on driven and driven and cast-in-place piles in glacial till have been reviewed.
6. Procedure recommended by Randolph and Wroth (1982) based on a very large number of pile load tests (see Figure 2.16). The method shows a correlation between the C_u/σ_{vo}' ratio and the adhesion factor, α . In addition, the method takes into account the flexibility and slenderness ratio of the pile by applying a length factor, F . The total skin friction takes the expression as:

$$Q_s = F\alpha C_u A_s \quad \text{Equation 2. 14}$$

where

Q_s = ultimate shaft resistance

α = adhesion factor

C_u = average undrained shear strength of the soil along the pile shaft

A_s = area of the pile shaft

7. Mooney et al., (1985) found that the shaft adhesion for screw piles in uplift condition ranged from 0.3 C_u (for stiff clays) to 0.9 C_u for soft clays

Burland (1973) suggested a β method to estimate shaft resistance for deep foundations installed in cohesionless soil.

$$q_s = \frac{1}{2} K_s \sigma'_{vo} \tan \delta$$

$$Q_s = q_s A_s \quad \text{Equation 2. 15}$$

where

σ'_{vo} = effective overburden pressure in soil at pile base level
 K_s = lateral earth pressure coefficient
 δ = soil-shaft effective friction angle, $\leq \phi'$, degrees

The value of the lateral earth pressure coefficient, K_s , is critical to evaluate the skin friction and is the most difficult to determine reliably because it is dependent on the angle of shearing resistance, the compressibility and the stress history of the soil. In addition, the installation process can also influence the value of K_s significantly. As indicated by Tomlinson (1994) driven piles displace the surrounding soil, thus, increases the horizontal soil stress. For bored pile, the drilling involved in installing can loosen dense sand and thus, decrease the horizontal stress. Kulhawy (1984) provided typical values of K_s in relation with the original soil stress K_o value as shown in Table 2.11 and Table 2.12. CFEM (1990) suggested that K_s is usually assumed to be equal to the coefficient of original earth pressure, K_o , for bored piles, and twice the value of K_o for driven displacement type piles. The relationship between K_s and the angle of internal soil friction, ϕ , for driven and bored pile is demonstrated in Figure 2.17 provided by Meyerhof (1982). The chart is only applicable for piles with length less than 15 to 20 pile diameters. Similar to the bearing capacity theory, Meyerhof suggested that conventional shaft capacity theory in terms of K_s should not be applied to piles longer than 15 to 20 pile diameters because the corresponding shaft friction became practically independent of the average overburden pressure along the shaft.

Kulhawy (1984) provided typical value of the angle of friction, δ , developed between the pile surface and the soil (Table 2.13). Canadian Foundation Engineering Manual (1992) suggested some typical value for a combined shaft factor, β coefficient for Cast-in-Place piles and Driven Piles where $\beta = K_s \tan \delta$. The values are summarized in Table 2.14.

2.3.3 Estimate Pile Capacity by Cone Penetrometer

Design of deep foundations based on direct in situ test data using static penetrometer is attractive because of the prominent advantages embedded within the method. The test is fast, economic, reliable and repeatable. In addition, the Cone Penetration test define not only a continuous soil profile but also provide a simple and direct correlation between cone tip resistance and cone shaft resistance to the pile toe resistance and pile shaft resistance. As stated by Lunne et al. (1997), almost all CPT methods use reduction factors to empirically account for influences caused by the "scale effect, rate of loading effects, difference of insertion technique, position of the CPT friction sleeve and differences in horizontal soil displacements". Nevertheless, methods are developed based on a large number of pile load tests with consideration of many different pile types, such as the LCPC-CPT method (Bustamante and Gianeselli, 1982). Lunne et al. (1997) compared case studies where CPT was used to predict capacity of a single pile including Robertson et al. (1988a), Briaud (1988), Tand and Funegard (1989), Sharp et al. (1988). These case studies investigated a large database where full-scale pile load tests were performed and a number of different in-situ test data were available. For example, Robertson et al. (1988a) illustrated the results of predicting ultimate capacity for eight steel pipe piles driven into deltaic soil. Thirteen methods including both static and dynamic methods were used in the exercise. The author illustrated that the static cone penetration methods gave much better prediction compared to methods that did not use the penetrometer method. Similarly, Briaud (1988) investigated 78 pile load tests in different soil types using different models including six CPT methods. Sharp et al. (1978) examined 28 pile load results with two CPT methods and three SPT methods. In all cases, the best method to predict the pile capacity was that of Bustamante and Gianeselli (1982) followed by methods by Ruiter and Beringen (1979) and by Schmertman (1978).

The review shows that CPT methods proposed by Bustamante and Giasenelli (1982) and Ruiter and Beringen (1979) give better predictions of pile capacity, hence, these methods are summarized here.

2.3.3.1 Bustamante and Giasenelli (1982) Method

The method is also known as the LCPC method that was developed based on the analysis of 197 full-scale compression and tension pile load tests with a wide variety of foundations and soil materials considered. The method is summarized as follow:

$$\begin{aligned} f_s &= \frac{q_c}{\alpha_{LCPC}} \\ q_p &= k_c q_{ca} \end{aligned} \quad \text{Equation 2. 16}$$

where

- f_s = pile unit side friction
- q_p = pile unit end bearing
- q_c = cone tip resistance
- q_{ca} = equivalent average cone resistance
- α_{LCPC} = friction coefficient
- k_c = end bearing coefficient

Bustamante and Giasenelli (1982) only adopted the measured CPT tip penetration resistance, q_c , for the calculation of both side friction and pile end bearing resistance. Lunne et al. (1997) stated that using only q_c could be considered as an advantage because interpreting f_s was difficult and could be unreliable. The method involved a procedure to calculate the equivalent average cone resistance, q_{ca} to smooth conservatively the cone tip resistance q_c profile in order to eliminate local irregularities (see Figure 2.19). In the procedure, the equivalent cone resistance, q_{ca} is calculated in several steps as follows (Lunne et al., 1997):

1. First, values of the cone tip resistance, q_c are averaged along a distance between $+a$ and $-a$ from the pile tip where a is taken as a length equivalent to $1.5 \times \text{Pile Diameter } (D)$. As the result, an arithmetic tip resistance mean, q_{ca}' is produced.
2. Then, values greater than $1.3 q_{ca}'$ along the length of $-a$ to $+a$, and values lower than $0.7 q_{ca}'$ along the length $-a$, are eliminated which produced a smoothed out thick curve as demonstrated in Figure 2.19.
3. At last, the mean tip resistance q_{ca} , is calculated.

As stated before, the method used the point bearing capacity coefficient k_c and the friction coefficient, α , to account for the scaling effect because of the difference in size between the cone penetrometer and the pile. The choice of point bearing capacity coefficient, k_c , and friction coefficient, α , was based on the various types of soils as illustrated in Table 2.15 and Table 2.16. Values for maximum unit shaft friction f_s , were also recommended unless local experience is available. Bustamante and Gianselli (1983) updated these tables to include the screw-in type of foundation. The descriptions of deep foundations are listed in Table 2.17, and the curves for determine the skin friction for different pile types based on the cone resistance, q_c are shown in Figure 2.20.

2.3.3.2 De Ruiter and Beringen (1979) Method

De Ruiter and Beringen (1979) proposed a method that uses both the cone tip resistance, q_c , and cone sleeve resistance, q_s in relation to the undrained shear strength, C_u of the soil. The procedure is self-explained and presented in Table 2.18. In cohesive soil material, the undrained shear strength C_u is calculated from the cone tip resistance, q_c . Then, pile shaft capacity and end bearing capacity are computed by applying empirical factors to C_u obtained. In cohesionless material, pile end bearing is determined by a procedure proposed by de Ruiter and Beringen (1979). They had found that an influence zone of 0.7 to 4.0 pile diameter below the pile tip governs the pile end bearing. The steps

involved to compute the pile bearing resistance, q_p , is self-explanatory as presented in Figure 2.21. In overconsolidated sands, reduction in capacity can happen due to pile driving. Figure 2.22 shows recommended corrections for sand relating to the OCR ratio for sand.

2.3.4 Helical Pile Under Compression Condition in Clay ($\phi = 0$)

Limited researches have been focused on the compressive capacity of screw piles. Narasimha Rao et al (1991) suggested that the load transfer phenomena for screw piles installed in clay can be described using a cylindrical shearing method as shown in Figure 2.23. The formulae proposed to approximate the ultimate compression capacity could be expressed as:

$$Q_c = A_p N_c C_p + A_a N_c C_a' + C_a' A_s' + \alpha C_a A_s \quad \text{Equation 2. 17}$$

where

- A_p = cross sectional area of the pile stem at the toe level = $\pi d^2/4$
- A_a = area of cross section of the helical plate = $\pi (D^2 - d^2)/4$
- A_s' = surface area of cylinder between top and bottom plates = $\pi D L_c$
- L_c = distance between top and bottom helical plate
- A_s = surface area of shaft
- N_c = bearing capacity factor
- C_p = cohesion of soil around pile toe
- C_a' = average cohesion of soil around cylinder of soil between top and bottom helical plates
- C_a = average cohesion of soil along the pile shaft
- α = adhesion factor

For uniform clay, it can be assumed that $C_p = C_a' = C_a = C_u$. Equation 2.17 was used to predict the model experiment results carried out by Narasimha et al. (1991). In general, the agreement is good for screw piles with helical plates welded at close intervals, such as, for a S/D ratio of 1.0 to 1.5 where S is the space between two helices and D is the helix diameter. The equation over

predicts the ultimate compression capacity for higher S/D ratio. This aspect is examined in detail in Section 2.4.

2.4 BEHAVIOR OF SCREW PILE UNDER VERTICAL UPLIFT LOADING

2.4.1 Introduction

Research on predicting the ultimate uplift capacity of individual plate anchors and shallow foundations was initiated with the development of the transmission line industry in the 1950's (e.g. Meyerhof and Adams, 1968; Adams and Hayes, 1967). During the last thirty years or so, a number of increasingly sophisticated theories have been developed to predict the ultimate uplift capacity of horizontal anchor foundations embedded in various types of soils. These researches set the framework for later works on predicting the uplift capacity of screw piles. Therefore, this section provides a brief review of major work carried out on predicting the uplift capacity of horizontal anchor and subsequently, the uplift capacity of screw pile.

2.4.2 Theories of Uplift Resistance for Anchors in Sand

Figure 2.24 shows a plate anchor having a width D installed to a depth of H . The embedment ratio (H/D) is defined as the ratio of the depth of the embedment, H , to the width of the anchor, D . If such an anchor is placed at a relatively shallow depth, the failure surface will extend to the ground surface at ultimate load. This type of behavior is referred to as shallow anchor condition. With increasing installation depth, the compressibility and deformation of the soil mass above the anchor prevent the failure surface from reaching the ground, and local shear failure in soil located around the anchor will take place. This is referred to as deep anchor condition. As stated by Meyerhof and Adam (1968), the ultimate uplift capacity can be estimated as the sum of the effective weight of

the soil located in the failure zone and the shearing resistance developed along the failure surface. However, the difficulties of estimating the uplift capacity of an anchor lie in the difficulties of predicting the geometry of the failure zone.

Das (1990) has summarized some of the early theories for predicting the uplift capacity of shallow anchor in sand as shown in Figure 2.25. Such theories include the Soil Cone method as proposed by Mores (1959), Friction Cylinder method proposed by Ireland (1963). In the Soil Cone theory, the slope surface rising at about 30 degrees from the vertical, forming a truncated cone with an apex angle of $\theta = 90^\circ + \phi/2$. The dead weight within the frustum was considered to predict the ultimate uplift capacity. For the Friction Cylinder method, the failure surface is assumed to rise vertically from the edge of the anchor, and the shear resistance developed along the cylindrical shear surface and the dead weight of the soil within the failure surface contributes the ultimate capacity of the anchor. Tuner (1962) suggested that the cone method is conservative at shallow depth but over-predicts at greater depth. Parr and Vanner (1962) indicated that the friction cylinder method works in cases where the strength of the soil medium can be effectively mobilized, therefore, the method might only apply to backfilled footing but not to flared-out footing. Balla (1961) established a more complicated failure surface for shallow circular anchors installed in dense sand. In Balla's theory, the failure surfaces composed with arcs of a circle which exit the ground surface at an angle of approximately $45^\circ - \phi/2$ to the horizontal. Das (1990) indicated that Balla's theory is in good agreement for the uplift capacity of anchors embedded in dense sand at an embedment ratio of $H/D \leq 5$. However, for anchors located in loose to medium sand and with embedment ratio $H/D > 5$, the theory overestimates the net ultimate uplift capacity. The main reason for this overestimation is that the failure surface does not extend to the ground surface in these cases. Balla (1961) suggested a simple non-dimensional factor, named the break out factor F_q , plotted with respect of the embedment ratio H/D , to determine the embedment ratio at which deep anchor condition is reached. The break out factor F_q , is developed based on the results of several laboratory

model and full-scale field tests. The breakout factor increases with H/D up to a maximum value at $H/D = (H/D)_{cr}$. For $H/D > (H/D)_{cr}$ the breakout factor remains practically constant. Therefore, anchors located at an embedment ratio less than the critical embedment ratio $(H/D)_{cr}$ are shallow anchors and those located greater than the critical are the deep anchor. The ultimate capacity of an anchor installed at shallow depth takes the following expression:

$$Q_t = H^3 \gamma \left[F_1 \left(\phi, \frac{H}{D} \right) + F_3 \left(\phi, \frac{H}{D} \right) \right]$$

Equation 2. 18

$$F_1 + F_3 = \frac{Q_t}{\gamma H^3}$$

where

Q_t = ultimate uplift capacity
 H = the depth to the top helix
 $F_1(\phi, H/D), F_3(\phi, H/D)$ = non-dimensional factors, determined using Figure 2.26

Similar to Balla's method, Macdonald (1963) demonstrated that the failure surface could be approximated by a parabolic function that produces a conical failure surface in shallow depths. Unlike Balla's method, for greater depths, he predicted a vertical failure surface as a cylinder with the diameter of the cylinder formed being about 1.75 times the base diameter of the footing. Mariupol'skii's (1965) extended Macdonald's model and proposed a theory that incorporates the progressive failure mechanism for shallow anchors and cavity expansion theory for deep anchor. According to this model, the progressive failure mechanism commences with compression of the soil located above the anchor plate. This compression occurs within a column of soil the same diameter as the anchor plate as shown in Figure 2.27. Compaction of the soil continues as pullout progresses, and this leads to an increase in the vertical compressive stress. Thus, there is a continued increase in the frictional resistance along the surface of the soil column. The increase of the frictional resistance progresses to the

adjacent rings of soil. Ultimately sufficient tensile stress is developed and the failure occurs as soil above the anchor separates in the form of a core with a curvilinear geneatrix. The net ultimate tension capacity can be given as:

$$Q_t = \frac{\pi}{4}(D^2 - d^2) \left\{ \frac{\gamma H \left[1 - \left(\frac{d}{D} \right)^2 + 2K_o \left(\frac{H}{D} \right) \tan \phi \right] + 4C \left(\frac{H}{D} \right)}{1 - \left(\frac{H}{D} \right)^2 - 2n \left(\frac{H}{D} \right)} \right\} \quad \text{Equation 2. 19}$$

where

- Q_t = ultimate uplift capacity
- D = the diameter of the anchor plate
- d = the diameter of the shaft
- C = cohesion and for sand C is equal to zero
- n = an empirical coefficient $\approx 0.025 \phi$
- ϕ = angle of internal soil friction
- H = embedment depth

For deep anchors, the concept of cavity expansion for a cylindrical cavity of height L and diameter D concept is used. The equation takes the following form:

$$Q_t = \left(\frac{\pi q_o}{2} \right) \left(\frac{D^2 - d^2}{2 - \tan \phi} \right) + f(\pi d)[H - (h - d)] \quad \text{Equation 2. 20}$$

where

- q_o = radial pressure under which the cavity is expanded
- f = unit skin resistance along the stem of the anchor
- h = effective length of anchor stem

However, in this model, the author recommended using the lower bound value calculated by both equations because there is no clear distinguishable guideline that can be established between shallow and deep anchor.

As a summary to these early studies, Meyerhof and Adam (1968) stated that there is a clear indication that the uplift behavior of deep footings is distinctly

different from that of shallow footings. In addition, for shallow footings installed in dense sand, the shape of the failure surface has been found to be generally parabolic in section near the footing edge. A vertical or cylindrical shape failure surface has been shown to provide better prediction for the ultimate uplift capacity, as the footing depth becomes greater. Based on these conclusions, Meyerhof and Adam (1968) proposed a semi-theoretical theory for estimation of the ultimate uplift capacity of strip footings. Solutions for rectangular and circular anchors are also derived with modifications on the principles developed for strip footings with consideration of the shape factors. Meyerhof and Adams (1968)'s model simplify the actual complex failure surfaces using a number of assumptions for both shallow and deep footing as shown in Figure 2.24.

For anchors installed in shallow depth ($H < H_{cr}$), at ultimate load, the truncated pyramidal shaped failure surface reaches the ground surface with an average angle varying between $\phi/3$ and $2\phi/3$ with the vertical. General shear failure is assumed to occur along the failure surface which a cohesive resistance, C and frictional resistance, F mobilized. In general, the theory considers the following components for predicting the ultimate uplift capacity of a strip footing installed in shallow depth. The ultimate capacity of a shallow footing would be simply the summation of the vertical component of the following forces:

1. The weight of the soil, W , bounded inside the failure surface
2. The total passive earth pressure P_p per unit length along the failure surface. The force P_p is inclined at average angle δ to the horizontal. For an average angle of $\phi/2$ between the failure surface to the vertical, δ has an approximate value of $2\phi/3$.

Based on the purposed failure surface, for circular shallow anchor, the uplift capacity can be obtained by the expression as:

$$Q_t = \pi DCH + W + s \frac{\pi}{2} \gamma D H^2 k_u \tan \phi \quad \text{Equation 2. 21}$$

$$s = 1 + m \left(\frac{H}{D} \right) \quad \text{Equation 2. 22}$$

with a maximum value of s taken as:

$$s = 1 + m \frac{H_{cr}}{D} \quad \text{Equation 2. 23}$$

$$W = \frac{\pi}{4} D^2 H \gamma \quad \text{Equation 2. 24}$$

or

$$Q_t = \pi DCH + \frac{\pi}{4} D^2 H \gamma + \left[1 + m \left(\frac{H}{D} \right) \right] \gamma D H^2 k_u \tan \phi \quad \text{Equation 2. 25}$$

where

- W = weight of the soil above the circular anchor
- D = diameter of the anchor plate
- s = shape factor governing the passive earth pressure on a convex cylindrical wall
- πDCH = cohesion along vertical plane through circular footing edge
- k_u = nominal uplift coefficient of earth pressure on vertical plane through footing edge
- ϕ = angle of internal friction of soil
- m = coefficient relating to the embedment depth (Table 2.19)

The failure surface for deep footings does not reach the ground surface because of the compressibility and deformation of the soil mass above the soil mass as the embedment ratio increases beyond a critical number, $(H/D)_{cr}$. This phenomenon, named the local shear failure, was modeled by limiting the vertical extent, H of the failure surface and adding the surcharge pressure above the level of the failure surface $\sigma_{vo}' = \gamma' (H - H_{cr})$ to Equation 2.21. Therefore, for deep circular anchors, the ultimate uplift capacity can be predicted using the following equation:

$$Q_t = \pi DCH_{cr} + W + S \frac{\pi}{2} \gamma D (2H - H_{cr})H_{cr}k_u \tan \phi \quad \text{Equation 2. 26}$$

where

H_{cr} = limiting embedment depth where the failure mechanism transfers from shallow to deep

The magnitude of H_{cr} was determined by laboratory observation on the failure surface and the values are given in Table 2.20. The magnitude of $sK_u = [1+m(H/D)]K_u$ for a given friction angle, ϕ , increases with the embedment ratio H/D to a maximum value of $(H/D)_{cr}$ and remains constant thereafter as shown in Figure 2.28.

Das (1990) further simplified Meyerhof and Adam's formula in terms of breakout factor, F_q , and Equation 2.21 can expressed as:

$$F_q = \frac{Q_t}{\gamma \frac{A}{H}} = 1 + 2 \left[1 + m \left(\frac{H}{D} \right) \right] \left(\frac{H}{D} \right) k_u \tan \phi$$

$$Q_t = F_q \gamma A H \quad \text{Equation 2. 27}$$

For a shallow circular anchor, the breakout factor, F_q variation with embedment ratio (H/D) for a given value of internal friction angle of soil, ϕ , is shown in Figure 2.29. Similarly, the breakout factor, F_q^* variation with a given ϕ for a deep circular anchor is plotted in Figure 2.30. Das (1990) summarized that for shallow anchors, the uplift capacity is the sum of the uplift capacity of the anchor plate and the weight of the anchor, W_a , which can be expressed as:

$$Q_t = F_q \gamma A H + W_a \quad \text{Equation 2. 28}$$

For deep anchors, the uplift capacity consists of three major components: the uplift capacity of the anchor plate, the frictional resistance along the anchor shaft, and the weight of the anchor. The equation takes the form as:

$$Q_t = F * \gamma AH + K_o P_s (H - H_{cr}) \bar{\sigma}'_o \tan \phi + W_a \quad \text{Equation 2. 29}$$

where

P_s = perimeter of the anchor shaft

$H - H_{cr}$ = effective length of the anchor shaft

$\bar{\sigma}'_o$ = average effective stress between $Z = 0$ to $Z = H - H_{cr} = \frac{1}{2}\gamma(H - H_{cr})$ as shown in Figure 2.31.

K_o = coefficient of earth pressure at rest $\approx 1 - \sin \phi$

Vesic (1965) studies the breakout resistance of objects embedded in the ocean bottom. He modeled the breakout force required to expand a spherical cavity in a semi-infinite, homogeneous, isotropic solid medium at shallow depth. Vesic indicated that the solution could be used to determine the ultimate uplift capacity of shallow circular anchor embedded in sand. Vesic's theory is fairly accurate in estimating the new ultimate uplift capacity for shallow anchors in loose sand. However, laboratory tests have shown that the theory can under estimate the actual capacity by as much as 100% or more for shallow anchors embedded in dense sand. The breakout factor for Vesic (1965)'s model is provided in Figure 2.32 for comparison with Meyerhof and Adam's theory.

Saeedy (1987) introduced a compaction factor for circular plate anchors embedded in sand. For shallow anchor, the failure surface is similar to Meyerhof and Adam (1968)'s theory. However, for deep anchors, the failure surface is assumed to have a shape of an arc and can be modeled as a logarithmic spiral. According to the author, the soil located above the anchor gradually becomes compacted during the pullout process. This compaction causes increase of shear strength of the soil, hence, increasing the net ultimate uplift capacity. An empirical compaction factor is introduced in order to model this phenomenon which is given in the form:

$$\mu = 1.044Dr + 0.44 \quad \text{Equation 2. 30}$$

The actual net ultimate uplift capacity can be expressed as:

$$Q_t = (F_q \gamma A H) \mu$$

Equation 2. 31

where

μ = compaction factor

Dr = relative density of compaction

F_q = breakout factor as shown in Figure 2.33

Veesaert and Clemence (1977) modified the Meyerhof and Adam's uplift capacity theory on shallow circular anchors. Based on laboratory experiments on model anchors, the results indicated that the failure surface may be modeled as a truncated cone with an apex angle of $90^\circ - \phi/2$ from horizontal. For deep anchors, Veesaert and Clemence (1977)'s model is essentially the same as the Meyerhof and Adam (1968)'s theory. Therefore, the breakout factor, F_q , takes the following form:

$$F_q = \frac{Q_t}{\gamma A H}$$

and

$$F_q = \left\{ 4K_o (\tan \phi) \left(\cos^2 \frac{\phi}{2} \right) \left(\frac{H}{D} \right)^2 \left[\frac{0.5}{\left(\frac{H}{D} \right)} + \frac{\tan\left(\frac{\phi}{2}\right)}{3} \right] \right\}$$

$$+ \left[4 + 8 \left(\frac{H}{D} \right) \tan\left(\frac{\phi}{2}\right) + 5.333 \left(\frac{H}{D} \right)^2 \tan^2\left(\frac{\phi}{2}\right) \right]$$

Equation 2. 32

Das (1990) provided a simpler chart plotting the breakout factor F_q against the embedment ratio, H/D , for sand with coefficient of lateral earth pressure $K_o = 1$, and the results are shown in Figure 2.34.

2.4.3 Anchor in Clay under Undrained Loading

Research has shown a number of anchor responses when it is subjected to an uplift force in soft saturated clay. The soil located above the anchor will be compressed and at the same time, the soil below the anchor will be relieved causing a decrease of stress. Consequently, this results in an increase of the pore water pressure above the anchor accompanied by a decrease of pore water pressure below the anchor. The difference results in a suction force that will increase the short term uplift capacity of the anchor. Nevertheless, the magnitude of the suction force and its variation with depth and type of clay soil is not properly understood by current research. Secondly, tension cracks at ground level have been reported for anchors typically installed to shallow depths. These tension cracks are created by substantiated tension force in the clay mass when the anchor is subjected to uplift forces. At greater depths, the overburden pressure above the anchor plate prevents the flexing of the clay mass, therefore, a failure surface begins to develop during uplift but disappears within a few anchor diameters from the anchor plate. In this case, the uplift capacity of an anchor plate can be determined by the shear strength of the clay. Therefore, the limiting uplift capacity of a plate can be approximately equal to the bearing capacity of the clay (Meyerhof and Adam 1968). Based on these observations, the uplift capacity can be given by the expression:

$$Q_t = Q_{bearing} + W + U \quad \text{Equation 2. 33}$$

where

Q_t	= ultimate uplift capacity
$Q_{bearing}$	= bearing capacity of the anchor in pullout loading
W	= weight of the soil mass above the anchor
U	= suction force below the anchor

For design purpose, the suction force is often neglected because of the difficulty in determining this force. Meyerhof and Adam (1968) indicates that the

failure surface is difficult to predict due to the formation of horizontal cracks caused by the tension stress in the soil mass is complicated to formulate. Therefore, an empirical procedure was adopted relating the uplift coefficient of clay to the undrained shear strength of the soil. Based on experimental results provided by Meyerhof and Adam (1968), Adams and Hayes (1967), Spence (1965) and Langley (1967), Meyerhof (1973) proposed the following relationship:

$$Q_t = A(\gamma' H + N_u C_u) \quad \text{Equation 2. 34}$$

$$N_u = 1.2 \left(\frac{H}{D} \right) \leq 9 \quad \text{Equation 2. 35}$$

where

- Q_t = ultimate uplift capacity of an anchor
- A = area of an anchor plate
- N_u = uplift capacity factor
- C_u = undrained shear strength of the clay
- γ' = unit weight of the clay

Experimental values of N_u were calculated from the model and field test with correction for the suction force below the anchors and plotted against the embedment ratio, H/D as shown in Figure 2.35. The uplift capacity factor, N_u increases with depth to a maximum value of approximately 9 or 10. A semi-theoretical line is determined based on the available data where the undrained shear strength of the clay is fully mobilized. However, for shallow anchors the uplift capacity may be as low as about one half the estimate from the theory. This is due to the influence of tension cracks formed due to the tensile stress in the soil mass. In addition, the undrained shear strength mobilized in fissured soil mass, such as stiff till material, may be considerably less than the peak value and possibly as low as the residual value. In such case, the uplift capacity factor N_u should be much lower. Detail discussion regarding this effect is provided in Section 2.5.

2.4.4 Failure Models of Screw Pile in Soil

A survey of literature indicates that a number of failure models are available for the analysis and design of individual screw piles subjected to axial uplift forces. Two methods, the cylindrical shear method and individual bearing method, are most commonly used as indirect methods to predict the uplift capacity of multi-helix screw piles with the support of conventional geotechnical engineering principles. A third method called the installation torque method is empirically developed based on a large database of over 2500 installed screw anchors. This method is currently used in the industry.

2.4.4.1 Cylindrical Shear Method

The cylindrical shear method assumes that a cylindrical shear failure surface, connecting the uppermost and lowermost helices, is formed as shown in Figure 2.23. The uplift capacity is mainly derived from the shear resistance along this cylindrical surface and bearing resistance above the top helix. The adhesion developed along the steel shaft is considered in cases where sufficient installation depth (deep pile) is provided. For a screw pile installed in shallow depth, the adhesion may not be reliably predicted, hence, it is ignored in many theories. The influence of installation depth on the screw pile's ultimate uplift capacity is discussed in a later section. The failure resistance can be summarized as follows:

$$Q_t = Q_{shaft} + Q_{helix} + Q_{bearing} \quad \text{Equation 2. 36}$$

where

- Q_t = ultimate uplift capacity
- Q_{shaft} = adhesion developed along the steel shaft
- Q_{helix} = shearing resistance mobilized along the cylindrical failure surface
- $Q_{bearing}$ = bearing capacity of the top helix

2.4.4.1.1. Helical Pile Under Uplift Condition in Sand

Vesic (1971) has shown that there is a weak zone surrounding the screw anchor in soil that is mainly caused by the screw action when installing the anchor. This disturbed zone causes a slip surface to develop in the shape of a cylinder around and above the anchor. Laboratory model tests performed by Mitsch and Clemence (1985) verified these observations. The sand around the helices was sheared and displaced laterally when the pile was screwed into the soil. This lateral movement introduced lateral stress to the surrounding sand, thus, densified the soil. Laboratory tests established that this increase in lateral stress during installation increases the potential for a cylindrical failure surface to develop as shown in Figure 2.36 and Figure 2.37.

Two distinct failure behavior patterns were observed for screw pile at failure under uplift loading. Similar to Meyerhof and Adam (1968)'s theory, the failure mechanism observed in the laboratory experiments could be approximated either to be shallow or deep depending on the relative density (D_r), the internal soil friction angle, ϕ , and the embedment ratio (H/D) of the sand. The maximum embedment ratio $(H/D)_{cr}$, where the failure mode changes from shallow to deep, increases with an increase in the relative density (D_r) and the internal soil friction angle, ϕ . For laboratory tests on sand with relative densities ranging from 47% to 90%, the screw pile behaves as a shallow anchor with an embedment ratio (H/D) less than 5. A truncated shape failure surface propagates from the top helix to the ground surface as shown in Figure 2.36. The central angle of the truncated cone is approximately equal to the soil friction angle, ϕ . A cylindrical failure surface is formed below the top helix. General shear failure occurs along this inter-helical cylinder failure surface. For sand with the same relative densities and embedment ratio (H/D) greater than 5, the screw pile is defined as a deep anchor where a failure zone develops directly above the top helix. However, this failure surface is confined by the overburden pressure, and

therefore the failure zone does not propagate to the ground surface as shown in Figure 2.37.

Based on the above observations, Mitsch and Clemence (1985) simplified the failure surfaces for shallow and deep screw pile under uplift loading condition as shown in Figure 2.38 and Figure 2.39.

Embedment ratio (H_1/D_1) is defined as the depth to the top helix, H_1 divided by the top helix diameter, D_1 . For a shallow circular screw pile with $H_1/D_1 \leq 5$, the ultimate uplift capacity of multi-helix screw pile in sand can be predicted by summing the uplift capacity of the top helix, the friction along the cylinder of soil between the helices. Frictional cylinder theory proposed by Meyerhof and Adams (1968) sets the basis for determining the bearing capacity of the top helix plate and the frictional resistance on the intra-helical cylindrical failure surface. Hence, the uplift capacity of a shallow anchor can be given as:

$$Q_t = \pi \gamma' K_u \tan \frac{\phi}{2} \left\{ \frac{D_1 H_1^2}{2} + \frac{H_1^3 \tan(\frac{\phi}{2})}{3} \right\} + \frac{\pi}{2} D_a \gamma' (H^2_3 - H^2_1) K_u \tan \phi + W_t \quad \text{Equation 2. 37}$$

For deep anchors with $H_1/D_1 > 5$, shaft resistance developed along the screw pile shaft can be considered since it can significantly contribute to the ultimate uplift capacity. The equation for estimating the shaft friction in homogeneous sand is provided by Meyerhof and Adam (1968). For deep anchors, the ultimate tensile capacity can be derived from:

$$Q_t = \gamma' H_1 A_1 N_{qu} + \frac{\pi}{2} D_a \gamma' (H^2_3 - H^2_1) K_u \tan \phi$$

$$+ P_s H_1 \left(\frac{\gamma' H_1}{2} \right) K_u \tan \phi \quad \text{Equation 2. 38}$$

where

Q_t	= ultimate screw pile uplift capacity
γ'	= effective unit weight of soil
K_u	= coefficient of lateral earth pressure in uplift for sands
ϕ	= friction angle of the soil
A_1	= area of the top helix
N_{qu}	= uplift capacity factor for cohesionless soils
H_1	= depth to top helix
D_a	= average helix diameter
D_1	= diameter of the top helix
H_3	= depth to the bottom helix
P_s	= perimeter of the screw pile shaft

The lateral earth pressure coefficient during uplift, K_u and uplift capacity factor, N_{qu} , derived from this study is also provided in Figure 2.40 and Figure 2.41. The major variable in the above equation is the lateral earth pressure coefficient in uplift (K_u). This coefficient is used to empirically quantify the lateral stress acting on the failure surface as the screw pile is pulled out from the soil. As indicated before, the lateral stress outside the cylindrical failure surface increases to a passive state due to the screw action during the installation process. The magnitude of the increase is dependent upon the amount of disturbance and the changes in stress level during the installation. Mitsch and Clemence (1985) provided the coefficients of lateral earth pressure K_u for screw piles and the values are listed in Table 2.21. The recommended values of K_u were calculated based on the model and field tests, and are 30% to 40% lower than those provided by Meyerhof and Adam (1968) which is mainly a result of the installation disturbance.

Das (1990) expressed the ultimate bearing capacity proposed in Mitsch and Clemence's theory in terms of breakout factor F_q for shallow anchor conditions and F_q^* as shown in Figure 2.42 and Figure 2.43. This approach simplifies computing steps involved in Mitsch and Clemence's method. Thus, for shallow anchor, equation 2.37 becomes:

$$Q_t = \frac{\pi}{4} F_q \gamma' D_1^2 H_1 + \frac{\pi}{2} D_a \gamma' (H_3^2 - H_1^2) K_u \tan \phi \quad \text{Equation 2. 39}$$

For deep anchors, equation 2.38 can be expressed as:

$$Q_t = \frac{\pi}{4} F_q^* \gamma' D_1^2 H_1 + \frac{\pi}{2} D_a \gamma' (H^2_3 - H^2_1) K_u \tan \phi$$

$$+ P_s H_1 \left(\frac{\gamma' H_1}{2} \right) K_u \tan \phi$$

Equation 2. 40

2.4.4.1.2. Helical Pile Under Uplift Condition in Clay ($\phi = 0$)

Mooney et al. (1985) proposed idealized failure surfaces for shallow and deep anchor conditions for helical piles in clay and silt based on laboratory model tests. A cylindrical failure surface was verified by measuring soil surface deflection in model experiments as shown in Figure 2.44. A procedure similar to the work conducted by Meyerhof and Adams (1968), Adams and Hayes (1967), Adams and Klym (1972), and Mitsch and Clemence (1985), was adopted in Mooney's model (see Figure 2.45). A simplified bearing capacity equation, similar to the bearing capacity equation used for deep foundation in compression, was used to predict the tension capacity of the screw pile. The common bearing capacity factor N_c is replaced by an uplift factor N_u . Research done on uplift anchor capacity by Ali (1968) and Kupferman (1971), Das (1980) and Narasimha Rao and Prasad (1989, 1991) indicated that the uplift bearing capacity factor N_u increases with the embedment ratio (H/D) to a constant maximum value of 9.4 at $(H/D)_{cr}$ as shown in Figure 2.46. Therefore, the helical plate failure in tension is similar to the bearing capacity condition in compression for deep screw piles. The critical value of the embedment ratio is a function of the undrained shear strength C_u of the material. Mooney et al. (1985) indicated that the critical embedment ratio $(H/D)_{cr}$ was approximately 5 for the soil tested in the experiment. Das (1990) proposed a design chart to approximate the critical embedment ratio in relation with the undrained shear strength C_u as shown in Figure 2.47 and the relationship can be expressed as follow:

$$\left(\frac{H}{D}\right)_{cr} = 0.107C_u + 2.5 \leq 7 \quad \text{Equation 2. 41}$$

A model that approximates the short term screw pile uplift capacity is shown in Figure 2.45. Similar to the model proposed by Mitsch and Clemence (1985), the pile uplift capacity is the sum of the bearing resistance on the top helix, the cohesion and frictional resistance on the cylindrical surface formed between the helices, and friction and adhesion on the pile shaft. For a shallow screw pile with an embedment ratio (H/D) of less than 4, the model does not consider the shaft resistance because it is considered insignificant, therefore, the uplift capacity equation for helical piles in clay under shallow condition can be given as:

$$Q_t = A_1 C_u N_u + \pi D_a C_u (H_3 - H_1) \quad \text{Equation 2. 42}$$

For deep anchors with embedment ratio (H/D) greater than 4, the contribution of the soil adhesion along the pile shaft can be substantial especially for those with enlarged central shafts. Therefore, the uplift capacity equation is expressed as:

$$Q_t = A_1 C_u N_u + \pi D_a C_u (H_3 - H_1) + P_s H_1 C_a \quad \text{Equation 2. 43}$$

Where

Q_t = ultimate uplift capacity of the multi-helix screw pile
 H_1 = depth to top helix
 H_3 = depth to bottom helix
 D_a = average helix diameter
 P_s = perimeter of anchor shaft
 A_1 = area of top helix
 N_u = uplift bearing capacity factor for cohesive soils
 C_u = undrained shear strength of the clay
 C_a = average cohesion of soil along the pile shaft

Narasimha Rao and Prasad (1993) conducted a series of laboratory model tests to study the behavior of multihelix screw anchor installed in soft marine clays. The study focused on the failure mechanism for different embedment ratio (H/D) and the impact of varying the space between the helices on the ultimate uplift capacity of a screw anchor. An empirical factor, named the spacing to diameter ratio (S/D), is used to estimate the resistance derived from the cylindrical failure surface formed by the top and bottom helices. The results of the study indicated that uplift capacity of screw pile increases with increasing embedment ratio, and this capacity increase is caused by different failure surfaces formed as the depth of embedment increase as shown in Figure 2.48. The cylindrical failure surface method proposed by Narasimha Rao and Prasad (1993) followed a similar procedure outlined by Mooney (1985). Therefore, the method considers bearing resistance from the top of the helical plate, the shear resistance between top and bottom helical plates and the shaft adhesion as the major components that contributes to the uplift capacity of screw pile. The suction force below the helical plate and the weight of the screw pile can be neglected for a conservative design procedure. The difference between Narasimha Rao and Prasad's method and the those proposed by Mooney's procedure is that more detail works were performed on the embedment ratio (H/D) and the space to diameter ratio (S/D), and these factors are incorporated into the design. The general formula can be expressed as:

$$Q_t = S_F (\pi D L_c) C_u + A(C_u N_u + \gamma' D) + \pi d H_{eff} \alpha C_u \quad \text{Equation 2. 44}$$

Where

$$\begin{aligned} S_F &= 1.0 && \text{for } S/D \leq 1.5 \\ S_F &= 0.683 + 0.069 (3.5 - SR) && \text{for } 1.5 \leq S/D \leq 3.5 \\ S_F &= 0.700 + 0.148 (4.6 - SR) && \text{for } 3.5 \leq S/D \leq 4.6 \end{aligned}$$

Q_t = ultimate anchor uplift capacity
 S_F = spacing ratio factor
 L_c = is the distance between top and bottom helical plates
 H_{eff} = effective length of the shaft, typically $8.6D$

α	= adhesion factor
d	= shaft diameter
D	= average helix diameter
γ'	= unit weight of soil
N_u	= uplift bearing capacity factor for cohesive soils
C_u	= undrained shear strength of the soil

Narasimha Rao and Prasad (1993) classified three different failure surfaces based on the laboratory observation. First, shallow condition occurs with an embedment ratio H/D up to 2. The characteristics of a shallow anchor failure are that tensile cracks and surface heave and a clear gap formed between the anchor shaft and the soil at the ground surface. There is no shaft adhesion because no relative movement between shaft and soil occurred because the tensile cracks and large deformations at the failure. Thus, the uplift load is transferred to the soil mainly by the bearing resistance of the top plate and the cylindrical cohesive resistance developed between the top and bottom helical plate. For embedment ratio between 2 and 4, the helical anchor is classified as transition anchor. The failure surface extends to the ground surface with observation of minute tensile cracks and a slight heaving-up of the soil surface. Shaft adhesion may contribute to the pile uplift capacity as the uplift bearing capacity factor, N_u approaches to the maximum value of 9. For an embedment ratio greater than 4, the helical anchor are consider as a deep anchor with no tensile cracks or surface heave can be observed during testing. For both transition and deep anchor conditions, the uplift capacities are derived from the bearing resistance above the top helix plate, the intra-helical cylindrical shearing resistance, and shaft resistance.

Narasimha Rao Prasad (1993) stated that there was an ineffective length of the pile shaft that could not be mobilized. The reason is supported by research done by Adams and Hayes (1967), Adams and Klym (1972), and Meyerhof and Adams (1968) which they assumed the soil above the top helix mobilized in uplift could be evaluated similar to that below a deep foundation in bearing. Zeevaert (1983) had shown that the failure zone extends over a depth of almost twice the

diameter below the tip of the pile loaded in compression. Based on the laboratory test results, Narasimha Rao and Prasad (1993) provided some values for estimating the effective shaft length that can be considered in design. For transition anchor with H/D of 3 and 4, the effective shaft length (H_{eff}) ranges from $0.7D$ - $0.9D$ and $1.7D$ - $2.5D$. For deeper anchor, the H_{eff} values are in the range $2.9D$ - $8.6D$.

Laboratory studies conducted by Narasimha Rao et al. (1991) investigated the effect of the spacing of helical plates on the ultimate uplift capacity of screw pile installed in soft to medium stiff clay. Spacing ratio (S/D) is defined as the spacing between any two adjacent helical plates divided by their average diameter. The results of the investigation showed that a near cylindrical shear surface could be formed for anchors with spacing to diameter ratios of 1.5 or less. With S/D ratio greater than 2, bearing failure occurs above each individual anchor helix and the cylindrical shear does not fully develop. The anchor capacity reduces with higher S/D ratio because less shearing resistance can be developed on a smaller shearing surface area. The study showed that as the spacing ratio (S/D) increases above 1.5 a significant uplift capacity reduction was observed (Narasimha et al., 1991). A reduction factor S_F is used to approximate such reduction of the resistance along the cylindrical failure surface with higher S/D ratio. Nevertheless, author suggested that at S/D ratio less than 1.5, the cylindrical failure surface method is valid. For a spacing ratio greater than 1.5, Hoyt and Clemence (1989) and Narasimha Rao et al. (1990) suggested that individual plate bearing method provides a better capacity prediction.

2.4.4.2 Individual Plate Method

The individual bearing method assumes that bearing failure occurs above each individual helix (Figure 2.49). The total uplift resistance is the sum of the individual capacities. Similar explanation of adhesion resistance along the pile shaft as discussed above is also applied here. The method depicts as:

$$Q_t = Q_{shaft} + \sum Q_{i(bearing)}$$

Equation 2. 45

where

Q_t = ultimate uplift capacity

Q_{shaft} = adhesion developed along the steel shaft

$\sum Q_{i(bearing)}$ = sum of the bearing capacity of each individual helix

The individual bearing method estimates the ultimate uplift capacity by assuming bearing failure had occurred above each individual helix. Therefore, the total capacity is the sum of the individual capacity. The theory is simply an extension work of the analysis and design of individual plate anchors and shallow foundations subjected to uplift forces (Adams and Hayes, 1967; Meyerhof and Adams, 1968; and Vesic, 1971). The method was adopted for predicting screw pile uplift capacity by Adams and Klym (1971), Johnston and Ladanyi (1974), Trofimenkov and Mariupolskii (1965), and Adams and Radhakrishna (1971) and results were well supported by full scale field tests conducted by these authors. Researchers have shown that at higher space to diameter ratio ($S/D > 2$), individual bearing method should provide better prediction of ultimate uplift capacity for screw pile. Adams and Klym (1971) stated that at $S/D \geq 2$, each helix plate can be assumed to be behaved independently of the other. Narasimha Rao et al. (1993) suggested that at higher S/D ratio, for example, $S/D > 2$, adhesion over a shaft length of $1.5D - 2.5D$ above each plate should be considered for multi-helix screw piles installed in cohesive soil. The modification of the individual bearing method provides much better agreement with field results obtained by previous researchers with maximum underestimation of 20%. For cohesionless soil, Adams and Klym (1971) suggested that the shaft resistance and weight of the screw pile should be neglected due to the relatively low magnitude of load involved. Methods to calculate the bearing capacity of each individual bearing plate are listed in Section 2.4.4.1.1.

2.4.4.3 Empirical Method

This method empirically correlates the torque monitored during the installation of the pile with the ultimate uplift pile capacity achieved, analogous to the relationship of pile driving effort to pile capacity. The method was developed empirically and lacks geotechnical explanation. Nevertheless, it is statistically analyzed based on a large database, and the method has been used successfully in the construction of thousands of anchors over the past twenty years as indicated by Hoyt et al., (1989). Due to the fact that this method is simply to use, therefore, it is widely accepted by the screw pile industry. The empirical relationship can be expressed as (Hoyt and Clemence, 1989):

$$Q_u = K_t T \quad \text{Equation 2. 46}$$

where

K_t = empirical factor

T = average installation torque

$K_t = 33 \text{ m}^{-1}$ for all square shafts and round shaft anchors less than 89 mm in diameter

$K_t = 23 \text{ m}^{-1}$ for 89 mm round shaft anchors

$K_t = 9.8 \text{ m}^{-1}$ for anchors with 219 mm diameter extension Shafts

2.5 THE EFFECTS OF TIME ON PILE RESISTANCE

The vertical capacity of multihelix screw piles installed in cohesive soil is governed by one major factor, the shear strength of the material. The shear strength of the clay can be difficult to determine because it depends on the rate of loading, the installation procedure and the type of soil tested.

When the pile is loaded rapidly, the soil next to the pile is failed under the undrained condition where the soil strength mainly consists of cohesion and the frictional resistance is assumed to be zero. If a pile is loaded with a sustained

force and failed over a long period of time allowing pore pressures to dissipate, the soil is assumed to fail under drained conditions where the soil strength consists of both the frictional and cohesive components. Bjerrum (1973) has reported such phenomenon on the skin friction of piles driven into soft clays. He observed that if a pile is loaded with a sustained load over a long period of time (i.e. permanent working load) the shearing stress in the clay surrounding the pile is carried partly by effective friction and partly by effective cohesion. The ultimate pile capacity increases with long term loading as a result of the consolidation of the clay in the stressed zone adjacent to the pile. However, creep behavior is often observed when the rate of loading was reduced from 10 mm per minute to 0.001 mm per minute. Bjerrum reported a reduction of 50 % in the adhesion for piles installed in soft clay in Mexico City. Skempton (1959) reported similar behavior for the skin friction of bored piles in London clay. Therefore, for friction piles installed in a soft clay where a substantial proportion of capacity is contributed by the skin friction, the softening behavior should be taken into account in assessing the safety factor. In addition, in the case of soft clays sensitive to remolding, the undrained shear strength used for design should be reduced to as low as its residual strength in order to account for soil disturbance caused by pile installation (Mooney et al., 1985).

Mooney et al., (1985) performed laboratory and full scale field tests on screw piles installed in clay and silt. Two types of tests were performed including rapid load tests and sustained load tests. These tests were designed to investigate the effect of loading rate on the uplift capacity of screw piles. The results indicated that the long term (drained loading condition) uplift capacities were approximately 20% higher than short term (undrained loading condition) tensile capacity. In long term tests for anchors installed in remolded and normally consolidated clays, a well defined stiff bulb of soil was formed above each helix, and a cavity filled with water was found below each helix. This observation suggests that consolidation occurred during the long term tests, which contributes to the increase in total uplift capacity. Nevertheless, the drained shear strength parameters are difficult to obtain from field samples due to sample disturbance

and complexity of recreating the field stress condition in the laboratory settings. For engineering applications where screw piles were used, it is uneconomical to perform drained tests to determine drained strength parameter. Therefore, the undrained shear strength parameters are commonly used which provides a more conservative prediction of the uplift screw pile capacity installed in normally consolidated clay.

For piles driven in stiff clays as described by Tomlinson (1994), the effects of sustained loading on piles are not well known, however, the author suggests that there may be a reduction in resistance with time. The pile installation procedure may create a softening of the soil in the fissure system surrounding the pile. Experiment data collected on reductions in resistance with time for piles in stiff clays. These data are compared with the results obtained from rapid pile loading tests and the results are shown in Table 2.22. Comparing the experiment data, Tomlinson suggests that there is a small change in pile resistance for periods of up to one year, therefore, there is little significance compared with other effects.

Skempton (1959) indicated that for soils like fissured stiff clay, the measured values of shear strength might differ greatly, depending on the method of test or size of test specimen. The strength determined along a fissure plane is usually much lower than the intact strength and may be close to the residual strength. Laboratory compression tests may vary over a fairly wide range, depending on the size of the test samples and on the spacing and orientation of the fissure planes in relation to the potential failure surface. The strength of fissured clay mobilized for a bell shape footing loaded in uplift condition as described by Adams and Radhakrishna (1971), was found to be much less than the intact strength. An approximation of the strength mobilized is about 30% of the intact strength as measured by the field vane, about 60% of the strength based on laboratory peak values, and about 100% of the undrained residual values from laboratory triaxial tests. As indicated by the author, the strength mobilized at the shallow depth is largely the fissured strength, whereas at greater depth a portion of the intact strength is mobilized. Therefore, adjustment to the uplift coefficient,

N_u proposed by Meyerhof and Adams (1968) is required for screw pile installed in stiff clay (see Figure 2.50). Adams and Hayes (1967) reported similar findings which they stated that the calculated N_u from the field tests are generally only about half the laboratory values. Most of the field tests carried out by Adams and Hayes (1967) were anchors installed in shallow depth in stiff clay. The soil was desiccated and was thus fissured. Therefore, the strength of these soils under pullout loads could be much less than the intact samples.

For the case where triple helix anchors were installed in medium dense to fine sand, Mitsch and Clemence (1985) investigated the effect of short and long term loading on the ultimate uplift capacity of pile. Uplift capacity of multihelix screw piles for both shallow ($H/D = 4$) and deep ($H/D = 8$) conditions were tested for short and long term conditions. The results indicated that the behavior of the screw piles in long term loading was essentially the same to that for short term conditions because the pore pressures in cohesionless material dissipates very quickly. Therefore, for free-draining material such as sand, long term and short term capacity should be the same. The author suggested that there were no discernible effects from creep or plastic deformation. Therefore, screw piles in sand can be designed for the short term loading as the critical condition.

2.6 EFFECT OF INSTALLATION METHOD

The installation method can affect the soil shear strength significant especially for piles installed in sensitive marine clay and fissured over-consolidated clay. The screw action involved when installing the screw pile in these materials will drive the soil shear strength from peak to a much lower residual value. This is due to the fact that the rotating motion continuously churns and remolds the surrounding soil during pile installation. For sensitive soft clay and fissured clay, there is a pronounced difference in the undrained strength determined at small strain comparing to strength at large strain as indicated by Adams and Radhakrishna (1971). The undrained shear strength of

fissured clays has a maximum difference of up to 35% between the peak and residual strength of the fissured clay.

Rigden, et al. (1979) performed a comparative study on open and closed end 457 mm diameter steel pile driven into stiff glacial till to a depth of 9.0 m. A clay plug was formed in the open end pile. The failure loads of the clay-plugged and steel plate closed piles were 1160 kN and 1400 kN. The author evaluated the ultimate skin friction and the base resistance of the piles and suggested that the skin friction on the open ended piles was 20 % less than that on the closed end piles. Therefore, it is recommended that if a clay plug is formed inside the pile tube, the skin friction obtained from Section 2.3.2 should be multiplied by a reduction factor of 0.8, and the ultimate base resistance, Q_b , reduced by a factor of 0.5. If an internal stiffening ring, such as a steel plate welded inside of the steel tube, is provided at the toe of a steel pile the base resistance should be calculated using the net cross sectional area of the steel.

If helical piles are placed too close to each other, the average net ultimate uplift capacity of each anchor may decrease due to the interference of the failure zones in soil located around the anchors. Das (1990) conducted Laboratory model test to study the group effect on the ultimate capacity of the pile. The results have shown that, for the non-interference of the anchor failure zones, the optimum center-to-center spacing in loose and dense sand should be $6 D_1$ and $10 D_1$, respectively. In any case, it is recommended that the minimum center-to-center spacing of the anchors should be about $5 D_1$. Trofimenkow and Mariupolskii (1965) conducted field load test on full scale screw piles. Twelve pile groups were tested each consisting of three small piles placed in one row at a distance from $1.5 D$ to $5 D$. The pile plate was at a depth of $8 D$. The experiments showed that the pulling out resistance of a deep installed pile group placed at a distance not less than $1.5 D$ is equal to that of the single pile in the same soil and at the same depth.

2.7 COMPRESSION CAPACITY VS. TENSION CAPACITY

Narasimha Rao, et al. (1991) investigated the compression and tension capacity of model screw pile installed in soft marine clay. The soils properties used in the laboratory testing are listed in Table 2.23. The undrained shear strength results were determined using the in situ vane shear apparatus. All the testing was carried out with a range of moisture contents of 26 % to 50.4%, with variation of pile length, number of helices and size of the shaft and helix diameter. Test results are presented in Table 2.24. It is concluded that the reduction of moisture content increases the capacities both in compression and tension. In addition, the number of plates also increases the capacities. The test results also indicate that the ultimate compression to tension capacity ratio (Q_c / Q_t) decreases with a decrease in moisture contents. At higher moisture content, w , such as 40.2 % to 50.4 %, the Q_c / Q_t ranges from 1.44 to 1.71, and at lower w , the Q_c / Q_t ratio decreases to a range of 1.03 to 1.17. The effect is independent on the installation depth, number of helices and pile diameter.

Trofimendkov and Mariupolskii (1965) conducted a series of field compression and tension tests using screw piles with various soil types. About two hundred piles were installed in soft to hard clays as well as loose to medium dense sands with pile helix diameter D ranging from 0.45 to 1.0 m to a depth up to 7 m. The test results indicated that the compression capacity was 1.4 to 1.5 higher than the uplift capacity. The author concluded that in the compression tests, the bearing plate was pressing on undisturbed soil, and the density of a typical soil increases with depth. A design procedure was proposed based on the test results and the author concluded that for the ultimate bearing capacity is 1.3 times more than that of a screw pile in the pulling out tests. Therefore, the compression to tension capacity ratio can be expressed as:

$$Q_{u(\text{compression})} = 1.3Q_{u(\text{tension})} \quad \text{Equation 2. 47}$$

2.8 CYCLIC LOADING

For engineering application such as surface vessels, the screw pile is subjected to a combination of sustained and repeated loads. Adams and Radhakrishna (1971) reported that for repeated loading cycles within a stress range comparable to transmission-load variations, the loading-unloading cycles did not show a marked influence on the ultimate uplift capacity of the test footings installed in stiff clay.

Strain softening response behavior under cyclic loading is a major concern for structures constructed on sand and sandy silt. Very few studies are available the influence of cyclic loading on the ultimate capacity of screw piles. Andreadis et al. (1978) carried out model studies on circular plate anchors with embedment ratio $H/D = 12$ installed in a medium uniform saturated sand. The type of tests were performed including a cyclic load test with sinusoidal 10 second duration cycle (N) and a sustained-repeated load test. The cyclic load test was performed with a sinusoidal duration cycle (N) of 10 second. In the sustained-repeated load test, the anchor was first load with a sustained static load ($Q_{sustain}$) and then a cyclic load (Q_{cyclic}). The author defined the relative anchor movement as:

$$\Delta\lambda = \frac{\text{Uplift Movement of Anchor, } \Delta}{\text{Anchor Diameter, } D} \quad \text{Equation 2. 48}$$

The relationship in terms of sinusoidal duration cycles (N), relative anchor movement $\Delta\lambda$, and relative cyclic load, $Q_{sustain}/Q_{ult}$ is presented in Figure 2.51. Figure 2.52 presents the relationship of Q_{cyclic}/Q_{ult} with the number of cycles applied to the pile for various values of $\Delta\lambda$. Based on the results of the model test, Andreadis et al. (1978) suggested that there is almost no reduction in ultimate uplift capacity obtained from static pile load test if the cyclic relative anchor displacement is maintained below about half of the relative movement to failure in static pullout test. Therefore, the relationship can be expressed as

$$\Delta\lambda_{(allowable)} = \frac{1}{2} \Delta_u$$

Equation 2. 49

where

$\Delta\lambda$ = allowable cyclic relative anchor displacement

Δ_u = ultimate displacement obtained from static pile load test

One can calculate maximum allowable value of $\Delta\lambda$ based on field pile load test, then, the ratio of Q_{cyclic} / Q_{ult} can be obtained from Figure 2.52, and the ultimate pile capacity used be determined corresponding to the number of load application cycles during the lift span of the pile.

Trofimenkov and Mariupolskii (1965) performed pile load testing on 200 screw piles installed in various soil conditions. Different loading methods including rapid loading test, sustained loading test, pulsating loading test were used to perform both compression and tension tests. Typical uplift test results using single 0.8 m diameter helix with 0.22 m diameter shaft installed to a depth of 5.0 m under different loading methods are shown in Figure 2.53. Based on the field results, author suggested that reduction factor m should be applied to ultimate capacity Q_u and the values of the reduction factor m are presented in Table 2.25.

2.9 FACTOR OF SAFETY USE FOR DESIGN

As discussed at the beginning of the chapter, in the present state of knowledge, a design method, that can be used to generally apply to all pile types, has not been developed. Empirical factors are embedded in the design methods to account for uncertainties, such as the difficulties of determining properties of the subsurface condition over the site, variation in the construction and installation procedure, and differences in rates of loading during the pile load test as compared to the service loading. Therefore, the usual approach to the problem is to apply a factor of safety to the ultimate capacity obtained by field pile

load testing and the result, called the allowable pile capacities, is typically used in design. The allowable net ultimate uplift capacity can be expressed as follow:

$$Q_{allow} = \frac{Q_{ultimate}}{FS} \quad \text{Equation 2. 50}$$

where

Q_{allow} = allowable net ultimate capacity used for design
 $Q_{ultimate}$ = ultimate capacity of the pile
 FS = factor of safe

The selection of the appropriate factor of safety depends on many factors. Lunne et al. (1998) stated that the selection of factor of safety is affected by "the reliability and sufficiency of the site investigation data, confidence in the method of calculation, and previous experience with similar piles in similar soils and whether or not pile load test results are available". Tomlinson (1994) states that a factor of 2.5 should be apply to the predicted ultimate capacity in order to ensure that settlement of more than 10 mm will not occur under working load. This recommended factor of safety is concluded based on a very large number of loading tests taken to failure with piles of diameters up to about 600 mm installed in clays and sands. For any cases, the factor of safety should not be taken as less than 2 even if the ultimate pile capacity is determined by the pile load test results (Terzaghi and Peck, 1996)

Das (1990) recommends that in most cases of screw pile subject to uplift force, a factor of 2 to 2.5 should be applied to the ultimate capacity as the safety factor. For screw pile group under uplift loading, the factor of safety should be taken as minimum of 2.5 to estimate the allowable uplift capacity of the pile group.

For the two direct methods using Cone Penetration test as outlined in Section 2.3.3, the values for the factor of safety provided by the authors are listed in Table 2.26.

For group piles, Terzaghi and Peck (1996) stated that the factor of safety should be taken as minimum of 3 in order to prevent base failure to occur.

2.10 REFERENCE

- Adams, J. I., and Klym, T. W. (1971). "A Study of Anchors for Transmission Tower Foundation"; *Canadian Geotechnical Journal*, Vol. 9, No. 1, pp. 89-104.
- Adams, J. I., and Hayes, D. C. (1967). "The Uplift Capacity of Shallow Foundation"; *Ontario Hydro Research Quarterly*, Vol. 19, pp. 1-13.
- Adams, J. I., and Radhakrishna, H. S. (1971). "Uplift Resistance of Augered Footings in Fissured Clay"; *Canadian Geotechnical Journal*, Vol. 8, pp. 452-462.
- Ali, M. S. (1968). "Pullout Resistance of Anchor Plates and Anchor Piles in Soft Bentonite Clay"; MSc. Thesis, Duke University, Durham, N.C.
- Andreadis, A., Harvey, R. C., and Burley, E. (1981). "Embedded Anchor Response to Uplift Loading"; *Journal of Geotechnical Engineering Division, ASCE*, Vol. 107, No. GT 1, pp. 59-78.
- ASCE (1993). "Bearing Capacity of Soils"; *Technical Engineering and Design Guides as Adapted from U.S Army Corps of Engineers*, No. 7, ASCE Press, New York, 147 pp.
- Bobbitt, B. E., and Clemence, S. P. (1987). "Helical Anchors: Application and Design Criteria"; *Proceedings of 9th Southeast Asian Geotechnical Conference*, Bangkok, Thailand, pp. 6-105 to 6-120.
- Ballisager, C. C. (1959). "Bearing Capacity of Piles in Aarhus Septarian Clay"; *Danish Geotechnical Institute, Bulletin No. 7*, pp. 14-19.
- Bella, A. (1961) "The Resistance to Breaking-out of Mushroom Foundations for Pylons"; *Proceedings of 5th International Conference on Soil Mechanics and Foundation Engineering*, Paris, France, Vol. 1, pp 569-576.
- Bjerrum, L. (1973). "Problems of Soil Mechanics and Construction in Soft Clay"; *Proceedings of the 8th International Conference, ISSMFE, Moscow*, Vol. 3, pp. 150-157.
- Bowles, J. E. (1988). "Foundation Analysis and Design"; 4th Edition, McGraw-Hill, New York, 1004 pp.
- Bradka, T. D. (1997). "Vertical Capacity of Helical Screw Anchor Piles"; *Master of Engineering Reports*, University of Alberta, Alberta, 97 pp.

- Bustamante, M., and Gianeselli, L. (1982). "Pile Bearing Capacity Prediction by Means of Static Penetrometer CPT"; Proceedings of the 2nd European Symposium on Penetration Testing, ESOPT-II, Amsterdam, 2, pp. 493-500, Balkema Pub., Rotterdam.
- Bustamante, M., and Gianeselli, L. (1983). "Prezision de la Capacite Portante des Pieux par La Methode Penetrometrique"; Compte Rendu de Recherche S.A.E.R.1/05.022. Available from Laboratoire Central des Ponts et Chaussees, 58 Boulevard Lefebvre, F-75732, Paris Cedex 15, France.
- Carville, C. A., and Walton, R. W. (1995). "Foundation Repair Using Helical Screw Anchors"; Foundation Upgrading and Repair for Infrastructure Improvement. Edited by William F. K. and Thaney, J. M. Geotechnical Special Publication No. 50, ASCE, pp. 56-76.
- CFEM (1992). Canadian Foundation Engineering Manual. 3rd Edition. Canadian Geotechnical Society, Technical Committee on Foundations, BiTech Publishers Ltd., Richmond, BC, 512 pp.
- Clemence, S. P. (1982). "Uplift and Bearing Capacity of Helix Anchors in Soil"; Research Contract Report TT-112-1, Vol. 1, Niagara Mohawk Power Corporation, Syracuse, NY.
- Clemence, S. P., and Pepe, F. D. Jr. (1984). "Measurement of Lateral Stress Around Multihelix Anchors in Sand"; Geotechnical Testing Journal, Vol. 7, No. 3, pp. 145-152.
- Das, B. M. (1990). Earth Anchors. Elsevier, Amsterdam, 241p.
- Das, B. M. (1980). "A Procedure for Estimation of Ultimate Uplift Capacity of Foundations in Clay"; Soils and Foundation, Japan, Vol. 20, No. 1, pp. 77-82.
- Das, B. M. (1968). "Model Tests for Uplift Capacity of Foundations in Clay"; Soils and Foundations, Vol. 18, No. 2, pp. 17-24.
- Davie, J. R., and Sutherland, H. B. (1977) "Uplift Resistance of Cohesive Soils"; Journal of the Geotechnical Engineering Division, ASCE, GT 9, Vol. 103, pp. 935-951.
- De Ruiter, J., and Beringen, F. L. (1979). "Pile Foundations for Large North Sea Structures"; Marine Geotechnology, 3(3), pp. 267-314.
- Ghaly, A. M., and Hanna, A. M. (1991a). "Experimental and Theoretical Studies on Installation Torque of Screw Anchors"; Canadian Geotechnical Journal, Vol. 28, No. 3, pp. 353-364.

- Ghaly, A. M., and Hanna, A. M. (1991b). "Stress Development in Sand due to Installation and Uplifting of Screw Anchors"; Proceedings of 4th International Conference on Piling and Deep Foundations, Stresa, Italy, Vol. 1, pp. 565-570.
- Ghaly, A. M., and Hanna, A. M. (1992). "Stresses and Strains Around Helical Screw Anchors in Sand"; Journal of Soil Foundations, Japanese Society of Soil Mechanics and Foundation Engineering, Vol. 32, No. 4, pp.27-42.
- Ghaly, A. M., Hanna, A. M., and Hanna, M. S. (1991). "Installation Torque of Screw Anchors in Dry Sand"; Journal of Soil Foundations, Japanese Society of Soil Mechanics and Foundation Engineering, Vol. 32, No. 2, pp.77-92.
- Ghaly, A. M., Hanna, A. M., and Hanna, M. S. (1991). "Uplift Behavior of Screw Anchors in Sand I: Dry Sand"; Journal of Geotechnical Engineering, ASCE, Vol. 117, No. 5, pp.773-794.
- Ghaly, A. M., Hanna, A. M., and Hanna, M. S. (1991). "Uplift Behavior of Screw Anchors in Sand II: Hydrostatic and Flow Conditions"; Journal of Geotechnical Engineering, ASCE, Vol. 117, No. 5, pp.794-808.
- Hanna, A. M., and Ghaly, A. M. (1992). "Effects of K_0 and Overconsolidation on Uplift Capacity"; Journal of Geotechnical Engineering Division, ASCE, Vol. 118, No. GT 9, pp.1449-1469.
- Hoyt, R. M., and Clemence, S. P. (1989). "Uplift Capacity of Helical Anchors in Soil"; Proceedings of 12th International Conference on Soil Mechanics and Foundation Engineering, Rio de Janeiro, Brazil, Vol. 2, pp. 1019-1022.
- Hoyt, R., Seider, G., Reese, L. C., and Wang, S. T. (1995). "Buckling of Helical Anchors Used for Underpinning"; Foundation Upgrading and Repair for Infrastructure Improvement. Edited by William F. K. and Thaney, J. M. Geotechnical Special Publication No. 50, ASCE, pp. 89-108.
- Huang, G. C., Mahmood, I., Joolazadeh, M., and Axten, G. W. (1995) "Design Considerations and Field Load Tests of a Helical Anchoring System for Foundation Renovation"; Foundation Upgrading and Repair for Infrastructure Improvement. Edited by William F. K. and Thaney, J. M. Geotechnical Special Publication No. 50, ASCE, pp. 76-89.
- Hansen, J. B. (1970). "A Revised and Extended Formula for Bearing Capacity"; Danish Geotechnical Institute Bul., No. 28 Copenhagen, 21 pp.
- Ireland, H. O. (1963). "Discussion, Uplift Resistance of Transmission Tower Footing"; Journal of Power Division, ASCE, 89(1), pp. 115-118.

- Janbu, N. (1976). "Static Bearing Capacity of Friction Piles"; Proceedings of 6th European Conference on SMFE, Vol. 12, pp. 479-488.
- Johnston, G. H., and Ladanyi, B. (1974). "Field Tests of Deep-Installed Screw Anchors in Permafrost"; Canadian Geotechnical Journal, Vol. 11, No. 3, pp. 348-358.
- Kupferman, M. (1971). "The Vertical Holding Capacity of Marine Anchors in Clay Subjected to Static and Cyclic Loading"; MSc. Thesis, University of Massachusetts.
- Kulhawy, F. H. (1984). "Limiting Tip and Side Resistance, Fact or Fallacy"; Symposium on Analysis and Design of Pile Foundations, American Society of Civil Engineers, San Francisco, pp. 80-98.
- Kulhawy, F. H. (1985). "Uplift Behavior of Shallow Soil Anchors – An Overview"; Uplift Behavior of Anchor Foundations in Soil Proceedings, ASCE, New York, N.Y., pp. 1-25.
- Langley, W. S. (1967). " Uplift Resistance of Groups of Bulbous Piles in Clay"; MSc. Thesis, Nova Scotia Technical College.
- Lunne, T.; Robertson, P. K., and Powell, J. J. M. (1997). "Cone Penetration Testing in Geotechnical Practice"; Blackie Academic & Professional. First edition. p. 312.
- Lutenegger, A. J., Bradford, L. S., and Mohammed G. K. (1988). "Use of In Situ Tests to Predict Uplift Performance of Mulihelix anchors"; Special Topics in Foundations, Edited by Das, B. M., Technical Special Publication No. 16, ASCE, New York, pp. 93-109.
- Mariupol'skii, L. G. (1965). "The Bearing Capacity of Anchor Foundation (English Translation)"; Soil Mechanics and Foundation Engineering, pp. 26-37.
- Meyerhof, G. G. (1976). "Bearing Capacity and Settlement of Pile Foundations"; Journal of the Geotechnical Engineering Division, Proceedings of the American Society of Civil Engineers, Vol. 102, No. GT3, March 1976, pp. 197-224
- Meyerhof, G. G. (1982). "The Bearing Capacity and Settlement of Foundations – Selected Papers with A Bibliography to 1981"; Tech-Press, Halifax, 424 pp.
- Meyerhof, G. G., and Adams, J. I. (1968). "The Ultimate Uplift Capacity of Foundations"; Canadian Geotechnical Journal, Vol. V, no. 4, pp. 225-244.

- Meyerhof, G. G., and Murdock, L. J. (1953). "An Investigation of the Bearing Capacity of some Bored and Driven Piles in London Clay"; *Geotechnique*, Vol. 3, No. 7, pp. 267-282.
- Mitsch, M. P., and Clemence, S. P. (1985). "The Uplift Capacity of Helix Anchors in Sand. Uplift Behavior of Anchor Foundations in Soil"; *Proceedings of ASCE*, New York, N.Y., pp. 26-47.
- Mooney, J. M., Adamczak, S., and Clemence, S. P. (1985). "Uplift Capacity of Helix Anchors in Clay and Silt"; *Uplift Behavior of Anchor Foundations in Soil. Proceedings of ASCE*, New York, N.Y., pp.48-72.
- Mores, H. (1959). "The Behavior of Mast Foundations Subjected to Tensile Forces"; *Bautechnik*, 36(10), pp. 367-378.
- Narasimha Rao, S., Prasad, Y.V.S.N., and Prasad, C. V. (1990). "Experimental Studies on Model Screw Pile Anchors"; *Proceedings of Indian Geotechnical Conference*, Bombay, pp. 465-468.
- Narasimha Rao, S., and Prasad, Y.V.S.N. (1991). "Uplift Behavior of Screw Anchors in Sand I: Dry Sand"; Discussion by Narasimha Rao, S., and Prasad, Y.V. S. N., *Journal of Geotechnical Engineering Division, ASCE*, Vol. 118, No. GT 9, pp.1474-1478.
- Narasimha Rao, S., and Prasad, Y.V.S.N (1991). "Estimation of Uplift Capacity of Helical Anchors in Clays"; *Journal of Geotechnical Engineering*, Vol. 119, No. 2, pp.352-357.
- Narasimha Rao, S., Prasad, Y.V.S.N (1990). "Experimental Studies on Model Screw Pile Anchors"; *Proceedings of Indian Geotech. Conf.*, Bombay, pp.465-468.
- Narasimha Rao, S., Prasad, Y.V.S.N., Shetty, M. D., and Joshi, V. V. (1989). "Uplift Capacity of Screw Anchors"; *Geotech. Engng.*, Vol. 20, No. 2, pp.139-159.
- Narasimha Rao, S., Prasad, Y.V.S.N., and Shetty, M. D. (1991). "The Behaviour of Model Screw Piles in Cohesive Soils"; *Journal of Soil and Foundations*, Japanese Society of Soil Mechanics and Foundation Engineering, Vol. 31, pp. 35-50.
- Narasimha Rao, S., Prasad, Y.V.S.N., and Veeresh, C. (1993). "Behaviour of Embedded Model Screw Anchors in Soft Clays"; *Geotechnique*, Vol. 43, pp. 605-614.
- Parr, R. G., and Vanner, M. J. (1962). "Strength Tests on Overhead Line Tower Foundations"; *Electrical Research Association*, Report O/T28.

- Poulos, H. G., and Davis, E. H. (1980). *Pile Foundation Analysis and Design*. John Wiley and Sons, New York, NY.
- Radhakrishna, H. S. (1975). "Helix Anchor Tests on Stiff Fissured Clay"; Ontario Hydro Research Division Research Report.
- Radhakrishna, H. S. (1976). "Helix Anchor Tests in Sand – Essa TS"; Research Report No. 76-130-K, Ontario Hydro Research Division, Toronto, Canada.
- Randolph, M. F., and Wroth, C. P. (1982). "Recent Developments in Understanding the Axial Capacity of Piles in Clay"; *Ground Engineering*, Vol. 15, No. 7, pp. 17-25.
- Reese, L. C., and O'Neill, M. W. (1988). "Drilled shafts: Construction Procedures and Design Methods"; Publication No. FHWA-HI-88-042/ADSC-TL-4.
- Rigden, W. J., Pettit, J. J., ST. John, H. D. and Poskitt, T. J. (1979). "Developments in Pilling for Offshore Structures"; *Proceedings of the Second International Conference on the Behaviour of Offshore Structures*, London, Vol. 2, pp. 276-296.
- Robinson, K. E., and Taylor, H. (1969). "Selection and Performance of Anchors for Guyed Transmission Towers"; *Canadian Geotechnical Journal*, Vol. 6, No. 2, pp.119-137.
- Rodgers, T. E. Jr. (1987). "High Capacity Multi-Helix Screw Anchors for Transmission Line Foundations"; In *Foundations for Transmission Line Towers*. ASCE, New Jersey, pp.81-95.
- Saeedy, H. S. (1987). "Stability of Circular Vertical Earth Anchors"; *Canadian Geotechnical Journal* 24(3), pp. 452-456.
- Skempton, A. W. (1959). "Cast in-situ Bored Piles in London Clay"; *Geotechnique*, Vol. 9, No. 4, pp. 153-173.
- Spence, B. E. (1965). "Uplift Resistance of Piles with Enlarged Bases in Clay"; MSc Thesis, Nova Scotia Technical College.
- Stewart, J. P., and Kulhawy, F. H. (1981). "Experimental Investigation of the Uplift Capacity of Drilled Shaft Foundations in Cohesionless soil"; Contract Report B-49 (6), Niagara Mohawk Power Corporation, Syracuse, NY 14853. Available as Geotechnical Engineering Report 81-2 from School of Civil an Environmental Engineering, Cornell University, Ithaca, NY 14850.
- Terzaghi, K. (1943). *Theoretical Soil Mechanics*; Wiley, New York, 510 pp.

- Terzaghi, K., Peck, R. B., and Mesri, G. (1996). "Soil Mechanics in Engineering Practice"; 3rd Edition, John Wiley & Sons, New York, 549 pp.
- Tomlinson, M. J. (1957). "The Adhesion of Piles Driven in Clay Soils"; Proceedings of 5th International Conference, ISSMFE, London, Vol. 2, pp. 66-71.
- Tomlinson, M. J. (1970). "The Adhesion of Piles in Stiff Clay"; Construction Industry Research and Information Association, Research Report No. 26, London.
- Tomlinson, M. J. (1994). Pile Design and Construction Practice, 4th Edition. E & FN Spon, London, 411 pp.
- Turner, E.A. (1962). "Uplift Resistance of Transmission Tower Footings"; Journal of Power Division, ASCE, 88, Paper 3187.
- Trofimenkov, J. G., and Mariupolskii, L. G. (1965). "Screw Piles Used for Mast and Tower Foundations"; Proceedings of Sixth International Conference on Soil Mechanics and Foundation Engineering, Montreal, Quebec, Vol. 11, pp. 328-332.
- Veesaert, C. J. and Clemence, S. P. (1977). "Dynamic Pullout Resistance of anchors"; Proceedings of International Symposium on Soil structure Interaction, Rourkee, India, Vol. 1, pp. 389-397.
- Vesic, A. S. (1965). "Cratering by Explosives as an Earth Pressure Problem"; Proceedings of VI International Conference on Soil Mechanics and Foundation Engineering, Montreal, Canada, Vol. 2, pp. 427-431.
- Vesic, A. S. (1971). "Breakout Resistance of Objects Embedded in Ocean Bottom"; Journal of Soil Mechanics and Foundation Division, ASCE, SM 9, Vol. 97, pp. 1183-1205.
- Vesic, A. S. (1973). "Analysis of Ultimate Loads of Shallow Foundations"; JSMFD, ASCE, Vol. 99, SM 1, Jan., pp. 45-73.
- Vesic, A. S. (1975). "Principles of Pile Foundation Design"; Soil Mechanics Series No. 38, School of Engineering., Duke University, 48 pp.
- Vesic, A. S. (1977). "Design of Pile Foundations"; NCHRP Synthesis of Practice No. 42, Transportation Research Board, Washington DC, 68 pp.
- Weikart, A. M., and Clemence, S. P. (1987). "Helix Anchor Foundations – Two Case Histories"; In. Foundations for Transmission Line Towers, ASCE, New Jersey, pp. 72-80.

Weltman, A. J. and Healy, P. R. (1978). "Piling in 'Boulder Clay' and other Glacial Tills"; Construction Industry Research and Information Association (CIRIA), Report PG5.

Winterkorn, H. F., and Fang, H. Y. (1975). Editor, "Foundation Engineering Handbook"; Van Nostrand Reinhold Company, New York, 751 pp.

Table 2.1: Bearing Capacity Equations by Several Authors (after Bowles 1988)

Terzaghi (1943)

$$q_{ult} = cN_c s_c + \bar{q}N_q + 0.5\gamma BN_\gamma s_\gamma$$

$$N_q = \frac{a^2}{2 \cos^2 (45 + \phi/2)}$$

$$a = e^{(0.75\pi - \phi/2) \tan \phi}$$

$$N_c = (N_q - 1) \cot \phi$$

$$N_\gamma = \frac{\tan \phi}{2} \left(\frac{K_{pr}}{\cos^2 \phi} - 1 \right)$$

For: strip round square
 $s_c = 1.0 \quad 1.3 \quad 1.3$
 $s_\gamma = 1.0 \quad 0.6 \quad 0.8$

Meyerhof (1976) – see Table 2.2 for shape, depth, and inclination factors

Vertical load: $q_{ult} = cN_c s_c d_c + \bar{q}N_q s_q d_q + 0.5\gamma BN_\gamma s_\gamma d_\gamma$

Inclined load: $q_{ult} = cN_c d_c i_c + \bar{q}N_q d_q i_q + 0.5\gamma BN_\gamma d_\gamma i_\gamma$

$$N_q = e^{\tan \phi \tan^2 \left(45 + \frac{\phi}{2} \right)}$$

$$N_c = (N_q - 1) \cot \phi$$

$$N_\gamma = (N_q - 1) \tan (1.4\phi)$$

Hansen (1970) – see Table 2.4 for shape, depth, and other factors

General: $q_{ult} = cN_c s_c d_c i_c g_c b_c + \bar{q}N_q s_q d_q i_q g_q b_q + 0.5\gamma BN_\gamma s_\gamma d_\gamma i_\gamma g_\gamma b_\gamma$

when $\phi = 0$

use $q_{ult} = 5.14s_u(1 + d'_c - i'_c - b'_c - g'_c) + \bar{q}$

$N_q = \text{same as Meyerhof above}$

$N_c = \text{same as Meyerhof above}$

$N_\gamma = 1.5(N_q - 1) \tan \phi$

Vesic (1973) – see Table 2.4 for shape, depth, and other factors

Use Hansen's equations above

$N_q = \text{same as Meyerhof above}$

$N_c = \text{same as Meyerhof above}$

$N_\gamma = 2(N_q + 1) \tan \phi$

Table 2.2: Shape, Depth, and Inclination Factors for the Meyerhof Bearing Capacity (after Bowles, 1988)

Factors	Value	For
Shape:	$s_c = 1 + 0.2K_p \frac{B}{L}$	Any ϕ
	$s_q = s_r = 1 + 0.1K_p \frac{B}{L}$	$\phi > 10^\circ$
	$s_r = s_c = 1$	$\phi = 0$
Depth:	$d_c = 1 + 0.2\sqrt{K_p} \frac{H}{B}$	Any ϕ
	$d_q = d_r = 1 + 0.1\sqrt{K_p} \frac{H}{B}$	$\phi > 10^\circ$
	$d_q = d_r = 1$	$\phi = 0$
Inclination:	$i_r = i_q = \left(1 - \frac{\theta^\circ}{90^\circ}\right)^2$	Any ϕ
	$i_c = \left(1 - \frac{\theta^\circ}{\phi^\circ}\right)^2$	$\phi > 0$
	$i_c = 0$	$\phi = 0$

Where $K_p = \tan^2(45^\circ + \phi/2)$

θ = angle of resultant measured from vertical without a sign



Table 2.3: Bearing Capacity Factors for Shallow Foundations for the Meyerhof, Hansen, and Vesic' Theory (after Bowles, 1988)

Note that N_c and N_q are same for all three methods; subscripts identify author for N_γ

ϕ	N_c	N_q	$N_{\gamma(H)}$	$N_{\gamma(M)}$	$N_{\gamma(V)}$	N_q/N_c	$2 \tan \phi (1 - \sin \phi)^2$
0	5.14	1.0	0.0	0.0	0.0	0.195	0.000
5	6.49	1.6	0.1	0.1	0.4	0.242	0.146
10	8.34	2.5	0.4	0.4	1.2	0.296	0.241
15	10.97	3.9	1.2	1.1	2.6	0.359	0.294
20	14.83	6.4	2.9	2.9	5.4	0.431	0.315
25	20.71	10.7	6.8	6.8	10.9	0.514	0.311
26	22.25	11.8	7.9	8.0	12.5	0.533	0.308
28	25.79	14.7	10.9	11.2	16.7	0.570	0.299
30	30.13	18.4	15.1	15.7	22.4	0.610	0.289
32	35.47	23.2	20.8	22.0	30.2	0.653	0.276
34	42.14	29.4	28.7	31.1	41.0	0.698	0.262
36	50.55	37.7	40.0	44.4	56.2	0.746	0.247
38	61.31	48.9	56.1	64.0	77.9	0.797	0.231
40	75.25	64.1	79.4	93.6	109.3	0.852	0.214
45	133.73	134.7	200.5	262.3	271.3	1.007	0.172
50	266.50	318.5	567.4	871.7	761.3	1.195	0.131

Table 2.4: Shape, Depth, Inclination, Ground and Base Factors for Use in Either the Hansen (1970) or Vesic (1973) Bearing Capacity Equations. Factors Apply to Either Method Unless Subscripted with (H) or (V). (after Bowels, 1988)

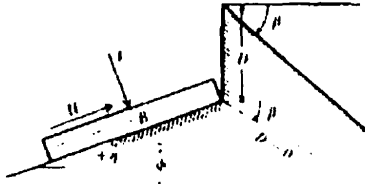
Shape factors	Depth factors	Inclination factors	Ground factors (base on slope)
$s'_c = 0.2 \cdot \frac{B}{L}$ $s'_q = 1 + \frac{N_q}{N_c} \cdot \frac{B}{L}$ $s'_c = 1$ for strip	$d'_c = 0.4k$ $d'_q = 1 + 0.4k$	$i'_{c(H)} = 0.5 - 0.5 \sqrt{1 - \frac{H}{A_f c_a}}$ $i'_{c(V)} = 1 - \frac{mH}{A_f c_a N_c}$ $i_c = i_q = \frac{1 - i_q}{N_q - 1}$ (Hansen and Vesic)	$\theta'_c = \frac{\beta''}{147^\circ}$ for Vesic use $N_c = -2 \sin \beta$ for $\phi = 0$ $\theta'_c = 1 - \frac{\beta''}{147^\circ}$
$s_q = 1 + \frac{B}{L} \tan \phi$	$d_q = 1 + 2 \tan \phi (1 - \sin \phi) k$		$g_{c(H)} = g_{c(V)} = (1 - 0.5 \tan \beta)^2$
$s_\gamma = 1 - 0.4 \cdot \frac{B}{L}$	$d_\gamma = 1.00$ for all ϕ $k = \frac{D}{B}$ for $\frac{D}{B} \leq 1$ $k = \tan^{-1} \frac{D}{B}$ for $\frac{D}{B} > 1$ (rad)	$i_{q(H)} = \left(1 - \frac{0.5H}{V + A_f c_a \cot \phi}\right)^n$ $i_{q(V)} = \left(1 - \frac{H}{V + A_f c_a \cot \phi}\right)^m$	$g_{q(H)} = g_{q(V)} = (1 - \tan \beta)^2$ Base factors (tilted base) $h'_c = \frac{\eta''}{147^\circ}$ $h_c = 1 - \frac{\eta''}{147^\circ}$
Where A_f = effective footing area B' 4.4) c_a = adhesion to base = cohesion or a reduced value D = depth of footing in ground (used with B and not B') e_a, e_L = eccentricity of load with respect to center of footing area H = horizontal component of footing load with $H \leq V \tan \delta + c_a A_f$ V = total vertical load on footing β = slope of ground away from base with downward = (+) δ = friction angle between base and soil usually $\delta = \phi$ for concrete on soil η = tilt angle of base from horizontal with (+) upward as usual case		$i_{c(H)} = \left(1 - \frac{0.7H}{V + A_f c_a \cot \phi}\right)^s$ ($\eta = 0$) $i_{c(H)} = \left(1 - \frac{(0.7 - \eta^2/450)H}{V + A_f c_a \cot \phi}\right)^s$ ($\eta > 0$) $i_{c(V)} = \left(1 - \frac{H}{V + A_f c_a \cot \phi}\right)^{m+1}$	$h_{c(H)} = \exp(-2\eta \tan \phi)$ $h_{c(H)} = \exp(-2.7\eta \tan \phi)$ $h_{q(V)} = h_{c(V)} = (1 - \eta \tan \phi)^2$ Notes: $\beta + \eta \leq 90^\circ$ $\beta \leq \phi$
General. 1. Do not use s_γ in combination with i_γ . 2. Can use s_γ in combination with d_γ, g_γ , and h_γ . 3. For $L/B \leq 2$ use ϕ_u . For $L/B > 2$ use $\phi_{p1} = 1.5\phi_u$ 17 For $\phi \leq 34^\circ$ use $\phi_{p1} = \phi_u$		$m = m_B = \frac{2 + B/L}{1 + B/L}$ H parallel to B $m = m_L = \frac{2 + L/B}{1 + L/B}$ H parallel to L . Note: $i_q, i_\gamma > 0$	

Table 2.5: Estimates for the Rigidity Index, I_r (after Bowles, 1988)

Soil	I_r
Sand ($D_r = 0.5-0.8$)	75-150
Silt	50-75
Clay	150-250

Table 2.6: Bearing Capacity Factors for Shallow Foundations for the Meyerhof, Hansen, and Vesic' Theory (after Bowles, 1988)

ϕ	Janbu			Vesic				
	$\psi = 75^\circ$	90	105	$I_r = 10$	50	100	200	500
0°	$N_q' = 1.00$	1.00	1.00	$N_q' = 1.00$	1.00	1.00	1.00	1.00
	$N_c' = 5.74$	5.74	5.74	$N_c' = 6.97$	9.12	10.04	10.97	12.19
5	1.50	1.57	1.64	1.79	2.12	2.28	2.46	2.71
	5.69	6.49	7.33	8.99	12.82	14.69	16.69	19.59
10	2.25	2.47	2.71	3.04	4.17	4.78	5.48	6.57
	7.11	8.34	9.70	11.55	17.99	21.46	25.43	31.59
20	5.29	6.40	7.74	7.85	13.57	17.17	21.73	29.67
	11.78	14.83	18.53	18.83	34.53	44.44	56.97	78.78
30	13.60	18.40	24.90	18.34	37.50	51.02	69.43	104.33
	21.82	30.14	41.39	30.03	63.21	86.64	118.53	178.98
35	23.08	33.30	48.04	27.36	59.82	83.78	117.34	183.16
	31.53	46.12	67.18	37.65	84.00	118.22	166.15	260.15
40	41.37	64.20	99.61	40.47	93.70	134.53	193.13	311.50
	48.11	75.31	117.52	47.04	110.48	159.13	228.97	370.04
45	79.90	134.87	227.68	59.66	145.11	212.79	312.04	517.60
	78.90	133.87	226.68	53.66	144.11	211.79	311.04	516.60

Note: a shape factor of s_c 1.3 may be used with Janbu's N_c'

Table 2.7: Bearing Capacity Factor N_c Related to the Pile Diameter (after CFEM, 1992)

Pile Toe Diameter (m)	N_c
Smaller than 0.5 m	9
0.5 m to 1.0 m	7
Larger than 1.0 m	6

Table 2.8: Range of N_q Factors (after CFEM, 1992)

Soil Type	Cast-In-Place Pile	Driven Piles
Silt	10 – 30	20 – 40
Loose sand	20 – 30	30 – 80
Medium sand	30 – 60	50 – 120
Dense sand	50 – 100	100 – 120
Gravel	80 - 150	150 - 300

Table 2.9: Adhesion Factors for Drilled Shafts in a Cohesive Soil (after Reese and O'Neill, 1988)

Shaft Depth (ft.)	Adhesion Factor α
0 - 5	0.0
Shaft diameter from bottom of straight shaft or from top of underream	0.0
All Other Points	0.55

Note: skin friction f_{si} should be limited to 5.5 ksf

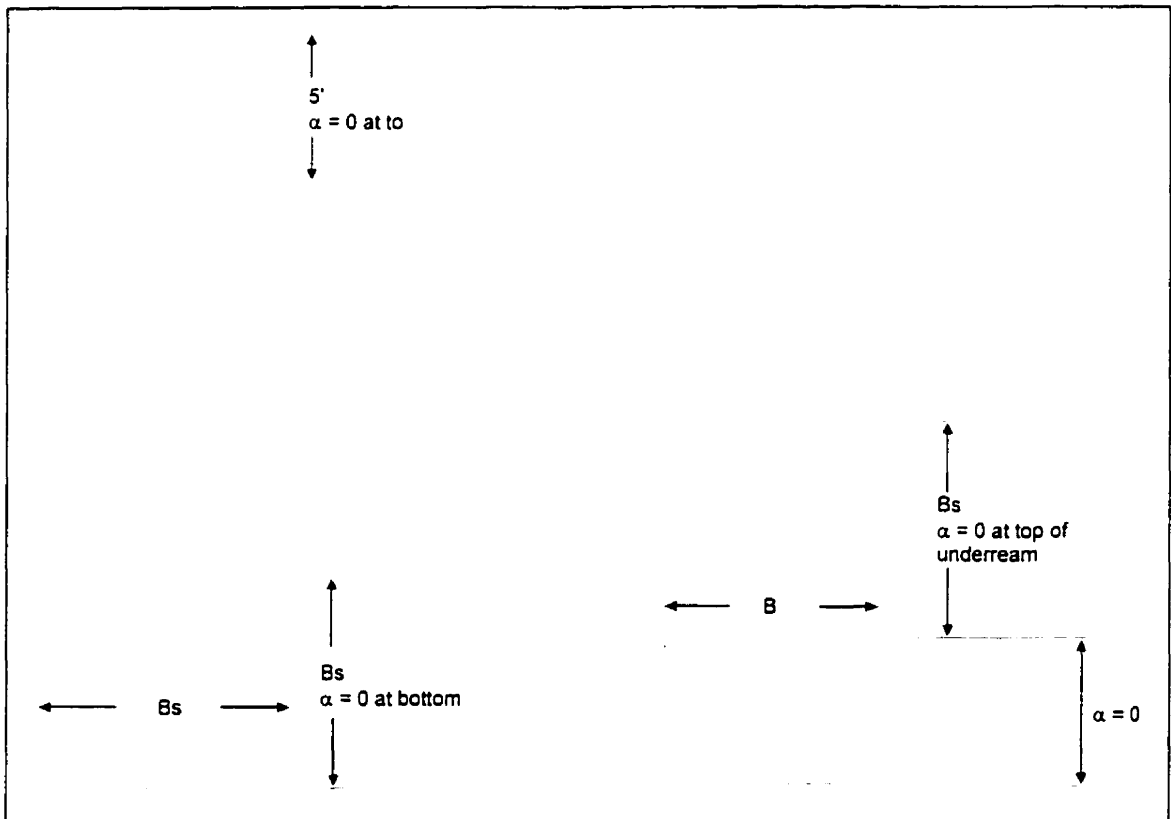


Table 2.10: Design Value of Adhesion Factors for Piles Driven into Stiff to Very Stiff Cohesive Soils (after Tomlinson, 1994).

Case	Soil Conditions	Penetration Ratio ^a	Adhesion Factor ^b
I	Sands of sandy gravels overlying stiff to very stiff cohesive soils	20	1.25
		20	Figure 2.14
II	Soft clays or silts overlying stiff to very stiff cohesive soils	8	0.40
		20	0.70
III	Stiff to very stiff cohesive soils without overlying strata	8	0.40
		20	Figure 2.14

^a Penetration ratio: Depth of penetration into stiff to very stiff soil/Diameter of pile.

^b total ultimate skin friction on length of pile embedded in stiff to very stiff cohesion soil = Adhesion factor x Undrained shearing strength x Embedded surface area.

Table 2.11: Values of the Coefficient of Horizontal Soil Stress, K_s (after Kulhawy, 1984)

Installation Method	K_s/K_0
Driven piles, large displacement	1 to 2
Driven piles, small displacement	0.75 to 1.25
Bored and cast-in-place piles	0.70 to 1
Jettied piles	0.50 to 0.7

Table 2.12: Typical Values of K_0 for a Normally Consolidated Sand (after Kulhawy, 1984)

Relative Density	K_0
Loose	0.5
Medium-dense	0.45
Dense	0.35

Table 2.13: Values of the Angle of Pile to Soil Friction for Various Interface Conditions (after Kulhawy, 1984)

Pile/Soil Interface Condition	Angle of Pile/Soil Friction, δ
Smooth (coated) steel/sand	0.5 ϕ to 0.7 ϕ
Rough (corrugated) steel/sand	0.7 ϕ to 0.9 ϕ
Precast concrete/sand	0.8 ϕ to 1.0 ϕ
Cast-in-place concrete/sand	1.0 ϕ
Timber/sand	0.9 ϕ to 0.9 ϕ

Table 2.14: Range of β Coefficients (after CFEM, 1992)

Soil Type	Cast-In-Place Piles	Driven Piles
Silt	0.2 – 0.30	0.3 – 0.5
Loose sand	0.2 – 0.4	0.3 – 0.8
Medium sand	0.3 – 0.5	0.6 – 1.0
Dense sand	0.4 – 0.6	0.8 – 1.2
Gravel	0.4 – 0.7	0.8 – 1.5

Table 2.15: Bearing Capacity Factors, k_c (after Bustamante and Gianeselli, 1982)

Nature of Soil	q_{ca} (MPa)	Factor k_c	
		Group I	Group II
Soft clay and mud	< 1	0.4	0.5
Moderately compact clay	1 to 5	0.35	0.45
Silt and loose sand	≤ 5	0.4	0.5
Compact to stiff clay and compact silt	> 5	0.45	0.55
Soft chalk	≤ 5	0.2	0.3
Moderately compact sand and gravel	5 to 12	0.4	0.5
Weathered to fragmented chalk	> 5	0.2	0.4
Compact to very compact sand and gravel	>12	0.3	0.4

Group I -	Plain bored piles Mud bored piles Micro piles (grouted under low pressure) Cased bored piles Hollow auger bored piles Piers Barrettes
Group II -	Cast screwed piles Driven precast piles Prestressed tubular piles Driven cast piles Jacked metal piles Micropiles (small diameter piles grouted under high pressure with diameter < 250 mm) Driven grouted piles (low pressure grouting) Driven metal piles Driven rammed piles Jacked concrete piles High pressure grouted piles of large diameter

Table 2.16: Friction Coefficient, α (after Bustamante and Gianeselli, 1982)

Nature of Soil	q_{ca} (MPa)	Category									
		Coefficients				Maximum Limit of q_s (MPa)					
		α									
		I		II		I		II		III	
		A	B	A	B	A	B	A	B	A	B
Soft clay and mud	< 1	30	90	90	30	0.015	0.015	0.015	0.015	0.035	-
Moderately compact clay	1 to 5	40	80	40	80	0.035 (0.08)	0.035 (0.08)	0.035 (0.08)	0.035	0.08	≥ 0.12
Silt and loose sand	≤ 5	60	150	60	120	0.035	0.035	0.035	0.035	0.08	-
Compact to stiff clay and compact silt	> 5	60	120	60	120	0.035 (0.08)	0.035 (0.08)	0.035 (0.08)	0.035	0.08	≥ 0.20
Soft chalk	≤ 5	100	120	100	120	0.035	0.035	0.035	0.035	0.08	-
Moderately compact sand and gravel	5 to 12	100	200	100	200	0.08 (0.12)	0.035 (0.08)	0.08 (0.12)	0.08	0.12	≥ 0.20
Weathered to fragmented chalk	> 5	60	80	60	80	0.12 (0.15)	0.08 (0.12)	0.12 (0.15)	0.12	0.15	≥ 0.20
Compact to very compact sand and gravel	> 12	150	300	150	200	0.12 (0.15)	0.08 (0.12)	0.12 (0.15)	0.12	0.15	≥ 0.20

CATEGORY:

IA - Plain bored piles
Mud bored piles
Hollow auger bored piles
Micropiles (grouted under low pressure)
Cast screwed piles
Piers
Barettes

IB - Cased bored piles
Driven cast piles

IIA - Driven precast piles
Prestressed tubular piles
Jacked concrete piles

IIIA - Driven grouted piles
Driven rammed piles

IIB - Driven metal piles
Jacked metal piles

IIIB - High pressure grouted piles with diameter > 250 mm

Micro piles grouted under high pressure
Maximum unit skin friction limit, q_s : bracket values apply to careful execution and minimum disturbance of soil due to construction.

NOTES:

Table 2.17: Descriptions of Deep Foundations Used in Combination with Figure 2.20 (after Bustamante and Gianselli, 1983)

Pile	Description	Remarks	Cone Resistance q_c (ksf)	Soil	Curve
Screwed - in	Screw type tool placed in front of corrugated pipe that is pushed or screwed in place; reverse rotation to pull casing while placing concrete		any	Clay-Silt	1
		$q_c < 53$ ksf	> 25	Clay-Silt	2
		Slow penetration	> 94	Clay-Silt	3
		Slow penetration	any	Sand-Gravel	1
		Fine Sands with load test	> 73	Sand-Gravel	2
		Coarse gravelly sand/gravel	> 153	Sand-Gravel	3
		Coarse gravelly sand/gravel	any	Chalk	1
		$q_c < 146$ ksf without load test	> 63	Chalk	2
		$q_c < 146$ ksf with load test	> 63	Chalk	3
		Above water table; immediate concrete placement; slow penetration	> 94	Chalk	3
		Above water table with load test	> 250	Chalk	4

Table 2.18: European CPT design method (after de Ruiter and Beringen, 1979)

	Sand	Clay
Unit skin friction, f_s	Minimum of: $f_1 = 0.12$ MPa $f_2 =$ CPT sleeve friction, f_s $f_3 = q_c / 300$ (compression) $f_4 = q_c / 400$ (tension)	$f = \alpha s_u$ where $\alpha = 1$ for N.C. clay $= 0.5$ for O.C. clay
Unit end bearing, q_p	Minimum: q_p from Figure 2.22	$q_p = N_c s_u$ Where: $N_c = 9$ $S_u = q_c / N_k$ $N_k = 15$ to 20

Table 2.19: Coefficient m and Maximum Factor, S used in Meyerhof and Adam's Theory (after Meyerhof and Adam, 1968)

Friction angle, ϕ	20°	25°	30°	35°	40°	45°	48°
Coefficient, m	0.05	0.1	0.15	0.25	0.35	0.5	0.6
Max factor, S	1.12	1.30	1.60	2.25	3.45	5.50	7.60

Table 2.20: Critical Embedment Ratio, $(H/B)_{cr}$ for Circular Anchor (after Meyerhof and Adam, 1968)

Friction angle, ϕ	20°	25°	30°	35°	40°	45°	48°
Depth $(H/B)_{cr}$	2.5	3	4	5	7	9	11

Table 2.21: Recommended Uplift Coefficients, K_u for Helical Anchors (after Mitsch and Clemence, 1985)

Soil Friction Angle (ϕ)	Meyerhof's Coefficient for Foundation Uplift	Recommended Coefficients for Helical Anchors
25	1.20	0.70
30	1.50	0.90
35	2.50	1.50
40	3.90	2.35
45	5.30	3.20

Table 2.22: Reduction in Ultimate Capacity with Time (after Tomlinson, 1994)

Type of Pile	Type of Clay	Change in Resistance	Reference
Driven precast concrete	London	Decrease of 10 to 20% at 9 months over first test at 1 month	Meyerhof and Murdock (1953)
Driven precast concrete	Aarhus (Septarian)	Decrease of 10 to 20 % at 3 months over first test at 1 month	Ballisager (1959)
Driven steel tube	London	Decrease of 4 to 25 % at 1 year over first test at 1 month	Tomlinson (1970)

Table 2.23: Soils – Index Properties Used in Test (after Narasimha Rao et al., 1991)

Soil Designation	Liquid Limit (%)	Plastic Limit (%)	Plasticity Index (%)	Grain Size Distribution			
				Clay (%)	Silt (%)	Fine Sand (%)	Undrained Shear Strength, C_u (kPa)
Soil 1	75	25	50	62	20	15	4.8 to 9.3
Soil 2	38	16	22	20	43	36	6.2
Soil 3	65	23	42	59	22	17	13.5

Table 2.24: Measured Ultimate Load Carrying Capacities for Model Piles Tests (after Narasimha Rao et al., 1991)

	S. No.	Screw Pile Designation	No. of Helical Plates	Placement Moisture Content w (%)	Consistency Index	Ultimate Capacity		
						Compression Q_{cu} (kN)	Tension Q_{tu} (kN)	Q_{cu}/Q_{tu}
Type I, Soil 1, Set I	1	P 1	2	40.2	0.696	1.44	0.84	1.71
	2	P 2	3	40.2	0.696	1.74	0.97	1.79
	3	P 3	4	40.2	0.696	1.94	1.34	1.45
	4	P 4	2	45.2	0.596	1.04	0.67	1.55
	5	P 5	3	45.2	0.596	1.36	0.91	1.49
	6	P 6	4	45.2	0.596	1.45	0.97	1.49
	7	P 7	2	50.4	0.492	0.84	0.55	1.53
	8	P 8	3	50.4	0.492	0.93	0.63	1.48
	9	P 9	4	50.4	0.492	1.05	0.73	1.44
Type I, Soil 1, Set II	1	P 4	2	45.2	0.596	2.38	1.48	1.61
	2	P 5	3	45.2	0.596	2.60	1.67	1.56
	3	P 6	4	45.2	0.596	2.71	1.72	1.58
Type II, Soil 2, Set I	1	P 7	2	26	0.545	0.81	0.69	1.17
	2	P 8	3	26	0.545	0.93	0.83	1.12
	3	P 9	4	26	0.545	0.99	0.90	1.10
Type II, Set II, Soil 2	1	P 10	2	26	0.545	0.68	0.65	1.05
	2	P 11	3	26	0.545	0.73	0.71	1.03

Note: Type I pile has a shaft diameter of 44 mm and helix diameter of 100 mm installed to a depth of 640.0 mm.

Type II pile has a shaft diameter of 25 mm and helix diameter of 75 mm installed to a depth of 1000.0 mm.

Set I pile has shaft diameter of 44 mm and helix diameter of 100 mm installed to depth of 1000.0 mm.

Set II pile has shaft diameter of 60 mm and helix diameter of 150 mm installed to depth of 1000.0 mm.

Table 2.25: Reducing Coefficient, m

Soil Type	Type of Load		
	Increasing by Steps	Pulsating	Alternate
Hard, very stiff and stiff clay	0.8	0.7	0.7
Medium stiff clay	0.8	0.7	0.6
Soft clay	0.8	0.6	0.4
Very soft clay	0.8	0.5	0.3
Partly saturated sand	0.8	0.7	0.7
Saturated sand	0.8	0.5	0.3

Table 2.26: Recommended Factors of Safety for Axial Capacity of Piles from CPT (after Lunne, et al., 1998)

Method	Factors of Safety
Bustamante and Gianeselli (1982)	2.0 (Q_s)
	3.0 (Q_b)
De Ruiter and Beringen (1979)	2.0 (static loads)
	1.5 (static + storm loads)

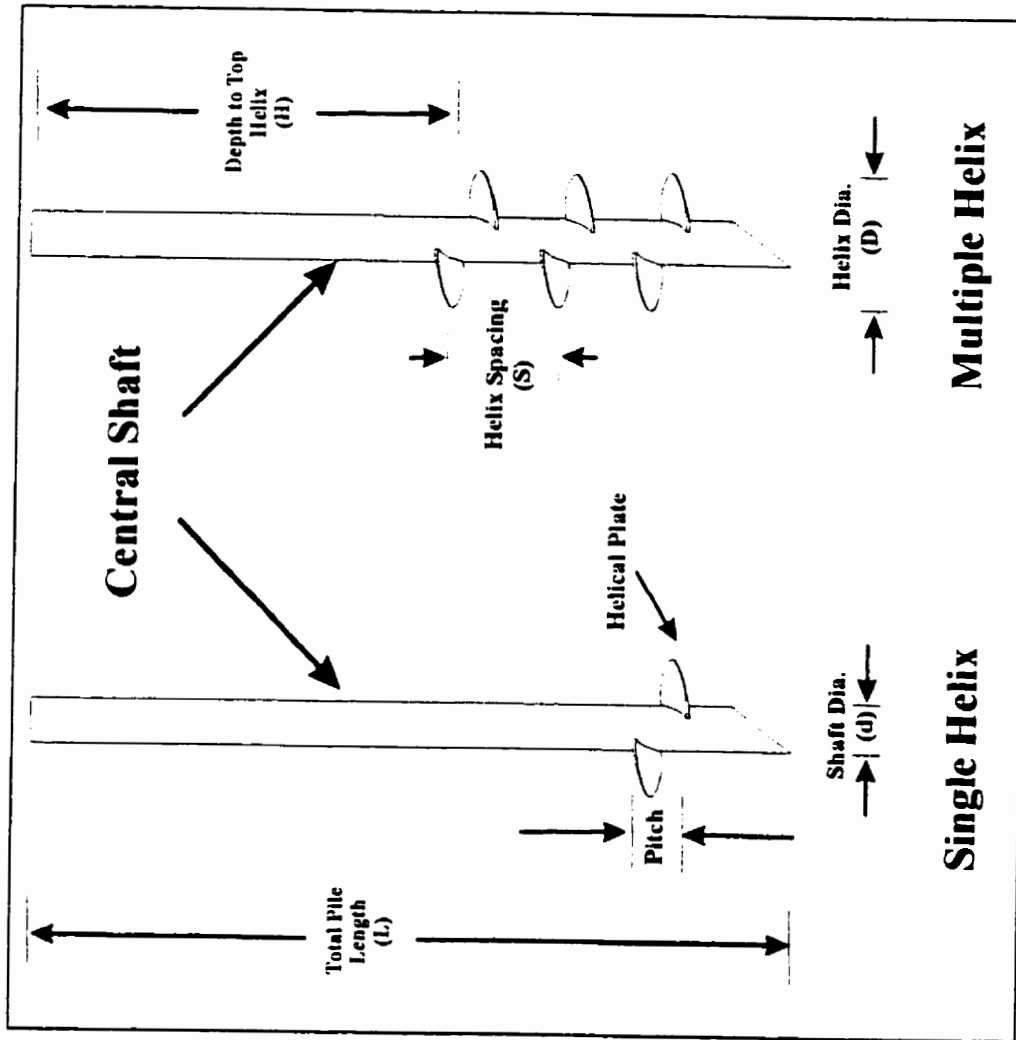


Figure 2.1: Configuration of Single and Multiple Helix

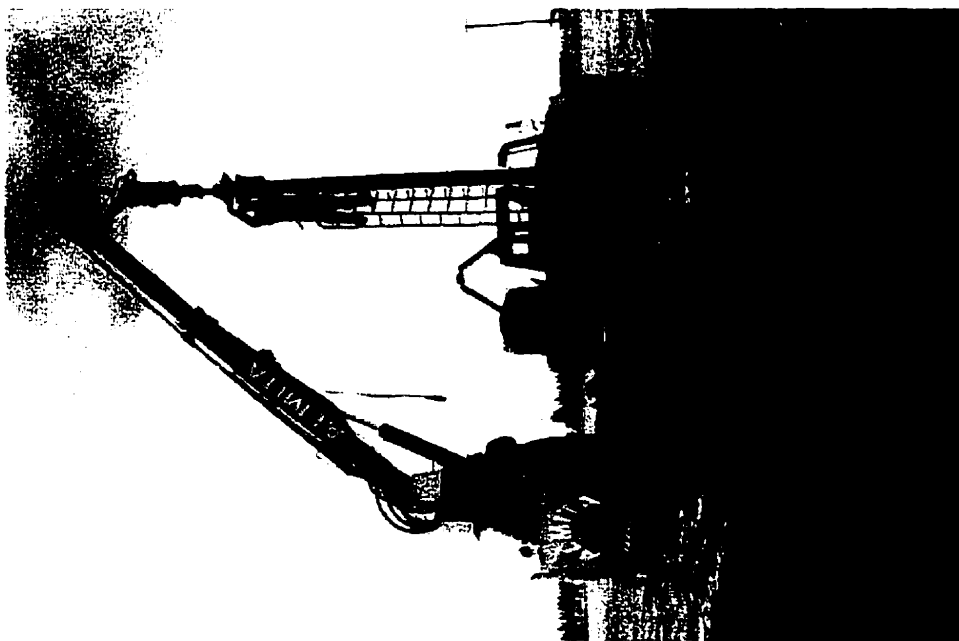


Figure 2.2: Pile Installation at University Farm Site



Figure 2.3: Leveling of the Pile during Installation

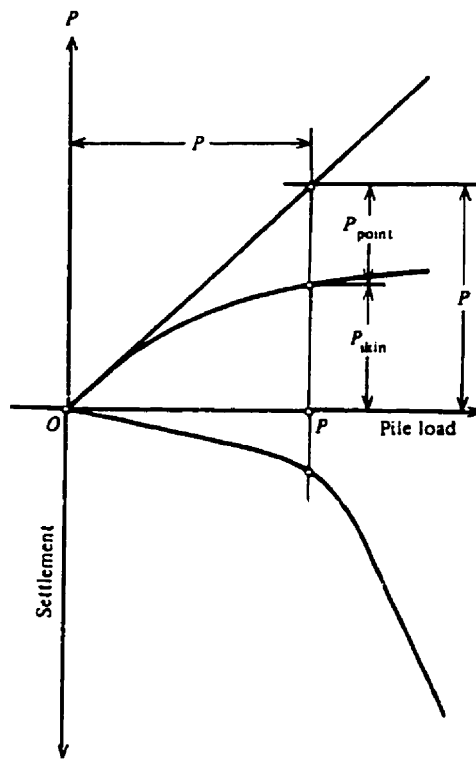


Figure 2.4: Stress Around Piles (after Winterkorn and Fang, 1975)

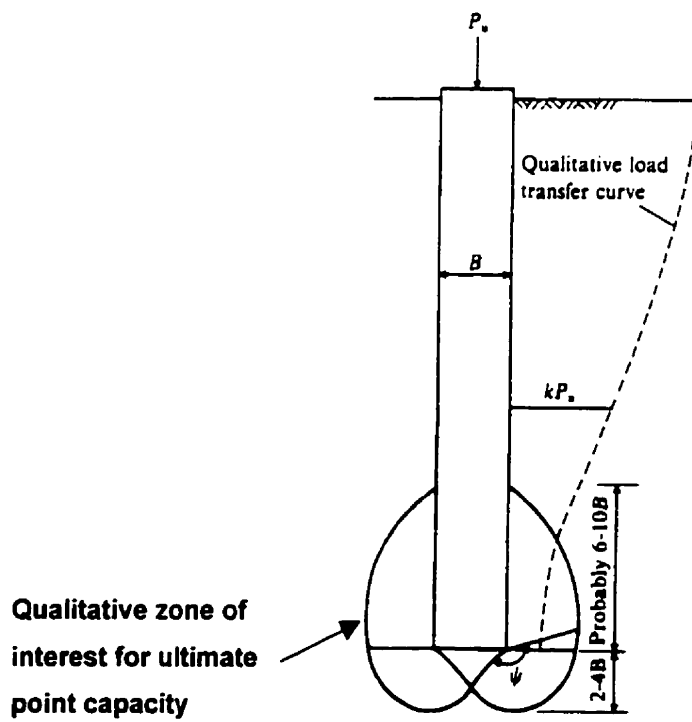


Figure 2.5: General Development of Pile Capacity (after Bowels, 1988)

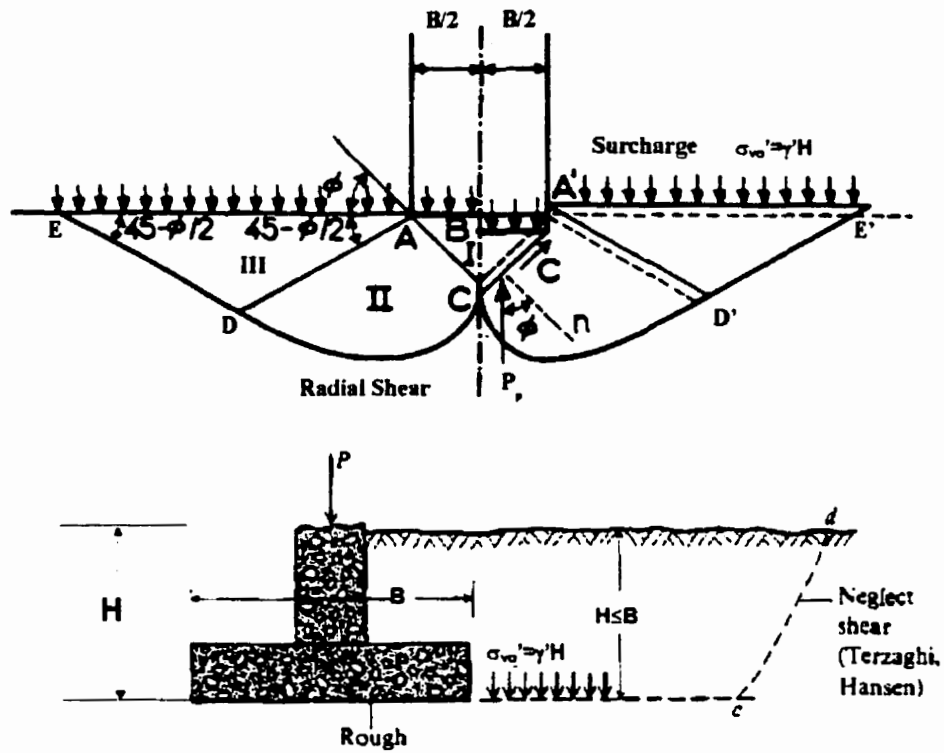


Figure 2.6: Boundaries of Zone of Plastic Equilibrium after Failure of Soil Beneath a Continuous Footing with Rough Base and Surcharge (after Terzaghi, 1943 and Bowles, 1988)

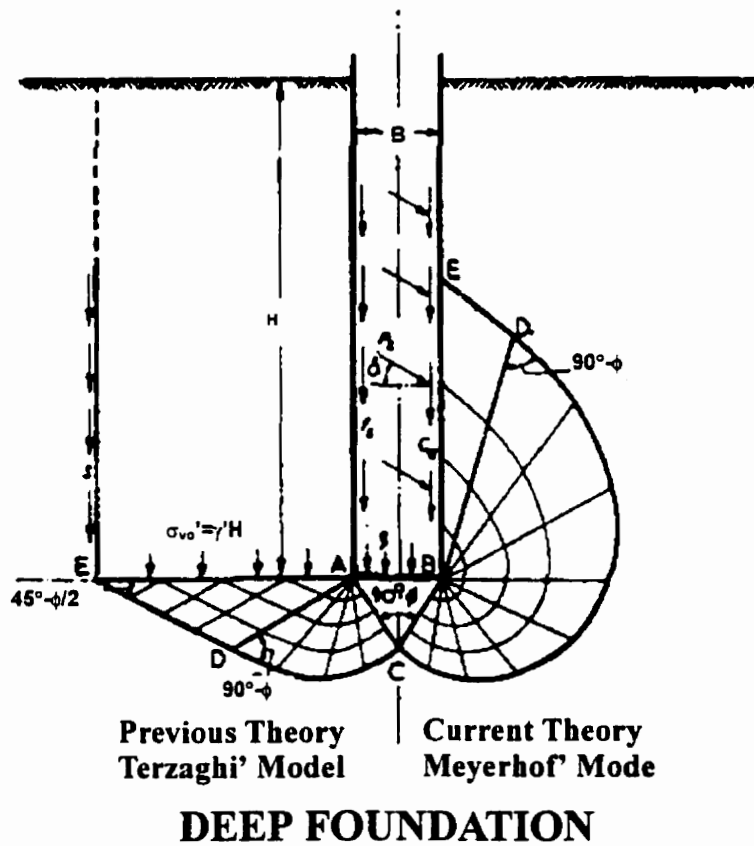
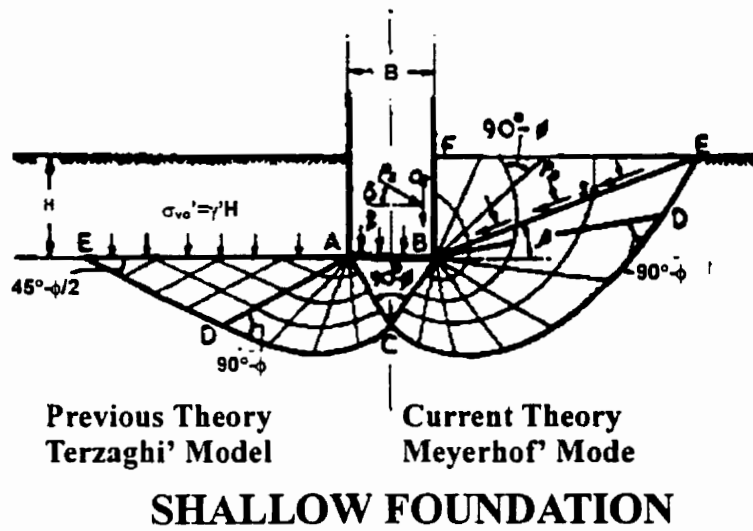


Figure 2.7: Terzaghi & Meyerhof's Pile Capacity Theories (after Meyerhof, 1982)

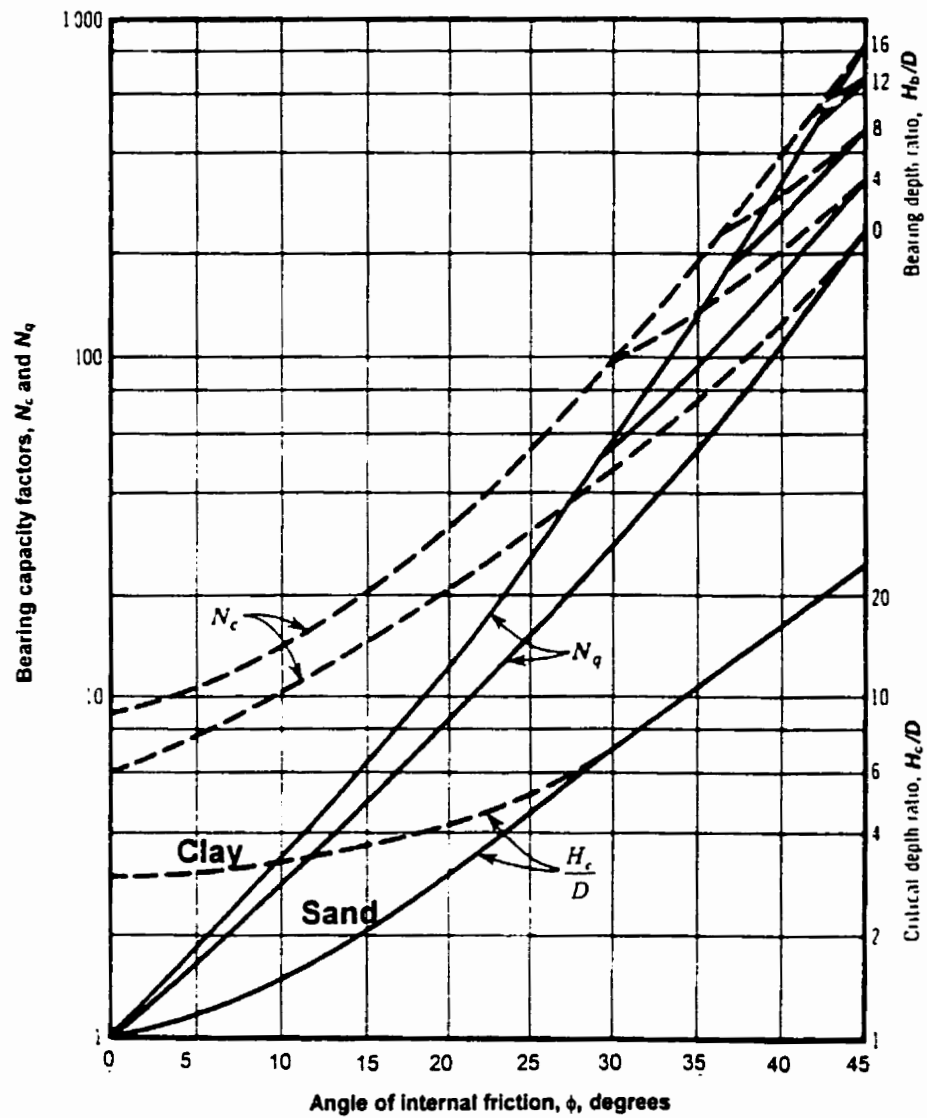


Figure 2.8: Bearing Capacity Factors and Critical Depth Ratios (after Meyerhof 1976)

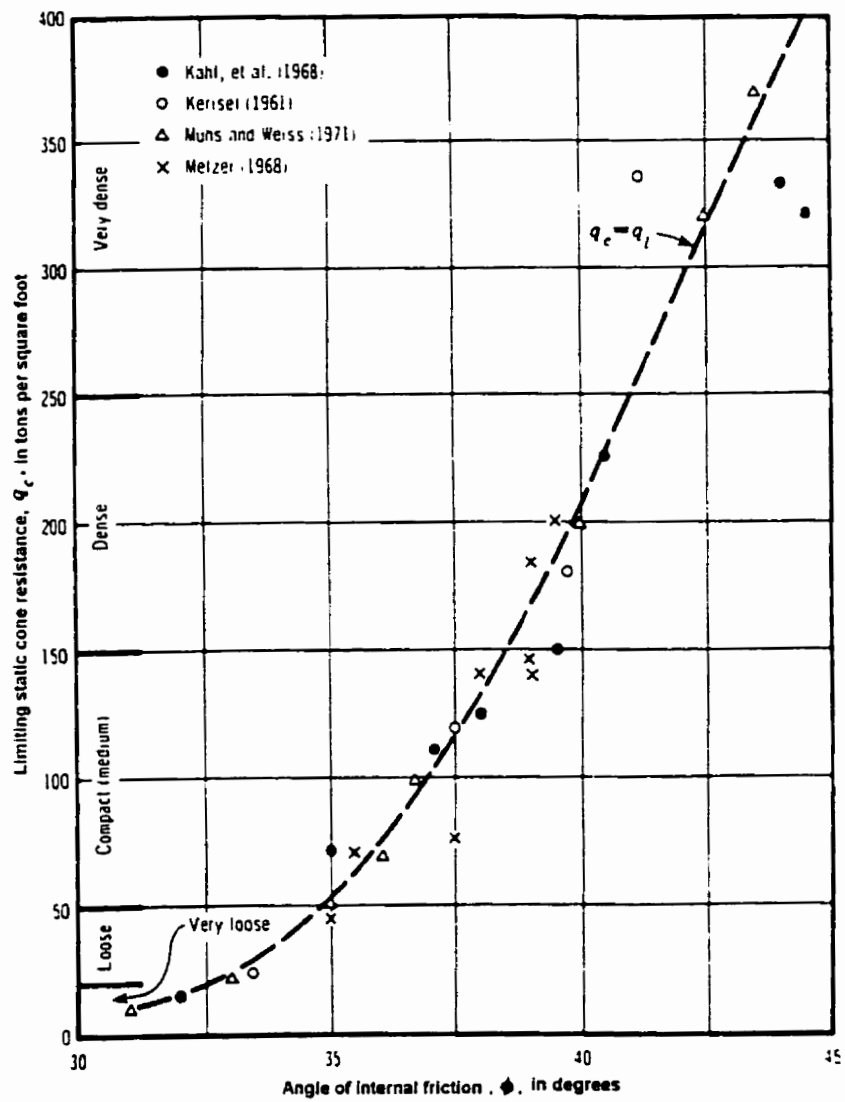


Figure 2.9: Approximate of Limiting Unit Point Resistance Based on the Static Cone Resistance (1 tsf = 95.8 kN/m², after Meyerhof 1976)

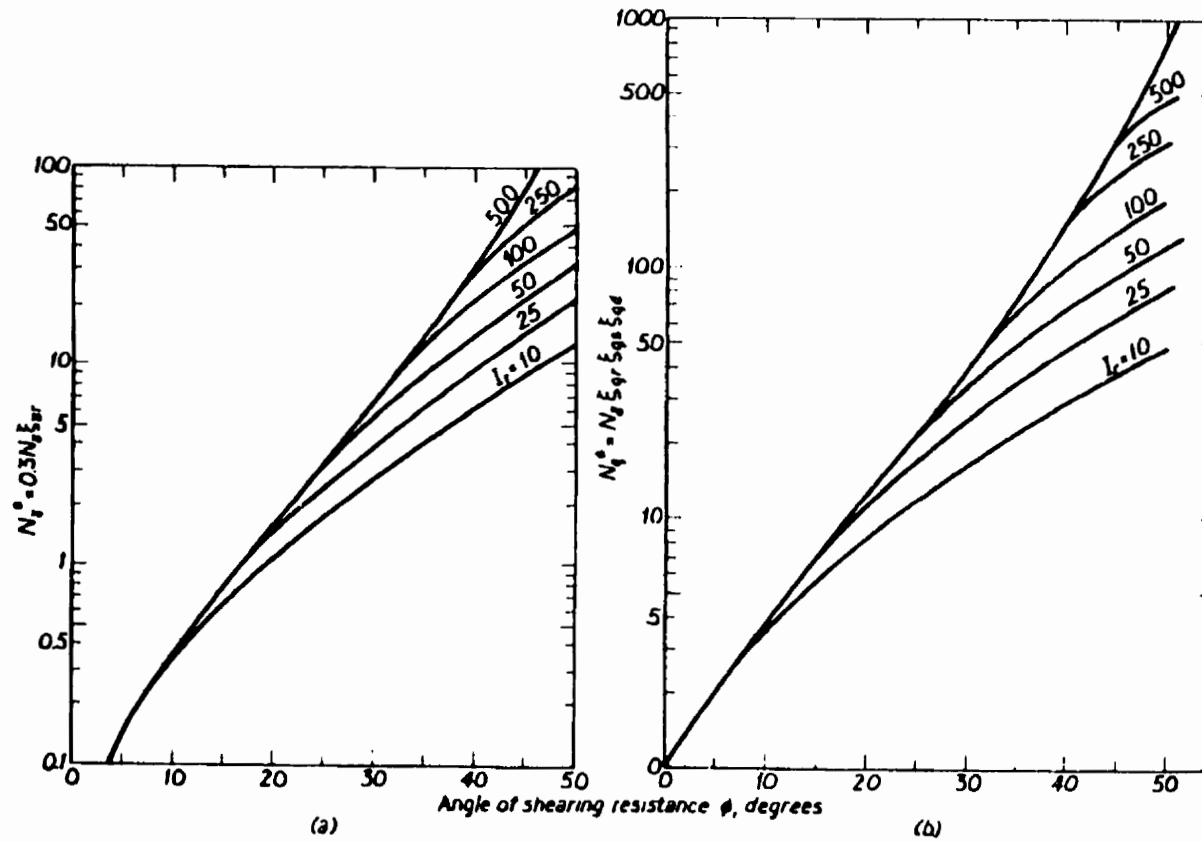


Figure 2.10: Bearing Capacity Factors of N , and N_q for Deep Foundations in Drained Loading: a) Values of N , b) Values of N_q (after Kulhawy, 1984)

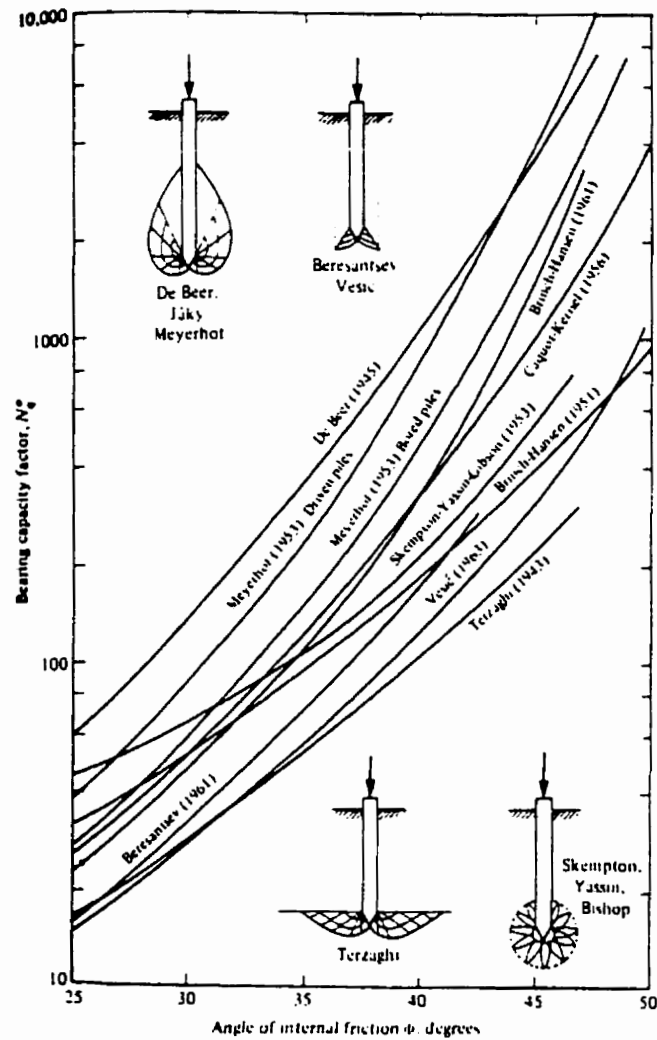


Figure 2.11: Bearing Capacity Factors vs. Angle of Internal Friction According to Various Authors (after Winterkorn and Fang, 1975)

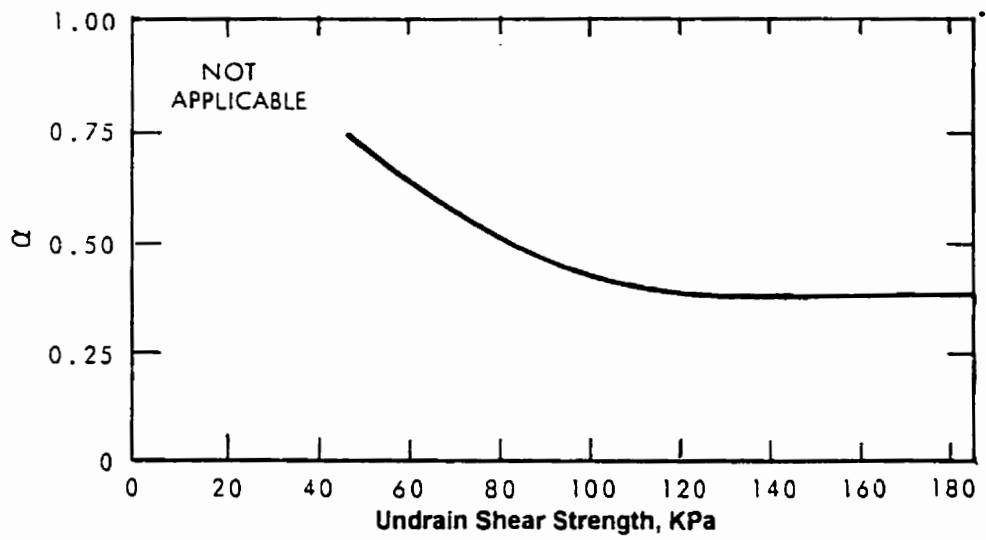


Figure 2.12: Reduction of Undrained Shear Strength for Anchorage Design (after CFEM, 1992)

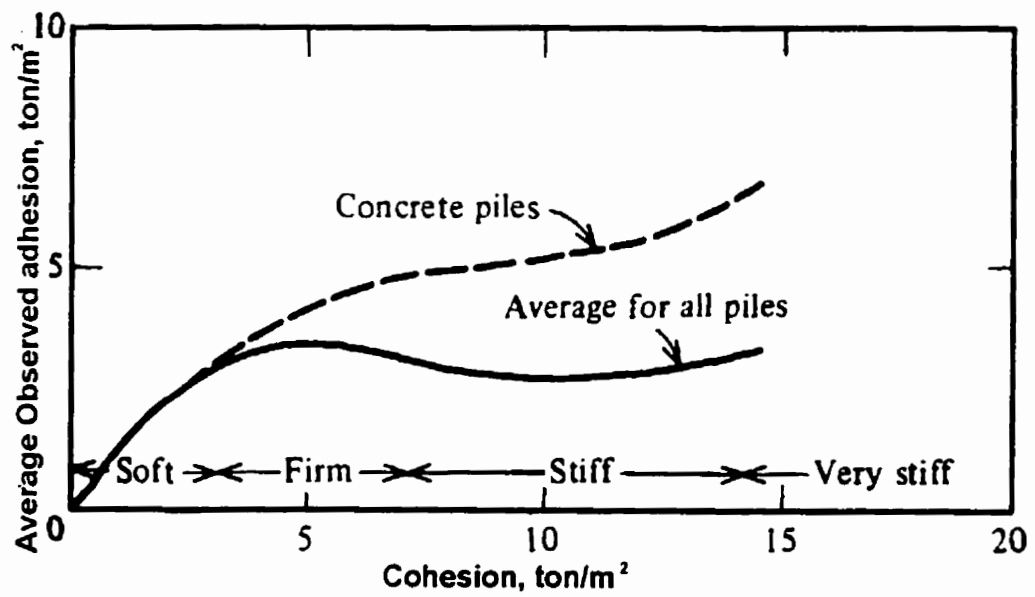


Figure 2.13: Limiting Adhesion for Soft to Stiff Clays. (after Tomlinson, 1957)

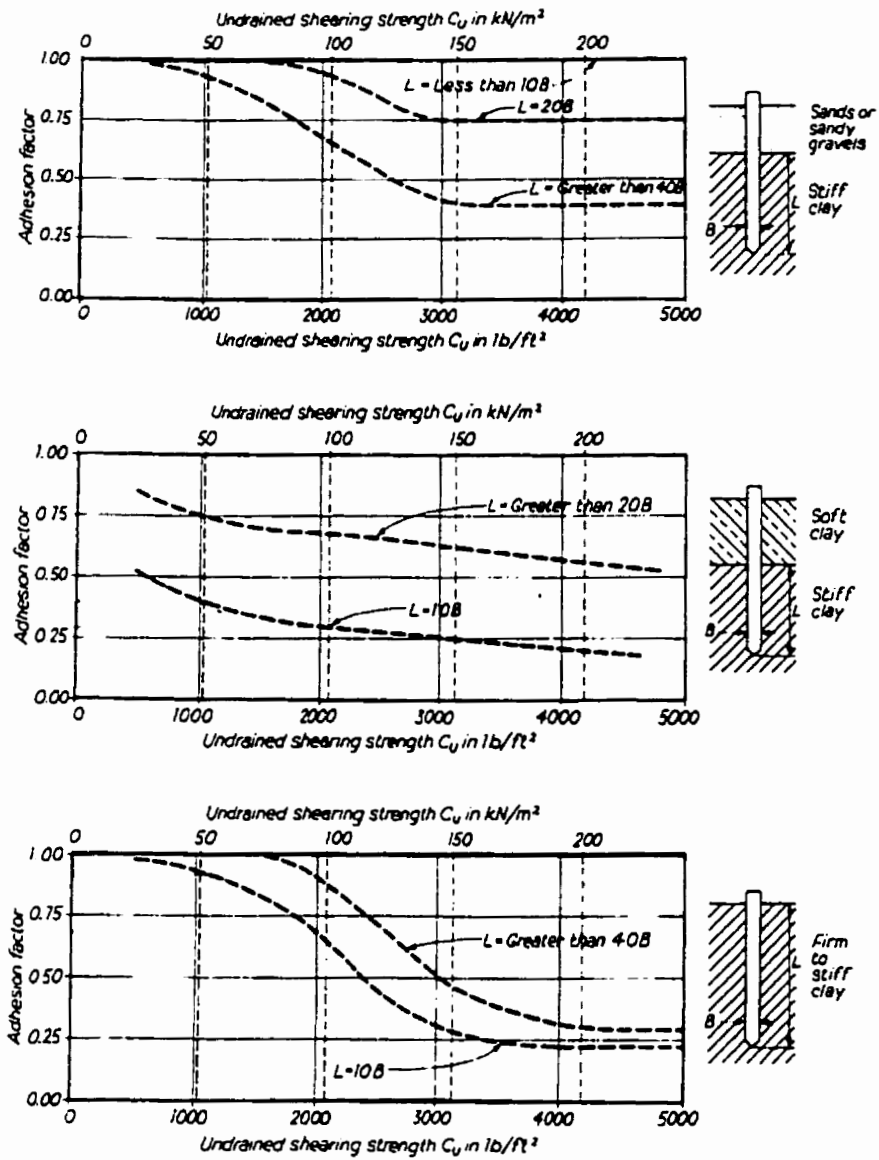


Figure 2.14: Design Curves for Adhesion Factors for Piles Driven into Clay Soils (after Tomlinson, 1994)

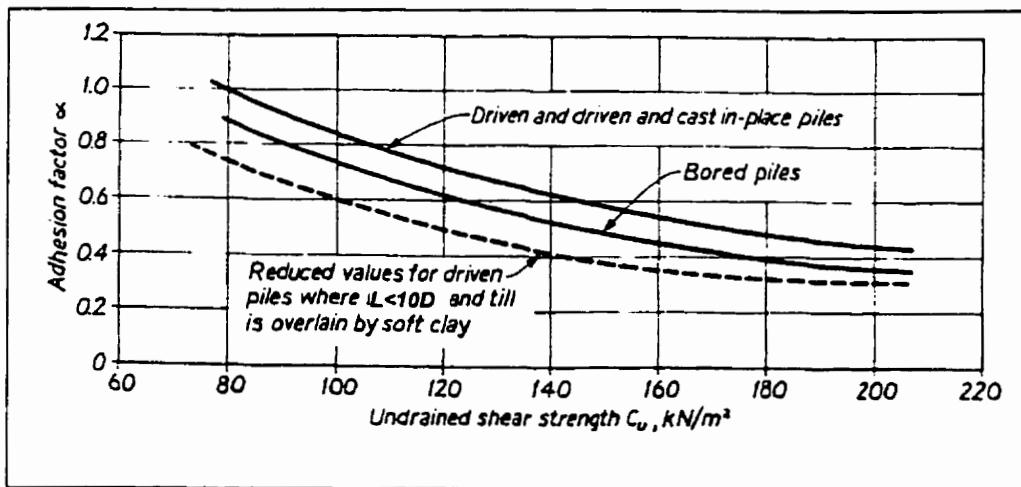


Figure 2.15: Adhesion Factor for Pile Driven in Till (after Weltman and Healy, 1978)

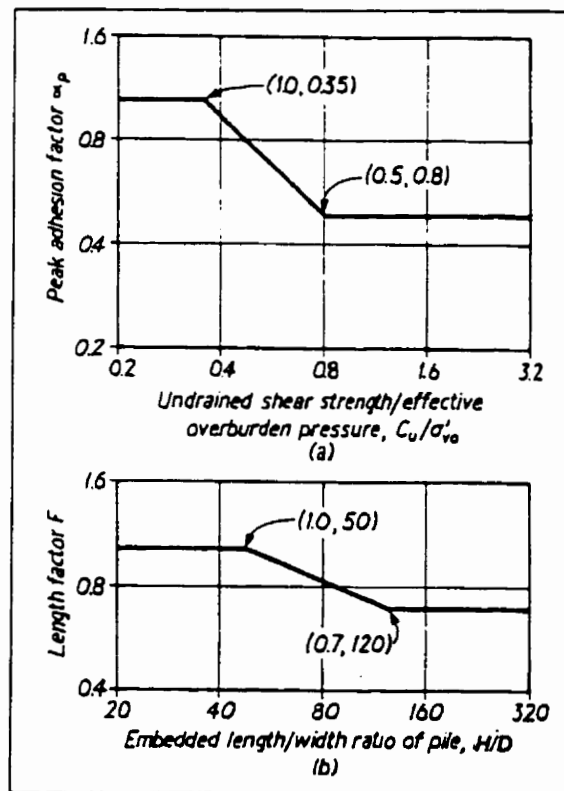


Figure 2.16: Adhesion Factors for Piles Driven to Deep Penetration into Clays: a) Peak Adhesion Factor vs. Shear Strength/Effective Overburden Pressure; b) Length Factor (After Randolph and Wroth, 1982)

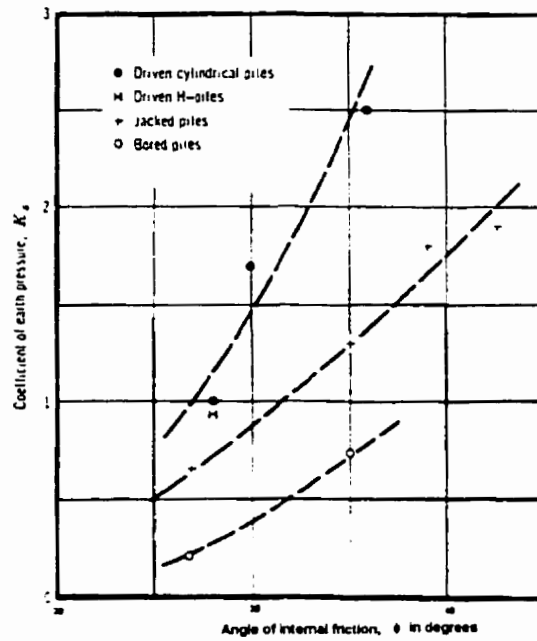


Figure 2.17: Coefficient of Earth Pressure on Shaft of Piles above Critical Depth in Sand (After Meyerhof, 1982)

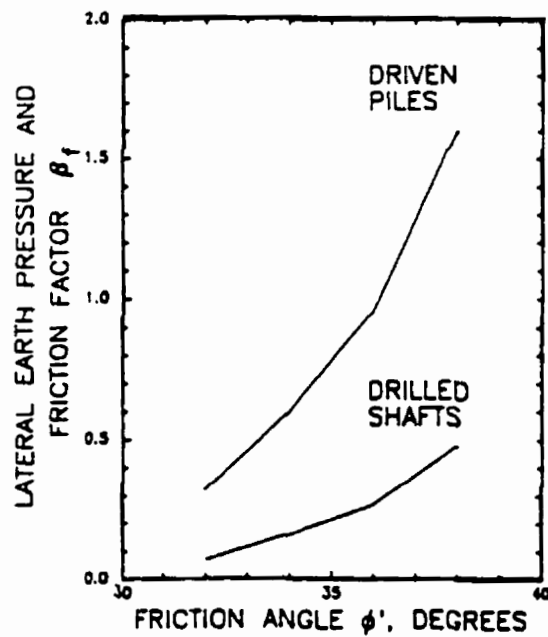


Figure 2.18: Lateral Earth Pressure and Friction Angle Factor, β as a Function of Friction Angle Prior to Installation (after ASCE, 1993, Data from Meyerhof, 1976 and Poulos and Davis, 1980)

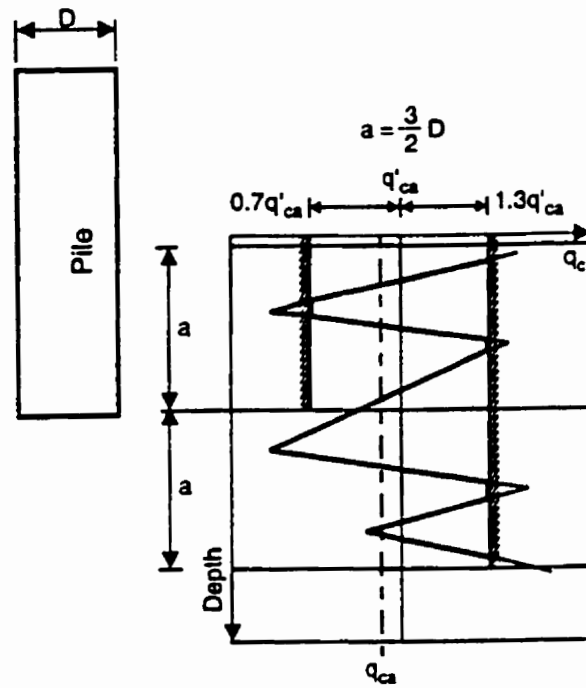
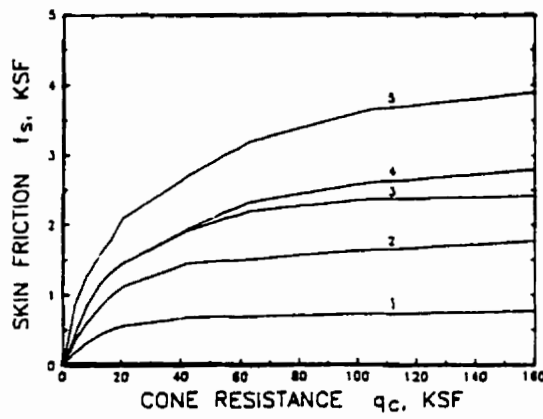
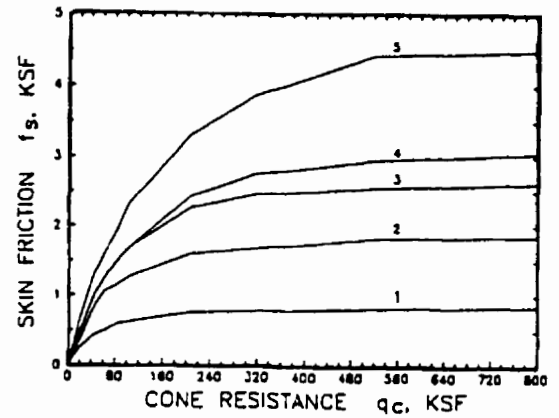


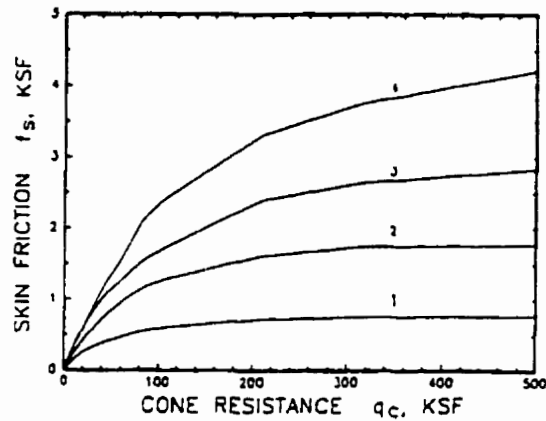
Figure 2.19: CPT Method to Determine Equivalent Cone Resistance at Pile Base (after Bustamante and Gianeselli, 1982)



a. CLAY AND SILT



b. SAND AND GRAVEL



c. CHALK

Figure 2.20: Pile Capacity Prediction Based on CPT - Curves Used with Table 2.17 (after Bustamante and Gianeselli, 1983)

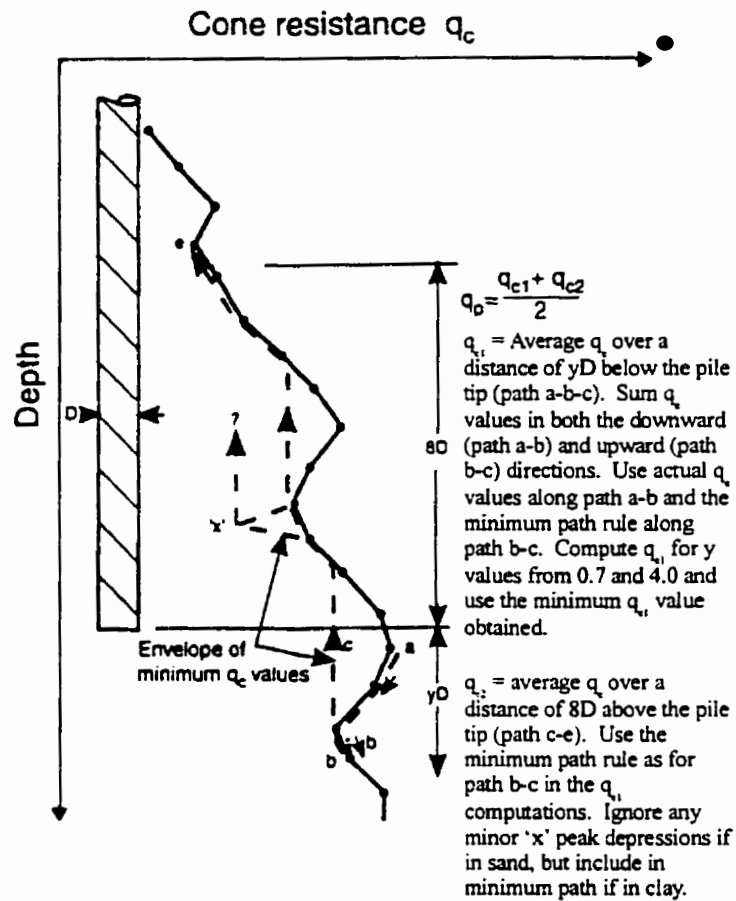


Figure 2.21: Predict Pile Capacity Using CPT – De Ruiter and Beringen Method (after De Ruiter and Beringen, 1979)

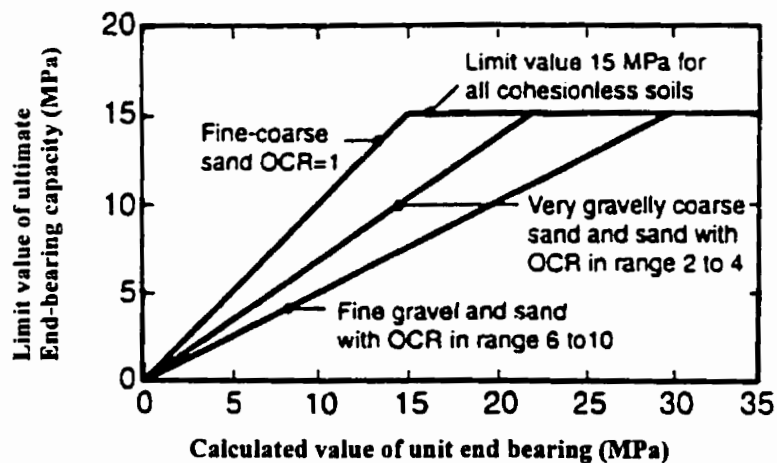


Figure 2.22: Correction for Over-Consolidated Sand for De Ruiter and Beringen Method (after De Ruiter and Beringen, 1979)

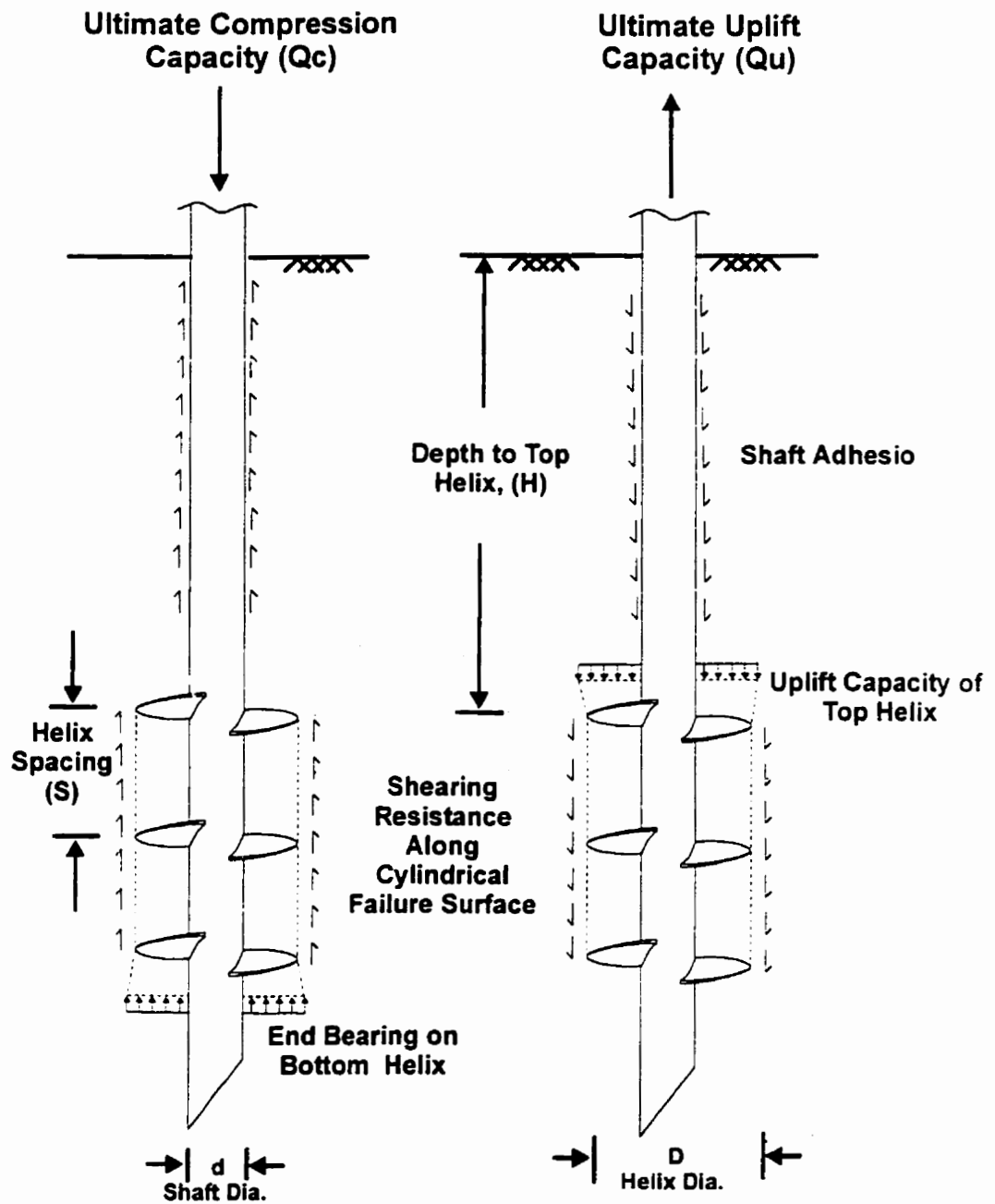
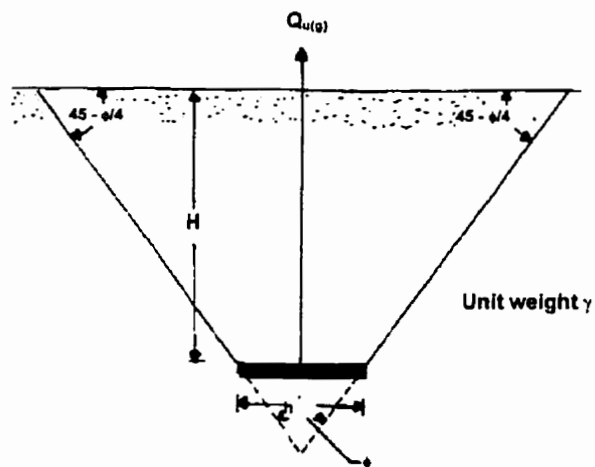
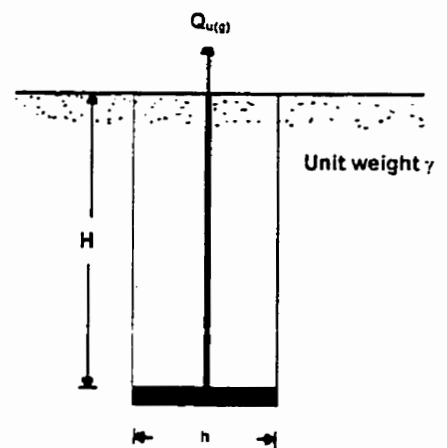


Figure 2.23: Screw Pile in Compression and Tension Loading (after Narasimha Rao et al., 1991)

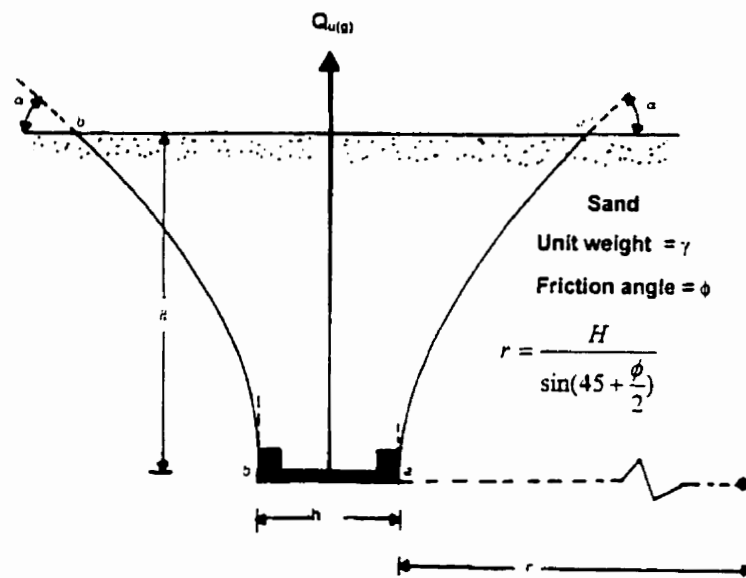




a) Soil Cone Method



b) Friction Cylinder Method



c) Balla's Theory for Shallow Circular Anchor

Figure 2.25: Previous Uplift Bearing Capacity Theories (after Das, 1990)

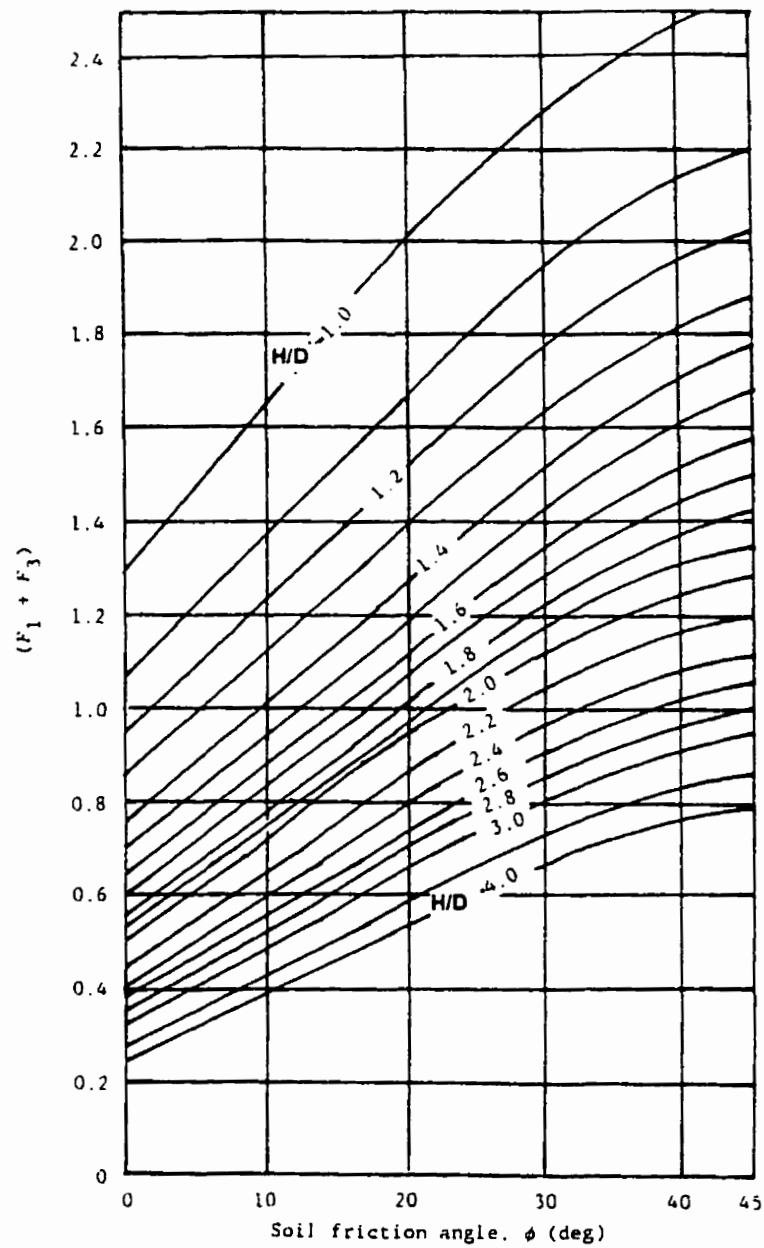
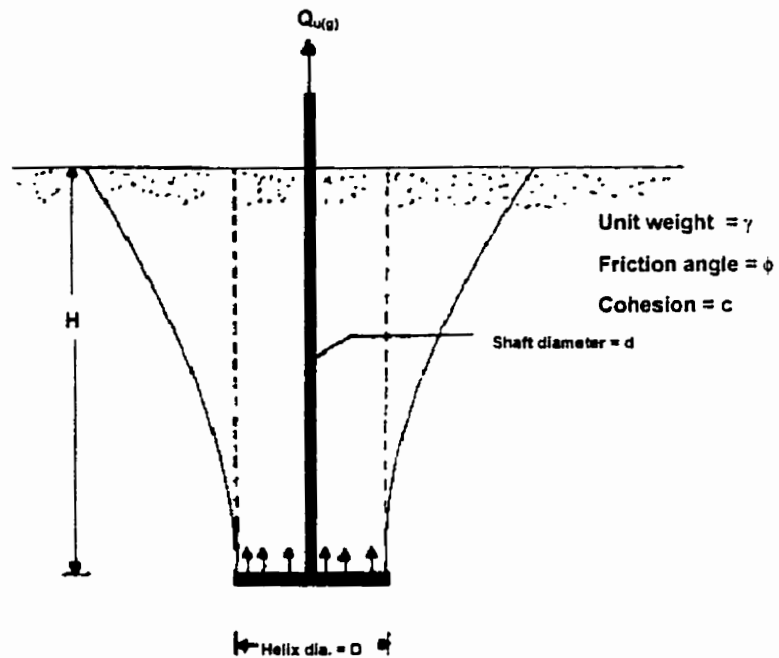
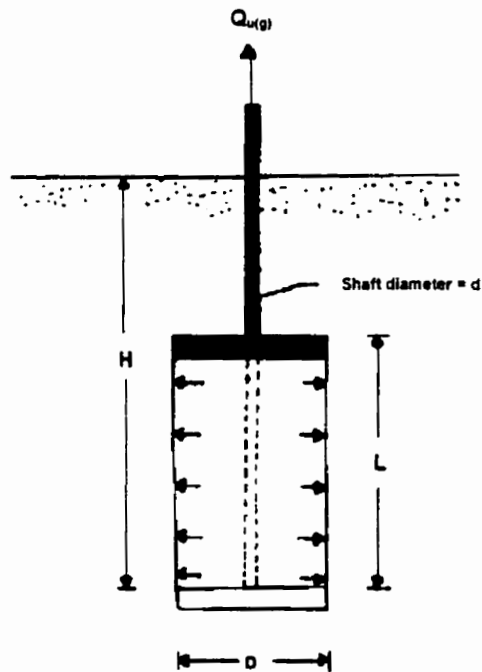


Figure 2.26: Variation of $F_1 + F_3$ Based on Balla's Theory (after Bella, 1961)



e) Mariupol'skii's Theory for Shallow Circular Plate Anchor



e) Mariupol'skii's Theory for Deep Circular Plate Anchor

Figure 2.27: Mariupol'skii's Uplift Capacity Model for Plate Anchor (after Das, 1990)

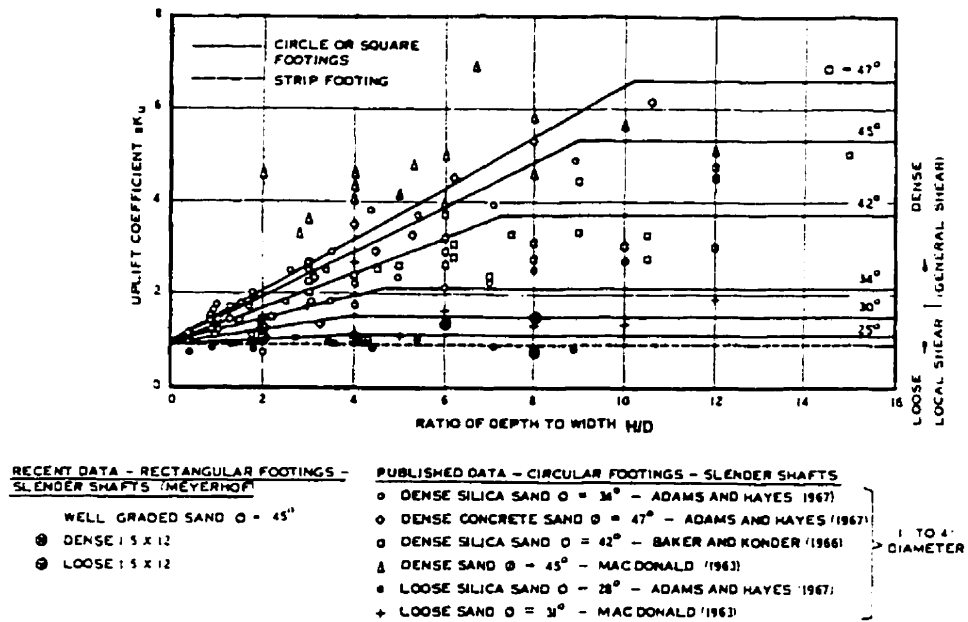


Figure 2.28: Uplift Coefficient sK_u used in Meyerhof and Adam's Uplift Capacity Theory (after Meyerhof and Adam, 1968)

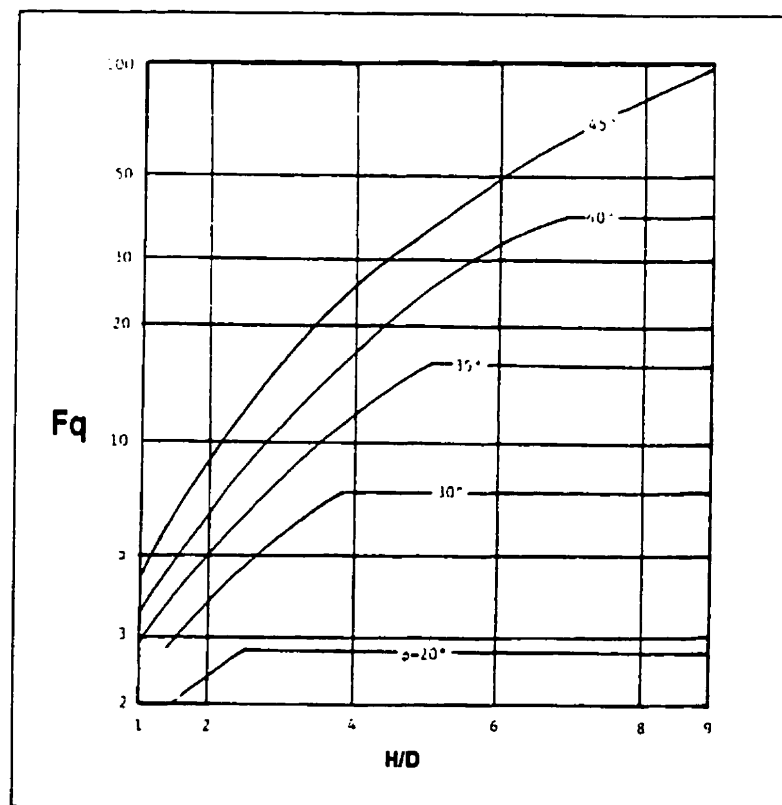


Figure 2.29: Plot of Breakout Factor, F_q , for Shallow Circular Anchors Based on Meyerhof and Adam's Theory (after Das, 1990)

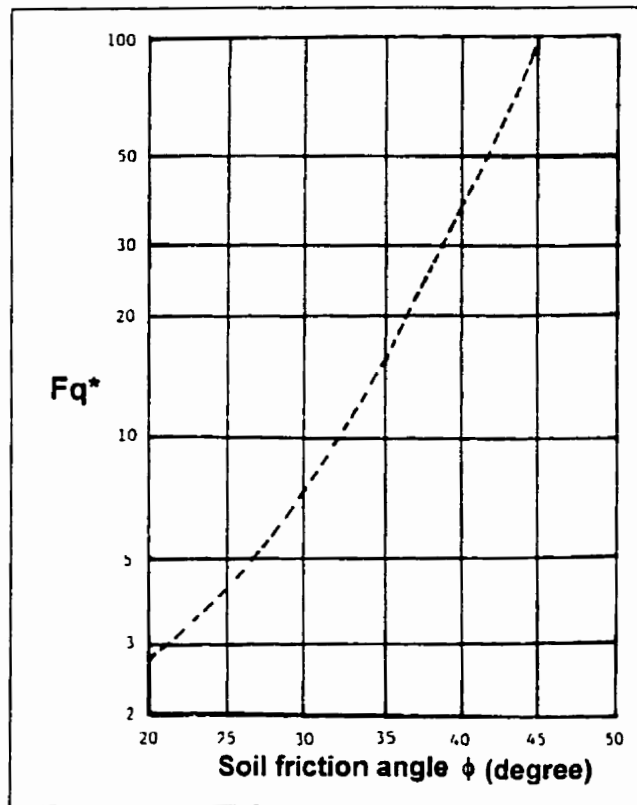


Figure 2.30: Plot of Breakout Factor, F_{q^*} , for Deep Circular Anchors Based on Meyerhof and Adam's Theory (after Das, 1990)

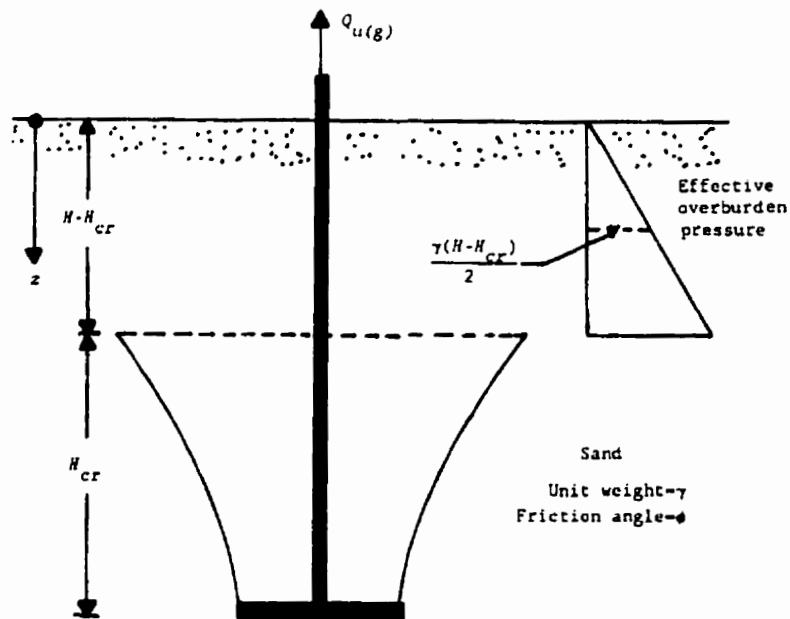


Figure 2.31: Failure Mechanism for Deep Anchor used in Meyerhof and Adam's Theory (after Das, 1990)

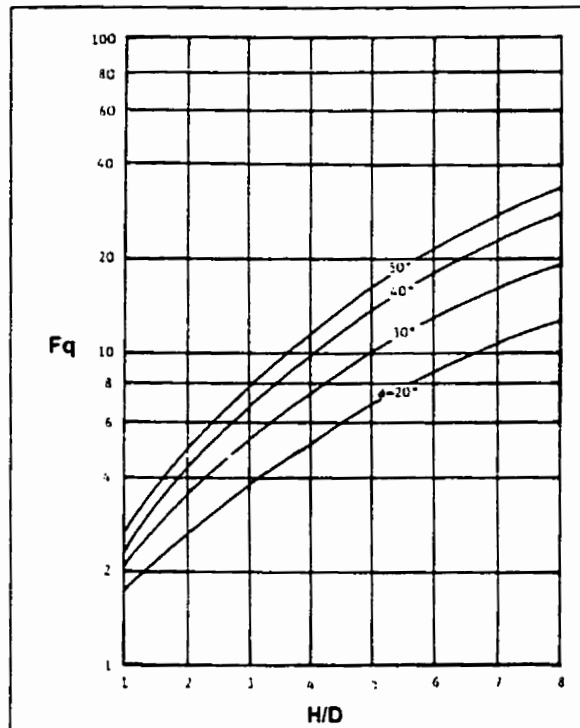


Figure 2.32: Variation of F_q for Shallow Circular Anchors Based on Vesic's Model (after Das, 1990)

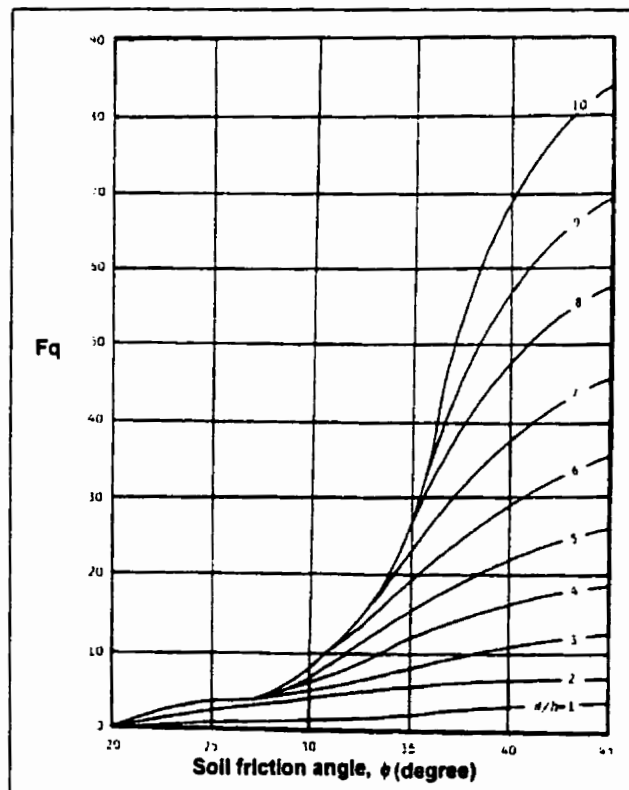


Figure 2.33: Breakout Factor Based on Saeedy's Theory (after Das, 1990)

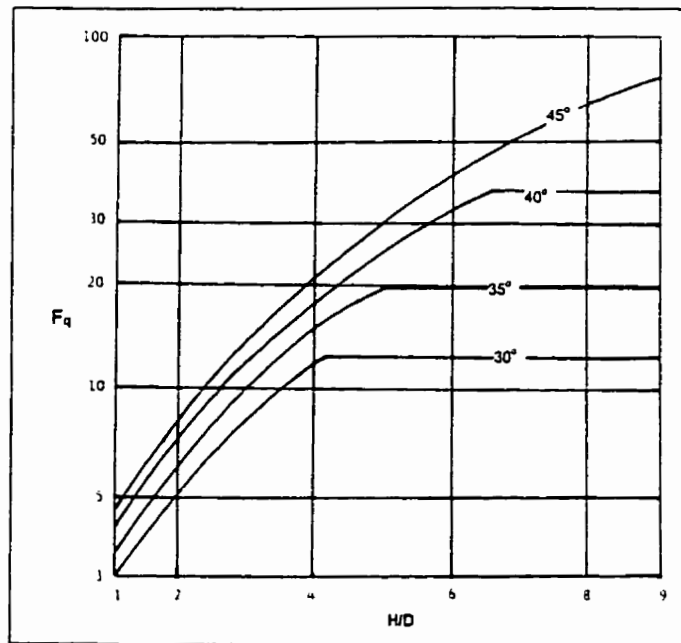


Figure 2.34: Breakout Factor, F_q for Shallow Circular Anchors Based on Veesaert and Clemence's Theory (after Das, 1990)

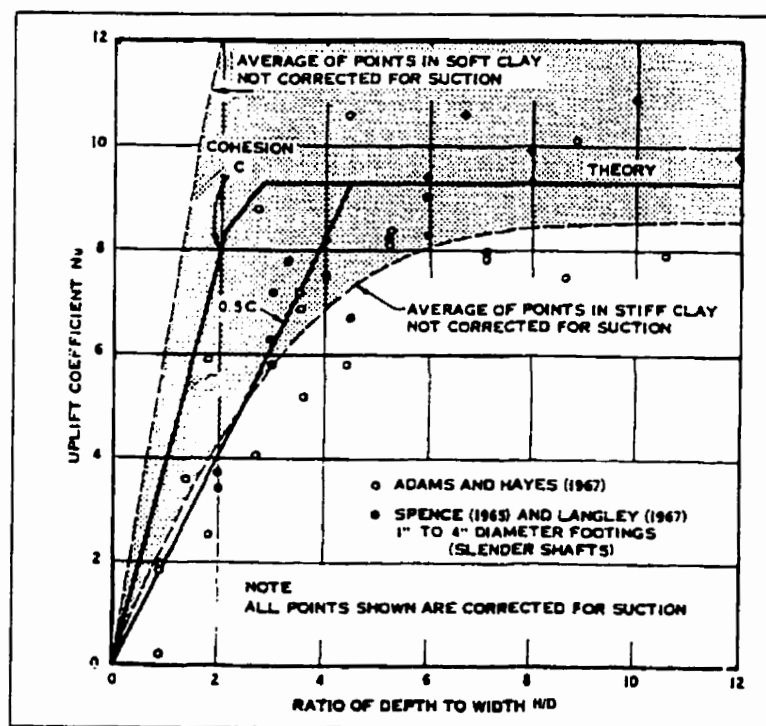


Figure 2.35: Uplift Coefficient N_u Based on Meyerhof and Adam Theory (after Meyerhof and Adam, 1968)

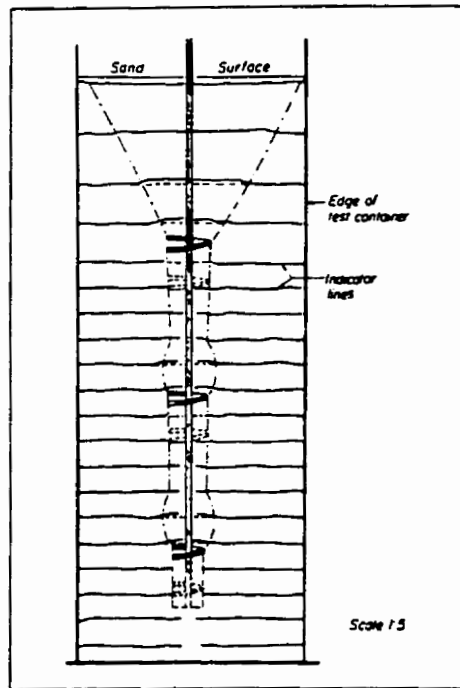


Figure 2.36: Shallow Model Screw Anchor Test with Marker Lines (after Mitsch and Clemence, 1985)

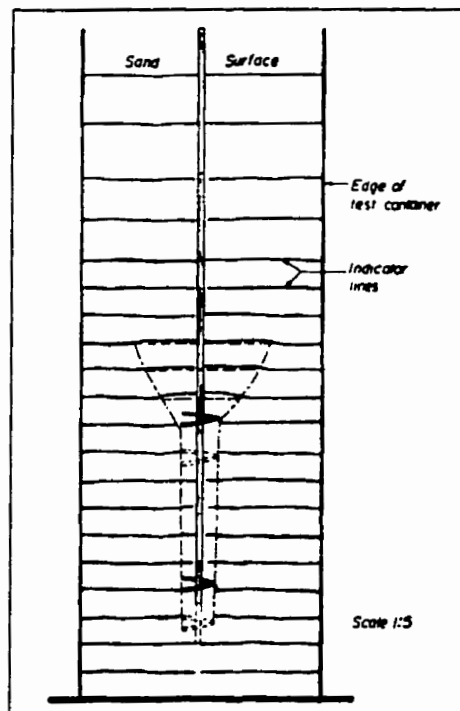


Figure 2.37: Deep Model Screw Anchor Test with Marker Lines (after Mitsch and Clemence, 1985)

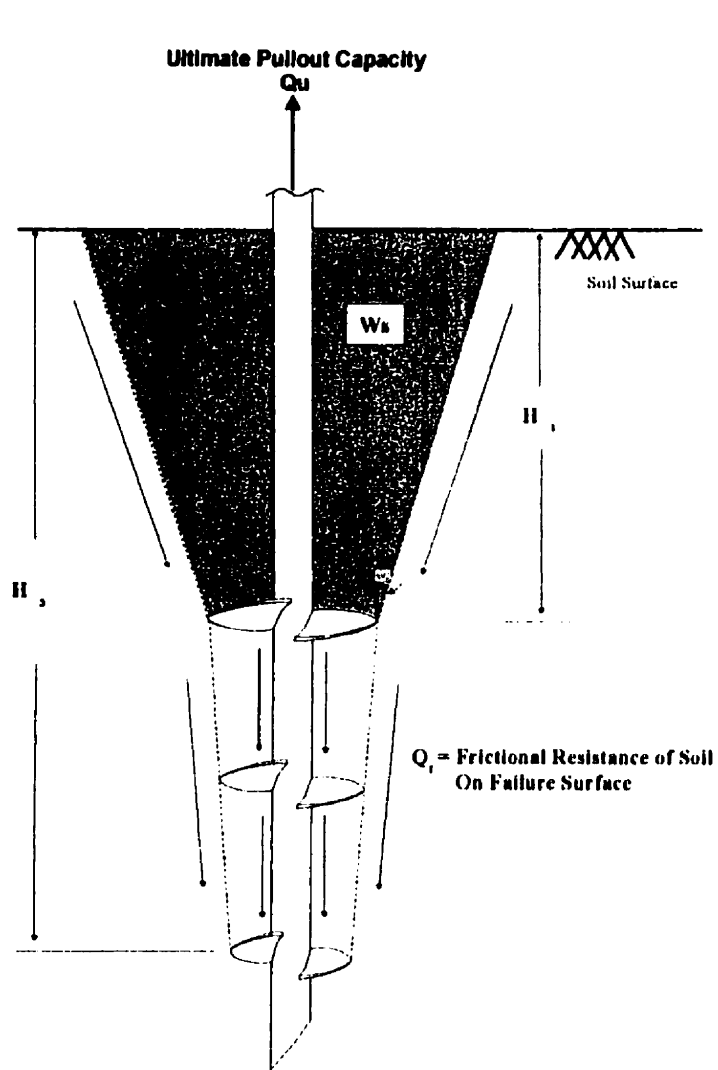


Figure 2.38: Failure Surface for Shallow Multihelix Anchor in Sand (after Mitsch and Clemence, 1985)

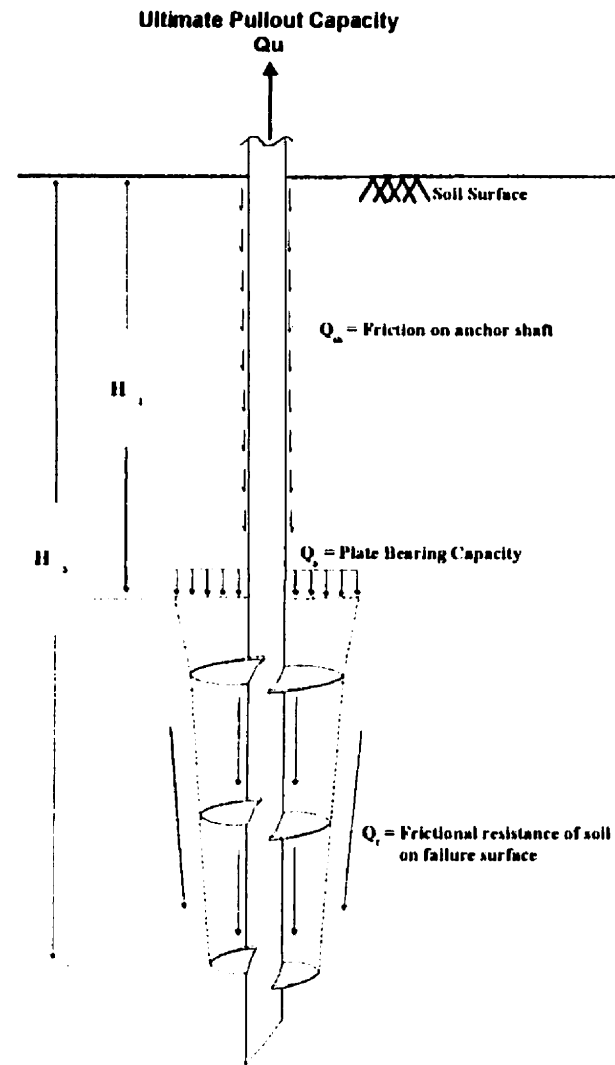


Figure 2.39: Failure Surface of a Deep Multihelix Anchor in Sand (after Mitsch and Clemence, 1985)

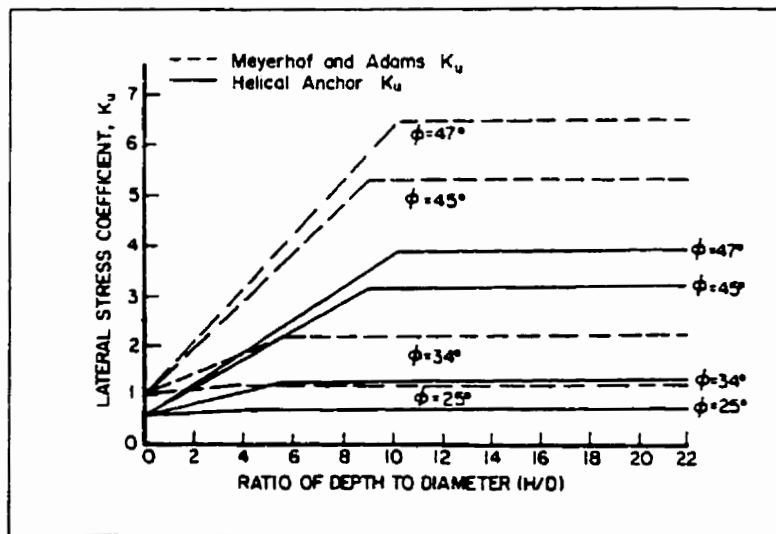


Figure 2.40: Recommended Lateral Stress Values, K_u , for Helical Anchors and Foundations in Uplift (after Mitsch and Clemence, 1985)

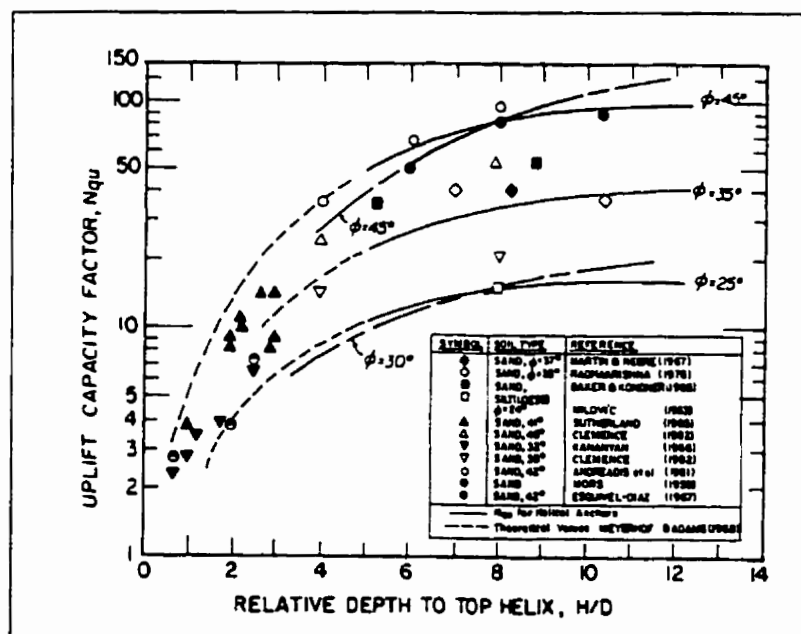


Figure 2.41: Uplift Capacity Factor, N_{qu} , vs. Embedment Ratio, H/D Ratio for Helical Anchors in Sand (after Mitsch and Clemence, 1985)

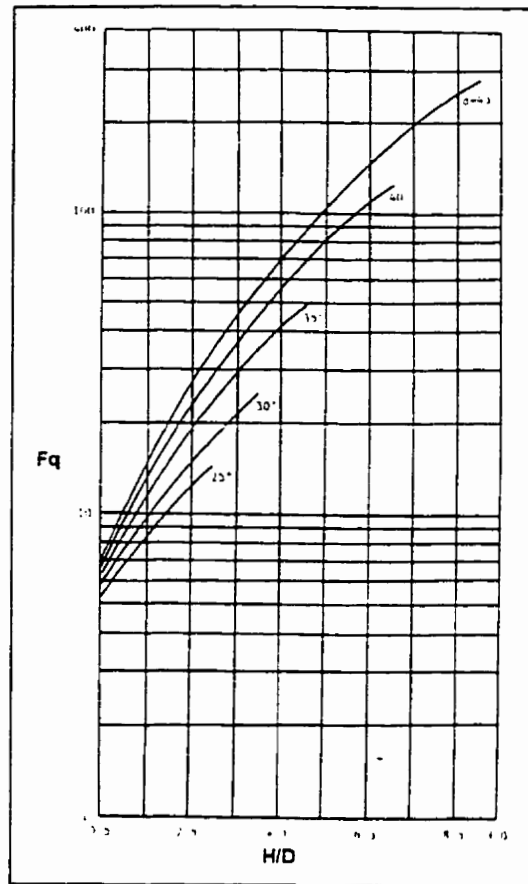


Figure 2.42: Variation of Breakout Factor with Embedment Depth for Shallow Anchor Condition based on Mitsch and Clemence's Theory (after Das, 1990)

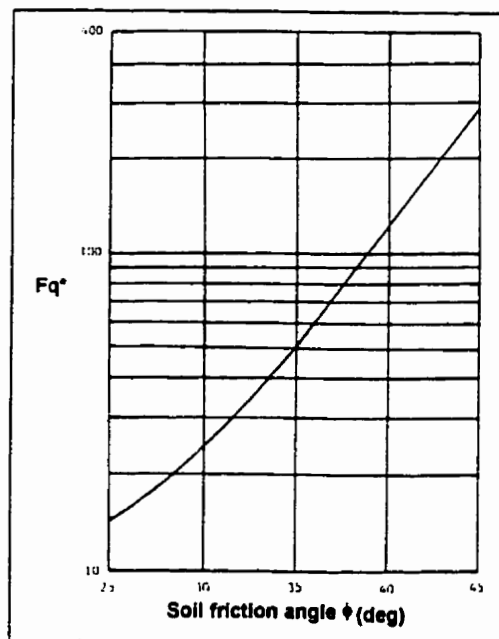


Figure 2.43: Variation of Breakout Factor with Embedment Depth for Deep Anchor Condition based on Mitsch and Clemence's Theory (after Das, 1990)

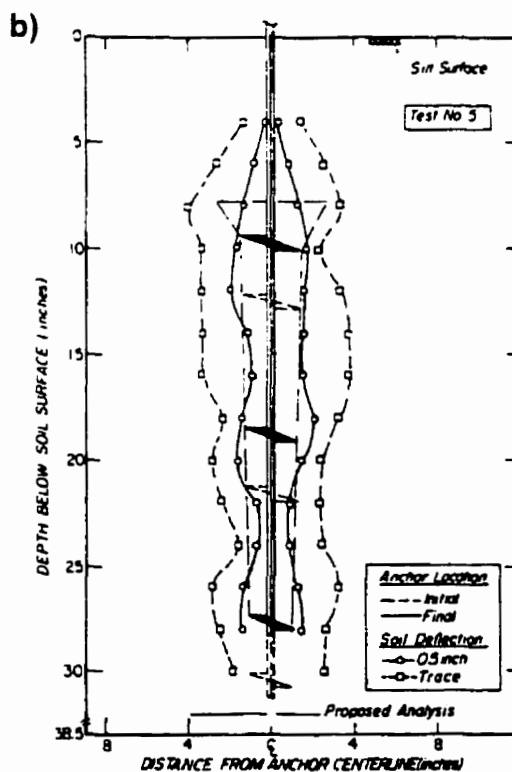
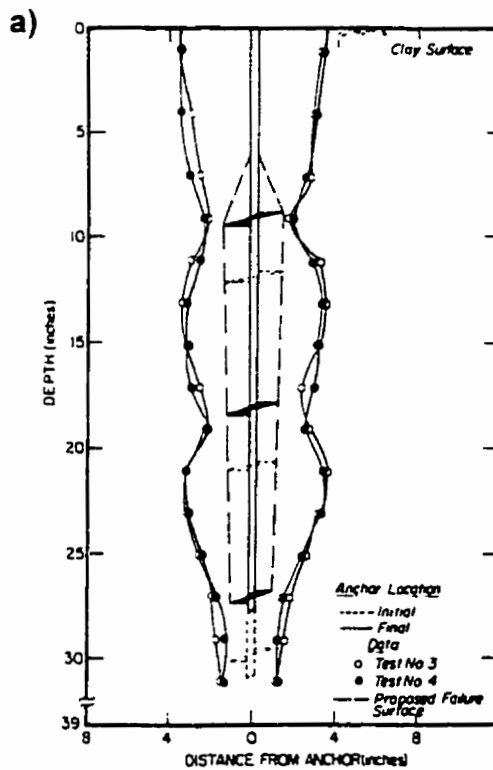


Figure 2.44: Comparison of Maximum Shear Strain Measured and Proposed Failure Surface for a) Shallow Model Tests in Clay and b) Deep Model Test in Lacustrine Silt (after Mooney et al., 1985)

Ultimate Pullout Capacity

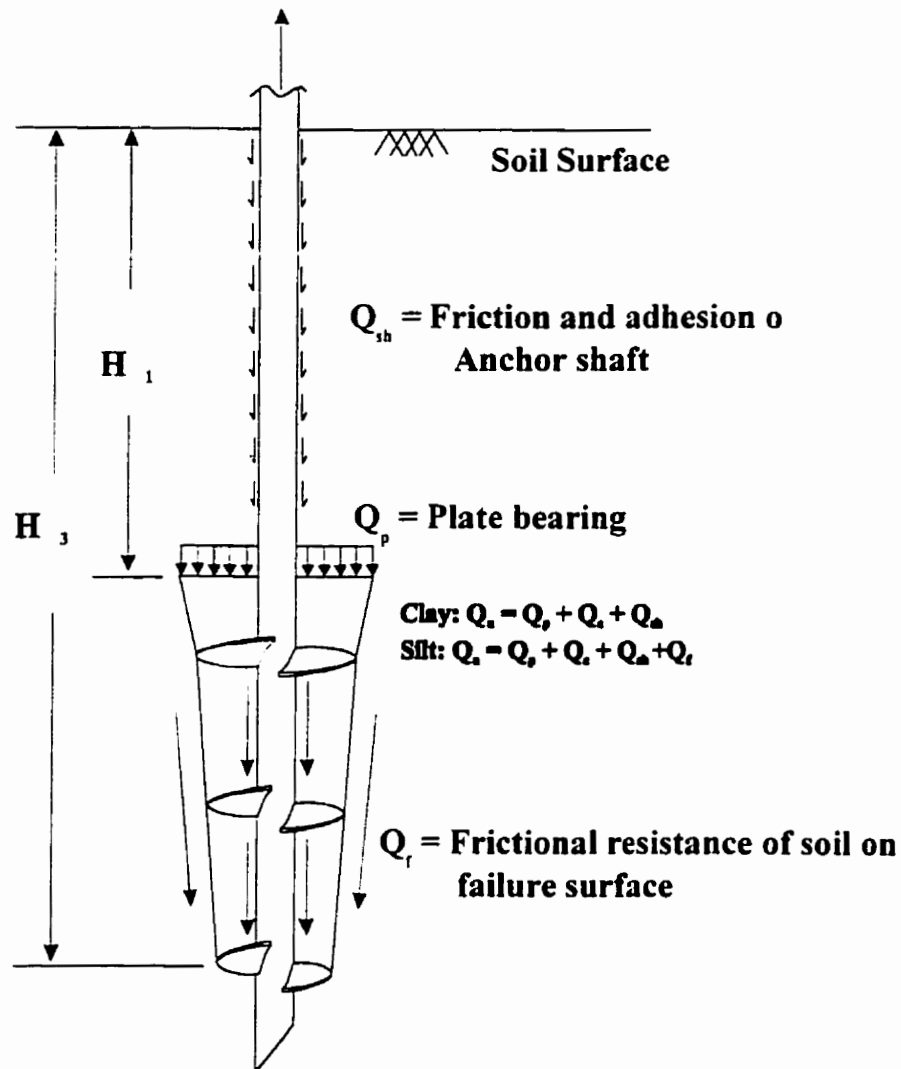


Figure 2.45: Proposed Failure Mode for Multihelix Anchors in Clay and Silt (after Mooney, et al., 1985)

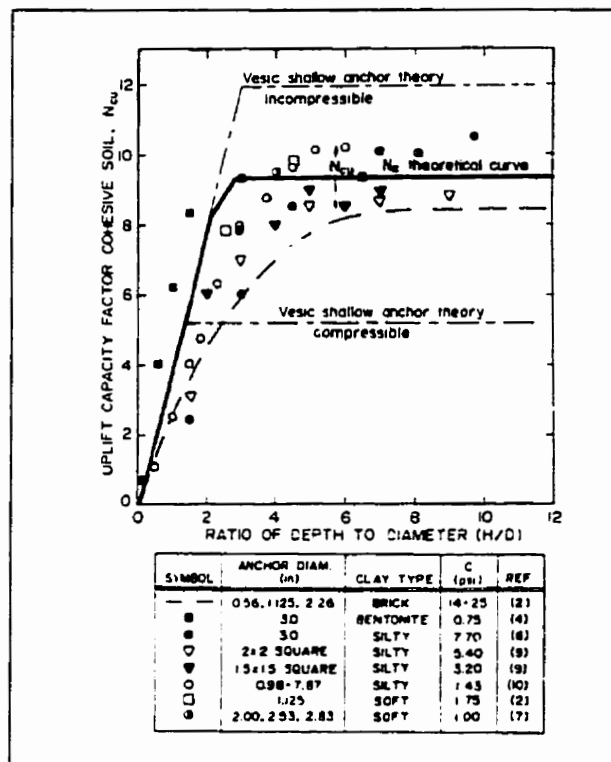


Figure 2.46: Uplift Capacity Factor, N_{cu} (after Mooney et al., 1985)

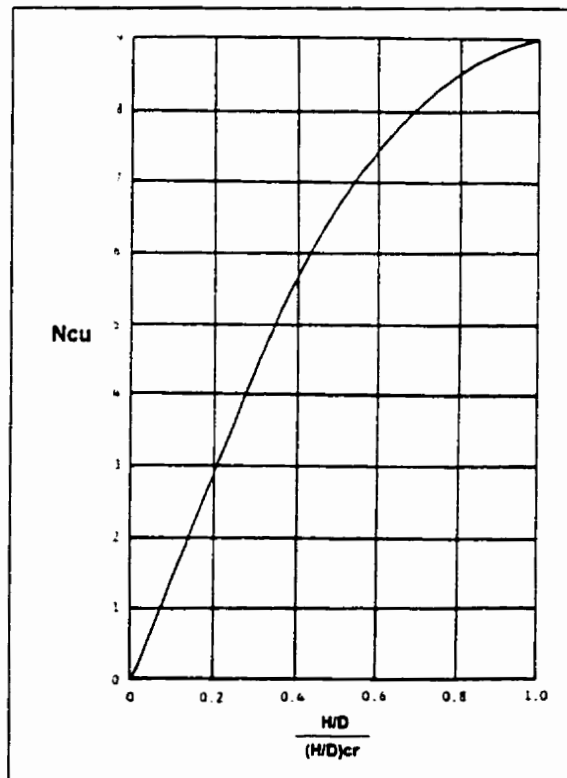


Figure 2.47: Variation of Uplift Capacity Factor N_{cu} with $(H/D)/(H/D)_{cr}$ Ratio (after Das, 1990)

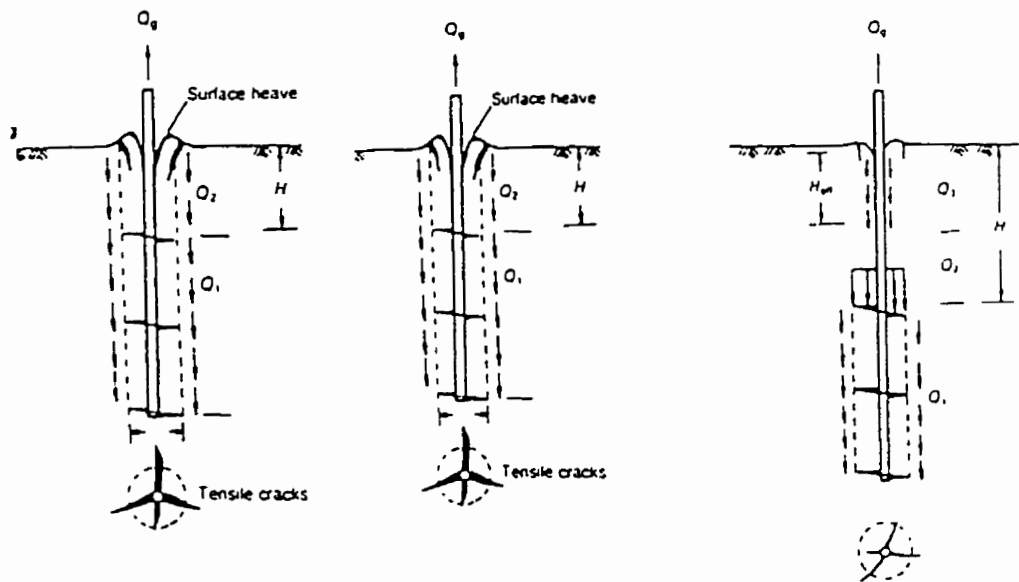


Figure 2.48: Behavior of Helical Anchor at Various Embedment Ratios: a) Shallow; b) Transitions; c) Deep (after Narasimha Rao and Prasad, 1993)

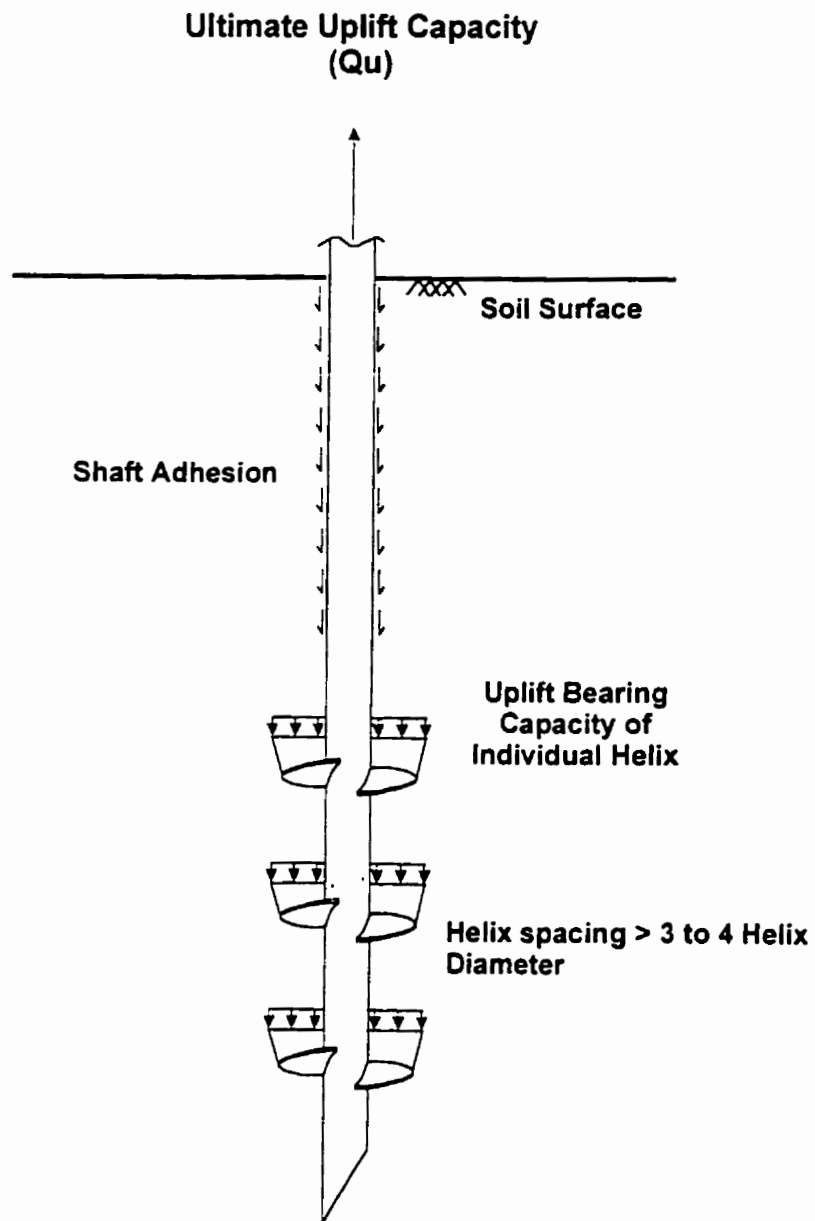


Figure 2.49: Individual Bearing Method

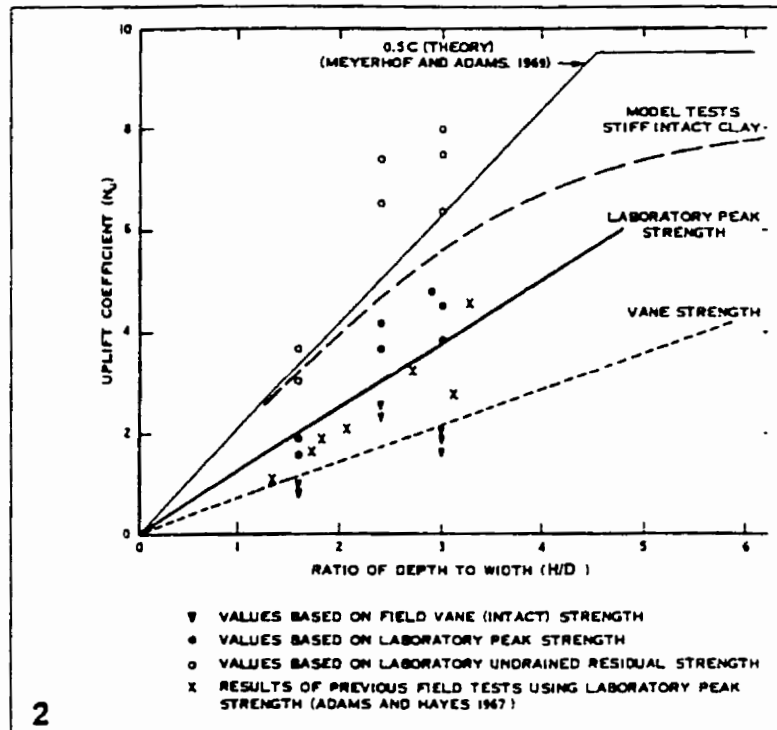


Figure 2.50: Comparison between Theory and the Results of the Full-Scale Tests of Belled Footings. (after Adams and Radhakrishna, 1971)

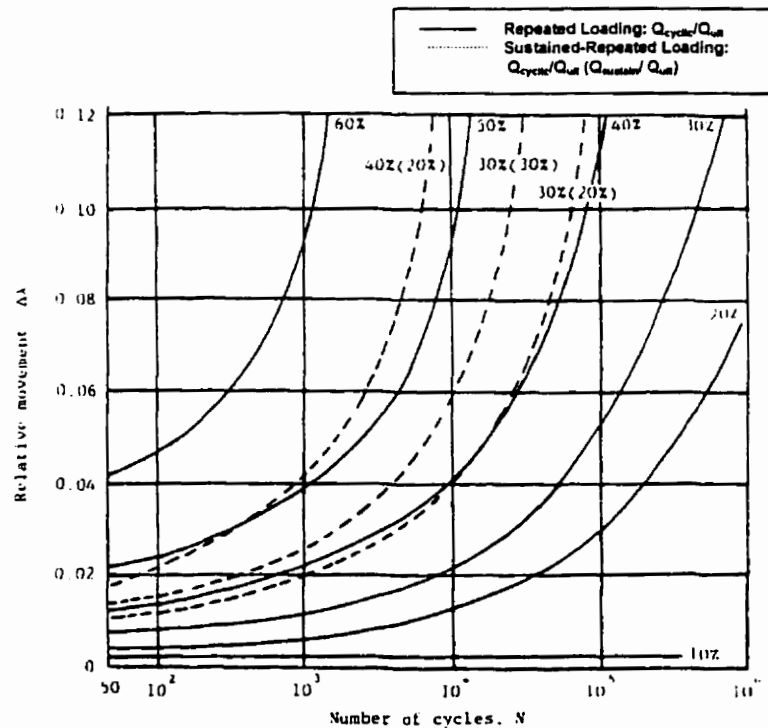


Figure 2.51: Relative Anchor Movement Versus Number of Cycles (after Andreadis et al., 1978)

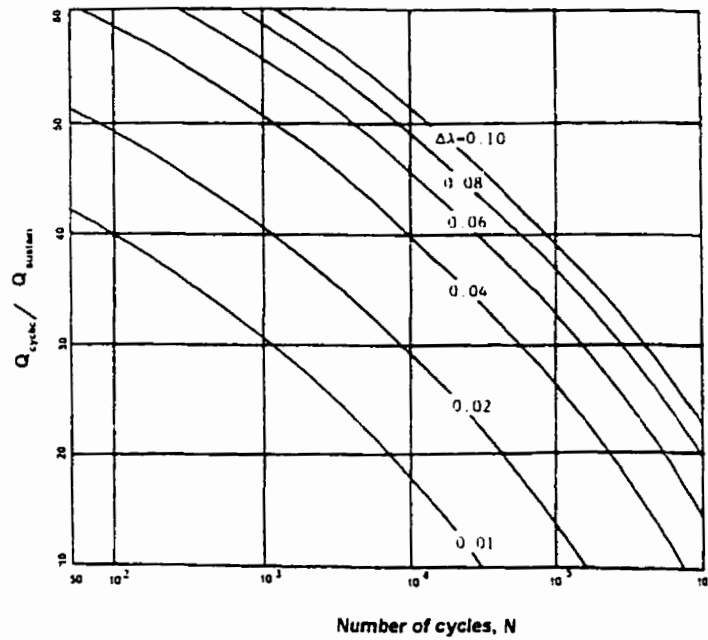


Figure 2.52: Relative Cyclic Load Versus Number of Cycles (after Andreadis et al., 1978)

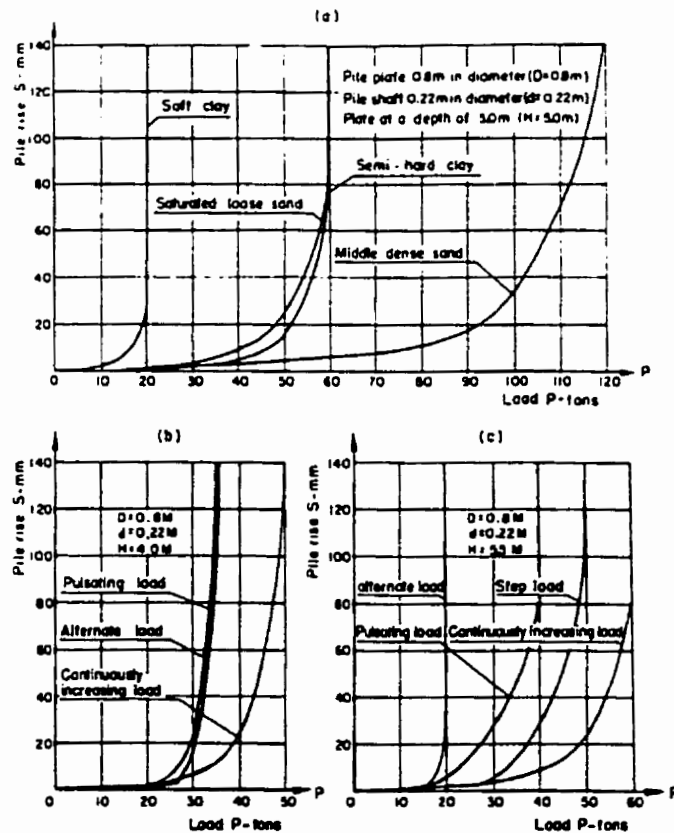


Figure 2.53: Results of Pile Load Tests: a) Continuous Uplift Tests in Various Soils; b) Uplift Test Under Different Loading Condition in Medium Stiff Clay; c) Uplift Tests Under Different Loading Condition in Saturated Loose Sands (after Trofimenkov and Mariupolskii, 1965)

CHAPTER 3 PILE DEVELOPMENT

3.1 SCOPE

This chapter describes the design, instrumentation and construction of the screw piles used for the field program. The test piles were designed to measure and study the following during the load testing of the pile:

1. The total load applied and settlement of the pile,
2. The distribution of load (stress) along the pile shaft as it was loaded,
3. The load carried by the end helix of the pile (end bearing),
4. The influence of installation depth (H) to helix diameter (D) ratio on the ultimate pile capacity, and
5. The influence of inter-helical space (S) to helix diameter (D) ratio on the ultimate pile capacity.

3.2 PILE GEOMETRY AND INSTRUMENTATION

ALMITA Manufacturing LTD. requested that tests be performed on the most commonly used screw piles used in engineering applications where large pile capacity are required. The company wanted to test large diameter screw pile for future use in foundation applications in which compressive load dominate. Therefore, the choice of the pile diameter and material thickness was pre-determined by the manufacturer. The length of the pile was limited by the installation equipment. The maximum length of the pile that the current installation truck can install is 6.10 m (20 ft). Figure 3.1 through 3.3 illustrate the geometry of the screw anchor piles used in the test program. Table 3.1 contains a summary of the pile characteristics. The steel properties used to manufacture these piles are provided in Appendix A.

The multi-helix screw pile adopted for the compression and tension test consisted of a 219 mm diameter pile with 6.71 mm thick steel shaft and three 356 mm diameter helices welded to the steel shaft, a typical screw pile geometry used in Alberta. The study considered two major geometric factors, the embedment ratio (H/D) and the inter-helix spacing or the spacing ratio (S/D), as the main variances that would significantly influence the ultimate load carrying capacity. Therefore, fully instrumented piles were installed to a depth of 3.05 m and 5.18 m to investigate the influence of the embedment ratio on the screw pile failure mechanism and load carrying capacity. The ratios were chosen based on the considerations of the installation equipment limitation and a review of the literature (Bradka, 1997). The instrumented piles are designed with 3 helices and they were to be compared with the standard production pile (non-instrumented) which had 2 helices. Figure 3.4 shows a schematic of the research piles with three helices installed to a depth of 3.05 m, 5.18 m, with a typical production pile having double helices installed to a depth of 5.18 m.

The helical piles used in lateral tests were designed to have the same geometry, and were installed to a depth of 5.18 m. Two types of wall thickness (t) were chosen 6.71 mm and 8.18 mm respectfully. The shaft wall thickness of the anchor was varied in order to compare the difference in ultimate capacity under lateral loading due to the structural stiffness.

Research screw piles were instrumented with five levels of strain gauges and a load cell at the base of the pile to evaluate the load transformation phenomena during the installation and load testing of the screw pile. Strain gauges were installed inside of the 219 mm diameter steel. The pipes were cut into short sections allowing strain gauges to be mounted inside to protect the instrumentation during installation. The sections were then welded together with the 356 mm diameter helices fully affixed to the central shaft at last. All the strain gauges were protected by a silicon shell and fiberglass insulation to avoid extreme heating during assembly of the pile and from excessive moisture during testing as shown

in Figure 3.5. The assembling and welding stages of preparing the research piles are presented in Figure 3.6, Figure 3.7, and Figure 3.8.

A systematic design was created for the strain gauge installation, wiring, and data collection. At each level, three strain gauges were installed 120° apart around the diameter to capture different loading conditions both for axial and lateral tests. Strain rosettes were used, with each rosette having three gauges whose axes are 45° apart. In addition, load cells were installed inside of the tip of the pile as demonstrated in Figure 3.9 and Figure 3.10. However, to protect the load cell from damage during installation, the load cell could only be installed about 0.3 m from the bottom of the screw pile. Consequently, there was a total of 49 channels, including 45 sensors from the 5 levels of strain gauges, 2 displacement transducers and 2 load cells, that all require monitoring during the test. A data logger system, CR10 with 3 multiplexers (AM416), was adopted to control the real time collection, and retrieve the stored data. Figure 3.11 shows the data acquisition system used. A laptop computer was connected to the data acquisition system as shown in Figure 3.12. The computer program provided real time plot data on screen for use in controlling the loading process.

3.3 STRAIN GAUGE AND END LOAD CELL CALIBRATION

The strain gauges and the end load cell were pre-calibrated at the University of Alberta. Sections of steel pile shaft with strain gauges installed inside were loaded in an unconfined compression machine. The output data are collected via the Data Acquisition system. The result were computed and compared to the load apply by the loading system (see Figure 3.13). The end load cells were calibrated in a same manner. The detailed results of the calibration are presented in Appendix A.

Table 3.1: Test Pile Properties

Test	Code	Instrumentation	Total No. of Test	Length L (m)	Shaft Dia. d (mm)	Helices Dia. D (mm)	No. of Helices	Wall Thick. t (mm)	Helix Spacing, S (mm)	H/D Ratio	S/D Ratio
Compression Long	CL	Strain Gauges, and Load Cell	3	5.18	219	356	3	6.71	533	10.46	1.5
Compression Short	CS	Strain Gauge, and Load Cell	2	3.05	219	356	3	6.71	533	4.69	1.5
Compression Production	Cprod.	Non	3	5.18	219	356	2	6.71	1067	10.46	3.0
Tension Long	TL	Strain Gauges	2	5.18	219	356	3	6.71	533	10.46	1.5
Tension Short	TS	Strain Gauges	2	3.05	219	350	3	6.71	533	4.69	1.5
Tension Production	TProd.	Non	2	5.18	219	356	2	6.71	1067	10.46	3.0
Lateral	L264	Strain Gauges	2	5.18	219	356	3	6.71	533	10.46	1.5
Lateral	L322	Strain Gauges	2	5.18	219	356	3	8.18	533	10.46	1.5

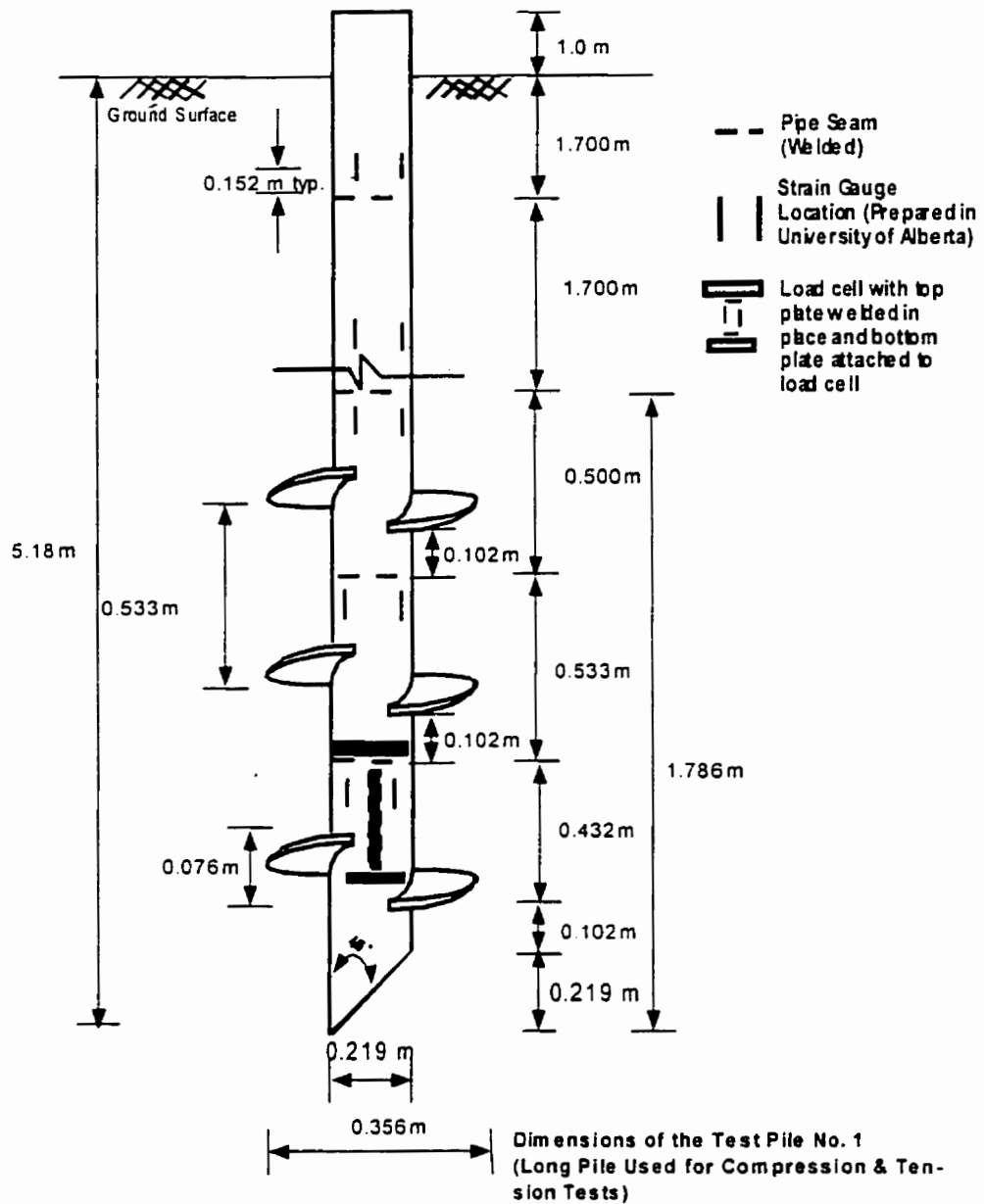


Figure 3.1: Dimensions of the Research Screw Pile Used in Compression & Tension Tests Installed to Depth of 5.18 m (Not to Scale)

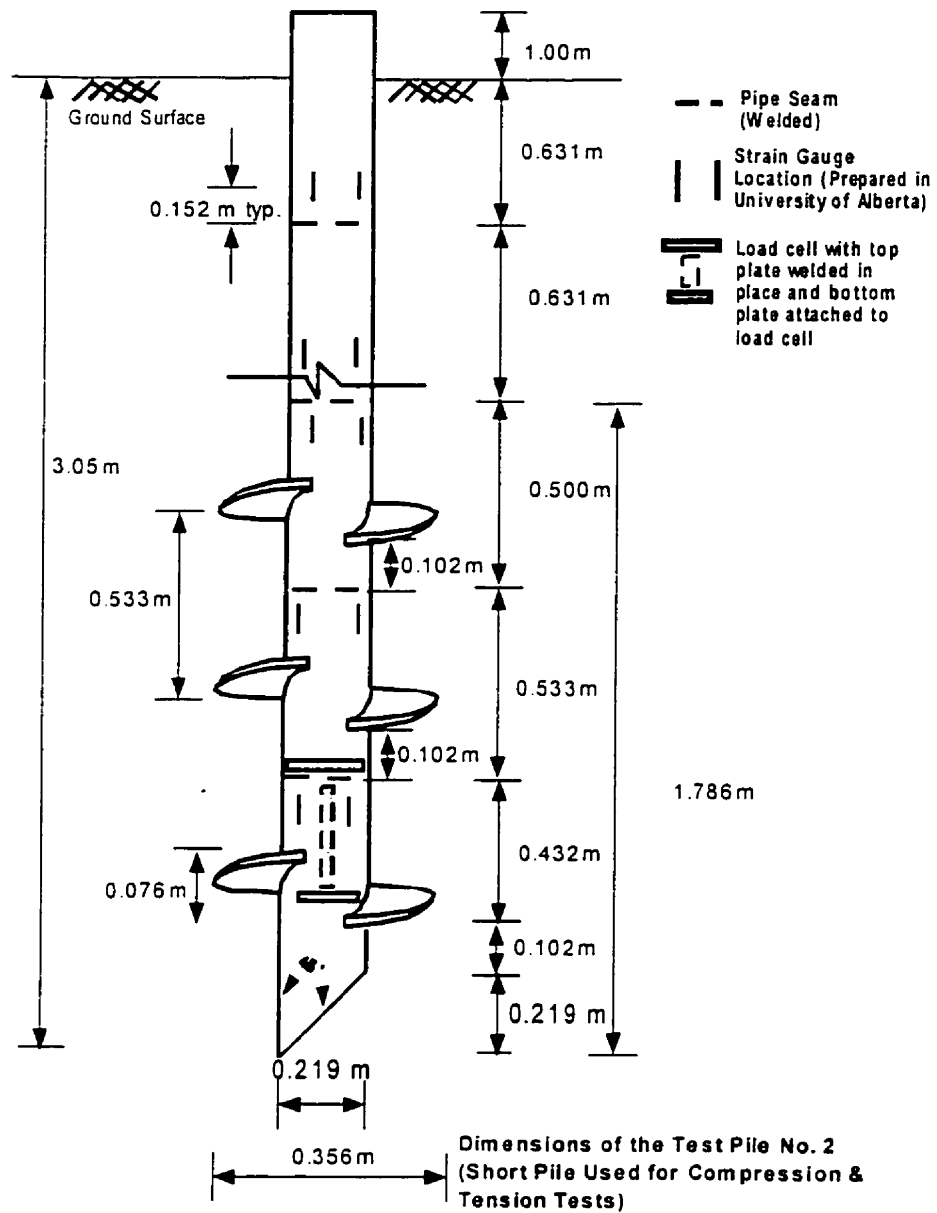


Figure 3.2: Dimensions of the Research Screw Pile Used in Compression & Tension Tests Installed to Depth of 3.05 m (Not to Scale)

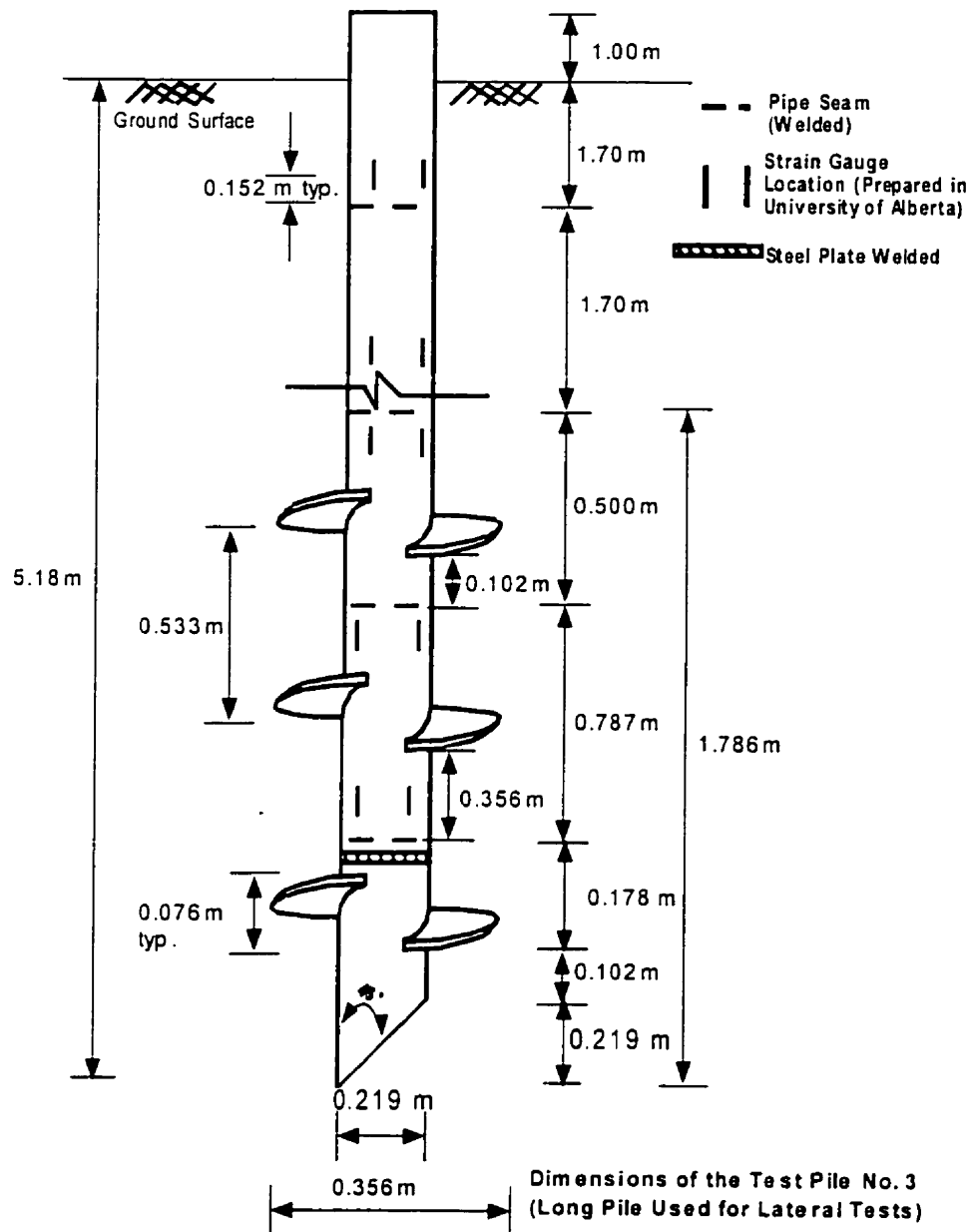
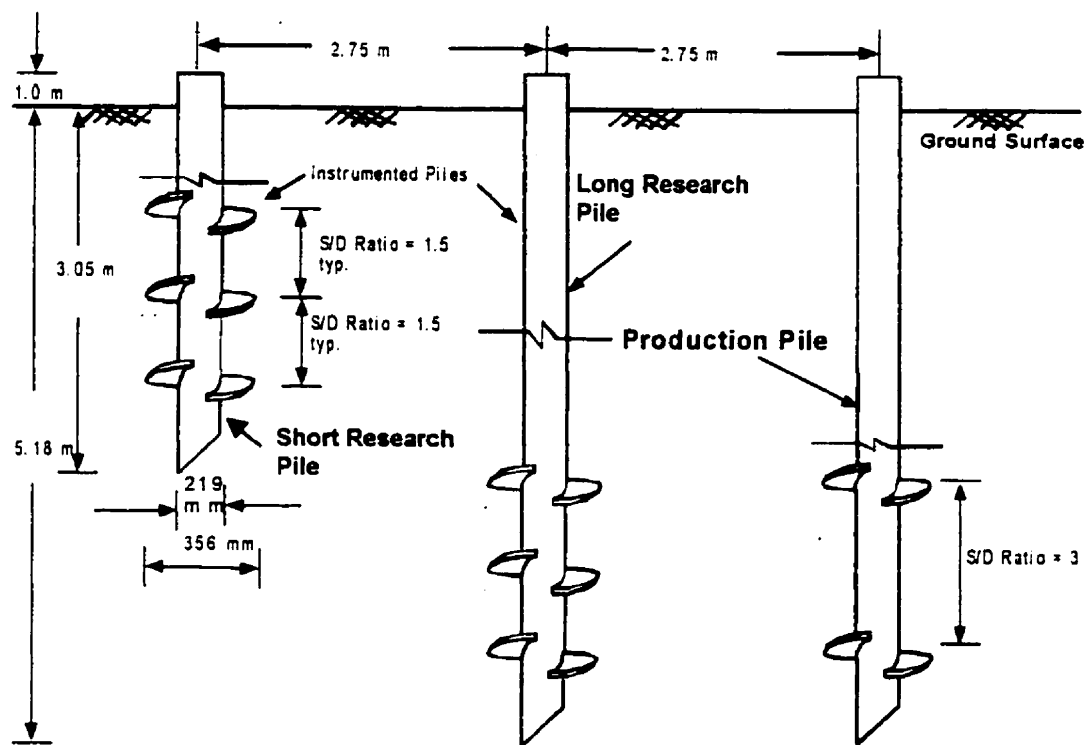


Figure 3.3: Dimensions of the Research Screw Pile Used in Lateral Tests Installed to Depth of 5.18 m (Not to Scale)



Site Profile for Compression and Tension Pile Load Test

Figure 3.4: Comparison of Short, Long, and Production Piles



Figure 3.5: Wires are Protected by Fiber Glass Insulation Prior to Welding of Sections



Figure 3.6: Pile Assembled at Manufacture's Floor Shop

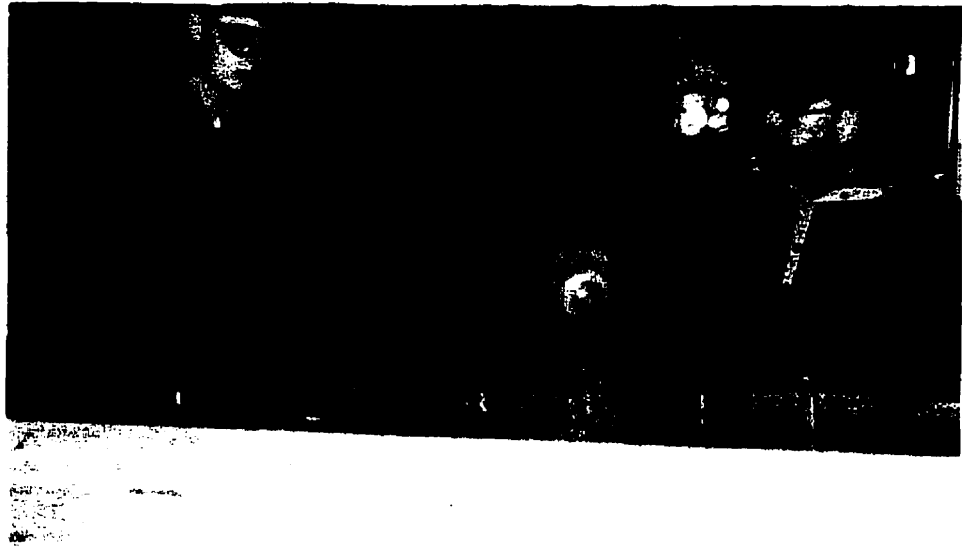


Figure 3.7: Protecting Strain Gauge during Welding by Water Cooling of Sections being Welded



Figure 3.8: Research Pile after Assembly

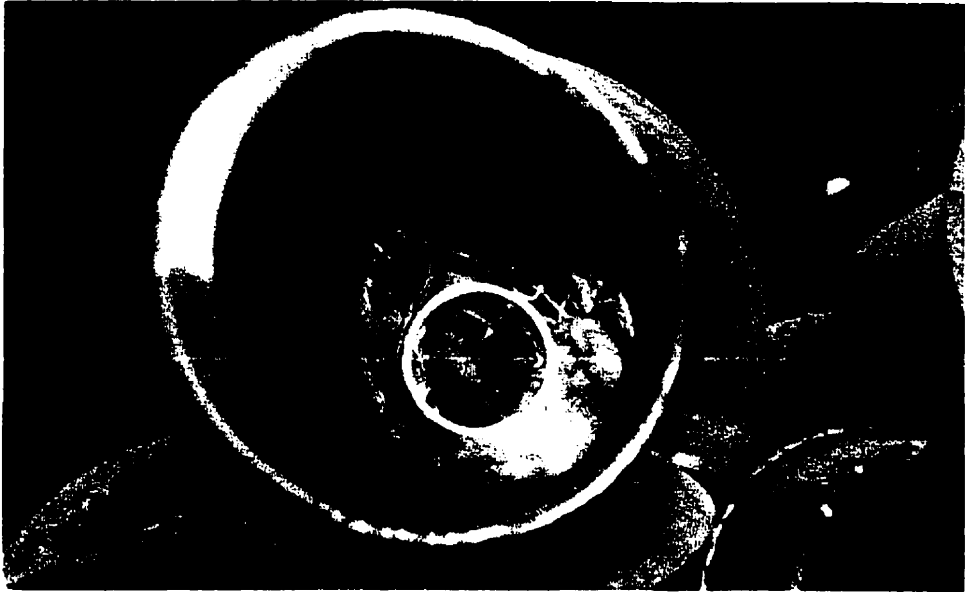


Figure 3.9: Pile End Load Cell Installed Inside of Compression Piles

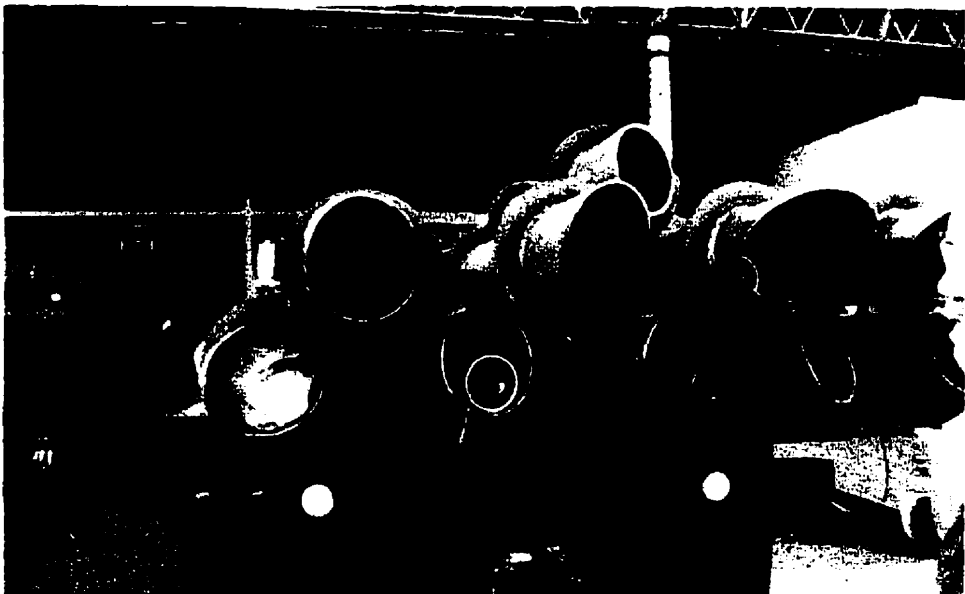


Figure 3.10: Size of Research Piles used in the Test Program

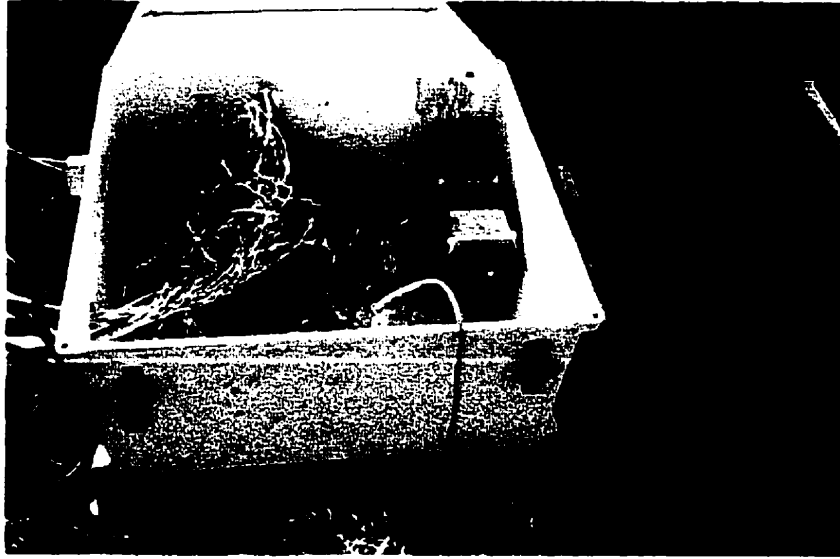


Figure 3.11: Data Acquisition System Used to Collect Test Data

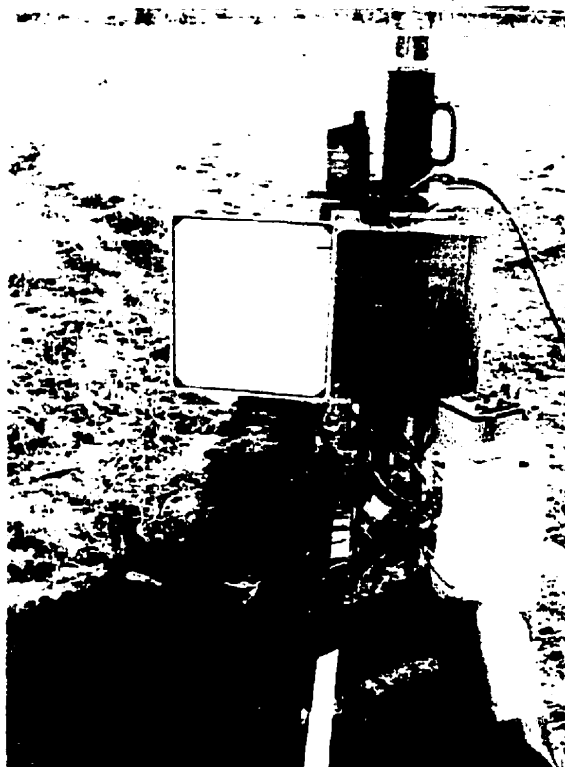


Figure 3.12: Complete Data Collection System Setup

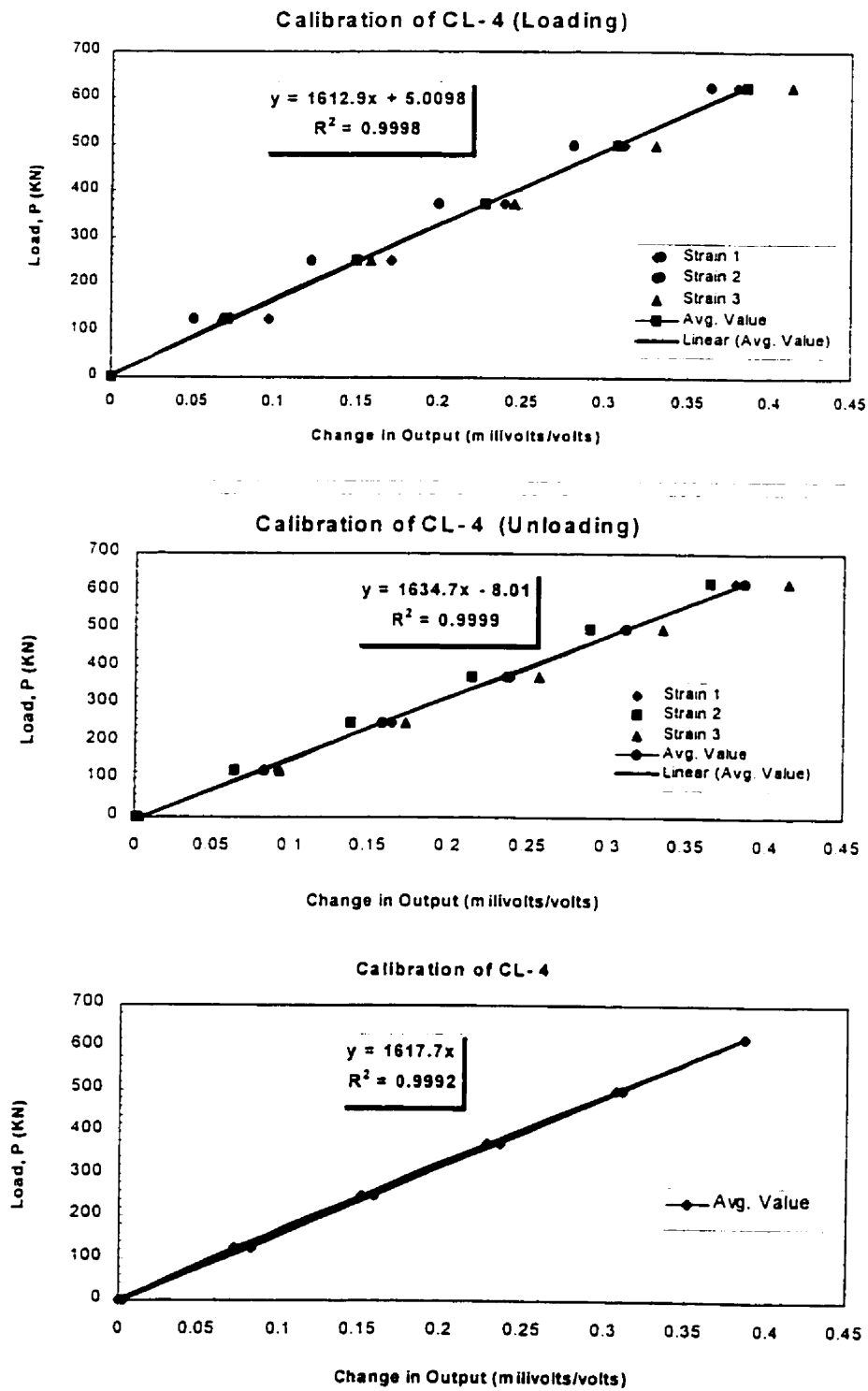


Figure 3.13: Strain Gauge Calibration

4.1 INTRODUCTION

The main objective of this research program is to test screw piles capacity installed in typical soil of Alberta. Therefore, it is important to determine the materials that are considered as representative soil for testing. The review of the geological literatures on Alberta soil indicated that the surficial deposits of Edmonton area consist mainly of well-sorted pre-glacial sands and gravels, glacial till and proglacial lake sediments. Based on the geological information, three "typical" test sites were proposed for the program. The soils chosen were: Lake Edmonton Clay at the University Farm site, Sand Dune at the Sand Pit site and Glacial Till at the Highway 14 Extension. These sites are located in the Edmonton area, allowing easy access for the test equipment. However, as outlined in section 4.3, the glacial till site was not used because the soil profile was determined as similar to the University Farm site. Nevertheless, the site investigation results for the glacial till site are included for future references. The following Chapter describes the geology of the field testing site and site investigation results.

4.2 SITE GEOLOGY**4.2.1 Glacial Lake Edmonton Sediments (University Farm Site)**

Glacial Lake Edmonton deposits are lacustrine sediments, laid down in a large proglacial lake at the close of the Wisconsin glacial period (Bayrock and Hughes, 1962). The general composition of the material includes varved silts and clays, with pockets of till, sand, or sandy gravel found in the sediments (Godfrey, 1993). The lake deposits are more clayey in the uppermost 0.6 m than in the lower bed. The lower lake sediment beds consist of fine sand and

till-like lenses of clay with scattered pebbles. The University Farm site, marked in Figure 4.1, is located in central Edmonton near 115 Street, and 58 Avenue.

4.2.2 Sand Dunes (Sand Pit Site)

The sand dunes are of minor loess that composes of medium- to fine-grained sand with silt. The material consists of dried sediments of the glacial lake, mainly lake-bed muddy silts and beach sand which were transported by wind and re-deposited in a nearby sand dune field after the drainage of the glacial lake. The testing site is located outside of Bruderheim, northeast of Edmonton. The Sand Pit site is approximately 7.5 km north of Bruderheim town center. Figure 4.2 illustrates the test site location.

4.2.3 Glacial Till

Sediments deposited by the glacier without washing or sorting make up the glacial till. Till is composed of mixed clay, silt and sand, with pebbles and boulders, lenses of sand, gravel and local bedrock. This material is the most significant parent material from which Alberta soil has developed (Bayrock and Hughes, 1962).

Cone Penetration tests were performed on a site located near 17 Street, and the highway 14 extension. The material is defined as lacustrine till but this site was later eliminated as a test site due to the similarity of the CPT profile with the University Farm Site.

4.3 SITE INVESTIGATION

4.3.1 Site Investigation Program

The site investigation for the field test program comprised both Cone Penetration tests (CPT) and Standard Penetration test (SPT) at each site. ConeTec Investigation Ltd. sponsored the in situ site investigation program by performing the Cone Penetration test with their cone truck with a penetration load capacity of 10 tons as illustrated in Figure 4.3 at the University Farm site and the Till site. Mobile Auger and Research Ltd. performed the SPT and a modified CPT test, called the Downhole Cone Penetrometer Test (DCPT), at the University Farm site and the Sand Pit site (see Figure 4.4).

Cone Penetration tests were performed at each site to a minimum depth of 7.5 m to assist in determining the soil stratigraphy and variation in shear strength within the soil profile. Two types of Cone Penetrometer were used for the site investigation. The conventional electric piezometer, a cone with an apex angle of 60° , 10 cm^2 base area, and a standard friction sleeve with surface area of 150 cm^2 (refers to Figure 4.5 and Figure 4.6), was used at the University Farm site where the material was cohesive, and uniform. The procedure to perform a CPT test is outlined in ASTM D3441-86. At the Sand Pit site, a simple but rugged electric cone penetrometer (DCPT) was used. Figure 4.7 compares the design of a standard Cone Penetrometer (CPT) and a Down Hole Cone Penetrometer (DCPT). The new cone developed at the University of Alberta, has a diameter of 46 mm with a projected area of 16.6 cm^2 (Treen et al., 1992). The DCPT modifies the equipment and procedure of the standard CPT and can be performed by using locally available drilling rigs (see Figure 4.8 and Figure 4.9). The DCPT is a useful and economic in situ test developed for regions where stiff glacial soils are the dominant surficial material. The robust and simple design allows the cone to be pushed through much stronger soil material ranging from

very stiff soils to soft bedrock. Treen et al. (1992) described the basic procedure of performing the DCPT as follows:

1. The electric Downhole Cone Penetrometer, attached to a 1.5 m length of standard AW drill rod (see Figure 4.10), is set up in the same manner as the SPT split spoon sampler. The penetrometer is then lowered to the bottom of the open borehole where the properties of the soil material are being investigated.
2. The Downhole Cone Penetrometer is pushed into the base of the borehole at a nearly constant rate of 2 cm/sec for a length of 1.5 m (see Figure 4.10). Data are recorded using a data acquisition system, which records a continuous cone tip penetration resistance over a length of 1.5 m. For soils that are more uniform and less stiff, the greater push force available allows a continuous cone tip resistance profile to whatever penetration depth is desirable. In this case, 1.5 m extension rod is attached to the AW rod and DCPT is pushed for another 1.5 m. The test continues to a depth where the DCPT meets refusal.
3. For stronger and non-uniform soil that might damage the cone, the penetrometer is removed from the borehole after the data are transferred to the computer. The borehole is then advanced using drilling and the above process is repeated. In this case, a near continuous, repeatable profile of cone penetration resistance profile is generated with gaps through the stiffer zones.

Treen et al. (1992) indicated that the equipment and procedures for performing the DCPT should not deviate significantly from the standard CPT in order to utilize existing research correlations developed for CPT. At the University Farm site, both cone penetrometers were used in order to compare the consistency of the field results. It can be seen from Figure 4.16 that the results from DCPT produced an almost identical profile of penetration resistance,

q_c , as compared to the standard CPT. This indicates that DCPT test can still maintain a degree of sensitivity in soft soils despite its robust and simple design. At the Sand Pit site, the DCPT was performed continuously to a depth of 7.5 m because the push force provided by the drill rig was sufficient to penetrate the medium dense sand deposit. Therefore, a continuous cone penetration profile that is comparable to CPT profile was generated.

One conventional boring using a solid stem auger was advanced at the University Farm site and the Sand Pit site. The Standard Penetration Test (SPT) was performed to a depth of approximately 6.0 m at intervals of about 0.76 m using a safety hammer as shown in Figure 4.12.

4.3.2 Site Investigation Result

4.3.2.1 Stratigraphic Interpretation

One application of the Cone Penetration Test (CPT) is to provide an estimate of the soil stratigraphy at a site. A typical summary report is shown in Figure 4.13 where the continuous CPT profiles of cone penetration resistance (q_c), sleeve friction (f_s), and friction ratio (R_f) are presented. Figure 4.13 to Figure 4.15 present a complete summary of the CPT soundings performed at three testing sites. The results for the Standard Penetration Test and the SPT “N” counts at various depths are shown in the figures.

In recent years, charts have been developed to classify soil type based on CPT data (Robertson and Camanella, 1983, Robertson, 1990). Researchers have shown that there is a relationship between the CPT friction ratio, the fines content and soil plasticity. Based on this observation, most classification chart proposed to use the friction ratio (ratio of the CPT sleeve friction f_s and the cone tip resistance q_c) to classify the soil type since this ratio increases with increasing fines content and soil plasticity. Robertson (1990) proposed a soil behavior type chart based on the normalized tip resistance, Q , and the normalized friction ratio,

F , as shown in Figure 4.17. Nine zones are used to define nine soil behavior types. In addition, a zone that represents normally consolidated soil is defined to provide an estimation of stress history of the material. In conjunction with the soil behavior type chart, Table 4.1 can be used to estimate the unit weight of the soil from each zone. Figure 4.18 to Figure 4.20 plots the result of CPT data for three sites on the soil behavior type chart.

The soil profile is interpreted according to the CPT data using the soil behavior type chart and the borehole information available. At the University Farm site, the top 0.45 m of the soil consists of clay mixed with gravels that are the result of the site being used as a snow dump for the University of Alberta. The CPT profile shows that the upper 4 m of soil consists of uniform clay. For the depth of 4.0 – 7.5 m, the soil consists of interbedded silty clay and clay silt. The soil becomes more silty and sandy beyond 7.5m. The ground water level was located around 3.0 m in depth. At the Till site, the top 0.8 m was drilled to avoid having the electronic cone damaged by pebbles. The zone, 0.8 m to 1.2 m consists of mainly clay. There is a thin layer of silt, approximately 0.3 m, located beneath the clay layer. From 1.5 m to 5.5 m, the soil profile was mainly clay. Between 5.5 m to 8.5 m, the soil consists of interbedded silty clay and clayey silt. The ground water table was found to be at approximately 3.5 m depth. For the Sand Pit site, the top soil are clean sand to a depth of 0.75 m. Between 0.75 m to 2.75 m, the soil is medium grain sand to silty sand. From 2.75 m to 5.0 m, the soil is a sand mixture of silty sand to sandy silt. Below 5.0 m, the soil is a silt mixture of clayey silt to silty clay. The ground water level was encountered at approximately 4.5 m in depth.

It can be seen from Figure 4.18 that the University Farm soil falls in zone 4, which is a slightly over-consolidated clayey silt to silty clay mixture. The Sand Pit material is classified as clean sand to silty sand (see Figure 4.19). Comparing the soil behavior type charts for the University Farm site and the Till site (see Figure 4.20), the results demonstrated that the CPT profiles of the Lake Edmonton Clay and the Glacial Till around Edmonton area are very

similar. The Glacial Till profile also falls in zone 4, which can be considered as a silt mixture consisting of clayey silt to silty clay. For zone 4 material found on the University Farm site, the unit weight estimated is approximately 18 kN/m³. For the Sand Pit site, the unit weight of the soil is around 18 to 19 kN/m³.

4.3.2.2 Soil Strength Properties

The tip resistance obtained from the cone penetration log can be used to evaluate the undrained shear strength, C_u of clays. Equation 4.1 is usually employed to estimate the C_u (Robertson and Campanella, 1988):

$$C_u = \frac{q_c - \sigma_{vo}}{N_k} \quad \text{Equation 4.1}$$

where

C_u = undrained shear strength of clay
 q_c = tip resistance from CPT profile
 σ_o = the in-situ total overburden pressure
 N_k = the cone factor

The cone factor is an empirical factor that is generally obtained from correlations. Lunne and Kleven (1981) indicated that the cone factor N_k has a range between 11 and 19, with an average of 15 for normally consolidated marine clays based on the field vane strength. Figure 4.21 shows the result of the undrained shear strength profile for the University Farm site and the Till site. At the University Farm site, the top 1.2 m is considered as soft to stiff clay and has an average undrained shear strength of 50 kPa. The material becomes stiffer between 1.2 m to 7.5 m, with an average value of 100 kPa.

The overconsolidation ratio (OCR) is used to describe the stress history of the material on site. It is typically defined as the ratio of the maximum past effective consolidation stress to the present effective overburden stress. If the

plasticity index, PI , is not known, a quick calculation of C_u / σ_{vo}' gives an estimate of overconsolidation ratio, OCR for clays. Schmertmann (1978a) indicates that $(C_u / \sigma_{vo}')_{NC}$ ratio for most normally consolidated post-pleistocene clay can be assumed be approximately equal to 0.33. The $(C_u / \sigma_{vo}')_{NC}$ ratio line, shown in Figure 4.21 indicating that the Lake Edmonton Clay is over-consolidated for the soil deposits found at the University Farm site. Schmertmann (1978a) suggested a chart for estimating OCR based on normalized C_u / σ_{vo}' ratio (see Figure 4.22). Based on this chart, the material at the University Farm site is over-consolidated in the upper 2.3 m having an OCR value, which ranges from 3.3 to 5.5. Below 2.3 m, the soil is less overconsolidated with a typical OCR value of between 1.1 to 3.0.

Standard Penetration Test, N count can be used to estimate shear strength of the soils. Many empirical correlations have been developed based on the SPT N count value. However, the major concern with using SPT correlations is the variability in equipment and test procedures encountered in practice throughout the world. A reliable SPT test result can only be obtained under controlled conditions, and by standardized equipment with measured energy ratio (ER_r = energy that is delivered to the drill stem) recorded during a SPT. N values measured with a known or estimated rod energy ratios (ER_r) should be normalized to a standard by the conversion (Robertson and Ghionna, 1987):

$$N_{60} = N \times \frac{ER_r}{60} \quad \text{Equation 4.2}$$

Table 4.2 gives a procedure to correct the SPT N count according to the energy ratios and test practices. To estimate the undrained shear strength of a cohesive material based on the corrected SPT N value, Bhanot (1968) provided a relationship as follow:

$$C_u = 0.87 N \quad \text{Equation 4.3}$$

Where

C_u = undrained shear strength
 N = SPT N count

Bhanot (1968) provided a detail study on the index properties and the laboratory shear strength values of the Lake Edmonton Clay. As part of his Ph. D thesis, Bhanot was involved in conducting a pile load testing program on a large diameter bored pile installed at the University Farm site. His test site was located approximately 1.0 km away from the current test site. The laboratory values that were presented in his thesis are considered as a valuable reference for the comparison with the CPT data collected in this study. Figure 4.23 presents the classification of the soil collected from various depths, based on the Casagrande's Plasticity chart. Soil composition, natural moisture content, liquid limit, plastic limit, degree of saturation and bulk density of the University Farm soil are shown in Figure 4.24. The upper 4.27 m (14 feet) is classified as mainly clay (> 50 % clay), with a bulk unit weight of approximately 18.5 kN/m³. Below 4.27 m, the soil is predominantly sandy silt, with a bulk unit weight of 21.5 kN/m³ for the rest of the depth. In addition, the author indicated that the upper layer is overconsolidated due to desiccation. In the lower layer till, soil is consolidated due to the weight of the receding glacier. Soil is highly plastic in the upper 4.27 m, but shows a rapid decrease in the value of plasticity index below this depth. Bhanot also presented the laboratory experiments results including unconfined compressive strength tests, shear box tests and undrained triaxial tests, and field SPT results. The results are presented in Figure 4.25 and Table 4.3. Figure 4.25 shows the moisture content, N values and shear strength versus depth. Table 4.3 summarizes the results of undrained triaxial compression tests on undisturbed and remolded recompacted samples of clay and till taken from the University Farm site.

The strength profile for the Till site is provided to compare the material strength variation with that of the Lake Edmonton Clay (the University Farm site). The profile indicates that between 0.8 m to 3.0 m, the material has an

undrained strength around 100 kPa. Below 3.0 m, the soil strength increases to around 140 kPa. The Glacial Till site is considered as stiff clay. On the basis of the results from soil classification and soil strength, the profile for the Glacial Till profile is comparable to the Lake Edmonton Clay with a slight increase of undrained shear strength. Therefore, no justification could be found for testing two cohesive sites with similar CPT profiles. Therefore, testing at the Glacial Till site was postponed until a more suitable location with a significantly greater cone resistance could be found.

Evaluation of sand strength parameter was performed using in situ test data, the Cone Penetration test (CPT) and the Standard Penetration test (SPT). In general, the soil internal friction angle, ϕ , and soil density, D_r , are the two important parameters that are needed in designing of a deep foundation.

Many theoretical and empirical correlations have been developed for estimating the friction angle, ϕ , of uncemented cohesionless soils by using cone tip resistance, q_c . A simplified empirical method, named state parameter approach developed by Robertson and Campanella (1983b), correlates the soil friction angle with the cone tip resistance q_c as shown in Figure 4.26. Durgunoglu and Mitchell (1975) proposed a method to evaluate ϕ based on the bearing capacity theory for sand with $K_o = 1.0$. The method is presented in a useful graphical form as shown in Figure 4.27. Balidi et al. (1986) proposed a relationship between the relative density D_r and the cone tip resistance q_c based on calibration chamber tests performed on Ticino sand. Figure 4.28(a) shows the correlation between D_r and q_c for normally consolidated (NC), uncemented, unaged silica Ticino sand. Skempton (1986) stated that the D_r versus q_c relationships are dependent on the aging of the cohesionless soil. The use of Figure 4.28(a) will overestimate D_r when applied to natural aged sands. Therefore, it is recommended to use Figure 4.28(b) if the stress history of the soil is unknown. Nevertheless, the correlations in Figure 4.28 should be used only as a guide to in situ relative density. Vesic (1975) indicated that the rigidity index I_r can be used to estimate the bearing capacity of a deep foundation based on

the cavity expansion theory (Vesic, 1975). Baldi et al. (1986) suggested that the pile tip behavior is similar to that of the CPT and the following relationship can be used to estimate I_r :

$$I_r = \frac{170}{R_f} \quad \text{Equation 4.4}$$

where

I_r = rigidity index

R_f = friction ratio in percent

Several empirical correlations have been proposed to estimate the soil friction angle, ϕ of normally consolidated sands based on in situ SPT results. Figure 4.29 shows an empirical approach developed by Peck, Hanson and Thornburn (1974) by relating SPT N-count value, ϕ , and σ'_{vo} for cohesionless soils. Similarly, De Mello (1971) developed a correlation based on the experimental data from Gibbs and Holtz (1957) as shown in Figure 4.30. Robertson and Ghionna (1987) indicated that De Mello's approach gave reasonable but more conservative results. However, the correlation was developed based on data without knowing the energy level during the SPT, therefore, using Figure 4.30 to estimate ϕ should be viewed with caution. Figure 4.31 shows a correlation for relative density D_r developed by Gibbs and Holtz (1957) using SPT data. It is important to understand that the empirical relationships provided to estimate D_r using SPT results has many uncertainties, such as SPT energy corrections, compressibility and age of sand and the in-situ horizontal stresses (Robertson and Ghionna, 1987). Therefore, the correlations should be used as an estimate. Bowles (1988) provided correlations for unit weight, relative density, and angle of internal friction angle, as shown in Table 4.4. The relationships shown in Table 4.4 for D_r and ϕ are related roughly to $N_{70} = {}^{60}_{/70} \times N_{60}$ and for borehole depths in the order of 4 to 6 m.

CPT profiles and SPT value are plotted on Figure 4.26 to 31. The estimated D_r and ϕ , based on Bowles (1988) method, is provided in Table 4.5 and Table 4.6 summarized the results from SPT correlations. Estimation of D_r and ϕ , based on CPT tip resistance q_c , indicated that ϕ ranges from 39° to 45° with D_r ranges between 80% to 90% for the upper 3.0 m of the soil stratigraphy. Friction angle ϕ decreases to a value of 30° and D_r decreases to approximately 30 % at depth of 5.0 m. The high friction angle is a result of a desiccated soil crust, therefore, the lower bound average value of 39° to the depth of 5.0 m, and a value of 30° for depth below 5.0 m, is recommended to use in design.

4.4 REFERENCES

- ASTM D1586-84 (1984). "Standard Method for Penetration Test and Split-Barrel Sampling of Soils"; (Reapproved 1984), Annual book of ASTM Standards, 1991, Philadelphia, PA, Vol. 04.08, pp. 232-236.
- ASTM D3441-86 (1986). "Standard Test Method for Deep, Quasi-Static, Cone and Friction-Cone Penetration Tests of Soil"; (Reapproved 1986), Annual book of ASTM Standards, 1991, Philadelphia, PA, Vol. 04.08, pp. 439-444.
- Balidi, G., Bellotti, R., Ghionna, V., Jamiolkowski, M. and Pasqualini, E. (1986). "Interpretation of CPTs and CPTUs; 2nd part: drained penetration of sands". Proceedings of the Fourth International Geotechnical Seminar, Singapore, 143-56.
- Bayrock, L. A. and Hughes, G.M. (1962). "Surficial Geology of the Edmonton District"; Alberta Research Council of Alberta, Preliminary Report 62-6.
- Bayrock, L. A., and Berg, T.E. (1966). "Geology of the City of Edmonton. Part I: Central Edmonton"; Research Council of Alberta, Report 66-1, pp.10-13.
- Bhanot, K. L. (1968). "Behavior of Scaled and Full-Length Cast-In-Place Concrete Piles"; Doctor of Philosophy Thesis, Department of Civil Engineering, University of Alberta, Edmonton Canada.
- Bowles, J. E. (1988). "Foundation Analysis and Design"; 4th Edition, McGraw-Hill International Editions.
- De Mello, V. F. B. (1971). "The Standard Penetration Test"; Proceedings of the Fourth Panamerican Conference on Soil Mechanics and Foundation Engineering, ASCE, Vol. 1, pp. 1-86.
- Durgunoglu, H. T., and Mitchell, J. K. (1975). "Static Penetration Resistance of Soils: I – Analysis"; Proceedings Special Conference on In Situ Measurement of Soil Parameters, Raleigh, Vol. I.
- Gibbs, H. J., and Holtz, W. G. (1957). "Research on Determining Density of Sand by Spoon Penetration Testing "; Proceedings 4th ICSMFE, London, Vol. 1, pp. 35-39.
- Godfrey, J. D., (1993). "Edmonton Beneath Our Feet: A Guide to the Geology of the Edmonton Region"; Edmonton Geological Society, Edmonton Canada.

- Lunne, T. and Kleven, A., (1981). "Role of CPT in North Sea Foundation Engineering"; Symposium on Cone Penetration Testing and Experience, Geotechnical Engineering Division, ASCE, Oct. 1981, pp. 49-75.
- Lunne, T.; Robertson, P. K., and Powell, J. J. M. (1997). "Cone Penetration Testing in Geotechnical Practice"; Blackie Academic & Professional. First edition. p. 312.
- Peck, R. B., Hanson, W. E., and Thornburn, T. H. (1974). Foundation Engineering, 2nd Edition, John Wiley, New York, 1974.
- Robertson, P. K., and Campanella, R. G. (1983a). "Interpretation of Cone Penetration Tests, Part I: Sand"; Canadian Geotechnical Journal, Ottawa, Vol. 20, no. 4, pp. 718-733.
- Robertson, P. K., and Campanella, R. G. (1983b). "Interpretation of Cone Penetration Tests, Part II: Clay"; Canadian Geotechnical Journal, Ottawa, Vol. 20, no. 4, pp. 718-733.
- Robertson, P. K., Campanella, R. G., Gillespie, D., and Greig, J. (1986). "Use of Piezometer Cone Data"; Proceedings of the ASCE Specialty Conference In Situ' 86: Use of In Situ Tests in Geotechnical Engineering, Blacksburg, 1263-80, American Society of Engineers (ASCE).
- Robertson, P. K., and Ghionna, V. N. (1987). "Capability of In-Situ Testing"; Received As Classnotes for Civ E 591 in the Department of Civil and Environmental Engineering at University of Alberta.
- Robertson, P. K., and Campanella, R. G. (1988). "Design Manual for Use of CPT and CPTU"; Pennsylvania Department of Transportation, (Penn Dot), 200 p.
- Robertson, P. K. (1990). "Soil Classification Using the CPT"; Canadian Geotechnical Journal, Ottawa, Vol. 21, no. 1, pp. 151-158.
- Schmertmann, J. H. (1978a). "Guidelines for Cone Penetration Test, Performance and Design"; Federal Highway Administration, Report FHWA-TS-78-209, Washington, July 1978, 145 p.
- Skempton, A. W. (1986). "Standard Penetration Test Procedures and the Effects in Sands of Overburden Pressure, Relative Density, Particle Size, Ageing and Overconsolidation"; Geotechnique, Vol. 36, No. 3, pp.425-447.

Treen, C.R., Robertson, P.K., and Woeller, D.J. (1992). "Cone Penetration Test in Stiff Glacial Soils using A Downhole Cone Penetrometer"; Canadian Geotechnical Journal, 29: 448-455.

Table 4.1: Estimate of Unit Weights based on Soil Behavior Type Classification System (see Figure 4.17, after Lunne et al., 1997)

Zone	Approximate Unit Weight
	(kN/m ³)
1	17.5
2	12.5
3	17.5
4	18
5	18
6	18
7	18.5
8	19
9	19.5
10	20
11	20.5
12	19

Table 4.2: Corrections for SPT Test (after Robertson and Ghionna, 1987)

RECOMMENDED GENERALIZED CORRECTIONS TO MEASURED SPT-N VALUES
FOR: ENERGY RATIOS, SAMPLER, ROD LENGTH AND BOREHOLE DIAMETER

$$N_{60} = N_{SPT} \cdot \frac{ER}{60} \cdot C_s \cdot C_r \cdot C_d$$

• ER = ENERGY RATIO

• $C_s = \frac{N_{SPT} \text{ (STANDARD SAMPLER)}}{N_{SPT} \text{ (SAMPLER WITHOUT LINER)}} = 1.2$

• $C_r \begin{cases} = 1: \text{ROD LENGTH (RL)} \geq 10 \text{ m} \\ < 1: \text{ROD LENGTH (RL)} < 10 \text{ m} \end{cases}$

• $C_d \begin{cases} = 1: \text{BOREHOLE DIAMETER (d)} \leq 115 \text{ mm} \\ > 1: \text{BOREHOLE DIAMETER (d)} > 115 \text{ mm} \end{cases}$

RL m	3 to 4	4 to 6	6 to 10	≥ 10
C_r	.75	.85	.95	1

d mm	65 115	150	200
C_d	1	1.05	1.15

Generalized energy corrections:

COUNTRY	HAMMER	RELEASE	ER(%)	$\frac{ER}{60}$
NORTH & SOUTH AMERICA	DONUT SAFETY AUTOMATIC	2 T. of R.	45	0.75
		2 T. of R.	55	0.92
		TRIP	55 to 83	0.92 to 1.38
JAPAN	DONUT DONUT -	2 T. of R.	65	1.08
		Auto-Trigger	78	1.30
CHINA	DONUT AUTOMATIC	2 T. of R.	50	0.83
		TRIP	80	1
U.K.	SAFETY AUTOMATIC	2 T. of R.	50	0.83
		TRIP	80	1
ITALY	DONUT	TRIP	65	1.08

2 T. of R. = TWO TURNS OF ROPE

Table 4.3: Results of Undrained Triaxial Compression Tests on Undisturbed and Remolded Recompacted Samples of Clay and Till (modified from Bhanot, 1968)

Depth below Ground Surface (ft.)	Soil Description	Undisturbed Samples		Remolded Recompacted Samples	
		Undrained Cohesion: C_u (psi.)	Angle of Shearing Resistance: ϕ_u (degrees)	Undrained Cohesion: C_{ru} (psi.)	Angle of Shearing Resistance: ϕ_{ru} (degrees)
3	Very hard brittle clay	-	-	13.8	25.4
6	Stiff clay with some silt	26.9	26.0	16.1	14.5
9	Stiff highly, Plastic clay	-	-	8.5	3.5
12	Stiff highly, plastic clay	13.1	4.5		
15	Stiff highly, plastic clay	-	-	8.5	3.5
16	Silty-sandy clay	10.1	4.5		
		9.0	3.5		
		13.5	8.5		
20	Silty-clay sand	7.8	11.5	-	-
24	-	-	-	3.0	19.5
27-30	-	-	-	5.5	25.0
30-45	-	-	-	4.9 to 5.5	15.5 to 25.0
45-50	-	-	-	5.5	25.0

Table 4.4: Empirical Values for ϕ , D_r , and Unit Weight of Normally Consolidated Granular Soils Based on the SPT (after Bowles, 1988)

Description	Very loose	Loose	Medium	Dense	Very dense
Relative density D_r	0	0.15	0.35	0.65	0.85
SPT N_{60} : fine	1-2	3-6	7-15	16-30	?
medium	2-3	4-7	8-20	21-40	>40
coarse	3-6	5-9	10-25	26-45	>45
ϕ : fine	26-28	28-30	30-34	33-38	
medium	27-28	30-32	32-36	36-42	<50
coarse	28-30	30-34	33-40	40-50	
γ_{wet} , pcf	70-100†	90-115	110-130	110-140	130-150
(kN/m ³)	(11-16)	(14-18)	(17-20)	(17-22)	(20-23)

† Excavated soil or material dumped from a truck will weigh 11 to 14 kN/m³ and must be quite dense to weigh much over 21 kN/m³. No existing soil has a $D_r = 0.00$ nor a value of 1.00—common ranges are from 0.3 to 0.7.

Table 4.5: Strength Determination of Sand Pit Soil Using SPT Data (after Bowles, 1988)

Depth (m)	SPT N	Relative Density D_r (%)	Friction Angle ϕ'	γ_{wet} (kN/m ³)
0.762	11	37.7	33	17.3
1.524	15	43.2	35	17.8
2.286	14	37.5	33	17.3
3.048	11	34.5	32	17
3.81	8	18.3	30	16
4.572	6	18	30	16
5.334	4	15	30	14

Table 4.6: Strength Determination of Sand Pit Soil Using SPT Data (after De Mello, 1971 and Gibbs and Holtz, 1957)

Depth (m)	SPT N	Relative Density D_r (%)	Friction Angle ϕ'
0.762	11	75	42
1.524	15	75	42
2.286	14	65	39
3.048	11	50	36
3.81	8	39	30
4.572	6	-	27.5
5.334	4	-	24

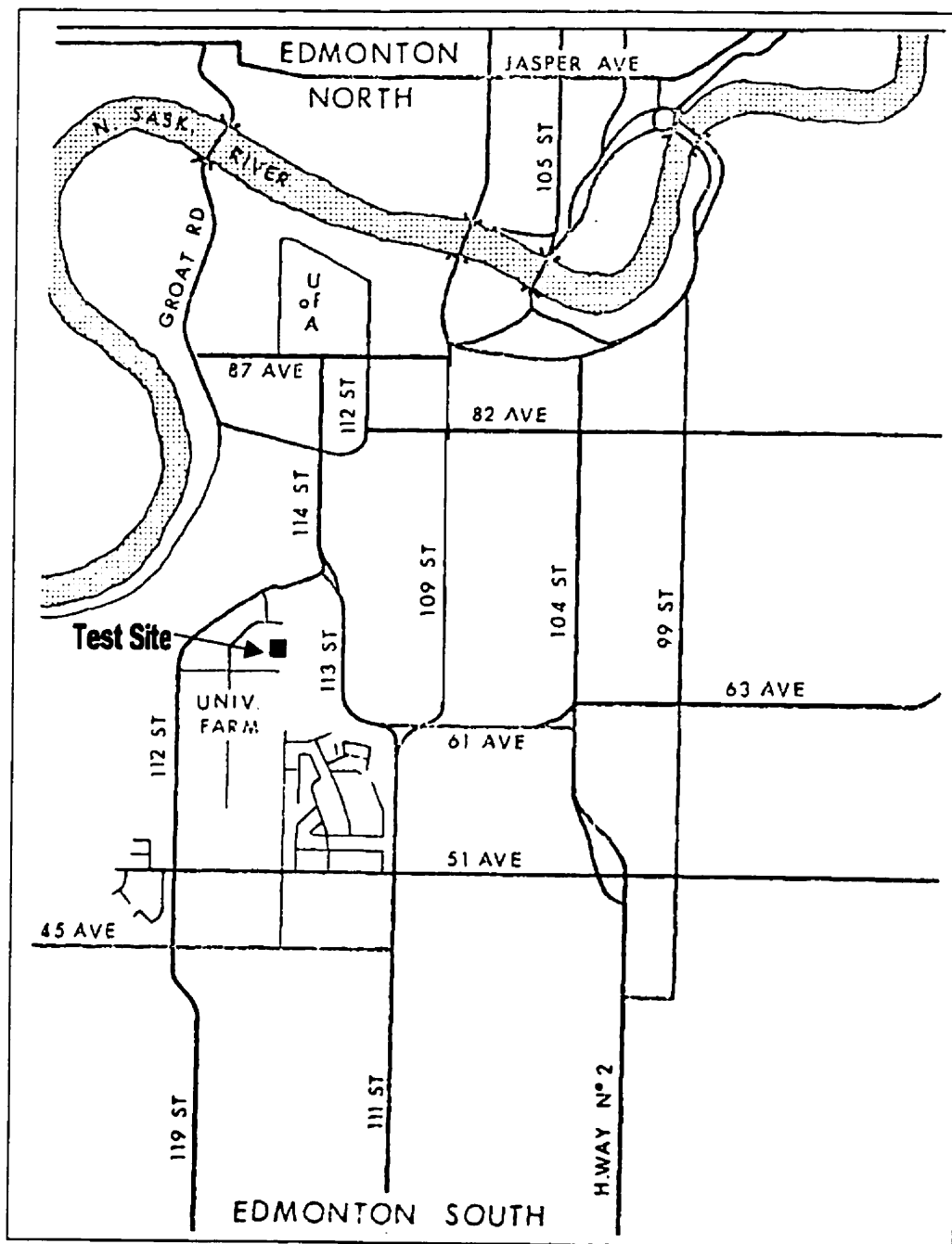


Figure 4.1: University Farm Pile Test Location (after Bhanot, 1968)

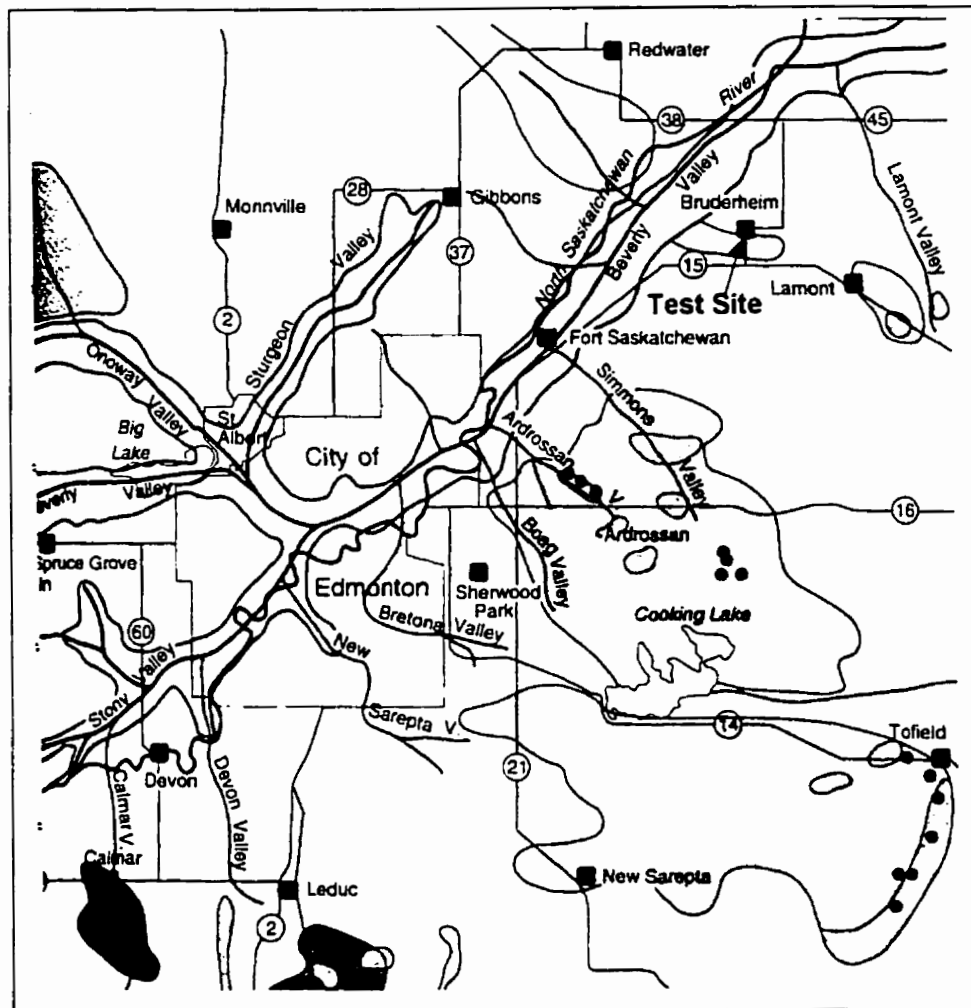


Figure 4.2: Sand Pit Pile Test Location (after Godfrey, 1993)

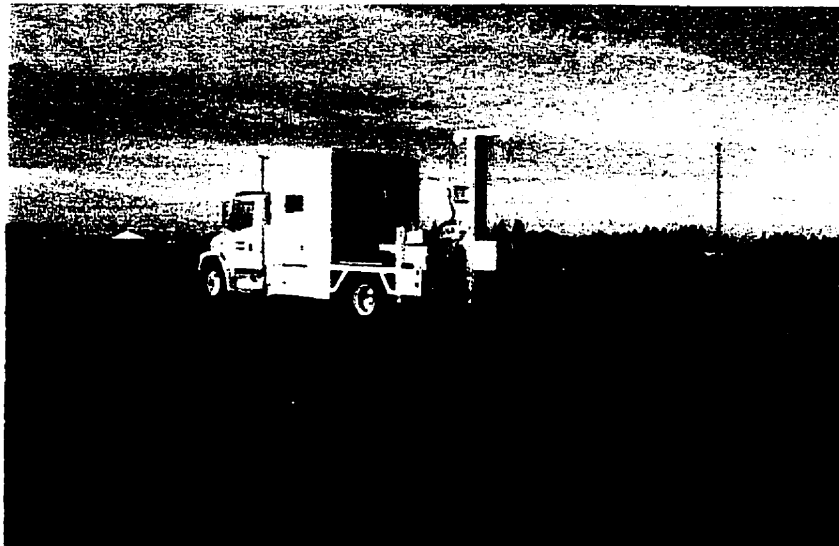


Figure 4.3: Cone Truck used to Perform CPT (Sponsored by ConeTec Investigation Ltd.)

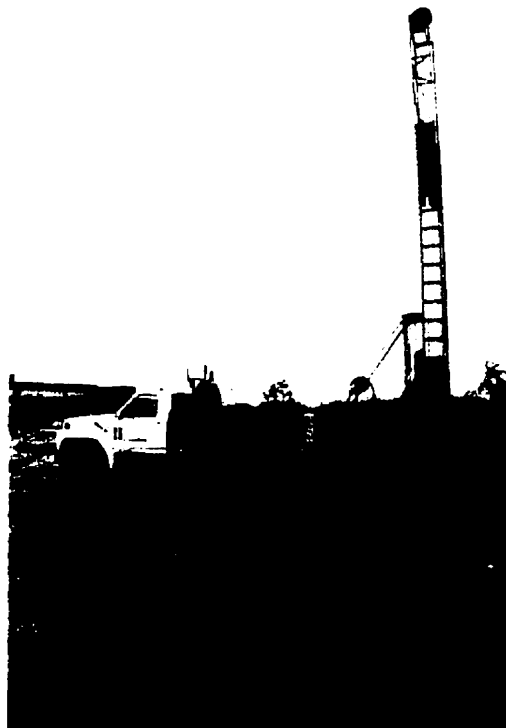


Figure 4.4: Drill Rig used to Perform SPT and CPT

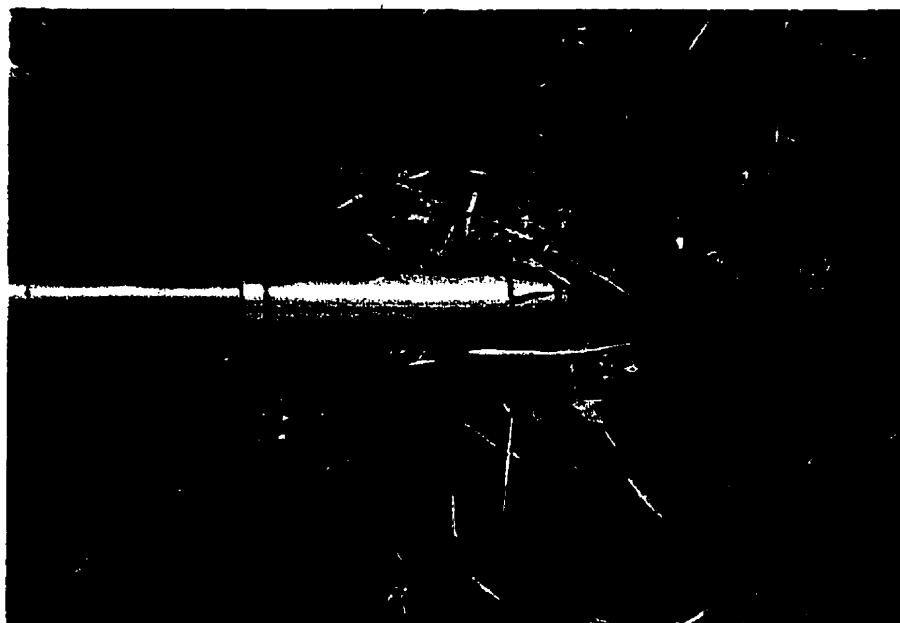


Figure 4.6: Standard CPT Cone



Figure 4.6: CPT Test at University Farm Site

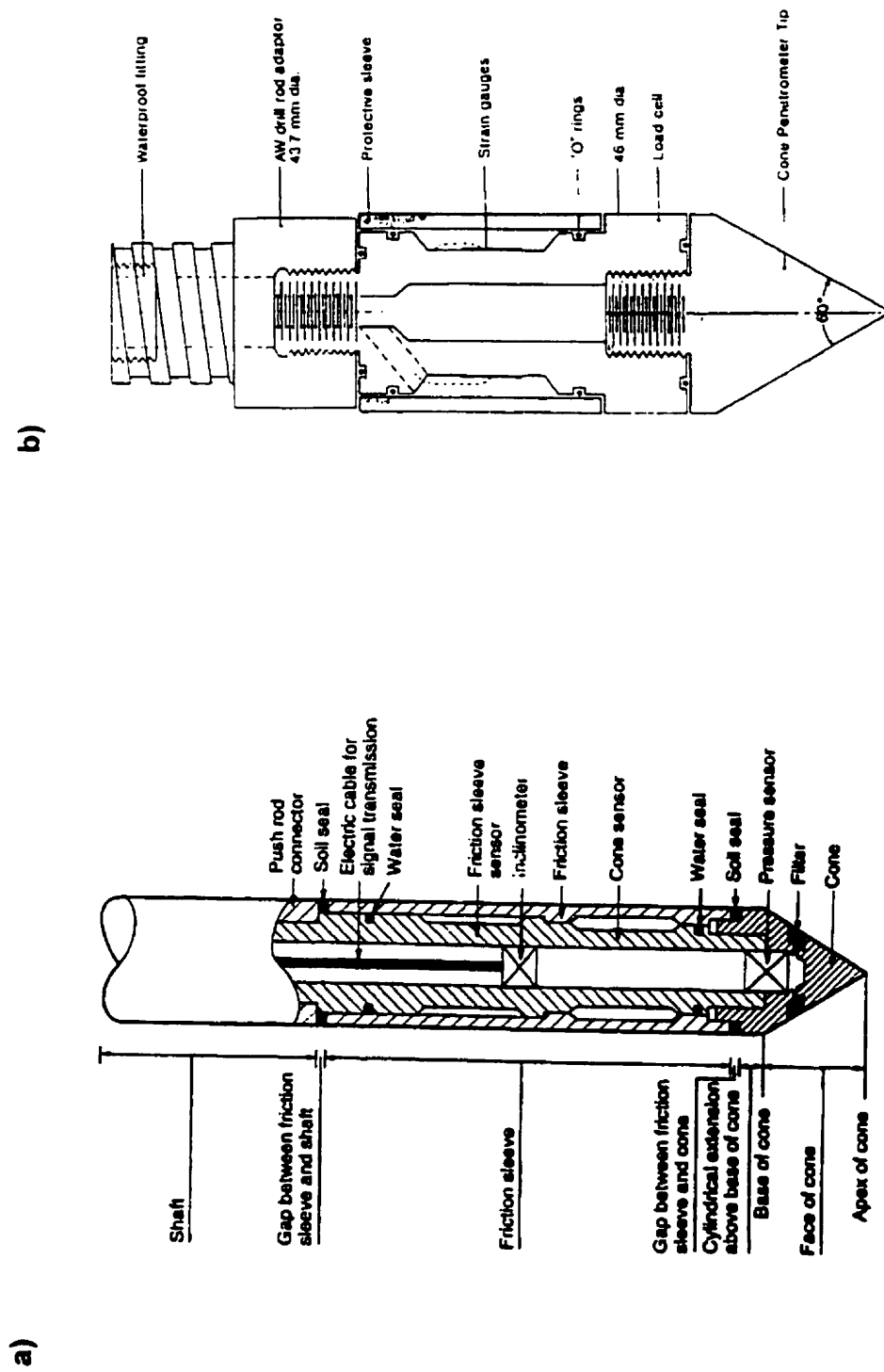


Figure 4.7: Comparison of Conventional CPT Cone and DCPT Cone: a) CPT Cone; b) DCPT Cone (after Robertson and Campanella, 1988 and Treen et al., 1992)

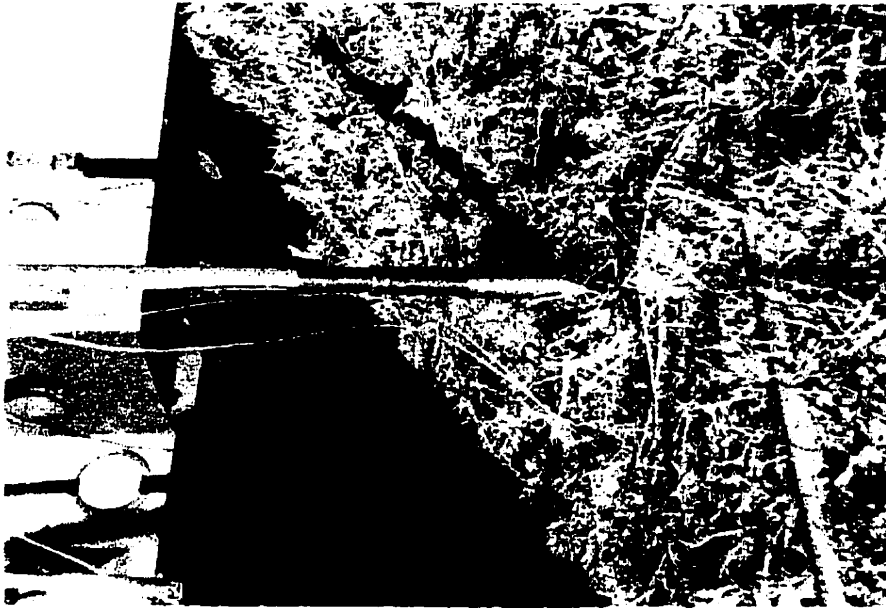


Figure 4.9: DCPT Cone

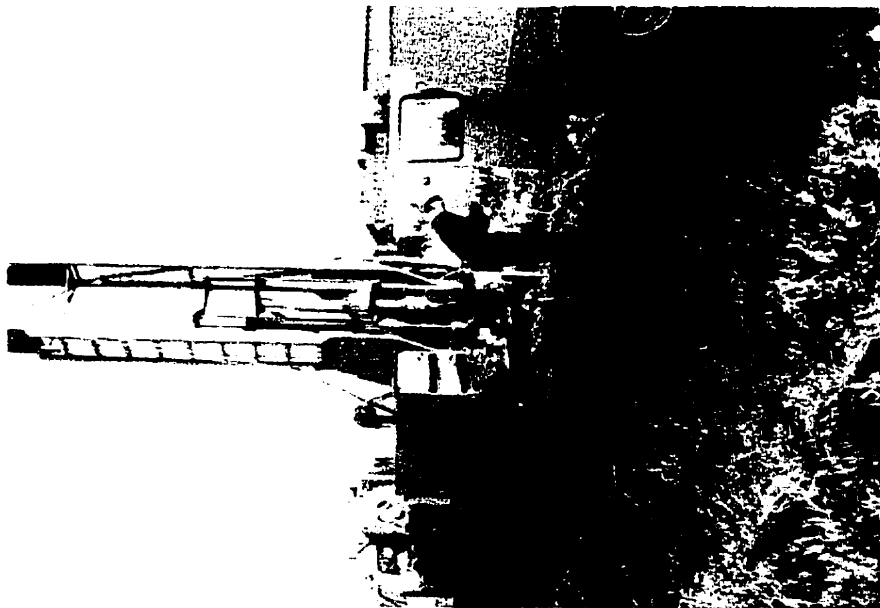


Figure 4.8: Preparation of DCPT Test

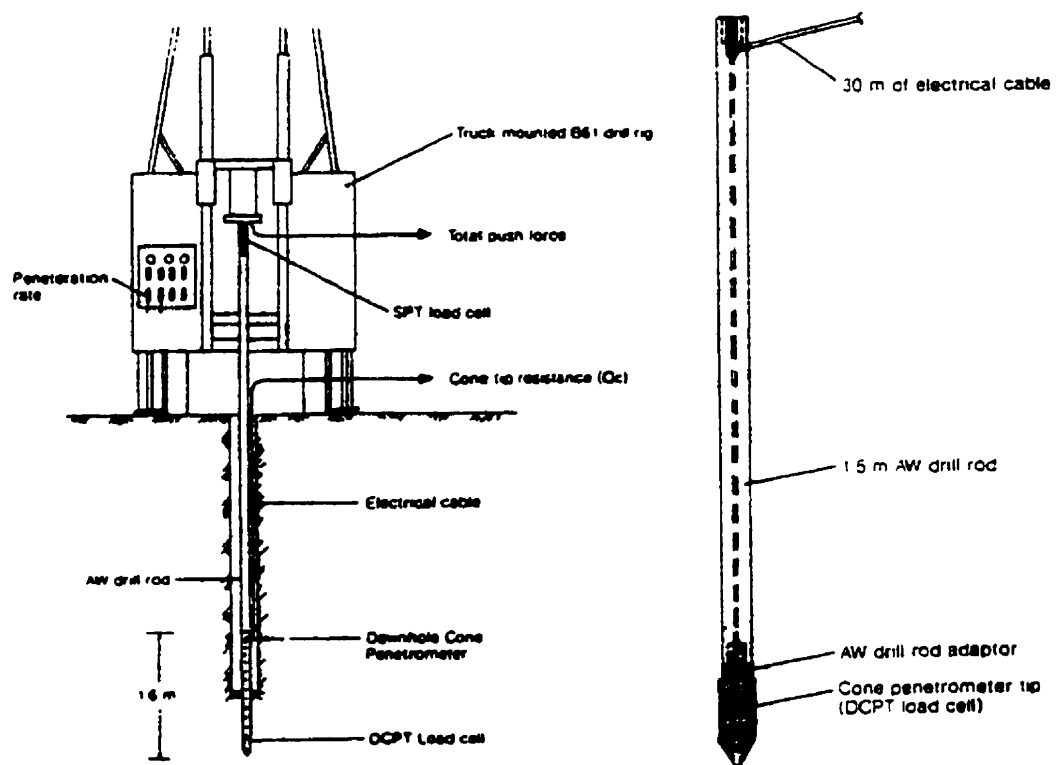


Figure 4.10: DCPT Performed by Conventional Drill Rig (after Treen et al., 1992)



Figure 4.11: Mobile Auger Performing DCPT at the University Farm Site



Figure 4.12: SPT Test Conducted by Mobile Auger at the Sand Pit Site

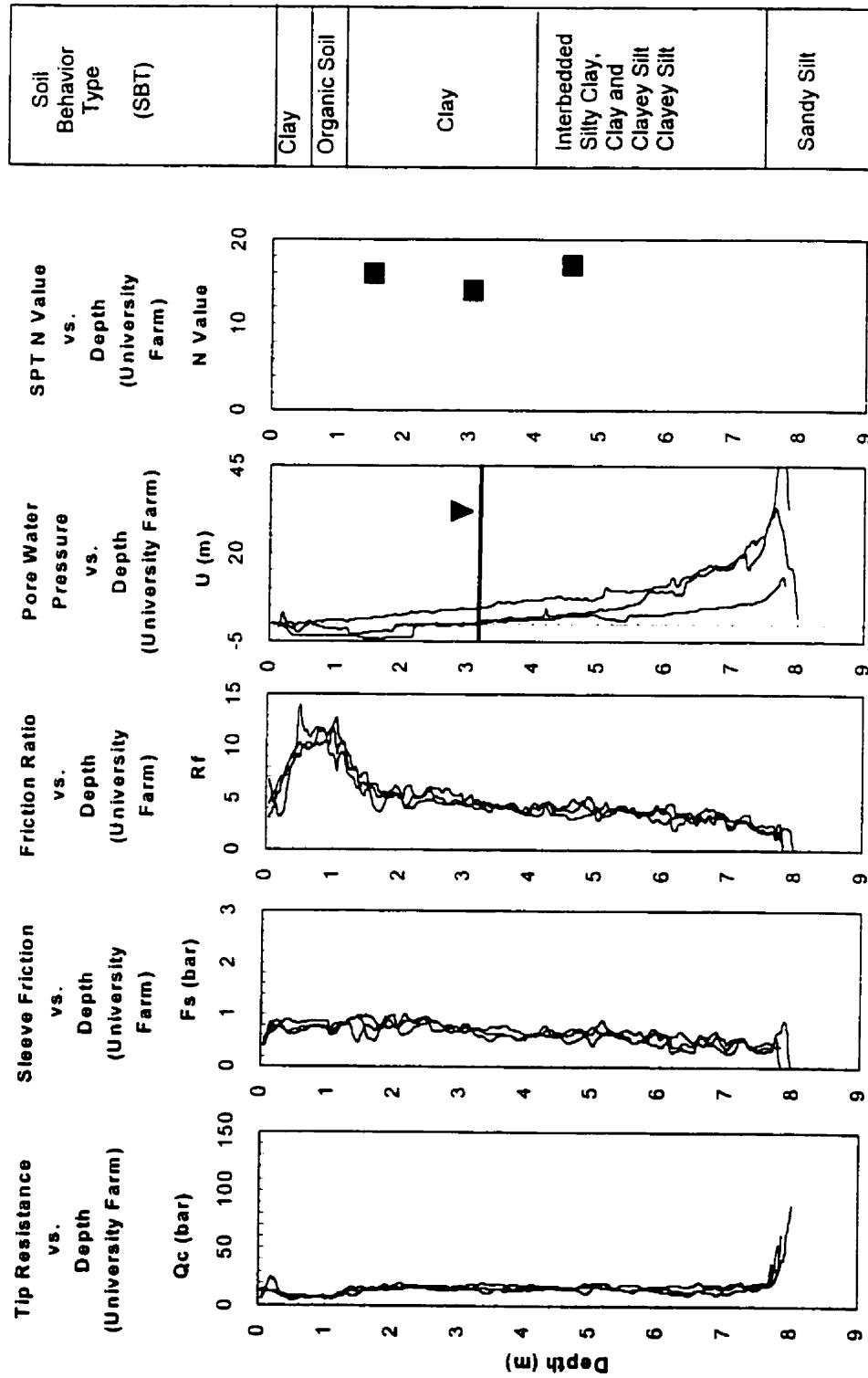


Figure 4.13: Cone Penetration Profile for the University Farm Site (after Robertson and Campanella, 1983b)

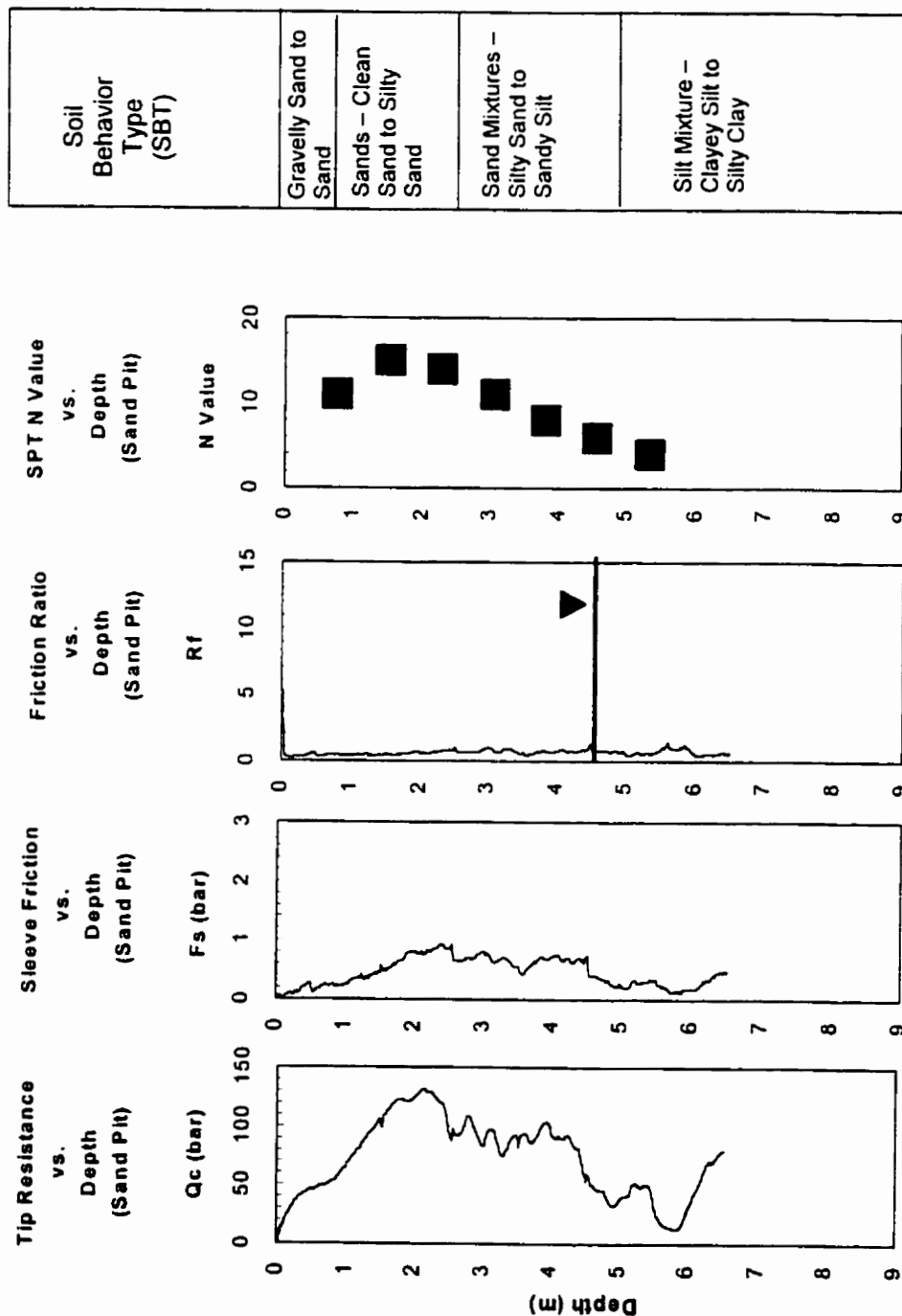


Figure 4.14: Cone Penetration Profile for the Sand Pit Site (after Robertson and Campanella, 1983a)

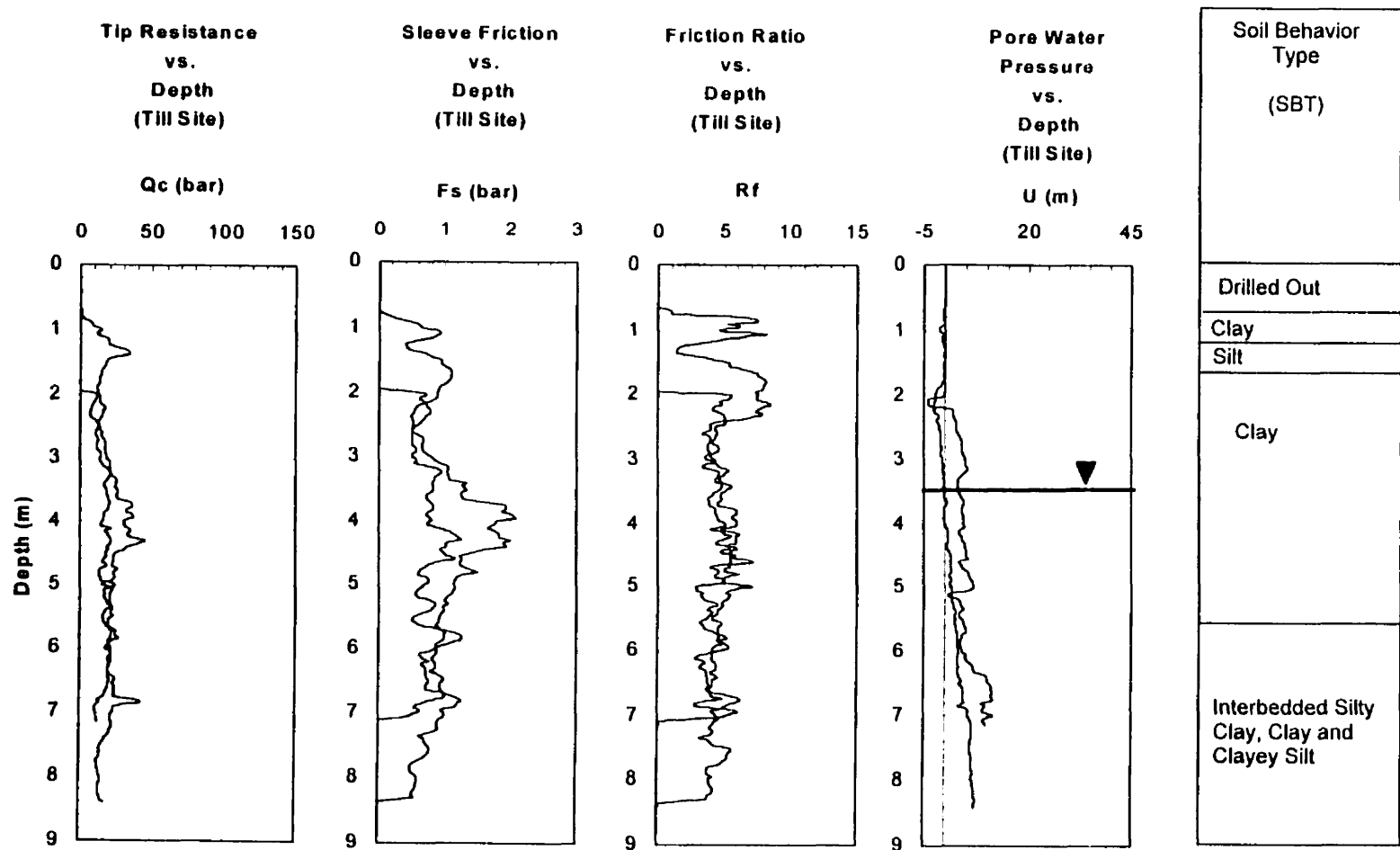


Figure 4.15: Cone Penetration Profile for the Till Site (after Robertson and Campanella, 1983b)

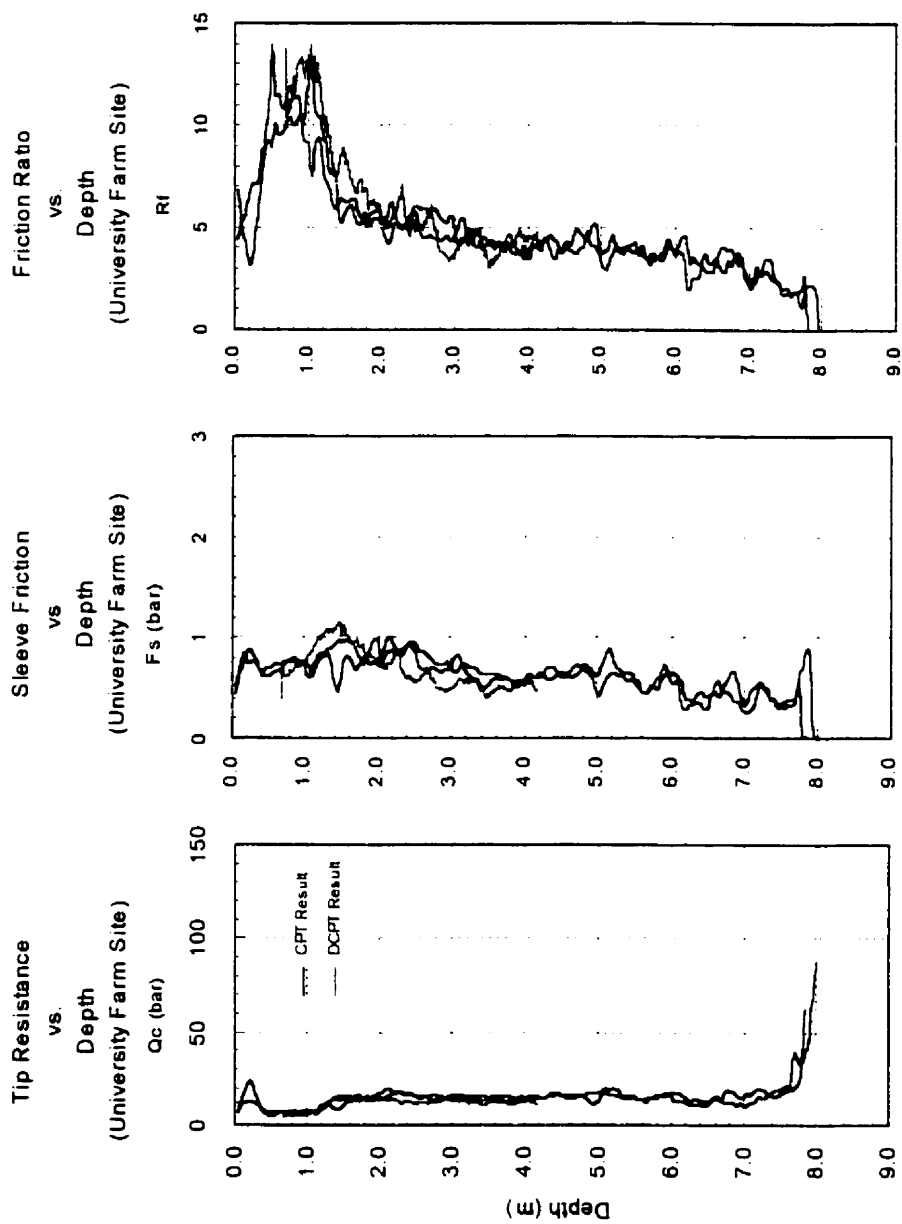
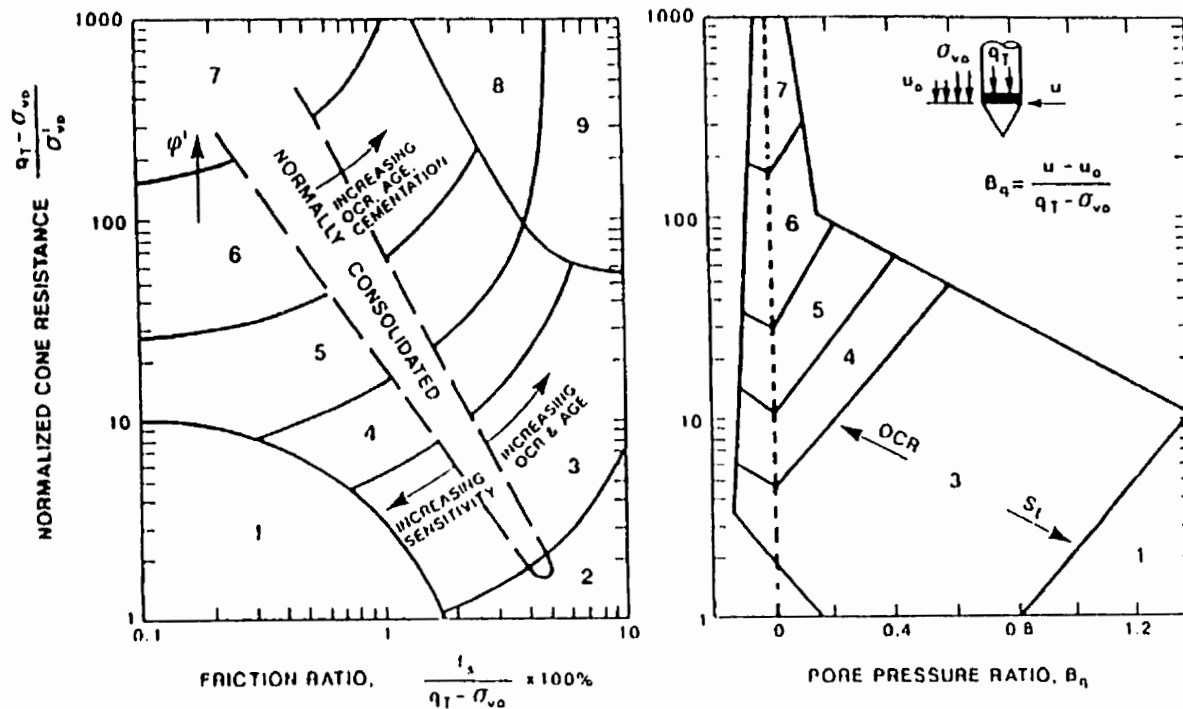


Figure 4.16: Comparing the CPT and the DCPT Result



1. Sensitive, fine grained
2. Organic soils – peats
3. Clays – silty clay to clay
4. Silt Mixture – clayey silt to silty clay
5. Sand Mixtures – silty sand to sandy silt
6. Sands – clean sand to silty sand

7. Gravelly sand to dense sand
8. Very stiff sand to clayey sand*
9. Very Stiff, fine Grained*

* Heavily overconsolidated or cemented

Figure 4.17: Normalized CPT Soil Behavior Type Chart (after Lunne et al., 1997)

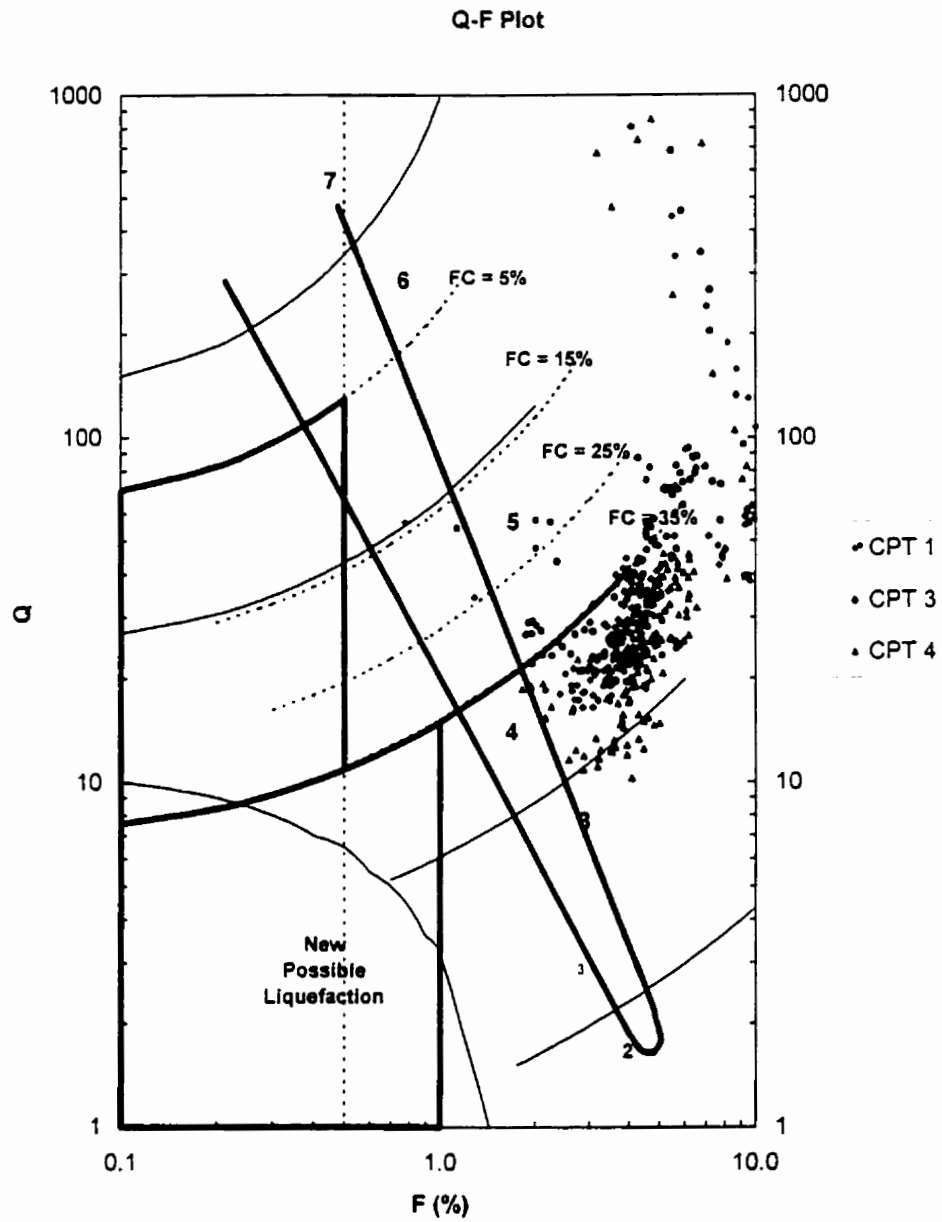


Figure 4.18: Soil Classification Result for the University Farm Site

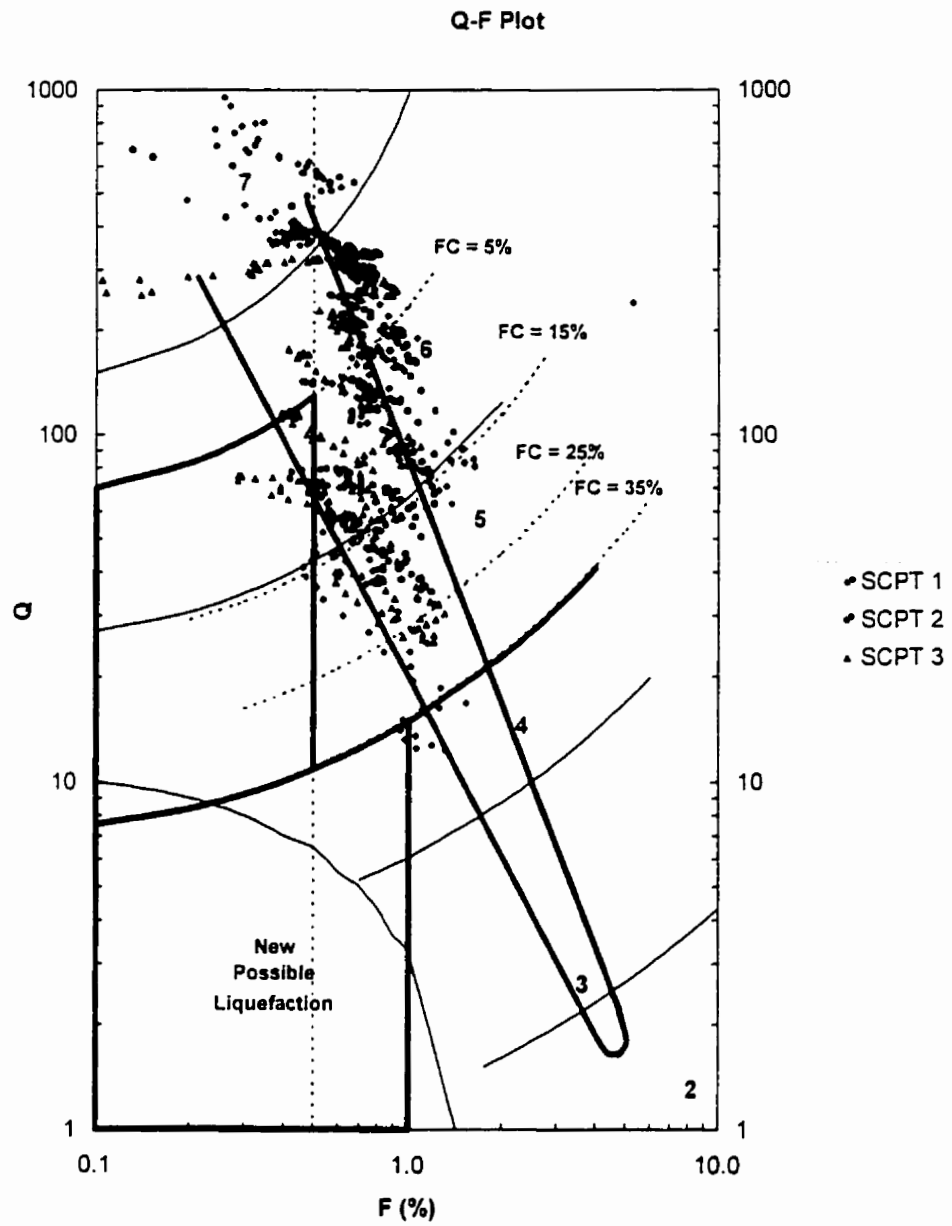


Figure 4.19: Soil Classification Result for the Sand Pit Site

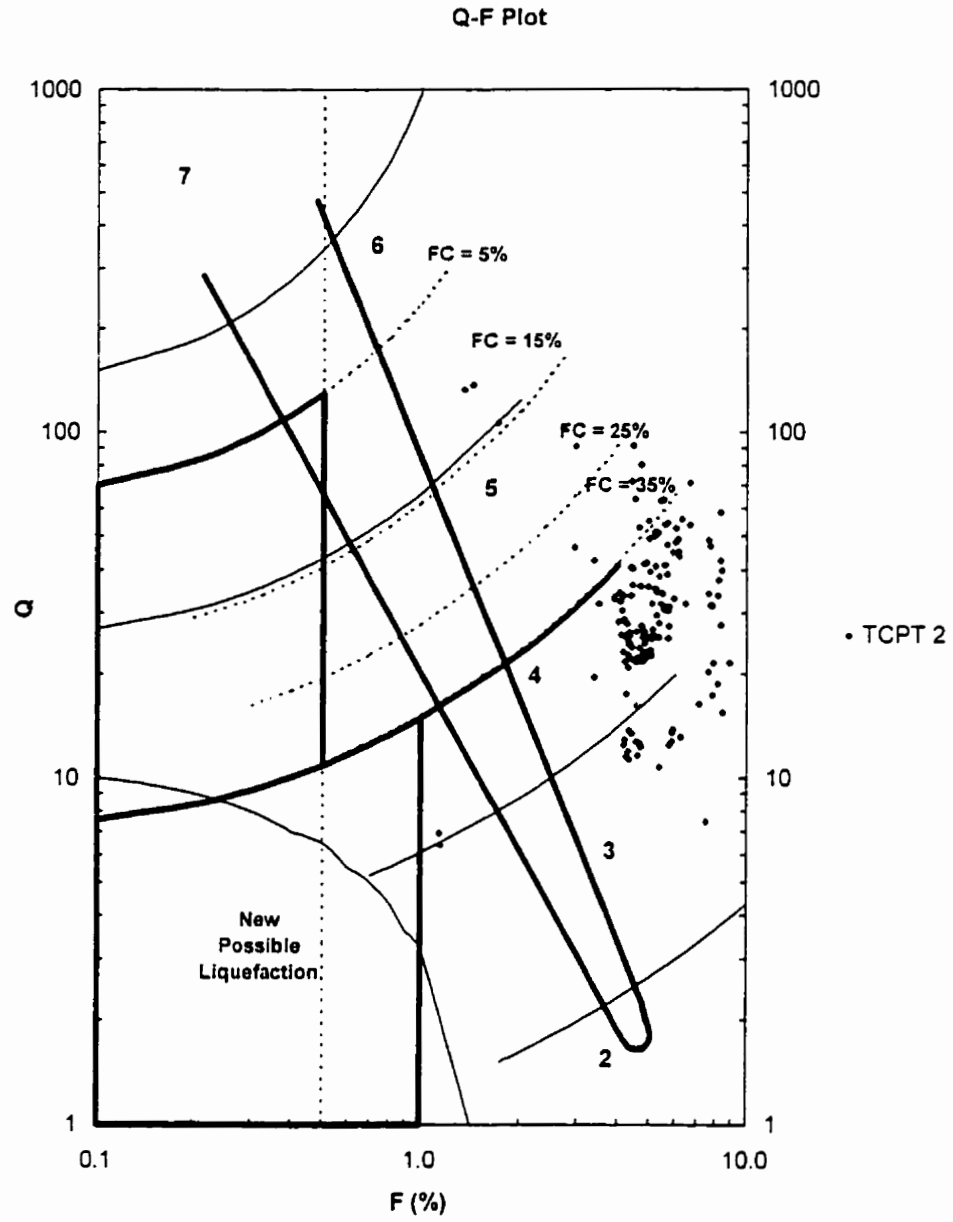


Figure 4.20: Soil Classification Result for the Till Site

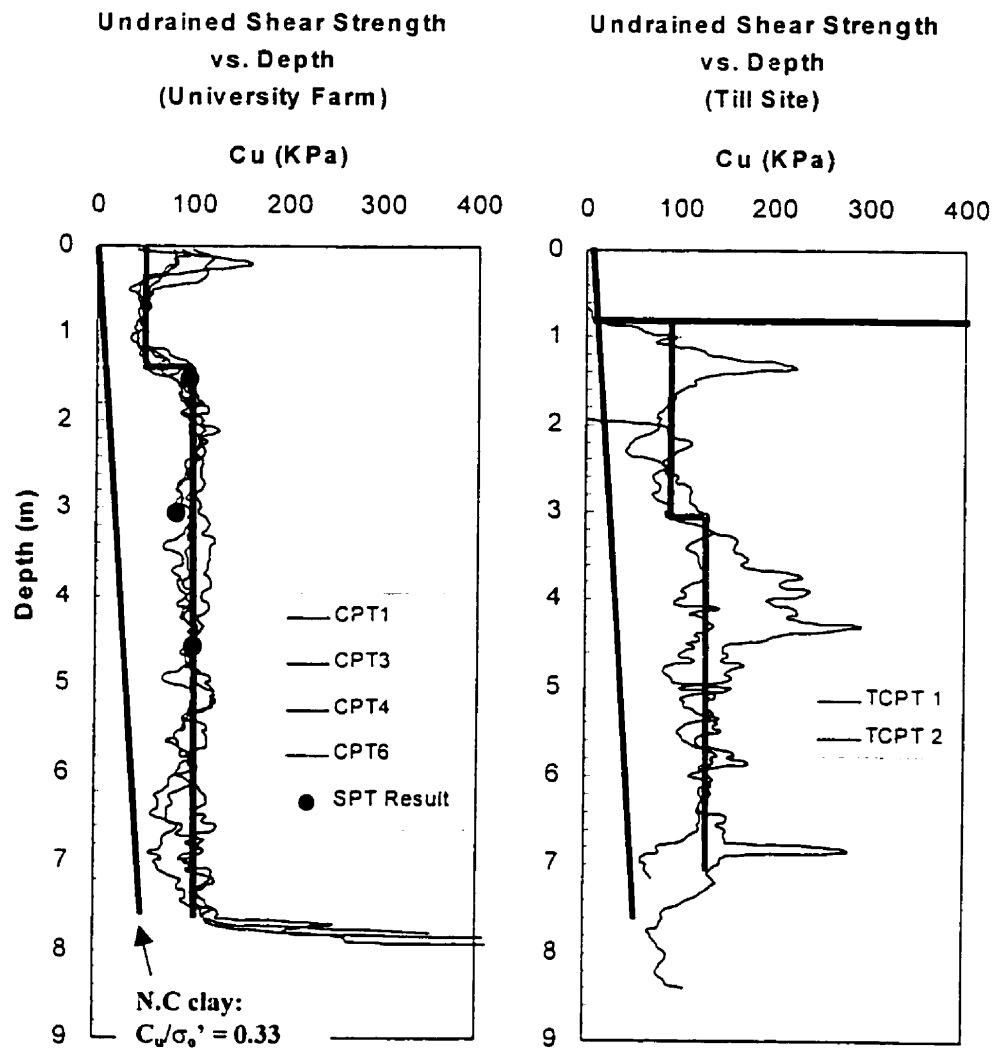


Figure 4.21: Undrained Shear Strength Profile for the University Farm Site and the Till Site

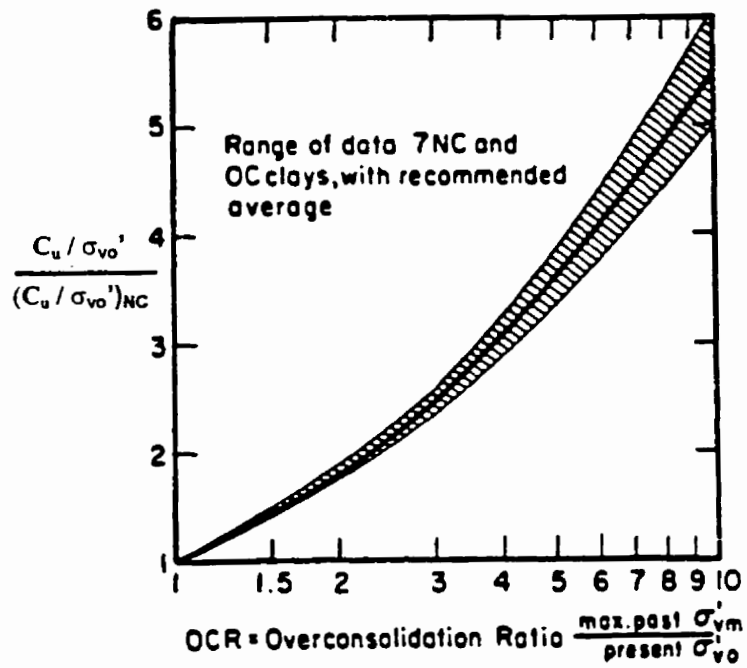
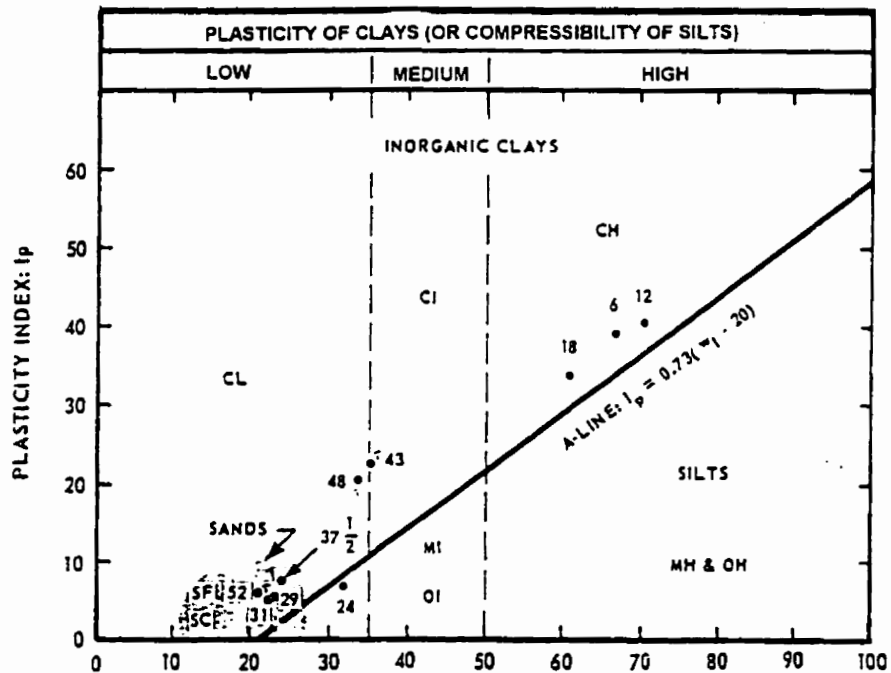
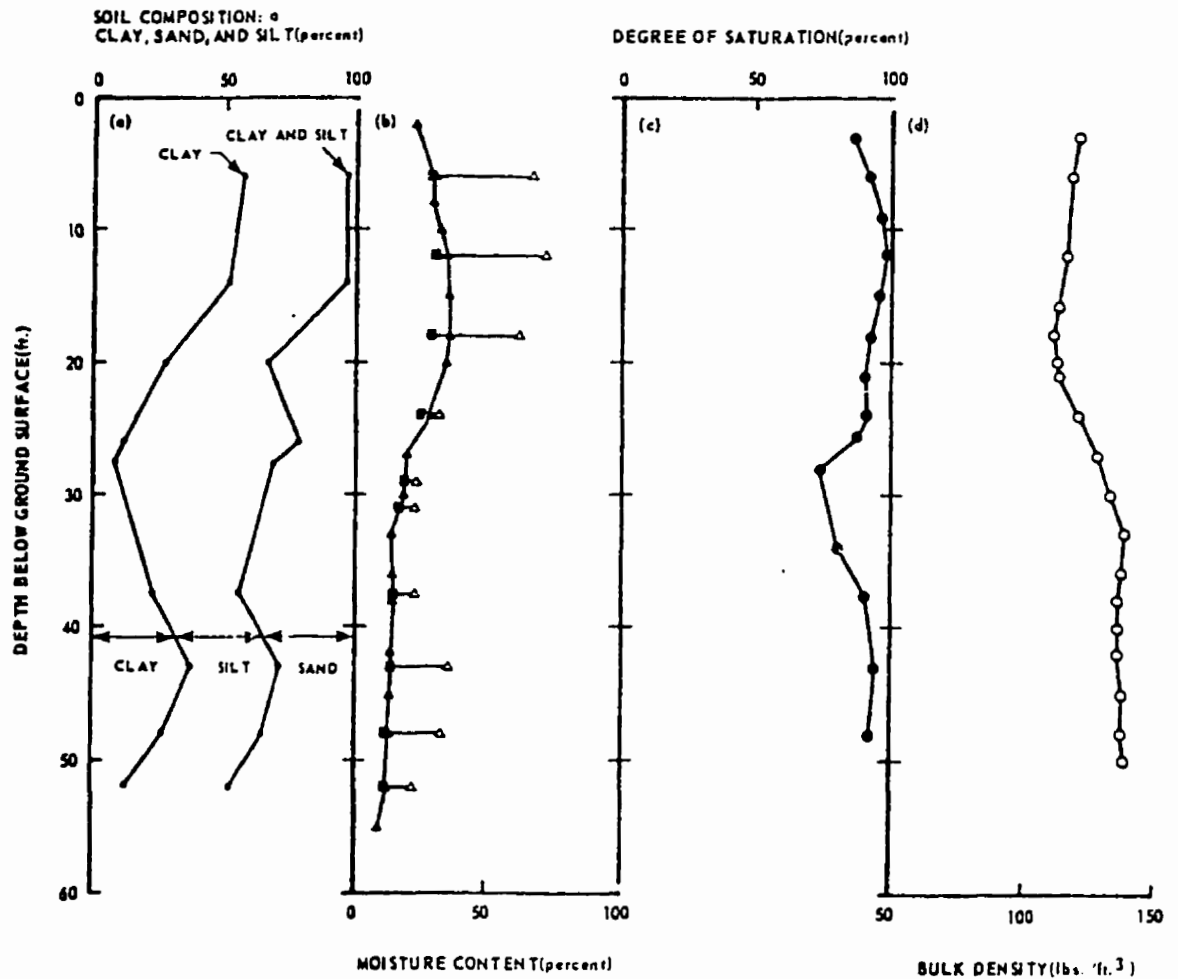


Figure 4.22: Normalized C_u/σ'_{vo} Ratio vs. OCR for Use in Estimating OCR (after Schmertmann, 1978a)



Note: The numbers appearing in the plat indicate the depth (ft.) at which the sample was removed.

Figure 4.23: Plasticity Chart for Field Soil at the University Farm Site (modified from Bhanot, 1968)



LEGEND:

- M.I.T. CLASSIFICATION
- ▲ NATURAL MOISTURE CONTENT(Average)
- △ LIQUID LIMIT
- PLASTIC LIMIT
- DEGREE OF SATURATION
- BULK DENSITY

NOTE: EACH POINT REPRESENTS AVERAGE OF THREE OR MORE VALUES.

Figure 4.24: Plots for Soil Composition, Natural Moisture Content, Liquid Limit, Plastic Limit, Degree of Saturation and Bulk Density of Soil (modified from Bhanot, 1968)

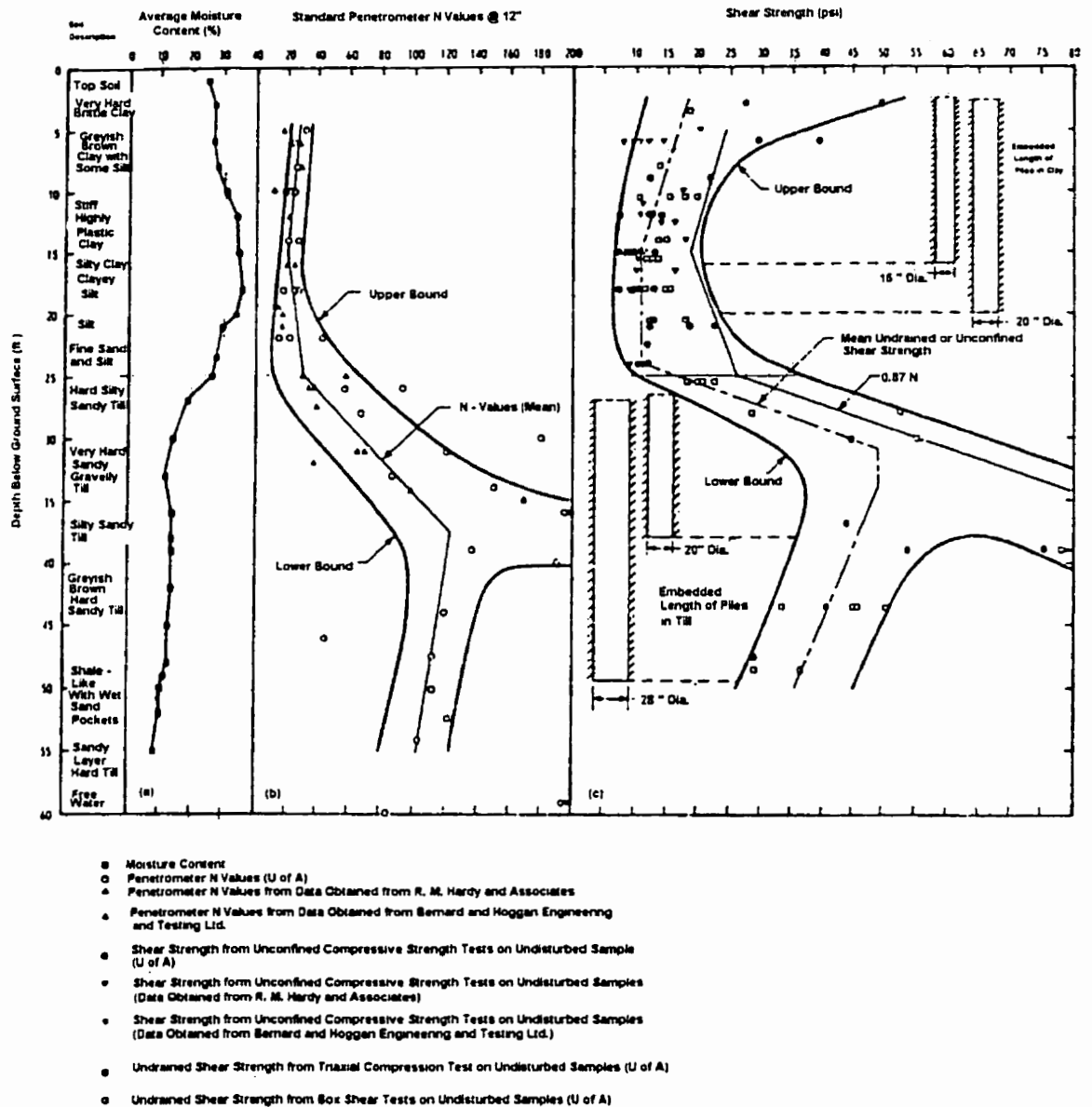


Figure 4.25: Strength Characteristics of Field Soil (modified from Bhanot, 1968)

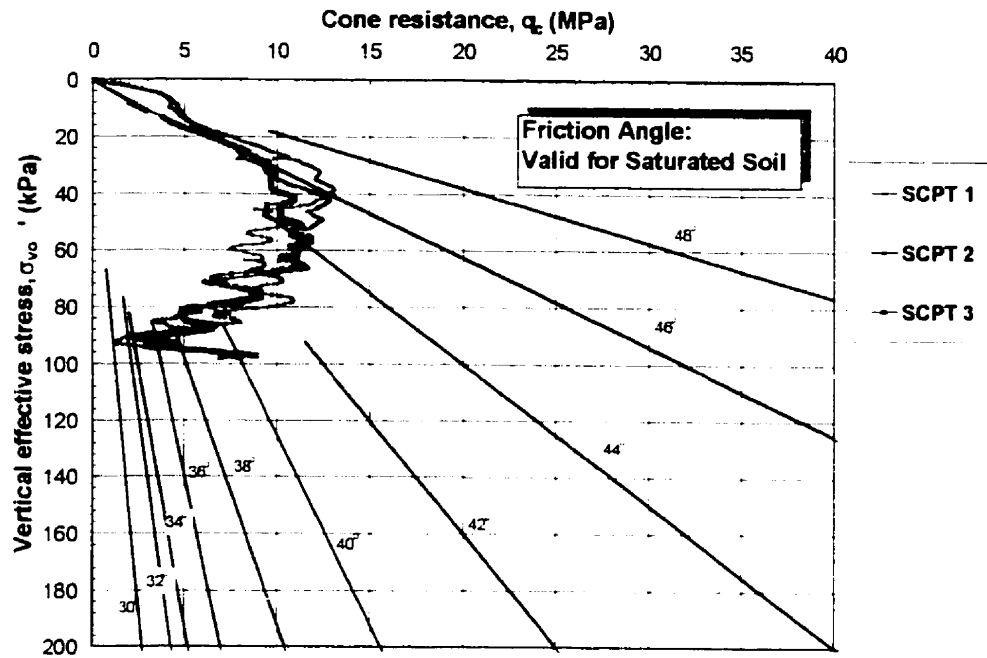


Figure 4.26: Correlation between Peak Friction Angle ϕ and q_c for the Sand Pit Site (after Robertson and Campanella, 1983)

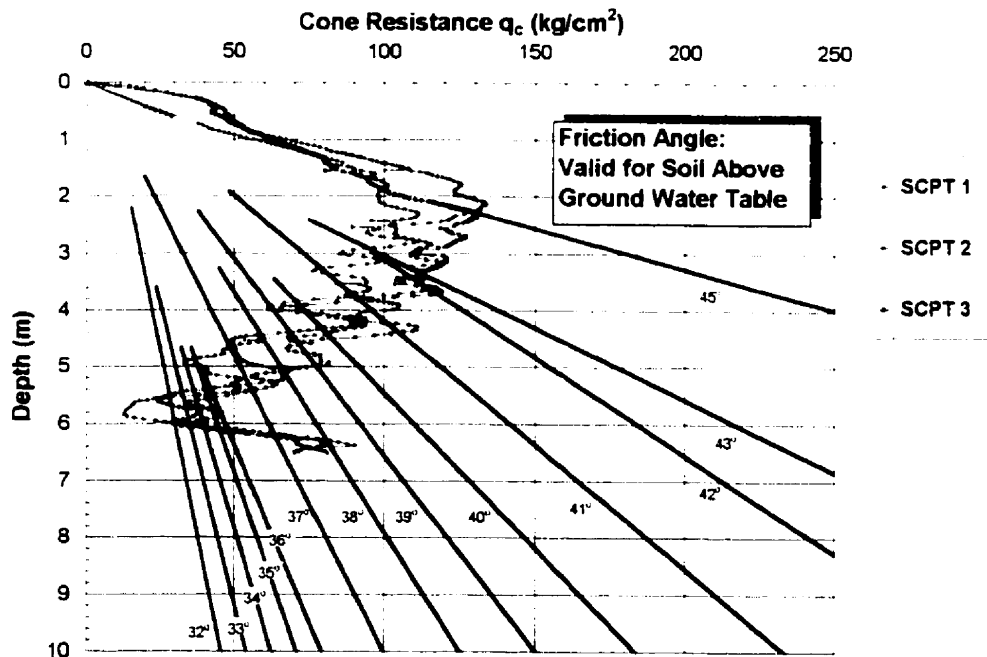


Figure 4.27: Correlation between Peak Friction Angle ϕ and q_c for the Sand Pit Site (after Durgunoglu and Mitchell, 1975)

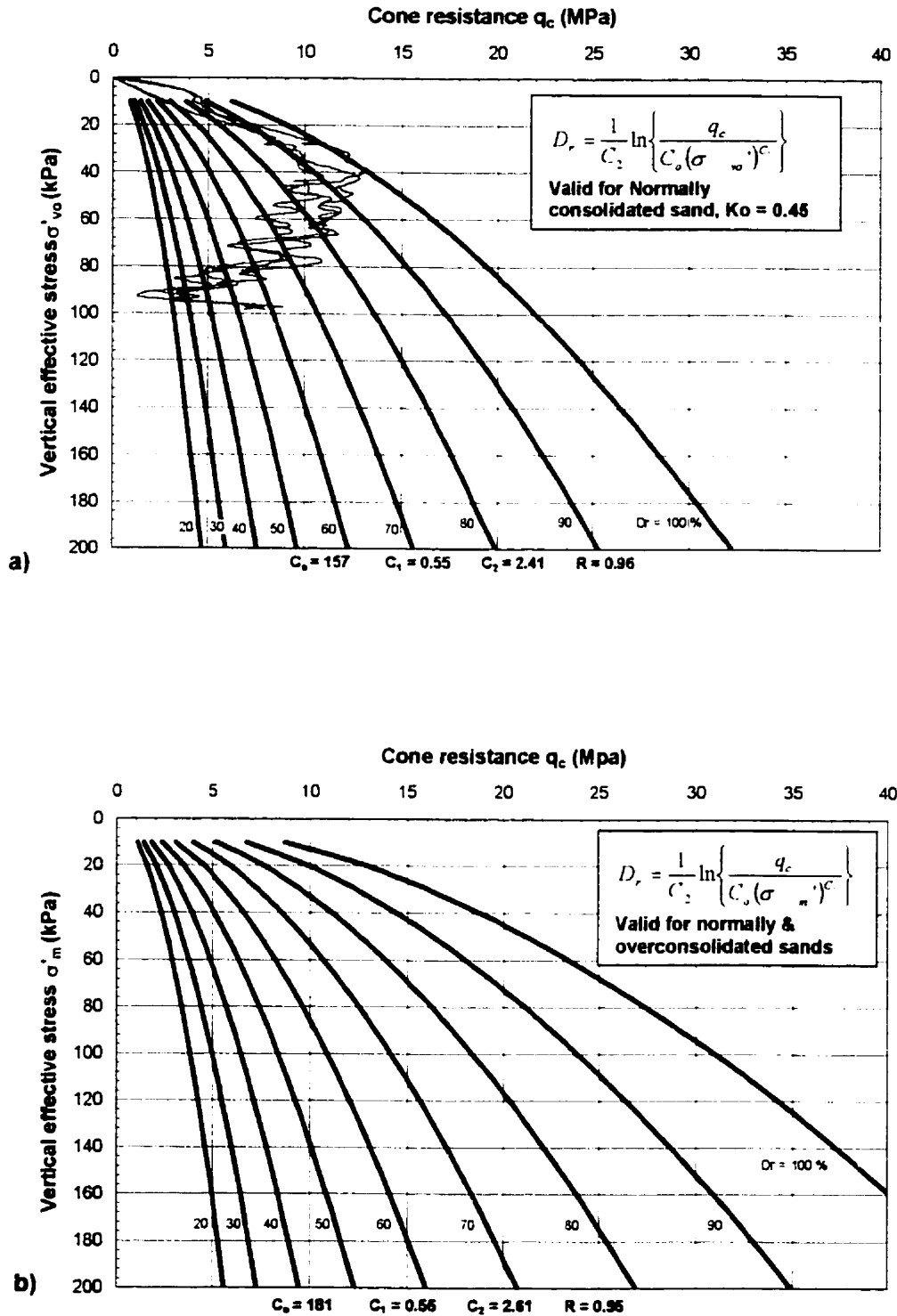


Figure 4.28: q_c , σ'_{vo} , D_r Relationship for Ticino Sand in Terms of (a) Normally and (b) Overconsolidated Behavior (after Baldi et al., 1986)

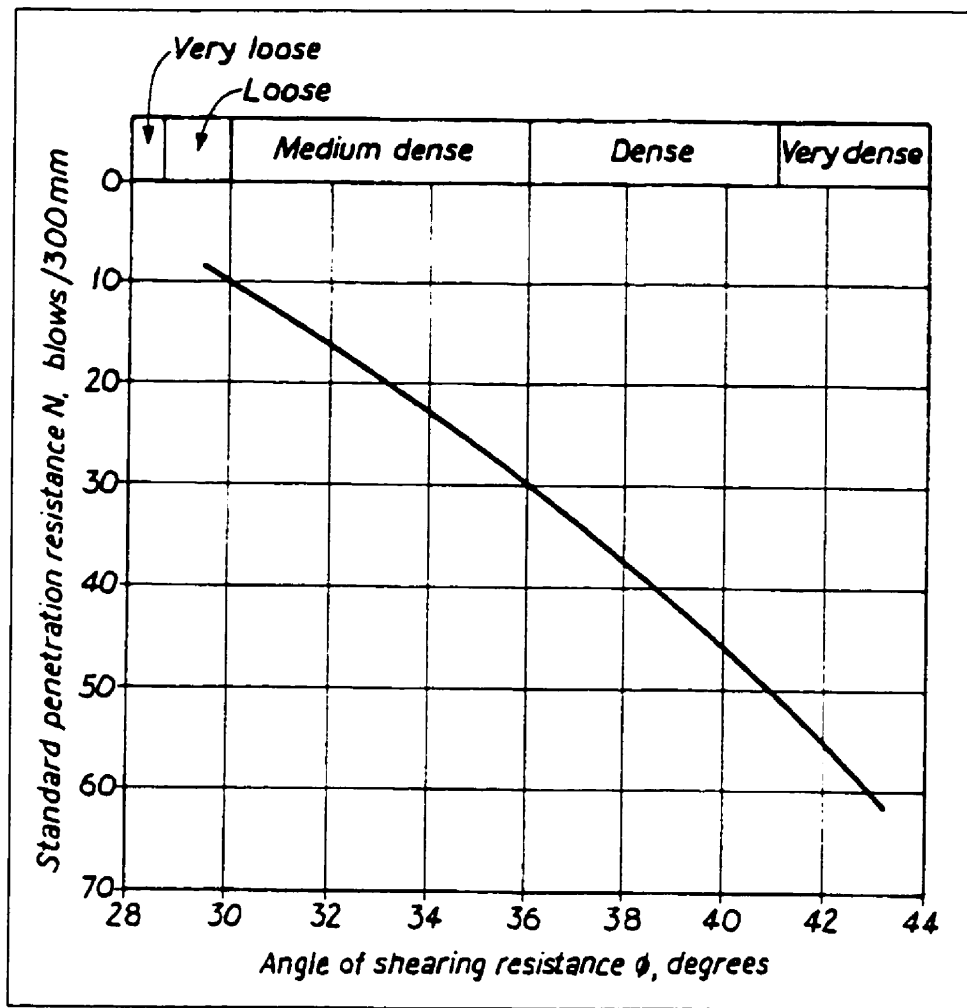


Figure 4.29: Relationship between Standard Penetration Test N -Values and Angle of Shearing Resistance (after Peck, Hanson and Thornburn, 1974)

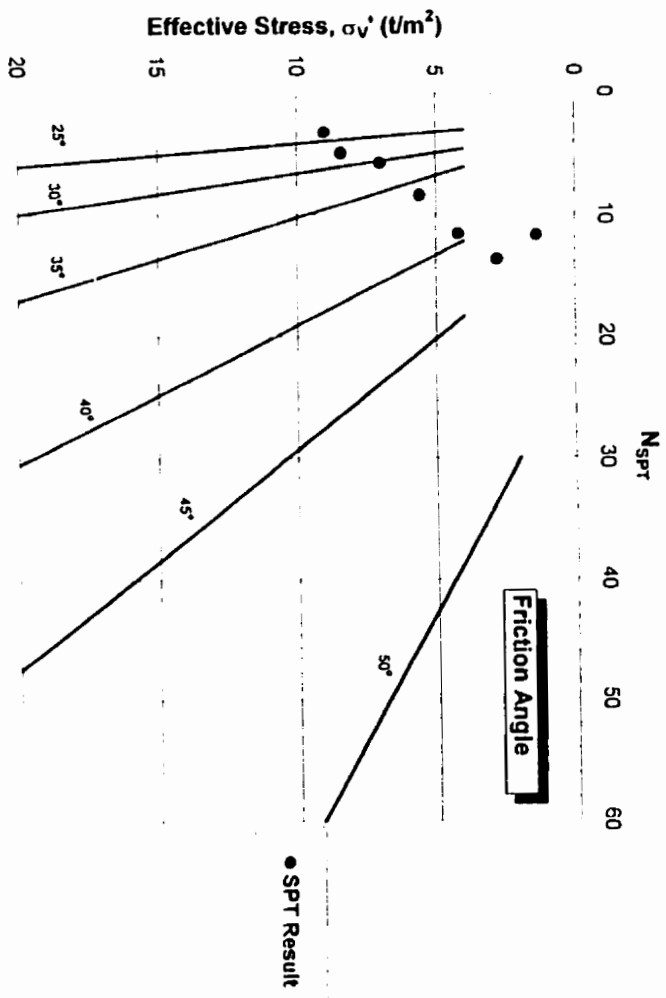


Figure 4.30: Correlation between Peak Friction Angle ϕ and N_{SPT} for Sand Pit site (after De Mello, 1971)

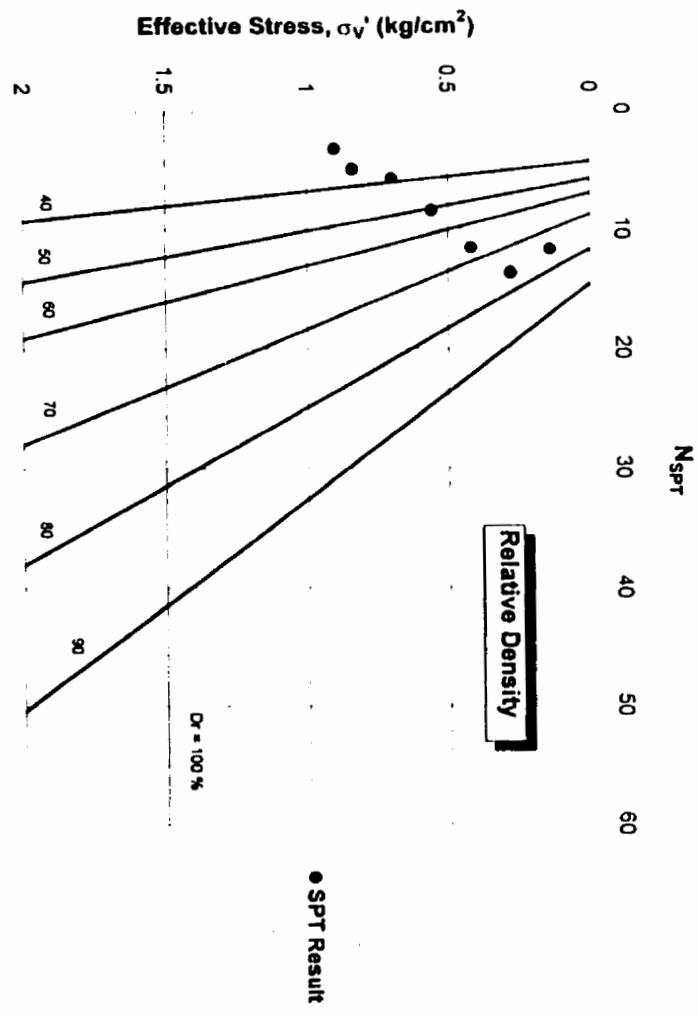


Figure 4.31: Correlation between Relative Density D_r and N_{SPT} for Sand Pit site (after Gibbs and Holtz, 1957)

CHAPTER 5 TESTING PROGRAM

5.1 INTRODUCTION

The original proposed field program included a total of 27 pile load tests to be performed at three sites underlain by different soil types that are considered as typical Alberta soils. The soil types chosen are: Lake Edmonton Clay (cohesive material), Sand dunes (cohesionless material), and Glacial Till. Six fully instrumented pile load tests including two compression piles, two pullout piles and two lateral piles would be performed at each site. Furthermore, three non-instrumented standard production piles would be loaded in compression and tension at each site to compare the result with the instrumented research piles.

However, Cone Penetration Test results demonstrated that the CPT profiles of the Lake Edmonton Clay and the Glacial Till found around Edmonton area are very similar. The Glacial Till behaves comparable to a stiff clay according to the soil behavior type based on the interpretation of CPT data (Robertson and Campanella, 1983). There was no justification to test two cohesive sites with similar CPT profiles. Therefore, the Glacial Till site was postponed until a more suitable location with a significantly greater cone resistance could be found. A total of 18 pile load tests, were performed at the two sites in the Edmonton area. Ten pile load tests including five compression tests, three tension tests and two lateral tests were conducted on the University Farm site. In addition, eight pile load tests, consisting of three compression, three pull out and two lateral pile load tests, were conducted at a Sand Pit site located at Bruderheim, northeast of Edmonton. This chapter describes the pile load tests performed including the test layout, test setup system, test loading system and test procedures.

5.2 TEST SITE LAYOUT

The site for the test piles was arranged in a systematic layout in order to minimize the number of reaction piles required. The layouts of the test sites were designed to meet the standard set by the ASTM standards for performing the pile load tests. In addition, the test sites were set out so that the reaction beam could be relocated easily for the next test. Figure 5.1 illustrates the site plan at the University Farm site with the indication of the location of the test piles, reaction piles, and in situ test locations. Similarly, Figure 5.2 presents the site layout at the Sand Pit site. The test piles were installed in rows requiring only a total of six piles as the reaction system. Timber cribbing was also used for tension pile load tests. The use of timber cribbing provides flexibility for the set up of pullout tests.

5.3 LOADING SYSTEM

For the test program, adequate capacity was delivered by a hydraulic jack with a 90 tonnes capacity (Figure 5.3) and a 1500 kN capacity electronic load cell (Figure 5.4). Load cell seats shown in Figure 5.5 was also used to ensure no eccentric loading during either the compression or the tension tests. Both the electronic load cell and the hydraulic jack were calibrated before use in field. The electronic load cell was loaded by an unconfined compression machine by applying incremental load steps to a maximum load of 600 kN and then, gradually unloaded to zero load. The maximum 600 kN was predicted to exceed the maximum ultimate capacity required in the field tests. The voltage output by the load cell was plotted against the load applied by the unconfined compression machine to produce the calibration curve for the load cell. The results can be found in Appendix B. The hydraulic jack was calibrated in the manufacturer's machine shop. The load applied by the jack was controlled by supplying fluid pressure through a manual hydraulic pump. The measurement of the axial

compressive or tensile load applied to the test pile was collected based on the load cell output and the pressure gauge reading on the hydraulic pump as a backup.

Two types of reaction beams were used in the program. At the University Farm Site, the reaction beam was a high strength hot rolled structure I-beam (S510 x 98.2) with a load capacity of 400 kN. At the Sand Pit site, higher ultimate load was expected for test piles installed in cohesionless material. Therefore, a high strength hot rolled wide flange structure beam (W 610 x 241) with a load capacity of 800 kN was used for testing.

5.4 DISPLACEMENT MEASUREMENT

The vertical pile movement was monitored by two electronic displacement potentiometers attached to the two 300 mm H-section steel reference beams. These reference beams were placed at a clear distance of not less than 2.5 m from the test pile and the reaction piles or the timber cribbing. They were securely supported by the sand bags placed at the end of the beams to ensure no excessive variations in readings due to ground movement or vibration. The pile movements during the compression and tension test were monitored using displacement potentiometers. The two potentiometers calibrated prior to testing, were placed on each side of the test pile diametrically and attached to the test pile using the magnetic setting. The potentiometers were calibrated similar to the procedure used to calibrate the load cells. The voltage output by the potentiometers were collected by the data acquisition system and then plotted against the measured distance. The results of the calibration are shown in Appendix B. Vertical deflection of the test beam was measured manually by a dial gauge, accurate to 0.01 mm. In addition, a survey level reading on both reaction piles and the test piles was used as a backup measurement on the pile movement. Figure 5.6 shows the measuring equipment used to monitor the displacement of the test pile and Figure 5.7 demonstrates how these electronic displacement transducers were attached to the pile. Figure 5.8 shows the

placement of reference beams from the test pile for the compression and tension tests. For the lateral pile load test, the pile head deflection was measured by one displacement potentiometers and one dial gauge attached to a 300 mm H-section reference beam located directly above the test pile (Figure 5.9).

5.5 REACTION SYSTEM

5.5.1 Axial Compression and Axial Tension Tests

Reactions for the axial compression and tension pile load tests were developed from two screw piles with 219 mm shaft diameter and three 406 mm diameter helices, installed to a depth of 5.18 m. The reaction piles had at least 2.6 times the capacity of the test piles in vertical loading condition. The factor of safety incorporated assumes that capacity delivered by three 406 mm diameter helices pile gave 30% higher capacity than three 356 mm diameter helices test pile.

For the compression tests, Load was transferred to the reaction piles by using 38 mm diameter, high strength steel bars as shown in Figure 5.10. The bars were bolted to the reaction frame and were connected to the tension reaction piles. A 20 mm thick steel plate was welded on top of the reaction piles and the test pile. As presented in Figure 5.11, four slots were cut from the plate allowing the steel bars to be connected. The calibrated hydraulic jack was placed on top of the steel jacking plate. A 1500KN capacity electronic load cell with a set of spherical bearing plates was placed between the jack and the reaction frame. Two 0.533 m tall spacers were located on top of the loading plates that were welded to the reaction piles. The spacers were used to allow sufficient space for placing the hydraulic jack, load cell, load cell seating and minimum of 50 mm vertical downward travel of the test pile. At the University Farm site, the ultimate pile capacities were expected to be less than 200 kN, therefore, the reaction frame was simply four steel bars connected with two 20 mm thick steel plate with lower

plate bolted to the test pile. A typical setup at University Farm site is shown in Figure 5.12. Figure 5.13 demonstrates the loading stage during a compression test. For system that requires higher loading capacity, the reaction frame was designed using two structure C-Channels connected back to back by welding to three 6.4 mm thick, 152 mm length square steel plates as shown in Figure 5.14. Figure 5.15 demonstrates the setup for the reaction piles including the use of spacer and structural frame.

A similar setup as the axial compression test was used for the tension tests. The hydraulic jack and the load cell were placed on top of the test beam as presented in Figure 5.16 and Figure 5.17. Similarly, four 38 mm diameter high strength steel bars bolted to the reaction frame were used to tie the loading system with the test piles as illustrated in Figure 5.18. Unlike the compression test, the reaction beam was placed on two rollers which were placed on top of the loading plate welded to the reaction piles. Figure 5.19 demonstrates details of the reaction system where the reaction was provided by timber cribbing. Figure 5.20 presents a schematic layout of the compression test setup and Figure 5.22 demonstrates the complete setup for the tension tests.

5.5.2 Lateral Load Test

The lateral load was delivered by pulling the test pile using a hydraulic jack connected to a reaction system with a tension member, such as a steel wire rope. The reaction system consisted of two 6.35 mm thick structure C-Channel plates connected by four 20 mm diameter high strength steel bars (Figure 5.22). The connection between the reaction frame and steel wire rope is demonstrated in Figure 5.23. The tension member was then connected to an adequate anchorage system, such as a structural I-beam supported by two reaction piles. The tension member was securely fastened so that the applied lateral load passed through the vertical central axis of the test pile as shown in Figure 5.24 and Figure 5.25. Figure 5.26 shows a schematic arrangement of the lateral pile load test.

5.6 PILE LOAD TESTING

For both the compression and tension tests, the loading was carried out following a quick load test procedure, as described in ASTM D 1143-81 and ASTM D 3689-90. Each pile was loaded to failure in increments of 10 to 15% of the proposed design load. Each loading increment was held until the rate of deflection was less than 0.25 mm per hour. Constant time intervals of a minimum of 5 minutes were used to permit adequate time for recording data manually in between readings. Electronic data were collected automatically every 20 second by the data acquisition system and transferred to the computer screen. Load increments were added until "failure" defined as continuous jacking was required to maintain the test load. This maximum load is held for 5 min and then removed. The load and settlement were continuously monitored by the computer, therefore, the time to failure could be observed and measures were taken to ensure sufficient loading time interval at failure was maintained in order to clearly define the load-settlement curve at failure. A similar procedure was followed for the "rebound" or the unloading portion of the test. The load was removed in increments of at least 2.5 min time intervals (Crowther, 1988). All the tests were carried out up to the ultimate load that was defined as the load corresponding to a pile top settlement greater than 10% of the helix diameter (i.e. 35.6 mm).

For the lateral piles, the tests were conducted using the quick load test procedure as described in ASTM D 3966-81. Loading procedure was the same as the axial compression or the tension tests. Lateral load was applied in increments of approximately 5 kN. Each increment was maintained for period of 5 to 10 min. The "failure" was assumed to be reached when more than 50 mm of lateral movement was observed (i.e. 23% of the shaft diameter).

5.7 REFERENCES

- ASTM D 1143-81 (1981). "Standard Test Method for Piles Under Static Axial Compressive Load"; (Reapproved 1984). Annual Book of ASTM Standards, 1997, Vol. 04.08, pp. 95-105.
- ASTM D 3689-90 (1990). "Standard Test Method for Individual Piles Under Static Axial Tensile Load"; (Reapproved 1995). Annual Book of ASTM Standard, 1997, Vol. 04.08, pp. 366-375.
- ASTM D 3966-90 (1990). "Standard Test Method for Piles Under Lateral Loads"; (Reapproved 1995). Annual Book of ASTM Standards, 1997, Vol. 04.08, pp. 389-399.
- Crowther, C. L. (1988). "Load Testing of Deep Foundations: the Planning Design and Conduct of Pile Load Tests"; John Wiley & Sons, New York.

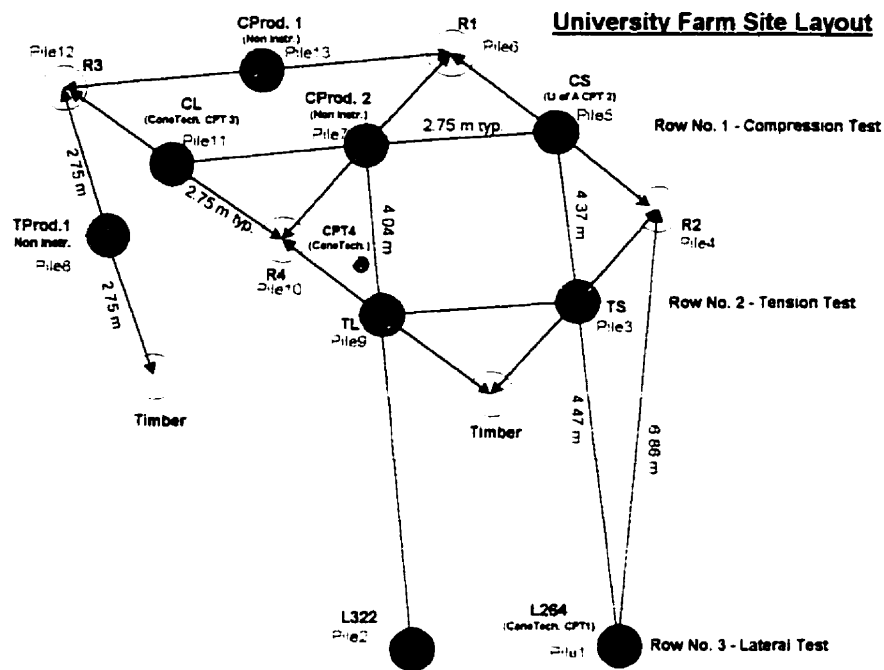


Figure 5.1: Site Layout at the University Farm Site

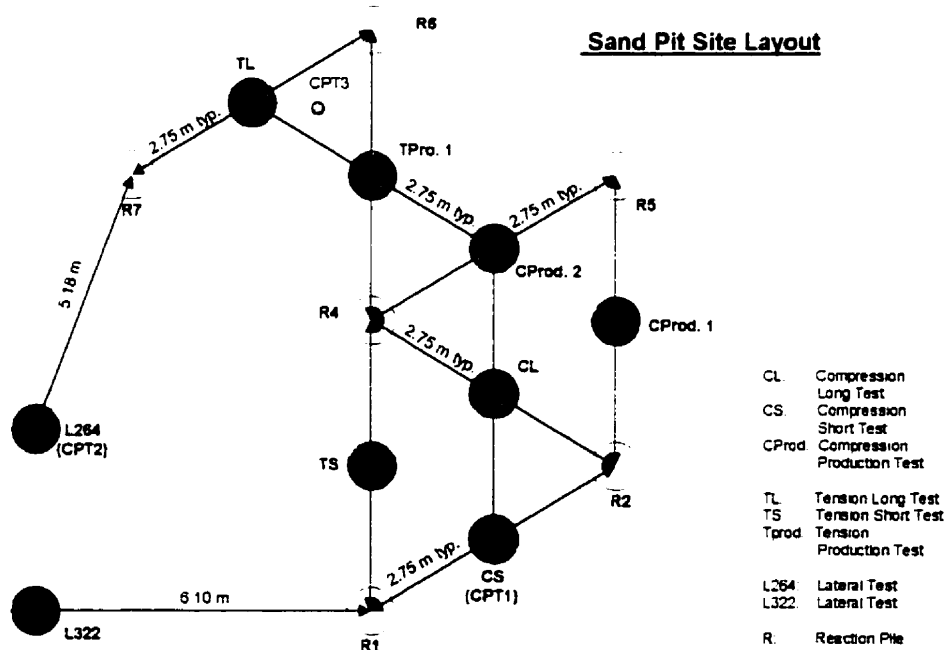
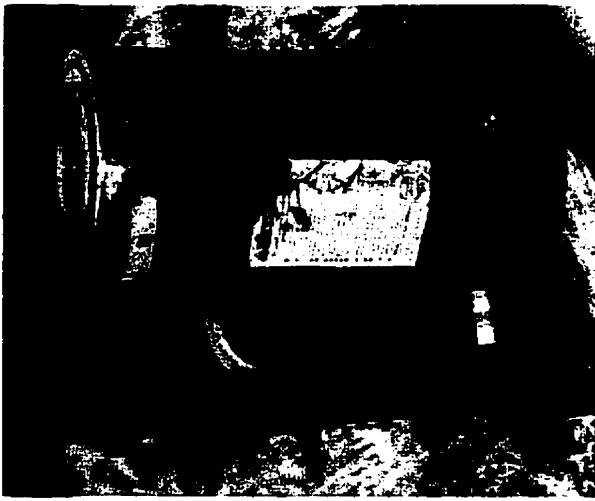
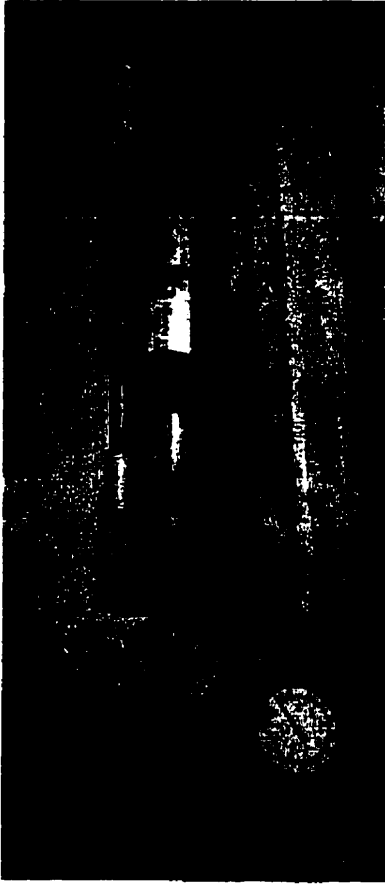


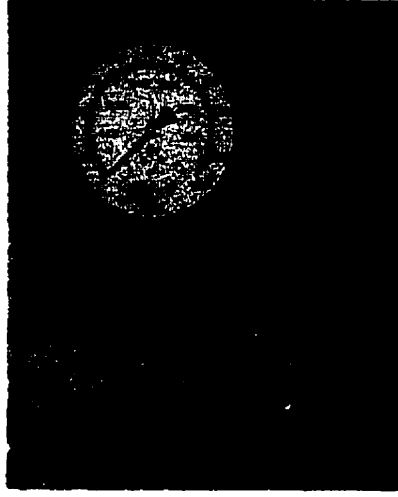
Figure 5.2: Site Layout at the Sand Pit Site



a)



b)



c)

Figure 5.3: The Loading System: a) Hydraulic Jack; b) Hydraulic Pump; c) Pressure Meter

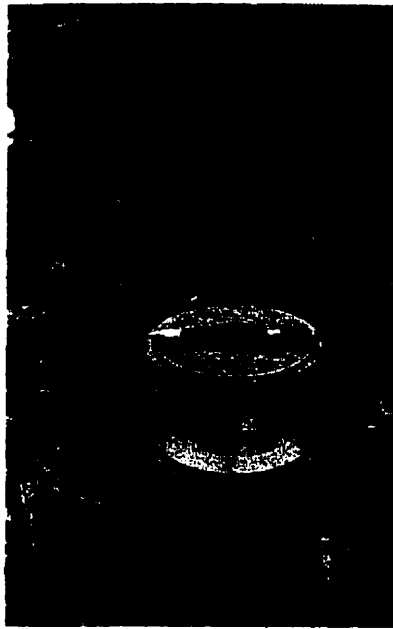


Figure 5.4: The Top Load Cell used to Measure Total Load Applied



Figure 5.5: Load Cell Setting is Used to Ensure No Eccentric Vertical Loading Applied

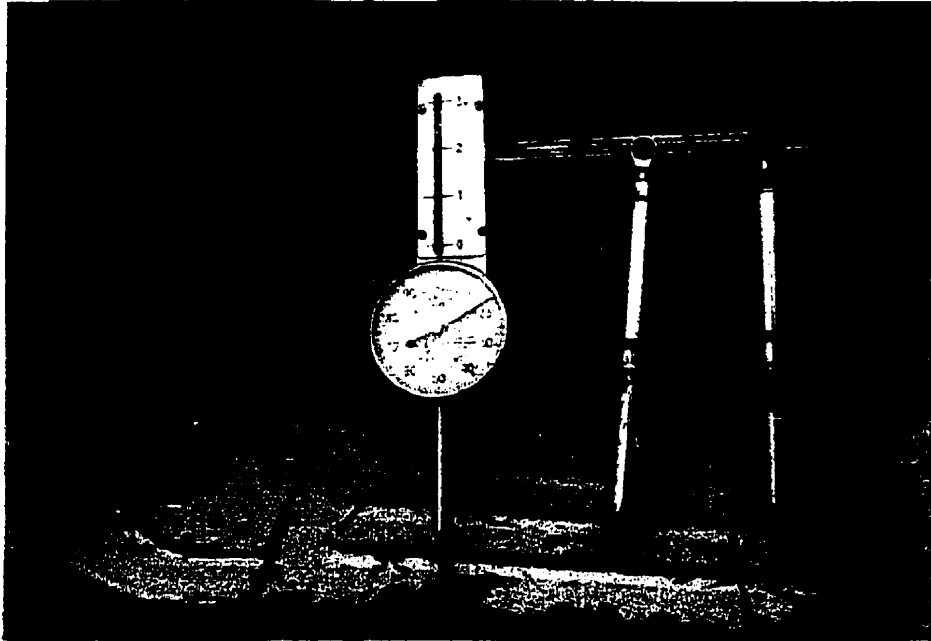


Figure 5.6: Electronic Displacement Potentiometers and Dial Gauge Used to Measure Displacement



Figure 5.7: Setup for the Electronic Displacement Transducers

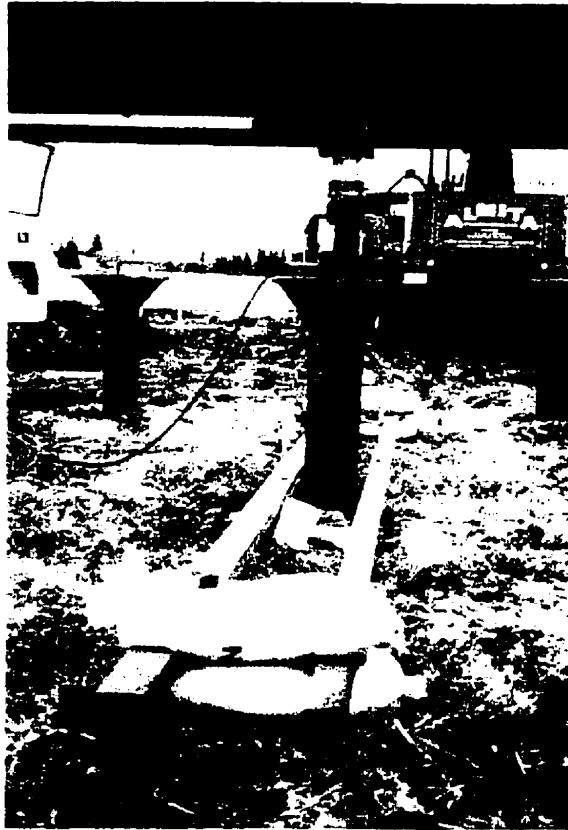


Figure 5.8: Reference Beam Location

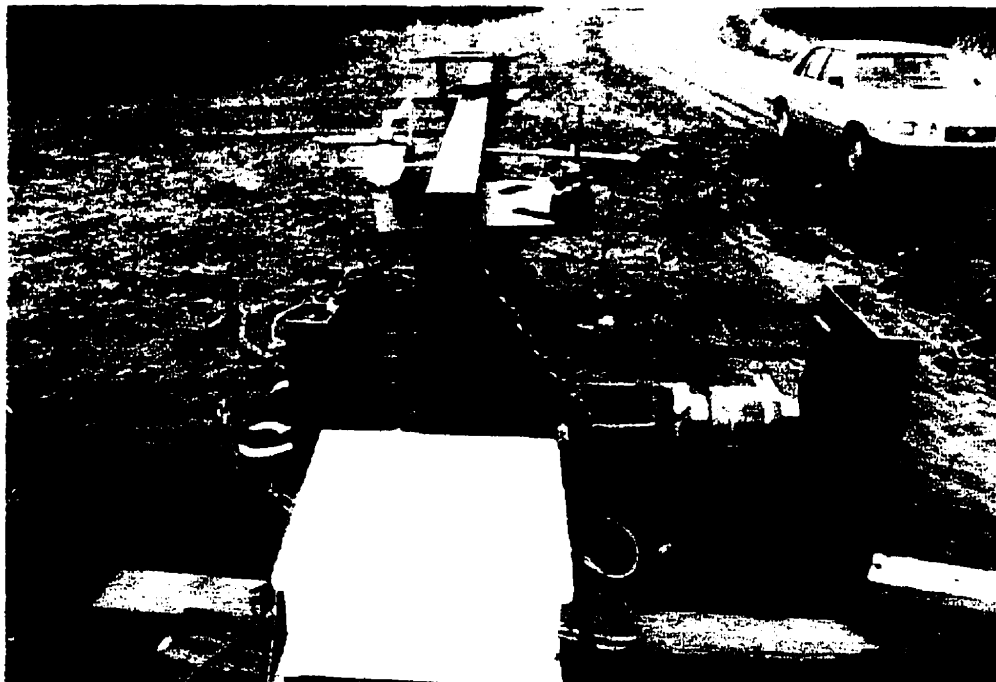


Figure 5.9: Displacement Transducer and Dial Gauge Location for Lateral Load Test

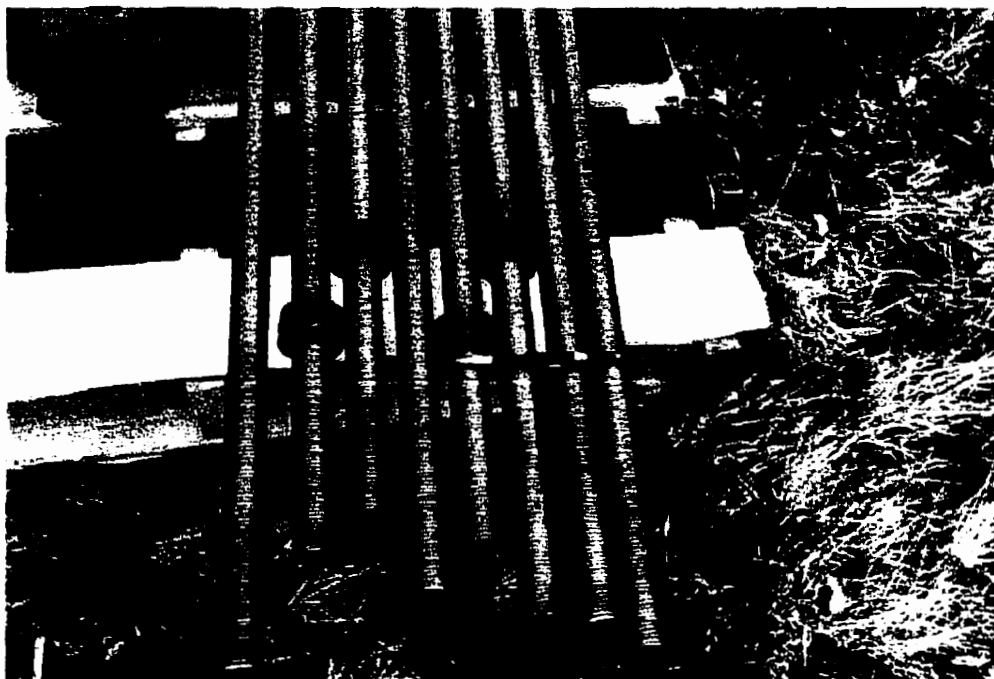


Figure 5.10: Steel Bars Used to Connect the Reaction Beam to the Test Pile



Figure 5.11: Plates Used to Connect the Test Piles to the Reaction Beam



Figure 5.12: Compression Test Setup at the University Farm Site

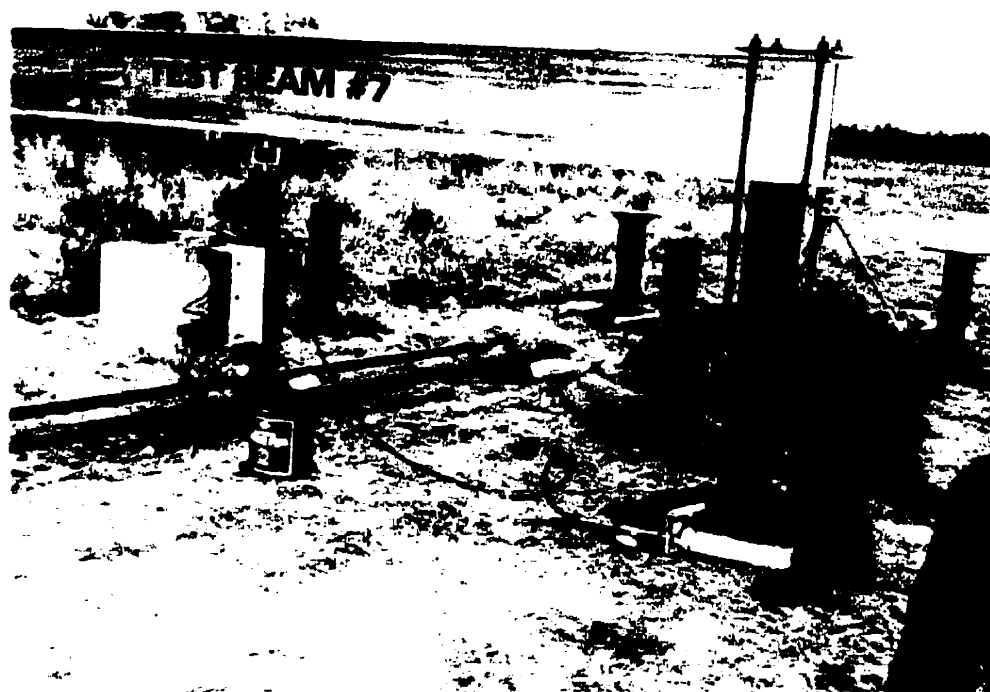


Figure 5.13: Loading the Test Pile during A Compression Test at the University Farm Site



Figure 5.14: Structure C-Channels Used for Making the Reaction Frame



Figure 5.15: Reaction Frame and Connection to the Reaction Pile at the University Farm Site

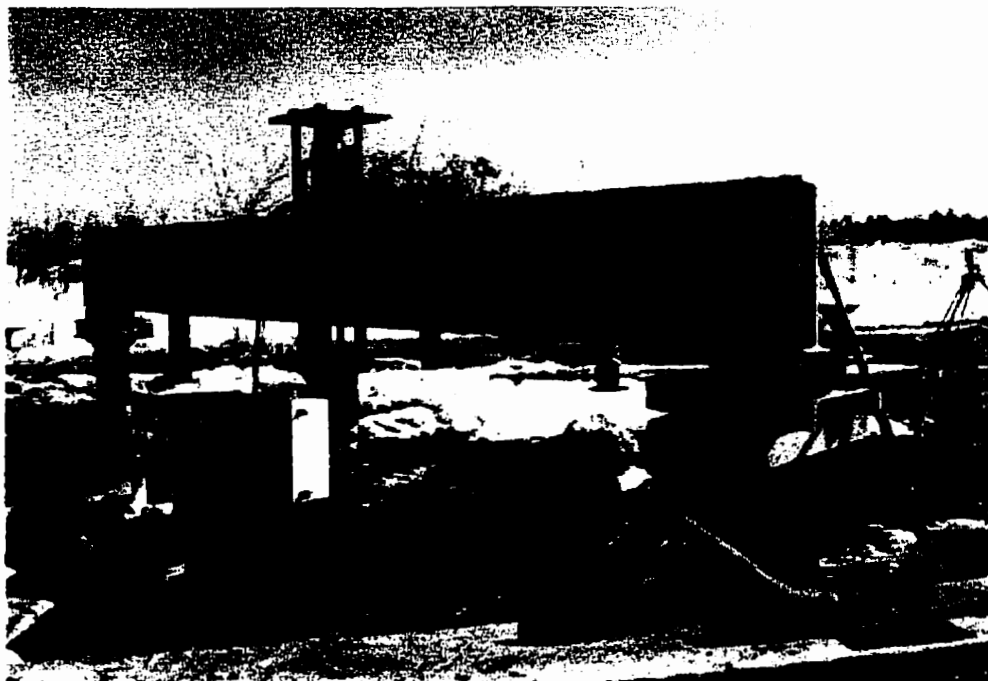


Figure 5.16: Tension Setup at the University Farm Site



Figure 5.17: Tension Setup at the Sand Pit Site



Figure 6.18: Setting Up the Tension Test at the Sand Pit Site



Figure 6.19: Reaction Setup Using Timber Cribbing for the Tension Test

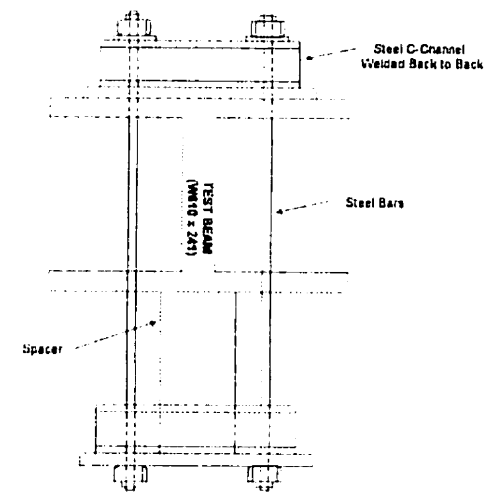
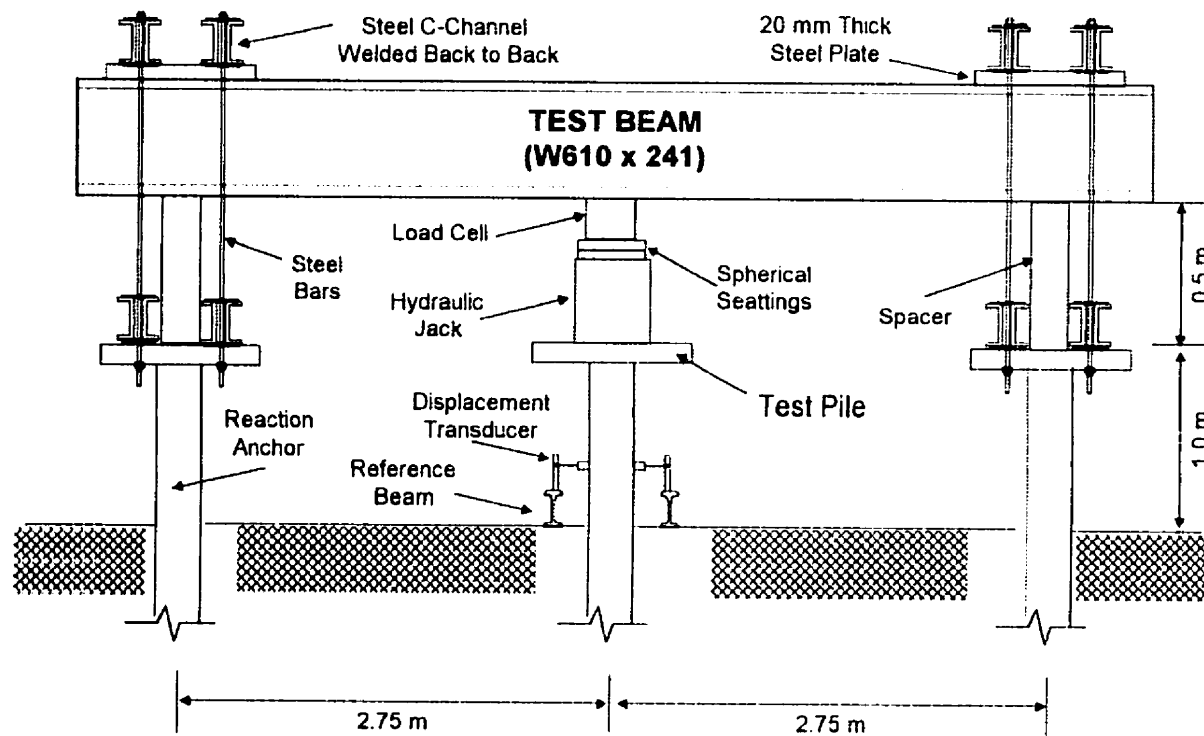


Figure 5.20: A Schematic Layout of the Compression Test

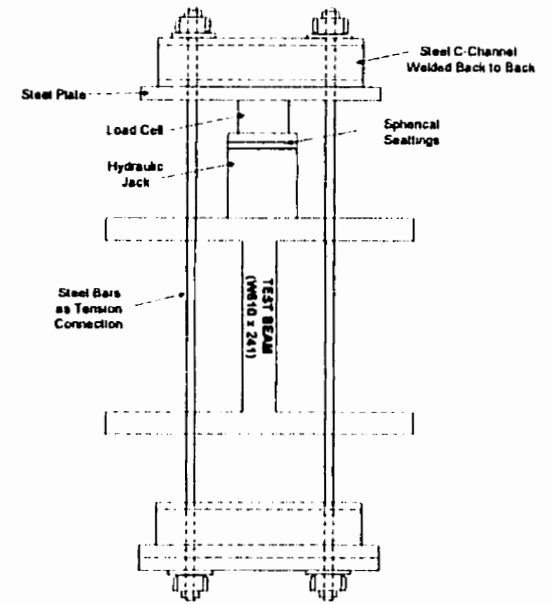
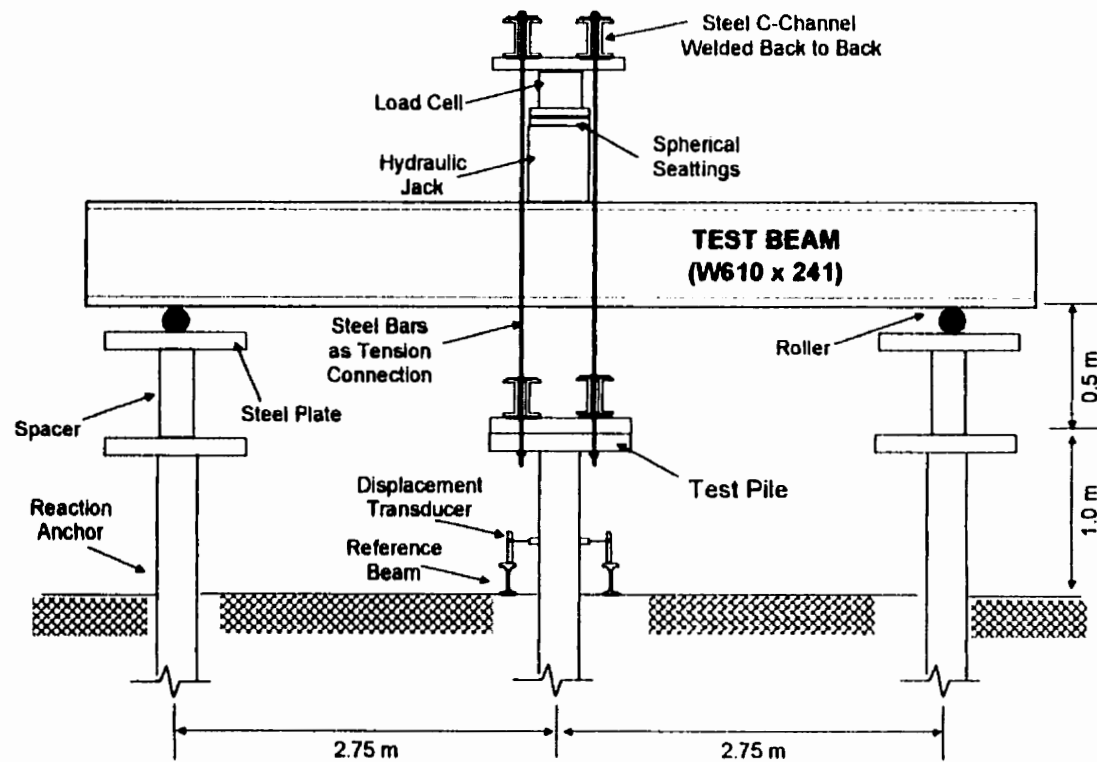


Figure 5.21: A Schematic Layout of the Tension Test



Figure 5.22: Reaction Frame Design for the Lateral Pile Load Test

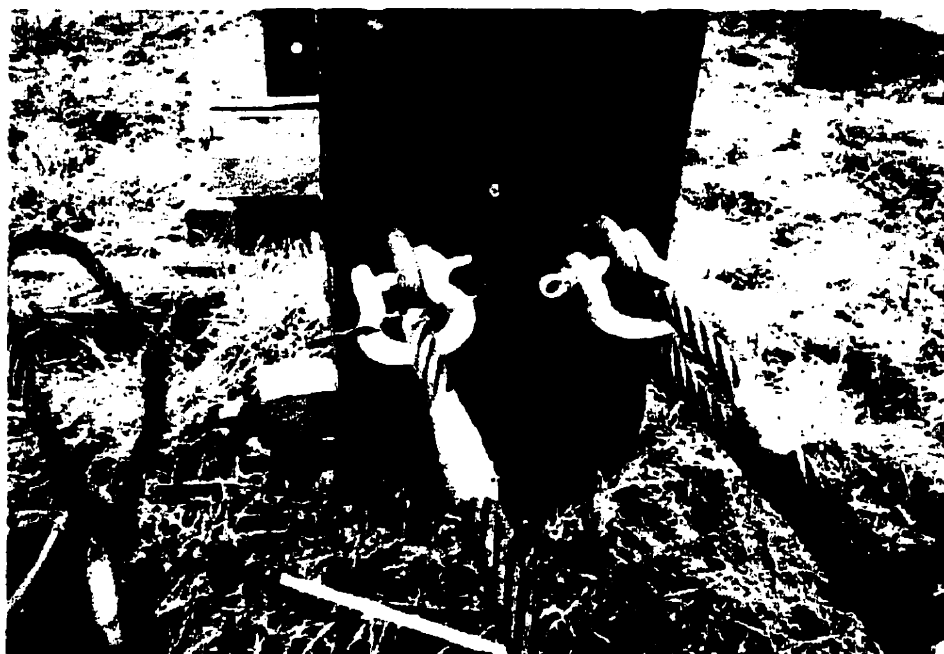


Figure 5.23: Steel Wire Rope Used in the Lateral Tests



Figure 5.24: Lateral Pile Load Test at the University Farm Site



Figure 5.25: Lateral Test Setup at the Sand Pit Site

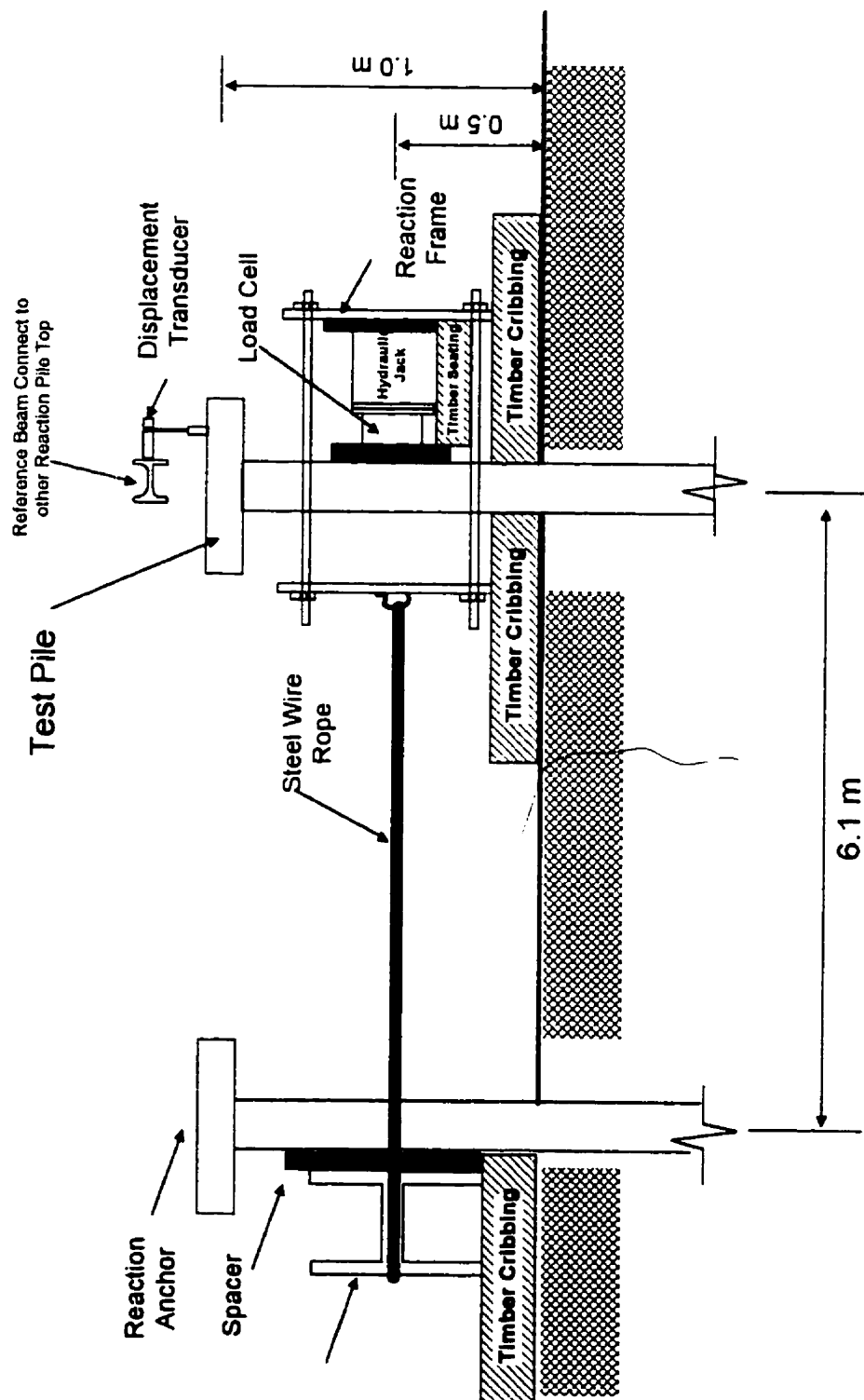


Figure 5.26: A Schematic Layout of the Lateral Test

CHAPTER 6 PILE LOAD TEST RESULTS

6.1 INTRODUCTION

This chapter presents the results obtained from the field test program conducted using full-scale screw piles. Ten pile load tests including five compression tests, three tension tests and two lateral tests were conducted on the University Farm site in central Edmonton. Eight pile load tests, including three compression, three pullout and two lateral pile load tests, were carried out on the Sand Pit site located near Bruderheim, northeast of Edmonton. A large amount of data were collected using the data acquisition system. It was difficult to present this data in their original format, therefore, the experimental data collected are summarized and are presented graphically. The original field data are saved to a hard diskette which can be found in Appendix C.

The results from the pile load test program are investigated to study the load-carrying behavior of screw piles installed in Lake Edmonton clay and sand. The discussion of the analysis is provided in this chapter. In addition, the predictions of the ultimate capacity in compression and tension of the screw pile using both indirect (theories) and direct (CPT) methods are presented. The predictions are compared to the field pile load test results. This comparison assists in providing recommendations for the future design of screw piles installed in these soils.

ALMITA Manufacturing Ltd. conducted an additional set of compression and lateral field pile load tests on the University Farm site in the winter of 1998 with assistance provided by the University of Alberta. The detailed test data are not included, however, the results obtained are compared to the first set of pile load test results presented in this thesis and these test results are used in the analysis on the ultimate capacity of screw piles at the University Farm site.

6.2 PILE CAPACITY RESULTS

6.2.1 Definition of Failure Load

For all the axial compression and tension tests performed, the screw piles were loaded according to the quick test procedure, described in ASTM D 1143 - 81 and ASTM D 3689 - 90. All the tests were carried out up to the ultimate load (failure) that was defined as the load corresponding to a pile top settlement greater than 10 % of the helix diameter (i.e. 35.6 mm). A similar quick loading procedure as described in ASTM D 3966-81, was used for all the lateral tests. The "failure" was assumed to be reached when more than 50 mm of lateral movement was observed (i.e. 23 % of the shaft diameter).

6.2.2 Axial Compression and Tension Test Results

For the compression piles tested at the University Farm site and the Sand Pit site, measurements were taken for each applied load increment in order to obtain the load-settlement curves, and these data are plotted in Figure 6.1 and Figure 6.2. For the tension tests at both sites, the total loads applied to pull the screw piles are plotted against the pile heave and the results are given in Figure 6.3 and Figure 6.4. The ultimate capacities obtained at failure for each test are summarized in Table 6.1 along with the geometry of the screw piles and the torque needed to install these piles.

As indicated in Table 6.1, the ultimate capacity in compression reached at the University Farm site were: 160 kN for screw pile with 3 helices installed to a depth of 3.05 m (CS test); 180 kN for screw pile with 3 helices installed to a depth of 5.18 m (CL test); and 210 kN for screw pile with 2 helices installed to a depth of 5.18 (Cprod.). Much higher capacities were obtained at the Sand Pit site with screw piles that have the same configurations, and the results were: 420 kN for CS test, 470 kN for CL test, and 380 kN for Cprod. test. For the tension tests, the results show that both TL test (3 helices installed to 5.18 m) and Tprod.

test (2 helices installed to 5.18 m) had the same uplift capacity, being 210 kN at the University Farm site and 360 kN at the Sand Pit site. For screw piles installed in shallower depth, the ultimate uplift capacity of TS test (3 helices installed to 3.05 m) was 140 kN at the University Farm site and 190 kN at the Sand Pit site.

6.2.3 Lateral Test Results

In lateral tests, the helical piles used were designed to have the same geometry as the compression and the tension test piles, and were installed to a depth of 5.18 m. The shaft wall thickness of the pile was varied in order to compare the difference in ultimate lateral capacity due to the change of the structural stiffness of the pile shaft. Two types of wall thickness (t) were chosen for testing, 6.71 mm and 8.18 mm. The load versus lateral movement curves are presented in Figure 6.5 and Figure 6.6. The results indicated that the ultimate lateral capacity achieved at the University Farm site were 40 kN for the L264 test ($t = 6.71$ mm) and 44 kN for the L322 test ($t = 8.18$ mm). At the Sand Pit site, the ultimate lateral capacity were 62 kN for the L264 test and 65 kN for the L322 test.

6.2.4 Load Transfer Mechanism

The distribution of the load along the pile shaft was established for each loading increment by analyzing the strain gauges installed at different locations inside of the pile shaft and end load cell installed inside the shaft at a distance approximately 0.3 m above the pile tip. The schematic of strain gauge and end load cell locations along with the site investigation results are presented in Figure 6.7 and Figure 6.8. The strain transducer output readings were used to determine the measured loads in the test pile at the strain gauge locations. Figure 6.9 and Figure 6.10 show the load distribution along the pile shaft at the various loading stages during the compression and tension tests carried out at the University Farm site. Figure 6.11 and Figure 6.12 present the load transfer

results at the Sand Pit site. The data points that are plotted in the graphs indicate the locations of the five levels of strain gauges installed along the pile shaft. The results of the measured load at failure indicated by the strain gauges for the compression and tension tests at the University Farm Site and the Sand Pit site are summarized in Table 6.2 and Table 6.3. The differences in measured load between strain gauge levels are presented in Table 6.4 and Table 6.5.

In the compression tests, the analysis of the data file indicated that the end load cells had measured no load in bearing. The reason is that a very stiff soil plug, consisting of a mixture of clay and gravel (previously the site was used as a snow dump by the University of Alberta), formed within the pile tip during the pile installation. The frictional resistance developed inside the shaft during the loading of the pile prevented this soil plug from being pushed up against the end load cell. The results provided by the end load cells were considered as unreliable and thus, excluded from the analysis. In addition, as indicated by Figure 6.9 and Figure 6.11, for the CS test pile, the heat, resulting from the welding process when assembling the pile sections, must have caused damage to the strain gauges installed at level 2 and level 3. Four out of six strain gauges installed at these levels gave no readings and the results for the remaining strain gauges were unreliable, therefore, the data were removed from the analysis and the graphical presentation.

By investigating the load from the strain gauges at various depths during each load increment, the load transfer mechanism to the surrounding soil can be studied. The observations, made on Figure 6.9 and Figure 6.10 (the University Farm site), indicated that the ultimate compression and tension capacity consist of three components: the shaft adhesion, the resistance along the cylindrical shear surface, and the bearing resistance from the bottom helix if loaded in compression or the top helix if loaded in tension. For piles installed in sand, similar behavior, as indicated by Figure 6.11 and Figure 6.12, can be drawn. Shaft frictional resistance, frictional resistance developed along the cylindrical failure surface formed around the helix area and bearing resistance contributed the ultimate capacity of screw pile installed in cohesionless soil. These

observations from the field test results verify previous studies carried out by Narasimha Rao et al. (1993) and Mitsch and Clemence (1985) in which they proposed a cylindrical failure surface to predict multi-helix screw pile capacity for piles with space to diameter ratio (S/D ratio) less than 2. According to the results from this study, it is reasonable to assume a cylindrical failure surface developed at failure for the three-helix screw pile ($S/D = 1.5$) used in the field tests. Figure 6.13 outlines the purposed cylindrical failure surfaces used for predicting the capacity for both the compression and the tension tests.

In order to assess the percentage of each component to the total ultimate resisted load, assumptions on the proposed cylindrical failure surface were made in order to evaluate the measured load according to each category (i.e. shaft resistance Q_{shaft} , bearing resistance $Q_{bearing}$ and cylindrical shearing resistance $Q_{interhelix}$). For example, for the compression tests at the University Farm site, the difference in measured load in the pile at any two points is the load transferred to the surrounding soil in the form of shaft adhesion or the cylindrical shear resistance. Since the surface area of the pile shaft and the cylindrical surface connecting the top and bottom helices is known, the average value of unit shaft adhesion or the resistance along the cylindrical shear surface can be calculated. Similarly, for piles loaded in compression in cohesionless soil, the shaft friction and cylindrical friction resistance can also be computed under the same assumption. For the CL tests at the University Farm site and the Sand Pit site, the differences in measured load between two levels of strain gauges are summarized in Table 6.4 and Table 6.5. Based on these results, the variations of the unit shear resistance over the pile length can be plotted and the results are shown in Figure 6.14. By assuming a cylindrical failure surface was mobilized at failure for both compression and tension tests, loads measured at failure by the five levels of strain gauges can be categorized into each component as shown in Table 6.6. Then, the percentage contribution by each component can be compared to the ultimate capacity, and these results are summarized in Table 6.7. Examining the values presented in Table 6.7, the following observation may be made:

1. Resistance developed along the pile shaft increases with the installation depth. At the University Farm site, the shaft adhesion increases from 20 % (CS test) to 32 % (CL) and 37 % (CL2) as the embedment depth increases from 3.05 m to 5.18 m. At the Sand Pit site, the shaft resistance increases from 6 % (CS) to 26 % (CL) with the same increase in installation depth.
2. At shallow depth (CS and TS tests with $H/D = 4.69$), the shaft resistance developed in tension was significantly higher than resistance in compression. At the University Farm site, the shaft adhesion contributed 36 % of the ultimate uplift capacity (TS test) comparing to 20 % to the ultimate capacity in compression (CS). At the Sand Pit site, 16 % of the ultimate capacity in tension was delivered by the shaft resistance and only 6 % of the total compression capacity was measured by the shaft friction. However, at greater depth ($H/D = 10.7$), there was no significant difference in shaft resistance due to loading direction.
3. The bearing resistance in compression contributes 20 % to 39 % of the total capacity and 14 % to 19 % of the ultimate pullout capacity for the tension tests. The bearing capacities for the compression tests at the Sand Pit site are slightly higher than the bearing capacities obtained at the University Farm site, being 36 % to 45 % for the compression tests and 19 % to 22 % for the tension tests respectively.
4. For the cohesive material (the Lake Edmonton clay), the load was mainly transferred to the surrounding soil by the shaft adhesion and the cylindrical shearing resistance. As indicated in Table 6.7, both components contribute 61 % to 80 % for the compression tests and 81 % to 86 % for the tension tests at the University Farm site. Similar behavior is observed for the screw piles installed in the cohesionless material (the Sand Pit site), 55 % to 65 % of the total compression capacity are obtained from the frictional components and 78 % to 81 % of total pull out capacity are developed from the shaft and cylindrical shear resistance.

6.3 DISCUSSION ON THE PILE LOAD TEST RESULTS

6.3.1 Effective Shaft Length, H_{eff}

At the University Farm site, as shown in Table 6.4, Table 6.5 and Figure 6.14, the outputs obtained from the strain gauge level 1 and Level 2 of the compression tests (CL tests) indicate the shaft adhesion developed at failure. For a length of approximately $1.0 \times D$ above the top helix, the shaft resistance was not mobilized at failure. This behavior is demonstrated in Figure 6.14 where the field results show no differential load measured between strain gauge level 2 to level 3. These experimental results support the study conducted by Trofimenkov and Mariupolskii (1965) and Narasimha Rao and Prasad (1991). These researchers indicated that the shaft adhesion along a length approximately equal to the helix diameter (D) could not be mobilized due to the formation of the shadow effect above the top helix in the compression test. Therefore, an effective shaft length ($H_{eff} = H - D$), where H is the installation depth and D is the diameter of the top helix, should be used to calculate the shaft adhesion.

For the tension tests performed, as explained in Section 2.4.4.1, the soil above the top helix mobilized in uplift could be evaluated similar to that below a deep foundation in bearing. For a pile loaded in compression, the failure zone could extend over a depth of almost twice the diameter below the tip of the pile. Similarly, a failure zone could form above the top of the helix when the screw pile is loaded in tension. For studies conducted using multi-helix screw piles installed in soft marine clay, Narasimha Rao and Prasad (1993) stated that there was an ineffective length of the pile shaft that could not be mobilized at failure. Based on the laboratory test results, Narasimha Rao and Prasad (1993) provided some insights for estimating the effective shaft length that can be used in design. For a transition pile with H/D of 3 and 4, the effective shaft length (H_{eff}) ranges from $0.7D - 0.9D$ and $1.7D - 2.5D$. For a deeper pile, the H_{eff} values are in the range of $2.9D - 8.6D$. The field test results performed by the current study indicated that for the shallow pile (TS tests) with $H/D = 4.69$ installed in stiff clay (Lake Edmonton clay), the H_{eff} is approximately

3.45 D and for the deep pile (TL tests) with $H/D = 10.7$, the H_{eff} is estimated as 9.45 D . Therefore, for the pile loaded in uplift, an effective shaft length ($H_{eff} = H - D$) as defined previously should also be used when evaluating the shaft adhesion for the tension tests. At the Sand Pit site, the same behavior can be shown from the field test results obtained from the CL and TL tests performed. Therefore, the ultimate resistance developed along an effective shaft length (H_{eff}) similar to that as described above should be used to predict the shaft friction for piles loaded in compression and tension in cohesionless soil.

The results shown in Table 6.6 indicated that the shaft adhesion mobilized at failure were higher than the results from the compression test. In theory, the shaft adhesion developed in the tension tests should be the same as in the compression tests because the failure surfaces were the same regardless of the loading direction (i.e. piles with same shaft length installed in the same soil). As explained previously, the zone of bearing failure above the top helix could be as much as twice that of the diameter of the helix diameter. Therefore, the difference in measured load is believed to be contributed partially by the bearing resistance of the top plate, but not necessarily entirely by the shaft adhesion.

6.3.2 Effect of the Bearing Capacity in Compression versus in Tension

The results obtained at both test sites indicated that the bearing capacity in compression is almost twice the capacity in tension. Adams and Hayes (1967), Adams and Klym (1972), Meyerhof and Adams (1968), Mooney et al. (1985) and Mitsch and Clemence (1985) all stated that the mechanism of mobilizing the soil above the top helix in uplift loading can be assumed to be similar to the failure conditions below a deep foundation in bearing. However, Bhanot (1968) indicated that laboratory experiments performed on clay samples collected at the University Farm site had shown a 40 % decrease in undrained shear strength (see Table 4.3 in Chapter 4) when the soil was remolded. For the tension tests, the soil above the top plate is disturbed by the rotary action during the installation of the screw pile and the decrease in undrained shear strength may be the

reason that cause the bearing capacities in tension to have a much lower value. For the cohesionless soil, the installation of helical piles induces significant stress changes in the soil, which can have a great influence on the screw pile uplift behavior. Vesic (1971) stated that the soil surrounding the anchor is disturbed by the anchor installation which results in loosening of soil within the disturbed zone, and the degree of loosening effect depends on the relative density of the sand. Therefore, the internal friction angle ϕ might be lower for the soil above the top helix, which causes the bearing capacity in tension to be lower than that for an undisturbed soil. In the case of compression tests, the soil below the bottom helix is undisturbed, therefore, the bearing capacity for the plate against an undisturbed soil should be higher than the capacity in tension.

6.3.3 Effect of the Cylindrical Resistance

The cylindrical resistance, developed along the failure surface formed around the helical plates, is significant despite the different soil types into which the piles were installed. At the University Farm site, the resistance consists of 31 % to 51 % of the total ultimate capacity for both compression and tension tests respectively. Similarly, at the Sand Pit site, the resistance for both tests ranges from 38 % to 62 % of the total ultimate capacity. Therefore, there is a significant increase in capacity by using multi-helix screw pile instead of single helix screw pile regardless of the pile loading direction.

6.3.4 Effect of Embedment Ratio (H/D)

The ultimate capacities shown in Table 6.1 are plotted in Figure 6.15 in order to compare the effect of embedment ratio on the ultimate capacities. As demonstrated in Figure 6.15, at the University Farm site, there is a 13 to 31 % increase in ultimate compression capacity (Q_c), and 50 % increase in ultimate uplift capacity (Q_t) as the embedment ratio increased from 4.69 to 10.7 for screw piles installed in cohesive soils. Similarly, for piles installed in cohesionless

material at the Sand Pit site, an 12 % increase in compression capacity and 90 % increase in tension capacity was found as embedment ratio increases. Therefore, the ultimate capacities in compression and tension increase with the increase of screw pile installation depth, however the increase is more significant in tension.

6.3.5 Effect of Space to Diameter Ratio (S/D)

The ultimate compression and tension capacities are plotted against the space to helix diameter ratio (S/D) and the results are shown in Figure 6.16. For the compression tests at the University Farm site, the production piles (Cprod. or Tprod. tests), installed to a depth of 5.18 m ($S/D = 3.0$), yielded a 17 % higher ultimate capacity in compression than the research pile ($S/D = 1.5$, i.e. CL or TL test's). However, at the Sand Pit site, different behavior was observed. Research piles with S/D of 1.5 resulted in higher ultimate capacity in compression than the production piles ($S/D = 3.0$). A 24 % increase in capacity was observed for the smaller S/D ratio. Nevertheless, both the research piles and production piles had essentially the same pullout capacity in tension tests at both test sites.

The reduction in ultimate capacity of the three-helix research pile ($S/D = 1.5$) in compression in the cohesive soil may be caused by soil disturbance due to pile installation. If the second and third helices do not follow the path of the first helix, then, the helical screws create a higher degree of soil disturbance along the surface surrounding the screw pile. This effect may reduce the undrained shear strength of the soil if the soil is sensitive to the disturbance (Bradka, 1997). Therefore, for screw pile installed in Lake Edmonton clay, the closer the helices are to each other, i.e. the lower the S/D ratio, the higher the soil disturbance due to installation if the helices are not properly designed. Soil disturbance is not a factor in cohesionless material, as the research pile ($S/D = 1.5$) reached a much higher capacity than the production pile ($S/D = 3.0$). In tension test, the S/D ratio

did not have an effect on the ultimate pullout capacity of the pile. Both piles ($S/D = 1.5$ & $S/D = 3.0$) showed essentially the same uplift capacity at both sites.

6.3.6 Ultimate Capacity in Compression versus in Tension

The ultimate capacity in compression and tension are similar in the cohesive material. However, for piles installed in cohesionless material, the ultimate capacity in compression is much higher than in tension especially for the short piles (121 % increase). As discussed previously, in the Lake Edmonton clay, the resistance of the screw pile was mainly developed by shaft adhesion and resistance developed along the cylindrical shear surface. Therefore, difference in loading direction does not affect the ultimate capacity significantly because resistance was developed by the same failure surface (see Figure 6.13). However, the contribution to the ultimate capacity from the end bearing becomes more significant in the cohesionless material. In addition, as discussed previously, the shear resistance of cohesionless soil is sensitive to the soil disturbance due to the pile installation process. The screwing action may loosen the soil surrounding the pile. Therefore, the disturbed soil strength property above the top helix (pile in tension) may be lower than the soil below the bottom helix that is less disturbed (pile in compression). As shown in Table 6.7, the measured bearing capacities in compression are more than twice of the bearing capacities in tension. Consequently, the ultimate capacity in compression is much higher than the ultimate capacity in tension for screw piles installed in cohesionless soil.

6.3.7 Lateral Capacity

CFEM (1992) states that the vertical piles resist lateral load or moment by deflecting until the reaction in the surrounding soil is mobilized. Therefore, the lateral capacity of a deep foundation depends essentially on the stiffness of the pile and the strength of the surrounding soil. Results shown in Figure 6.5 to 6.6

demonstrate that there is no significant increase in lateral capacity due to the increase in shaft wall thickness or the increase in structure stiffness. The results indicated that for a 22 % increase in structure stiffness, only 10 % increase in ultimate lateral load for piles installed in clay (Lake Edmonton clay) and 5 % increase in ultimate lateral capacity for piles installed in cohesionless soil (Sand). Hence, the load versus lateral movement response in lateral loading for these screw piles in these soils is mainly dependent upon the soil characteristics, such as the coefficient of horizontal subgrade reaction (k_{sub}), the undrained shear strength of a cohesive soil, the soil internal friction angle and the relative density of a cohesionless soil.

6.4 PILE CAPACITY PREDICTION

The design of pile foundations using in situ test results can be categorized into two separate approaches; the direct and indirect. Campanella et al. (1989) provided a clear explanation for each approach and their definitions are adopted as follows:

“Direct Approach: provides the opportunity to pass directly from in situ measurements to the performance of foundations without the need to evaluate any intermediate soil parameters.

Indirect Approach: leads to design methods that require the evaluation of parameters such as, strength, stiffness and consolidation. These parameters are then applied to the solutions of boundary value problems”.

The prediction of ultimate pile capacity using both indirect and direct methods is separated into four stages. As indicated by the test results, three components including the shaft, cylindrical shearing and bearing resistance contributed to the ultimate capacity regardless of the loading direction. Therefore, analyses are performed for each component using the indirect methods reviewed in Chapter 2 with the assumption that a cylindrical failure

surface was formed at failure (see Figure 6.13). Schematic layouts of both short and long research piles are presented in Figure 6.7 and Figure 6.8 indicating the dimensions of the research piles along with the soil strength property results obtained from the site investigation. Lastly, some of the design methods proposed by previous works are used to predict the screw pile capacities and the results are compared to the measured pile load capacity. In addition to the prediction using indirect methods, the direct methods, namely the CPT methods, are also used to estimate the ultimate pile capacities. The prediction results obtained from the direct methods are then compared to the values obtained using the indirect methods.

6.4.1 Prediction of Shaft Resistance

Methods used to evaluate the shaft adhesion for tests performed at the University Farm site are listed in Table 6.8. The adhesion factor α and undrained shear strength of the cohesive material used in the calculations are also indicated in the table. Similarly, the shaft resistance developed for piles installed at the Sand Pit site is computed using theoretical methods indicated in Table 6.9. The soil internal friction angle ϕ and lateral earth pressure coefficient used in the analysis are also presented in Table 6.9. The predictions are compared with the experimental measured values as shown in Table 6.6, and the comparison are presented graphically in Figure 6.17 and Figure 6.18. As explained in Section 6.3.1, an effective length ($H_{eff} = H - D$) was used to compute the shaft resistance regardless of the loading direction. Therefore, the shaft resistance predicted results for the compression tests are essentially the same as for the tension tests.

In the cohesive soil, the indirect methods used to evaluate the shaft adhesion tend to underestimate the shallow conditions and over predict the deep conditions. All the methods underestimate the shaft adhesion in tension significantly. The underestimation ranges from 31 % to 71 % for the research pile installed in shallow depth. As explained previously, the shaft adhesion in

compression and tension should be the same because the areas that shaft adhesion can be mobilized are the same for both of the tests. This increase in shaft adhesion for the TS test may be contributed partially by the bearing resistance of the top helix. Comparing the prediction results, the adhesion factors provided by Mooney et al. (1985) and the chart provided by Tomlinson (1957) is useful for preliminary assessment of the shaft adhesion.

For a pile installed in cohesionless soil, the behavior of the shaft resistance developed is comparable to those found for driven piles in the literature. The lateral earth pressure coefficient for a pile loaded in compression (K_s) given by CFEM (1992) and Meyerhof (1982) provides reasonable results. For piles loaded in tension in sand, the reduced lateral earth pressure (K_u) value provided by Mitsch and Clemence (1985) provides better prediction of shaft resistance for piles installed in deep condition ($H/D = 10.7$). However, K_u provided by Meyerhof (1968) gives a better prediction for piles installed in shallow condition ($H/D = 4.69$).

6.4.2 Ultimate Pile Bearing Resistance

The design approaches used to evaluate the bearing capacity of the pile installed in the Lake Edmonton clay and sand are presented in Table 6.10 and Table 6.11. The prediction results are compared with the experimental measured values and these comparisons are shown in Figure 6.19 and Figure 6.20.

In the cohesive soil, the bearing capacity theory, proposed by Meyerhof (1976), provides reasonable results for piles loaded in compression regardless of the embedment depth of the piles. For the tension tests, the methods used to predict the uplift bearing capacity overestimate for both TS and TL tests with significant over prediction of as much as 144 % for the TS test. As discussed in Section 6.3.2, Bhanot (1968) reported a 40 % decrease in undrained shear strength when the soil is remolded. Therefore, the soil disturbance created by

the rotary action during the pile installation may remold the undrained shear strength of the surrounding soil to a much lower value. In addition, as indicated by Adams and Radhakrishna (1971), the strength mobilized at the shallow depth is largely the fissured strength, whereas at a greater depth a portion of the intact strength is mobilized. Thus, the uplift coefficient, N_u proposed by Meyerhof and Adams (1968) should be adjusted for the screw pile installed in stiff clay. Adams and Hayes (1967) reported similar findings for shallow anchors installed in stiff clay, here they state that the calculated N_u from the field tests were generally only about half the laboratory values. The authors reasoned that this reduction in uplift bearing capacity factor N_u was due to the desiccated soil crust in which the screw piles were installed. In this desiccated zone, the soil is mostly fissured, and the undrained shear strength of the fissured clay mobilized under pullout loads could be much less than the undrained shear strength determined using intact samples (i.e. laboratory samples). For screw piles installed in greater depth, a portion of the intact strength was mobilized which contributed higher uplift bearing capacity. Nevertheless, for the TL test, a theoretical limiting value of $N_u = 9$ provides reasonable uplift bearing capacity prediction for the TL test.

For screw piles installed in cohesionless soil, as shown in Table 6.11 and Figure 6.20, bearing capacity theories available grossly overestimate the pile bearing capacity in compression for the shallow condition (CS test), and give better results for deep conditions (CL test). Vesic (1963) calculated the bearing capacity factors N_q based on the cavity expansion theory. Kulhawy (1984) reviewed and extended Vesic's concepts and proposed his modified bearing capacity factor for deep foundations. The bearing capacity factors proposed by both authors are shown in Figure 2.10 and Figure 2.11 in Chapter 2. The bearing capacity factor N_q developed based on a cylindrical failure surface as proposed by Vesic (1963) provides better bearing capacity prediction comparing to the model provided by Meyerhof (1976). The prediction results using methods provided by Vesic (1963) and Kulhawy (1984) provide excellent agreement with the measured field test results for screw piles installed in greater depth (CL test). For screw pile in shallow condition (CS test), the bearing capacity calculated

based on N_q value provided by Vesic (1963) over predicts the measured $Q_{bearing}$ by as much as 50 %. As discussed in Section 4.3.2.2, Chapter 4, the site investigation results (SPT and CPT) obtained from the Sand Pit site correlate to a very high soil internal friction angle ϕ (39° to 45°) and soil relative density D_r (ranges between 80 % to 90 %) for the upper 3.0 m of the soil stratigraphy. The results obtained from these in situ tests are unreasonably high for a medium sand dune deposit with a typical ϕ value of 30° to 35° . It is reasoned that this high friction angle is a result of the desiccated soil crust. The site investigation was performed in the early winter season when the water table was very low (around 4.5 m). The matrix suction force in the upper soil crust, as a result of the surface vegetation drawing water from the ground water table, can be significant. This suction force might be the reason that causes unreliably high friction angle and relative density of the soil. However, the pile installation process eliminated the suction force due to the rotary action when screwing the pile into the ground and thus, resulting a lower friction angle compared to the site investigation results. However, the degree of change in friction angle can not be properly assessed by the in situ tests available currently. For deep piles where the bottom helix was located around the water the table, this effect is not a factor that might effect the capacity prediction, and therefore, the prediction provided by Vesic (1963) and Kulhaway (1984) agrees with the measured experimental value well.

For piles loaded in uplift condition, the breakout factor F_q based on research work carried out by Meyerhof (1968) provides good agreement prediction with the measured bearing capacity for shallow pile in tension. For deep pile condition, F_q based on Saeedy (1987) gives much better prediction of the bearing capacity in uplift.

6.4.3 Ultimate Cylindrical Shearing Resistance

Analysis on the shearing resistance developed along the cylindrical failure surface formed between the top and bottom pile helix are presented in Table 6.12

and Table 6.13. The results are compared to the measured value and graphically presented in Figure 6.21 and Figure 6.22. The full length of cylindrical shear resistance could not be measured due to the location of the strain gauges installed inside of the pile shaft. Therefore, the measured load only indicates the shear resistance over the length that could be measured by the strain gauges as indicated in Table 6.6. The prediction of the cylindrical resistance is calculated based on the length as shown in Table 6.6.

For a cohesive soil, the cylindrical shear method provides reasonable results comparing to the measured values, although over prediction of as much as 91 % is observed for the TS test. However, the disagreement may be caused by number of reasons. Most importantly, the variation in soil strength properties over the soil profile can not be estimated accurately because only three cone penetration tests were performed across the University Farm site as a part of site investigation program. For instance, if the screw pile was installed with helices located in a soft clay pocket that was not detected by the CPT test, much lower shear resistance can develop.

For piles installed in sand, the lateral earth pressure value provided by ASCE (1992) for driven piles in dense sand provide good agreement with the measured values for the compression tests. For the tension tests, the lateral earth pressure in uplift (K_u) provided by Meyerhof (1968) over estimate by 45 % for shallow anchor and 15 % for deep anchor. Predicted values using K_u proposed by Mitsch and Clemence (1985) agrees with the measured value for shallow anchor, but under estimate by 31 % for deep anchor. However, using K_u provided by Mitsch and Clemence (1985) for shallow anchor and K_s value provided by ASCE (1993) for deep anchor, the predictions agree with the measured values very well.

6.4.4 Ultimate Screw Pile Axial Capacity Prediction Using Both Indirect and Direct Methods

A summary of the methods used to predict the axial pile capacities is shown in Table 6.14 and Table 6.15. The prediction results are compared graphically with the measure ultimate capacity and the results are presented in Figure 6.23 and Figure 6.24. As explained in Chapter 2, previous researches have focused on predicting the uplift capacity of the screw piles because they are commonly used for engineering applications where the pullout capacity of screw piles are most important. As a result, little published research works done on screw piles are available to predict the compression capacity. Therefore, the capacity prediction is mainly performed using the direct method. For the tension tests, approaches proposed by different studies, including the cylindrical shear, the individual bearing and the empirical approaches, are used to predict the screw pile tension capacity. These indirect methods require correlations to predict soil parameters and these parameters are shown in Figure 6.7 and Figure 6.8. In addition to the indirect methods, the direct methods, the cone penetration methods (CPT methods) are also used to estimate the pullout capacity.

For the cohesive soil, Table 6.15 and Figure 6.24 show that both direct and indirect methods provide reasonable predictions for screw piles loaded in compression and tension. For the compression tests, the cylindrical shearing method, proposed by Narasimha Rao et al. (1991), overestimated the screw pile capacity in compression with a maximum over prediction of 52 % for the CL test. In comparison to the indirect method, the direct methods, namely the LCPC method proposed by Bustamante and Gianeselli (1982) and the de Ruiter and Beringen (1979) method, provided satisfactory prediction results. The best results were obtained using CPT method proposed by de Ruiter and Beringen (1979). The LCPC method underestimated the compression capacity by as much as 30 % for the CS test. For the tension tests, all the methods provided good prediction. In general, the indirect methods tend to over predict the uplift capacity especially for the screw piles in shallow condition (TS test). For the

CPT method, the direct method by de Ruiter and Beringen (1979) provides excellent prediction and the LCPC method underestimated the pullout capacity by as much as 25 %.

For the cohesionless soil, only the direct methods were used to predict the compression capacity of the piles. Both methods provided reasonable results with best predictions given by the LCPC method. For the pullout tests, the direct methods gave satisfactory results for the deep pile condition, but over predicted the pullout capacity by as much as 164 % for the shallow pile condition. This large discrepancy may be a result of number of factors. First, as discussed previously, the site investigation results are believed to be unreliably high for the shallow depth due to the presence of the desiccated soil crust, which results over prediction of the pile uplift capacity. Secondly, the direct methods were developed for more conventional pile types, such as the bored pile, driven pile with simple failure surface and the capacity are mainly contributed by the shaft resistance and bearing resistance. Although methods provided by Bustamante and GIANESSELLI (1982) included various pile types including the cast concrete screw pile, however, the method was developed mainly for predicting the compression capacity and the methods was not formulated for predicting the uplift capacity. Therefore, modifications of the methods are required in order to properly assess the uplift capacity of a multi-helix screw pile. For the indirect methods, both the cylindrical shear and the individual bearing methods provide satisfactory results. The empirical method provided good uplift capacity prediction for deep condition screw pile and overestimated significantly for the shallow condition.

6.5 REFERENCE

- Adams, J. I, and Klym, T. W. (1972). "A Study of Anchors for Transmission Tower Foundation"; Canadian Geotechnical Journal, Vol. 9, No. 1, pp. 89-104.
- Adams, J. I., and Hayes, D. C. (1967). "The Uplift Capacity of Shallow Foundation"; Ontario Hydro Research Quarterly, Vol. 19, pp. 1-13.
- Adams, J. I., and Radhakrishna, H. S. (1971). "Uplift Resistance of Augered Footings in Fissured Clay"; Canadian Geotechnical Journal, Vol. 8, pp. 452-462.
- ASCE (1993). "Bearing Capacity of Soils"; Technical Engineering and Design Guides as Adapted from U.S Army Corps of Engineers, No. 7, ASCE Press, New York, 147 pp.
- ASTM D 1143-81 (1981). "Standard Test Method for Piles Under Static Axial Compressive Load"; (Reapproved 1984). Annual Book of ASTM Standards, 1997, Vol. 04.08, pp. 95-105.
- ASTM D 3689-90 (1990). "Standard Test Method for Individual Piles Under Static Axial Tensile Load"; (Reapproved 1995). Annual Book of ASTM Standard, 1997, Vol. 04.08, pp. 366-375.
- ASTM D 3966-90 (1990). "Standard Test Method for Piles Under Lateral Loads"; (Reapproved 1995). Annual Book of ASTM Standards, 1997, Vol. 04.08, pp. 389-399.
- Bella, A. (1961) "The Resistance to Breaking-out of Mushroom Foundations for Pylons"; Proceedings of 5th International Conference on Soil Mechanics and Foundation Engineering, Paris, France, Vol. 1, pp 569-576.
- Bhanot, K. L. (1968). "Behavior of Scaled and Full-Length Cast-In-Place Concrete Piles"; Doctor of Philosophy Thesis, Department of Civil Engineering, University of Alberta, Edmonton Canada.
- Bradka, T. D. (1997). "Vertical Capacity of Helical Screw Anchor Piles"; Master of Engineering Reports, University of Alberta, Alberta, 97 pp.
- Bustamante, M., and Gianceselli, L. (1982). "Pile Bearing Capacity Prediction by Means of Static Penetrometer CPT"; Proceedings of the 2nd European Symposium on Penetration Testing, ESOPT-II, Amsterdam, 2, pp. 493-500, Balkema Pub., Rotterdam.
- Das, B. M. (1990). Earth Anchors. Elsevier, Amsterdam, 241p.

- Das, B. M. (1980). "A Procedure for Estimation of Ultimate Uplift Capacity of Foundations in Clay"; *Soils and Foundation, Japan*, Vol. 20, No. 1, pp. 77-82.
- De Ruiter, J., and Beringen, F. L. (1979). "Pile Foundations for Large North Sea Structures"; *Marine Geotechnology*, 3(3), pp. 267-314.
- Campanella, R. G., Robertson, P. K., Davies, M. P., and Klohn, A. S. Y. (1989). "Use of In Situ Tests in Pile Design"; *Proceedings of Seventh International Conference of the International Society for Soil Mechanics and Foundation Engineering*, Rio de Janeiro, pp. 199-203.
- CFEM (1992). *Canadian Foundation Engineering Manual*. 3rd Edition. Canadian Geotechnical Society, Technical Committee on Foundations, BiTech Publishers Ltd., Richmond, BC, 512 pp.
- Hoyt, R. M., and Clemence, S. P. (1989). "Uplift Capacity of Helical Anchors in Soil"; *Proceedings of 12th International Conference on Soil Mechanics and Foundation Engineering*, Rio de Janeiro, Brazil, Vol. 2, pp. 1019-1022.
- Kulhawy, F. H. (1984). "Limiting Tip and Side Resistance, Fact or Fallacy"; *Symposium on Analysis and Design of Pile Foundations*, American Society of Civil Engineers, San Francisco, pp. 80-98.
- Meyerhof, G. G., and Adams, J. I. (1968). "The Ultimate Uplift Capacity of Foundations"; *Canadian Geotechnical Journal*, Vol. V, no. 4, pp. 225-244.
- Meyerhof, G. G. (1982). "The Bearing Capacity and Settlement of Foundations – Selected Papers with A Bibliography to 1981"; *Tech-Press*, Halifax, 424 pp.
- Meyerhof, G. G. (1976). "Bearing Capacity and Settlement of Pile Foundations"; *Journal of the Geotechnical Engineering Division, Proceedings of the American Society of Civil Engineers*, Vol. 102, No. GT3, March 1976, pp. 197-224.
- Mitsch, M. P., and Clemence, S. P. (1985). "The Uplift Capacity of Helix Anchors in Sand. Uplift Behavior of Anchor Foundations in Soil"; *Proceedings of ASCE*, New York, N.Y., pp. 26-47.
- Mooney, J. M., Adamczak, S., and Clemence, S. P. (1985). "Uplift Capacity of Helix Anchors in Clay and Silt"; *Uplift Behavior of Anchor Foundations in Soil. Proceedings of ASCE*, New York, N.Y., pp.48-72.

- Narasimha Rao, S., Prasad, Y.V.S.N., and Shetty, M. D. (1991). "The Behaviour of Model Screw Piles in Cohesive Soils"; *Journal of Soil and Foundations*, Japanese Society of Soil Mechanics and Foundation Engineering, Vol, 31, pp. 35-50.
- Narasimha Rao, S., Prasad, Y.V.S.N., and Veeresh, C. (1993). "Behaviour of Embedded Model Screw Anchors in Soft Clays"; *Geotechnique*, Vol, 43, pp. 605-614.
- Saeedy, H. S. (1987). "Stability of Circular Vertical Earth Anchors"; *Canadian Geotechnical Journal* 24(3), pp. 452-456.
- Reese, L. C., and O'Neill, M. W. (1988). "Drilled shafts: Construction Procedures and Design Methods"; Publication No. FHWA-HI-88-042/ADSC-TL-4.
- Randolph, M. F., and Wroth, C. P. (1982). "Recent Developments in Understanding the Axial Capacity of Piles in Clay"; *Ground Engineering*, Vol. 15, No. 7, pp. 17-25.
- Tomlinson, M. J. (1957). "The Adhesion of Piles Driven in Clay Soils"; *Proceedings of 5th International Conference, ISSMFE, London*, Vol. 2, pp. 66-71.
- Tomlinson, M. J. (1994). *Pile Design and Construction Practice*, 4th Edition. E & FN Spon, London, 411 pp.
- Trofimenkov, J. G., and Mariupolskii, L. G. (1965). "Screw Piles Used for Mast and Tower Foundations"; *Proceedings of Sixth International Conference on Soil Mechanics and Foundation Engineering, Montreal, Quebec*, Vol. 11, pp. 328-332.
- Veesaert, C. J. and Clemence, S. P. (1977). "Dynamic Pullout Resistance of anchors"; *Proceedings of International Symposium on Soil structure Interaction, Rourkee, India*, Vol. 1, pp. 389-397.
- Vesic, A. S. (1963). "Bearing Capacity of Deep Foundations in Sand"; *National Academy of Sciences, National Research Council, Highway Research Record* 39, pp.112-153.
- Vesic, A. S. (1965). "Cratering by Explosives as an Earth Pressure Problem"; *Proceedings of VI International Conference on Soil Mechanics and Foundation Engineering, Montreal, Canada*, Vol. 2, pp. 427-431.
- Vesic, A. S. (1971). "Breakout Resistance of Objects Embedded in Ocean Bottom"; *Journal of Soil Mechanics and Foundation Division, ASCE, SM* 9, Vol. 97, pp. 1183-1205.

- Vesic, A. S. (1973). "Analysis of Ultimate Loads of Shallow Foundations"; JSMFD, ASCE, Vol. 99, SM 1, Jan., pp. 45-73.
- Vesic, A. S. (1975). "Principles of Pile Foundation Design"; Soil Mechanics Series No. 38, School of Engineering., Duke University, 48 pp.
- Vesic, A. S. (1977). "Design of Pile Foundations"; NCHRP Synthesis of Practice No. 42, Transportation Research Board, Washington DC, 68 pp.
- Weltman, A. J. and Healy, P. R. (1978). "Piling in 'Boulder Clay' and other Glacial Tills"; Construction Industry Research and Information Association (CIRIA), Report PG5.
- Winterkorn, H. F., and Fang, H. Y. (1975). Editor, "Foundation Engineering Handbook"; Van Nostrand Reinhold Company, New York, 751 pp.

Table 6.1: Summary of the Test Pile Geometry and Test Results

Test	No. of Helix	Helix Dia. (D, mm)	Helix Spacing (S, mm)	Depth to Top Helix (H, m)	Wall Thickness (t, mm)	Embed. Ratio (H/D)	Space to Dia. Ratio (S/D)	Ultimate Load, Qu		Installation Torque	
								Unv. Farm (kN)	Sand Pit (kN)	Unv. Farm (ft. lbs.)	Sand Pit (ft. lbs.)
Compression Long (CL)	3	356	533	3.79	6.71	10.7	1.50	180	470	15000	33000
Compression Short (CS)	3	356	533	1.67	6.71	4.69	1.50	160	420	11500	30000
Compression Production (Cprod. No. 1)	2	356	533	3.79	6.71	10.7	3.00	210	380	14375	33000
Compression Production (Cprod. No. 2)	2	356	1067	3.79	6.71	10.7	3.00	210	-	15000	32250
Tension Long (TL)	3	356	533	3.79	6.71	10.7	1.50	210	360	16250	37500
Tension Short (TS)	3	356	533	1.67	6.71	4.69	1.50	140	190	15000	31500
Tension Production (Tprod.)	2	356	1067	3.79	6.71	10.7	3.00	210	360	16875	35250
Lateral (L264)	3	356	533	3.79	6.71	10.7	1.50	40	62	17500	36000
Lateral (L322)	3	356	533	3.79	8.18	10.7	1.50	44	65	15000	33000

Note: 1 ft. lbs. = 1.356 N. m.

Table 6.2: Measured Load at Failure at Each Strain Gauge Level for the University Farm Site

**(a) Measured Load at Each Strain Gauge Level for the Compression Tests
(University of Alberta Farm Site)**

Description Gauge Location	Depth (m)	CL Load Measured (kN)	CL 2 Load Measured (kN)
Load Applied	0	175	187
Level 1	1.55	124	164
Level 2	3.24	119	119
Level 3	3.55	121	117
Level 4	4.05	86	77
Level 5	4.58	66	38

Description Gauge Location	Depth (m)	CS Load Measured (kN)
Load Applied	0	155
Level 1	0.58	125
Level 2	0.78	-
Level 3	1.41	-
Level 4	1.91	118
Level 5	2.45	60

**(b) Measured Load at Each Strain Gauge Level for the Tension Tests
(University of Alberta Farm Site)**

Description Gauge Location	Depth (m)	TL Load Measured (kN)
Load Applied	0	217
Level 1	1.55	196
Level 2	3.24	142
Level 3	3.55	132
Level 4	4.05	101
Level 5	4.58	46

Description Gauge Location	Depth	TS Load Measured (kN)
Load Applied	0	155
Level 1	0.58	108
Level 2	0.78	100
Level 3	1.41	92
Level 4	1.91	79
Level 5	2.45	50

Table 6.3: Measured Load at Failure at Each Strain Gauge Level for the Sand Pit Site

**(a) Measured Load at Each Strain Gauge Level for the Compression Tests
(Sand Pit Site)**

Description Gauge Location	Depth (m)	CL Load Measured (kN)
Load Applied	0	484
Level 1	1.55	409
Level 2	3.24	356
Level 3	3.55	360
Level 4	4.05	312
Level 5	4.58	172

Description Gauge Location	Depth (m)	CS Load Measured (kN)
Load Applied	0	439
Level 1	0.58	414
Level 2	0.78	-
Level 3	1.41	-
Level 4	1.91	269
Level 5	2.45	197

**(b) Measured Load at Each Strain Gauge Level for the Tension Tests
(Sand Pit Site)**

Description Gauge Location	Depth (m)	TL Load Measured (kN)
Load Applied	0	369
Level 1	1.55	358
Level 2	3.24	260
Level 3	3.55	233
Level 4	4.05	189
Level 5	4.58	72

Description Gauge Location	Depth (m)	TS Load Measured (kN)
Load Applied	0	192
Level 1	0.58	170
Level 2	0.78	162
Level 3	1.41	149
Level 4	1.91	120
Level 5	2.45	72

Table 6.4: Measured Load Differences between Strain Gauge Levels as Indicated for the University Farm Site

**(a) Load Differences between Strain Gauge Levels for the Compression Tests
(University of Alberta Farm Site)**

Description	Length (m)	CL Load Differences (kN)	CL 2 Load Differences (kN)
Ground to Level 1	0-1.55	50.5	23.5
Level 1 to Level 2	1.55-3.24	4.71	45.0
Level 2 to Level 3	3.24-3.55	-1.50	1.94
Top Helix to Level 4	3.722-4.05	34.5	40.2
Level 4 to Level 5	4.05-4.58	20.3	38.8

Description	Length (m)	CS Load Differences (kN)
Ground to Level 1	0-0.58	30.5
Level 1 to Level 4	0.58-1.91	6.15
Level 4 to Level 5	1.91-2.45	58.1

**(b) Load Differences between Strain Gauge Levels for the Tension Tests
(University of Alberta Farm Site)**

Description	Length (m)	TL Load Differences (kN)
Ground to Level 1	0-1.55	20.8
Level 1 to Level 2	1.55-3.24	53.4
Level 2 to Level 3	3.24-3.55	10.3
Level 3 to Level 4	3.55-4.05	31.4
Level 4 to Level 5	4.05-4.58	54.6

Description	Length (m)	TS Load Differences (kN)
Ground to Level 1	0-0.58	47.1
Level 1 to Level 2	0.58-0.78	7.85
Level 2 to Level 3	0.78-1.41	7.93
Level 3 to Level 4	1.41-1.91	13.2
Level 4 to Level 5	1.91-2.45	28.5

Table 6.5: Measured Load Differences between Strain Gauge Levels as Indicated for the Sand Pit Site

**(a) Load Differences between Strain Gauge Levels for the Compression Tests
(Sand Pit Site)**

Description	Length (m)	CL Load Differences (kN)
Ground to Level 1	0-1.55	75.5
Level 1 to Level 2	1.55-3.24	52.6
Level 2 to Level 3	3.24-3.55	-3.19
Top Helix to Level 4	3.55-4.05	47.1
Level 4 to Level 5	4.05-4.58	140.2

Description	Length (m)	CS Load Differences (kN)
Ground to Level 1	0-0.58	24.5
Level 1 to Level 4	0.58-1.91	146
Level 4 to Level 5	1.91-2.45	71.5

**(b) Load Differences between Strain Gauge Levels for the Tension Tests
(Sand Pit Site)**

Description	Length (m)	TL Load Differences (kN)
Ground to Level 1	0-1.55	11.0
Level 1 to Level 2	1.55-3.24	98.8
Level 2 to Level 3	3.24-3.55	26.8
Level 3 to Level 4	3.55-4.05	43.5
Level 4 to Level 5	4.05-4.58	117

Description	Length (m)	TS Load Differences (kN)
Ground to Level 1	0-0.58	22.5
Level 1 to Level 2	0.58-0.78	8.08
Level 2 to Level 3	0.78-1.41	12.1
Level 3 to Level 4	1.41-1.91	29.8
Level 4 to Level 5	1.91-2.45	48.0

Table 6.6: Measured Shaft Resistance, Bearing Capacity and Cylindrical Shearing Resistance at Failure for the Length Indicated for Both Test Sites

Test	Description Gauge Location	Length (m)	Q_{shaft} (measured)	
			University Farm Site (kN)	Sand Pit Site (kN)
CS	Ground to Level 1	0-0.58	30.5	24.5
CL	Ground to Level 2	0-3.24	55.2	128
CL 2	Ground to Level 2	0-3.24	68.5	-
TS	Ground to Level 2	0-0.78	55.0	30.5
TL	Ground to Level 2	0-3.24	74.2	110

Test	Description	Depth (m)	Q_{bearing} (measured)	
			University Farm Site (kN)	Sand Pit Site (kN)
CS	-	2.45	60.3	197.3
CL	-	4.58	66.2	172.2
CL 2	-	4.58	38.0	-
TS	Level 2-Level 4	1.584	21.1	41.9
TL	Level 2-Level 4	3.722	41.7	70.3

Test	Description Gauge Location	Length (m)	$Q_{\text{interhelix}}$ (measured)	
			University Farm Site (kN)	Sand Pit Site (kN)
CS	Level 4 to Level 5	1.91-2.45	58.1	71.5
CL	Top Helix to Level 5	3.722-4.58	54.8	187
CL 2	Top Helix to Level 5	3.722-4.58	79.0	-
TS	Level 4 to Level 5	1.91-2.45	28.5	48.0
TL	Level 4 to Level 5	4.05-4.58	54.6	117

Table 6.7: Comparison of Each Load Contribution Components to the Ultimate Load Measured by the Tests for Both Test Sites

Test	Q _{ultimate} (measured)		Q _{shaft} (measured)		Q _{bearing} (measured)		Q _{interhelix} (back calculated)		Q _{shaft} / Q _{ultimate}		Q _{bearing} / Q _{ultimate}		Q _{interhelix} / Q _{ultimate}	
	UAF (kN)	SP (kN)	UAF (kN)	SP (kN)	UAF (kN)	SP (kN)	UAF (kN)	SP (kN)	UAF (%)	SP (%)	UAF (%)	SP (%)	UAF (%)	SP (%)
CS	155	439	30.5	24.5	60.3	197	64.2	217	19.7	5.57	38.9	45.0	41.4	49.5
CL	175	484	55.2	128	66.2	172	53.3	184	31.6	26.4	37.9	35.6	30.5	38.0
CL 2	187	-	68.5	-	38.0	-	81.0	-	36.5	-	20.3	-	43.2	-
TS	155	192	55.0	30.5	21.1	41.9	78.8	120	35.5	15.9	13.6	21.8	50.9	62.3
TL	217	369	74.2	110	41.7	70.3	101	189	34.3	29.7	19.2	19.0	46.5	51.2

Note:

1. $Q_{interhelix} \text{ (back calculated)} = Q_{ultimate} \text{ (measured)} - Q_{shaft} \text{ (measured)} - Q_{bearing} \text{ (measured)}$
2. UAF: University Farm Site
3. SP: Sand Pit Site

Table 6.8: Shaft Adhesion Prediction for the Compression and Tension Tests at the University Farm Site

See Figure 6.17 & Figure 6.18 for Comparison		α		CS (kN)	TS (kN)	CL (kN)	TL (kN)
		C_u 50 kPa	C_u 90 kPa				
Shaft Adhesion Measured				30.5	35.0	55.2	71.2
Q_{shaft} (predicted)	ASCE (1993)	0.38	0.38	16.1	16.1	66.7	66.7
	CFEM (1992)	0.72	0.469	30.4	30.4	92.6	92.6
	Mooney et al. (1985)	0.9	0.3	38.0	38.0	77.4	77.4
	Tomlinson (1957)	-	-	26.6	26.6	63.3	63.3
	Tomlinson (1994)	0.4	0.3	16.9	16.9	56.7	56.7
	Reese & O'Neill (1988)	0.55	0.55	23.2	23.2	96.5	62.7
	Weltman & Healy (1978)	0.9	0.7	38.0	38.0	131.0	131.0
	Randolph & Wroth (1982)	0.5	0.5	21.1	21.1	87.7	87.7
Percent Difference (%)	ASCE (1993)			-47.4	-70.8	20.7	-10.2
	CFEM (1992)			-0.3	-44.7	67.8	24.8
	Mooney et al. (1985)			24.7	-30.9	40.2	4.3
	Tomlinson (1957)			-12.8	-51.6	14.7	-14.7
	Tomlinson (1994)			-44.6	-69.3	2.8	-23.5
	Reese & O'Neill (1988)			-23.8	-57.8	74.8	-15.5
	Weltman & Healy (1978)			24.7	-30.9	137.4	76.6
	Randolph & Wroth (1982)			-30.7	-61.6	58.9	18.2

Table 6.9: Shaft Resistance Prediction for the Compression and Tension Tests at the Sand Pit Site

See Figure 6.17 & Figure 6.18 for Comparison		ϕ (39°) (Dense Sand)		CS	TS	CL	TL
		k_s	k_u	(kN)	(kN)	(kN)	(kN)
Shaft Resistance Measured (kN)				24.5	30.5	128	110
Q_{shaft} (predicted)	ASCE (1993)	3.195	-	24.1	-	178.3	-
	CFEM (1992)	2.325	-	17.6	-	129.7	-
	Kulhawy (1984)	0.70	-	5.3	-	39.1	-
	Meyerhof (1982)	2.75	-	20.8	-	153.5	-
	Meyerhof (1968)	-	3.62	-	27.3	-	202
	Mitsch & Clemence (1985)	-	2.18	-	16.5	-	122
	Winterkorn & Fang (1975), $Q_s(\text{limit})^*$	-	-	8.7	8.71	84.3	84.3
Percent Difference (%)	ASCE (1993)			-1.55	-	39.2	-
	CFEM (1992)			-28.4	-	1.28	-
	Kulhawy (1984)			-78.4	-	-69.5	-
	Meyerhof (1982)			-15.3	-	19.8	-
	Meyerhof (1968)			-	-10.4	-	84.0
	Mitsch & Clemence (1985)			-	-46.0	-	10.8
	Winterkorn & Fang (1975), $Q_s(\text{limit})^*$			-64.4	-71.4	-34.2	-23.2

Note:

$Q_s(\text{limit})^*$: Maximum Mantle Friction for Screw and Bored Piles

Table 6.10: Predicting Plate Bearing Capacity for the Compression and Tension Tests at the University Farm Site

See Figure 6.19 & Figure 6.20 for Comparison		N _c		N _{cu}		CS	CL	TS	TL
		CS	CL	TS	TL	(kN)	(kN)	(kN)	(kN)
Bearing Capacity Measured						60.3	66.2	21.1	41.7
Q_{bearing} (predicted)	Meyerhof (1976)	9	9	-	-	50.1	50.1	-	-
	Meyerhof (1968)	-	-	9.23	9.23	-	-	51.4	51.4
	Mooney et al. (1985)	-	-	9	9	-	-	50.1	50.1
	Narasimha Rao et al. (1991)			9	9	-	-	51.9	54.3
	Das (1990)	-	-	7.5	9	-	-	41.8	50.1
Percent Difference (%)	Meyerhof (1976)					-16.9	-24.3	-	-
	Meyerhof (1968)					-	-	144	23.3
	Mooney et al. (1985)					-	-	138	20.2
	Narasimha Rao et al. (1991)					-	-	146	30.1
	Das (1990)					-	-	97.9	20.2

Table 6.11: Predicting Plate Bearing Capacity for the Compression and Tension Tests at the Sand Pit Site

See Figure 6.19 & Figure 6.20 for Comparison		N_q		N_{qu}		$F_1 + F_2$	F_q	F_q^*	$Q_{bearing}$ (predicted)			
		ϕ 39 ° (Dense)	ϕ 30 ° (Loose)	ϕ 39 °	ϕ 39 °	ϕ 39 °	ϕ 39 °	ϕ 39 °	CS	CL	TS	TL
		CS	CL	TS	TL	TS	TS	TL	(kN)	(kN)	(kN)	(kN)
Bearing Capacity Measured									197.3	172.2	141.9	70.3
$Q_{bearing}$ (predicted)	Meyerhof (1976)	169	60	-	-	-	-	-	499	320	-	-
	Vesic (1963)	100	30	-	-	-	-	-	295	160	-	-
	Kulhaway (1984)	120	32.5	-	-	-	-	-	354	173	-	-
	Bella (1961)	-	-	-	-	0.77	-	-	-	-	55.1	-
	Meyerhof (1968)	-	-	-	-	-	25	35	-	-	44.1	145
	Vesic (1965)	-	-	-	-	-	11.67	-	-	-	20.6	-
	Saeedy (1987)	-	-	-	-	-	-	66.67	-	-	-	88.9
	Veesaert & Clemence (1977)	-	-	-	-	-	21.25	-	-	-	37.5	-
	Mitsch & Clemence (1985)	-	-	22	50	-	-	-	-	-	40.0	207
Percent Difference (%)	Meyerhof (1976)								153	85.8	-	-
	Vesic (1963)								49.6	-7.10	-	-
	Kulhaway (1984)								79.5	0.64	-	-
	Bella (1961)								-	-	31.5	-
	Meyerhof (1968)								-	-	5.25	106
	Vesic (1965)								-	-	-50.9	-
	Saeedy (1987)								-	-	-	26.4
	Veesaert & Clemence (1977)								-	-	-10.5	-
	Mitsch & Clemence (1985)								-	-	-4.58	195

Table 6.12: Predicting Cylindrical Shear Resistance for the Compression and Tension Tests at the University Farm Site

See Figure 6.21 & Figure 6.22		CS (kN)	CL (kN)	TS (kN)	TL (kN)
Cylindrical Shear Resistance Measured		58.1	54.8	28.5	154.6
Q_{interhelix} (predicted)	Narasimha Rao et al. (1991)	54.4	86.4	-	-
	Mooney (1985)	-	-	54.4	53.1
Percent Difference (%)	Narasimha Rao et al. (1991)	-6.45	57.7	-	-
	Mooney (1985)	-	-	91.1	-2.73

Table 6.13: Predicting Cylindrical Shear Resistance for the Compression and Tension Tests at the Sand Pit Site

See Figure 6.21 & Figure 6.22		ϕ (39°) (Dense Sand)		CS	CL	TS	TL
		k_s	k_u	(kN)	(kN)	(kN)	(kN)
Cylindrical Shearing Resistance Measured				171.5	187.3	148.0	116.9
$Q_{\text{interhelix}}$ (predicted)	ASCE (1993)	3.195	-	63.5	192	-	-
	CFEM (1992)	2.325	-	44.6	140	-	-
	Kulhawy (1984)	0.7	-	13.4	42.1	-	-
	Meyerhof (1982)	2.75	-	52.8	165	-	-
	Meyerhof (1968)	-	3.62	-	-	69.5	135
	ASCE (1993)	-	3.195	-	-	61.3	119
	Mitsch and Clemence (1985)	-	2.18	-	-	41.8	81.3
Percent Difference (%)	ASCE (1993)			-11.1	2.61	-	-
	CFEM (1992)			-37.6	-25.3	-	-
	Kulhawy (1984)			-81.2	-77.5	-	-
	Meyerhof (1982)			-26.2	-11.7	-	-
	Meyerhof (1968)			-	-	44.6	15.4
	ASCE (1993)			-	-	27.7	1.88
	Mitsch and Clemence (1985)			-	-	-12.9	-30.5

Table 6.14: Summary of Predicted and Measured Axial Pile Capacity for Screw Piles Installed at the University Farm Site

University Farm Site		(see Figure 6.23 for Comparison of Predicted and Measured Capacity Results)									
				Ultimate Compression Capacity Q_c			Ultimate Tension Capacity Q_t				
				CS	CL	Cprod.	TS	TL	Tprod.		
Predicting the Ultimate Screw Pile Capacity Using Listed Methods	Indirect Method	Cylindrical	Narasimha Rao et al. (1991)	239	273	262					
		Shear	Mooney et al. (1985)				209	243	243		
		(kN)	Narasimha Rao and Prasad (1993)				181	233	222		
		Individual	Hoyt and Clemence (1989)				172	222	172		
		Bearing (kN)	Narasimha Rao et al. (1991)						202		
	Direct Method	Empirical (kN)	Hoyt and Clemence (1989)				200	217	225		
		CPT	Bustamante and Ganeselli (1982)	112	164	164	106	161	161		
		(kN)	Ruiter and Beringen (1979)	149	220	220	142	220	220		
		Cylindrical	Narasimha Rao et al. (1991)	49.6	51.6	24.8					
		Shear	Mooney et al. (1985)				49.3	15.5	15.5		
Percent Difference between the Predicted Capacity and the Measured Values	Indirect Method	(%)	Narasimha Rao and Prasad (1993)				29.4	10.9	5.66		
		Individual	Hoyt and Clemence (1989)				22.7	5.49	-18.3		
		Bearing (%)	Narasimha Rao et al. (1991)						-3.92		
		Empirical (%)	Hoyt and Clemence (1989)				43.0	3.26	7.23		
		CPT	Bustamante and Ganeselli (1982)	-30.0	-8.76	-21.8	-24.6	-23.2	-23.2		
	Direct Method	(%)	Ruiter and Beringen (1979)	-7.11	22.3	4.79	1.22	4.68	4.68		

Table 6.15: Summary of Predicted and Measured Axial Pile Capacity for Screw Piles Installed at the Sand Pit Site

Sand Pit Site (see Figure 6.24 for Comparison of Predicted and Measured Capacity Results)				Ultimate Compression Capacity Q_c			Ultimate Tension Capacity Q_t		
				CS	CL	Cprod.	TS	TL	Tprod.
Predicting the Ultimate Screw Pile Capacity Using Listed Methods	Indirect	Cylindrical Shear (kN)	Mitsch and Clemence (1985)				137	490	490
		Individual Bearing (kN)	Adams and Klym (1971)				120	267	178
		Empirical (kN)	Hoyt and Clemence (1989)				500	420	470
	Direct Method	CPT (kN)	Bustamante and Ganeselli (1982)	455	409	409	429	527	527
			Ruiter and Beringen (1979)	482	257	257	501	230	230
Percent Difference between the Predicted Capacity and the Measured Values	Indirect	Cylindrical Shear (kN)	Mitsch and Clemence (1985)				-28.1	36.1	36.1
		Individual Bearing (kN)	Adams and Klym (1971)				-36.8	-25.9	-50.6
		Empirical (%)	Hoyt and Clemence (1989)				163.4	16.8	30.7
	Direct Method	CPT (%)	Bustamante and Ganeselli (1982)	8.31	-13.0	7.65	125.6	46.4	46.4
			Ruiter and Beringen (1979)	14.8	-45.4	-32.5	163.8	-36.0	-36.0

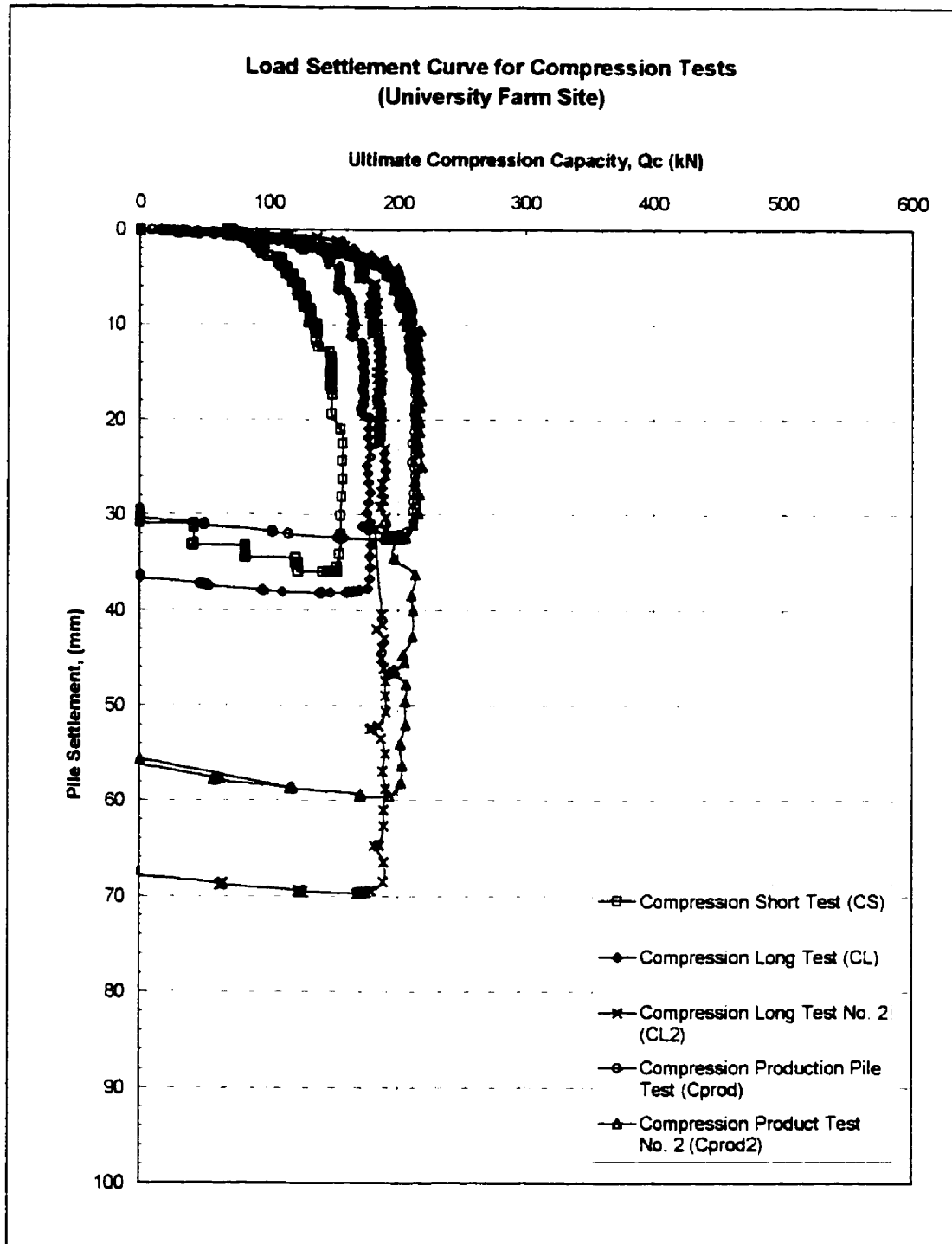


Figure 6.1: Compression Pile Load Test Results from the University Farm Site

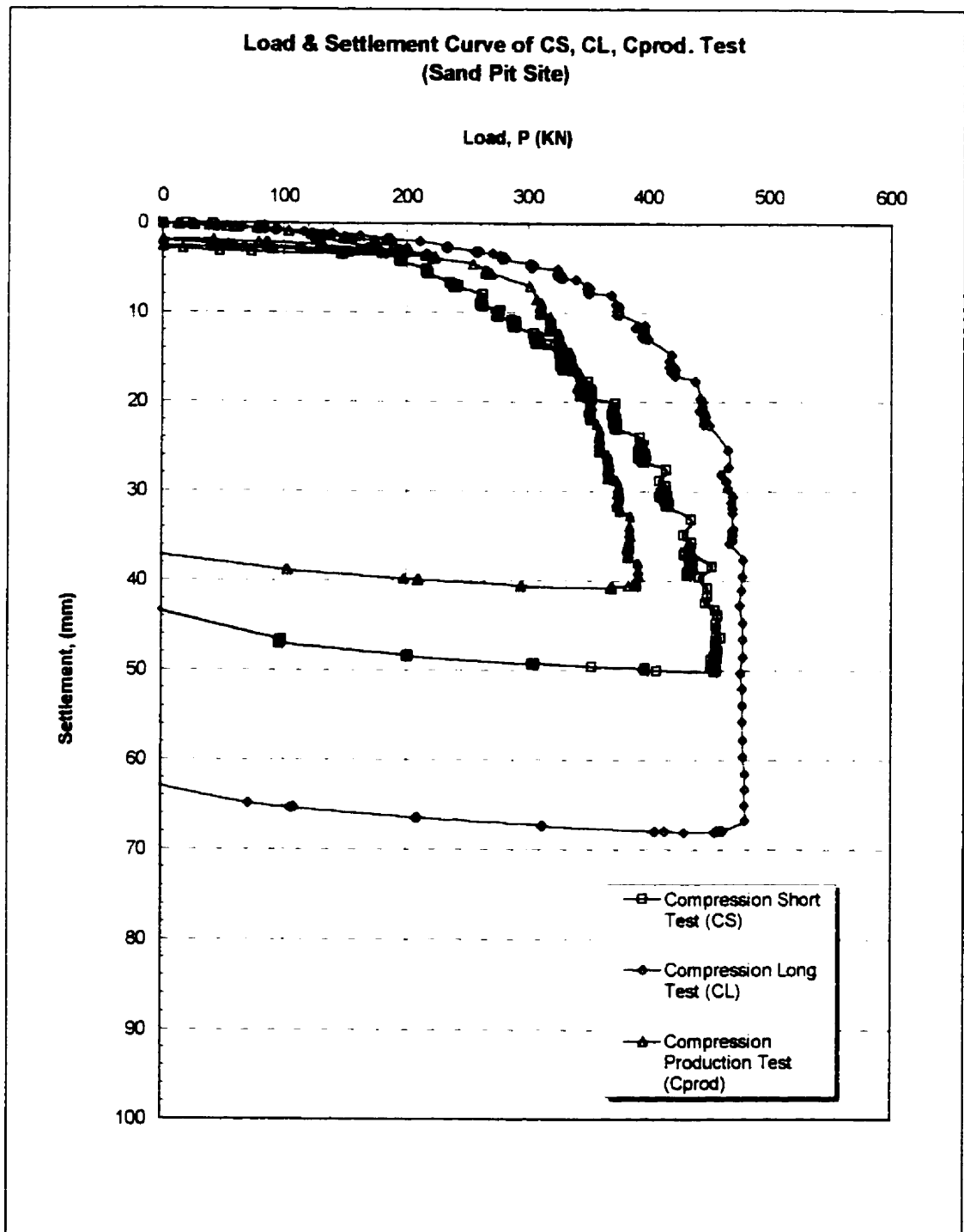


Figure 6.2: Compression Pile Load Test Results from the Sand Pit Site

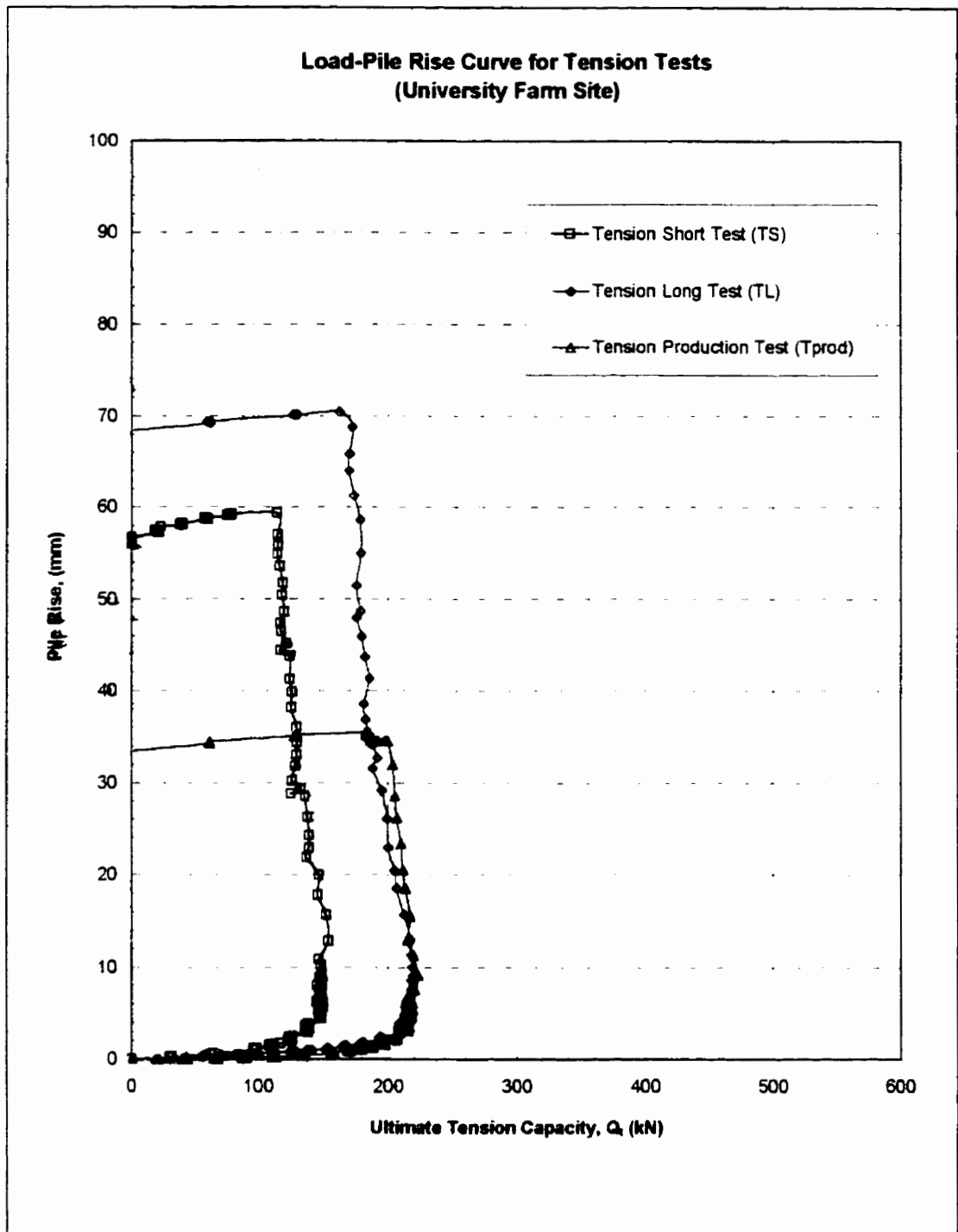


Figure 6.3: Tension Pile Load Test Results from the University Farm Site

**Load-Pile Rise Curve of TS, TL, Tprod. Test
(Sand Pit Site)**

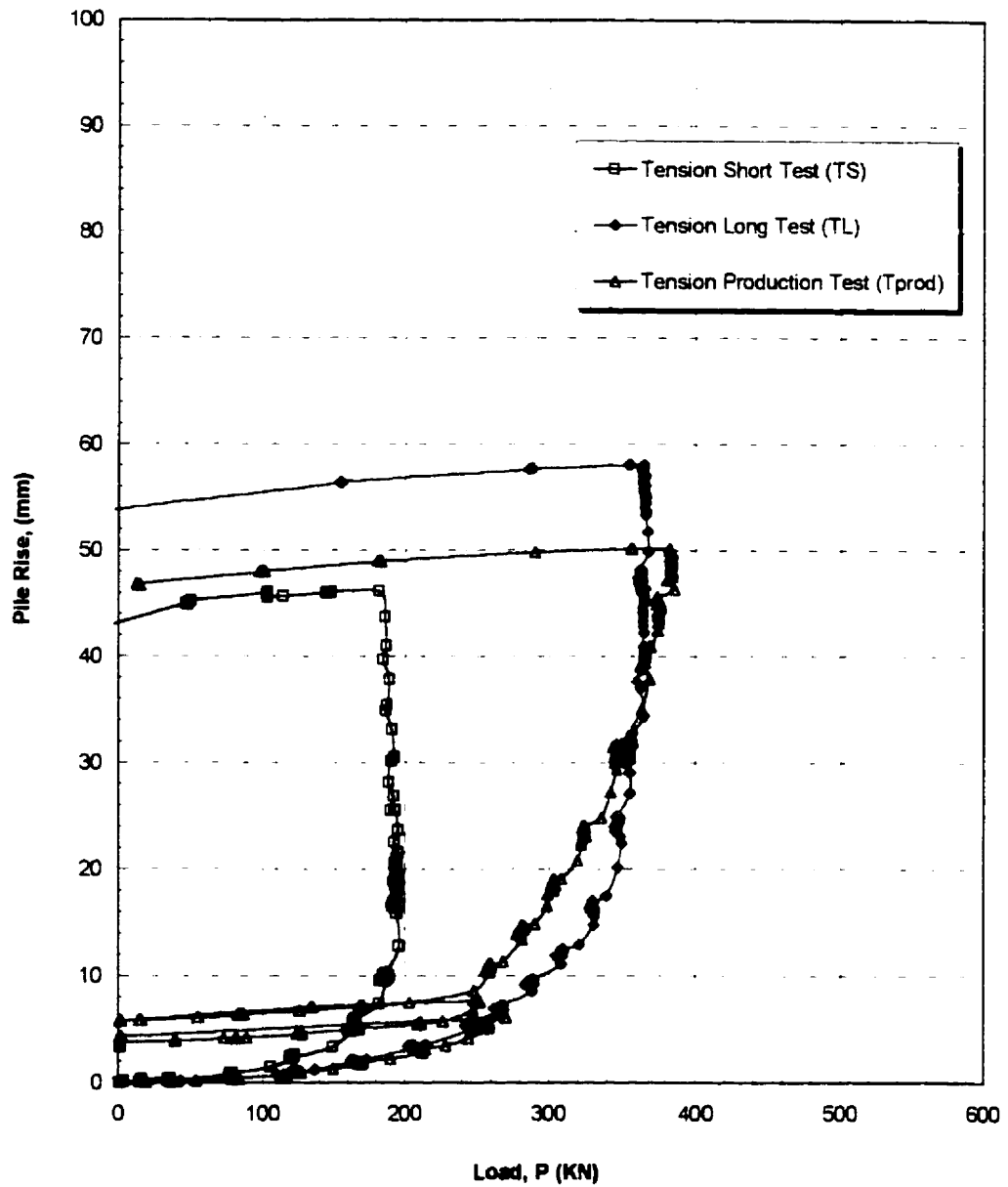


Figure 6.4: Tension Pile Load Test Results from the Sand Pit Site

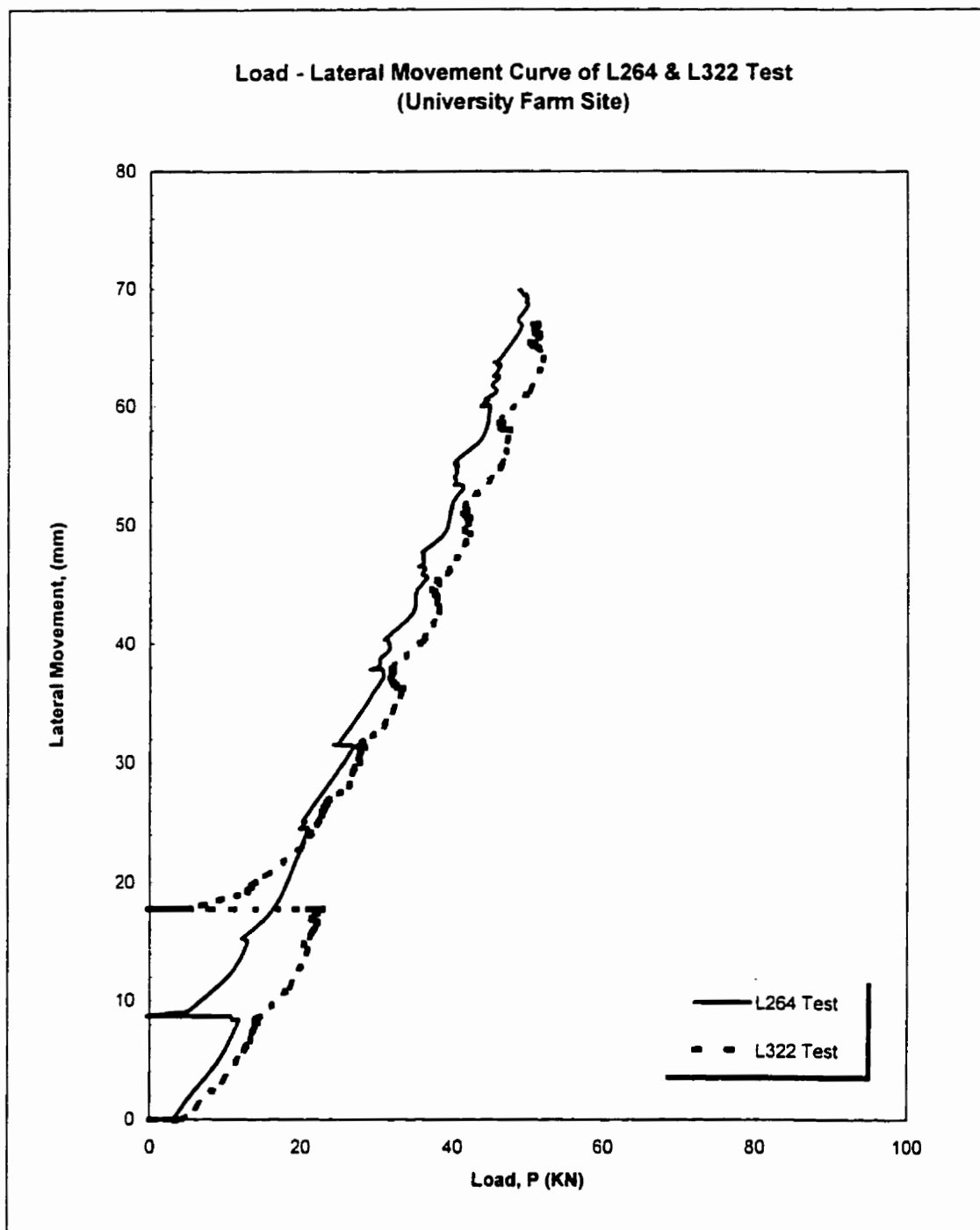


Figure 6.5: Lateral Pile Load Test Results from the University Farm Site

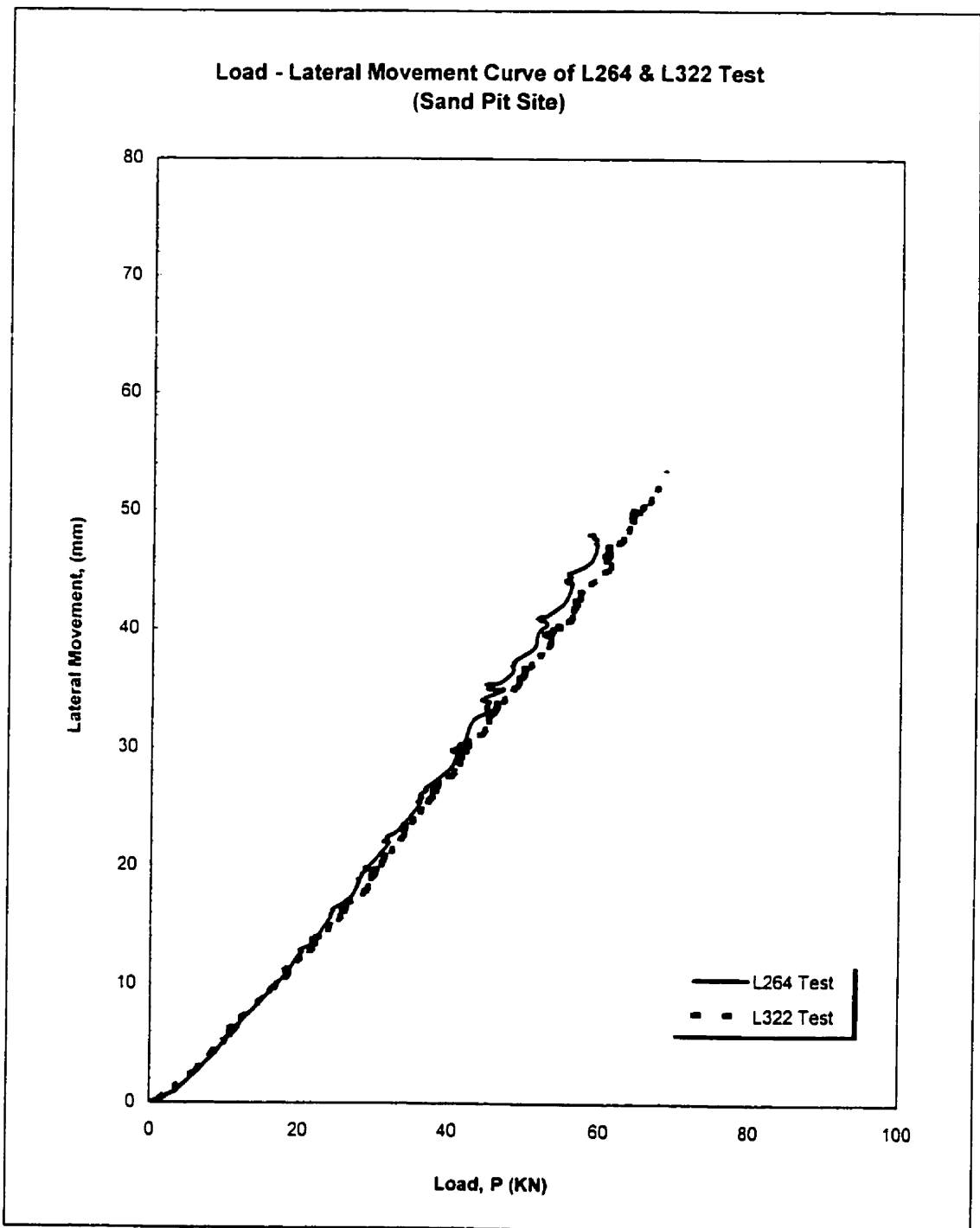


Figure 6.6: Lateral Pile Load Test Results from the Sand Pit Site

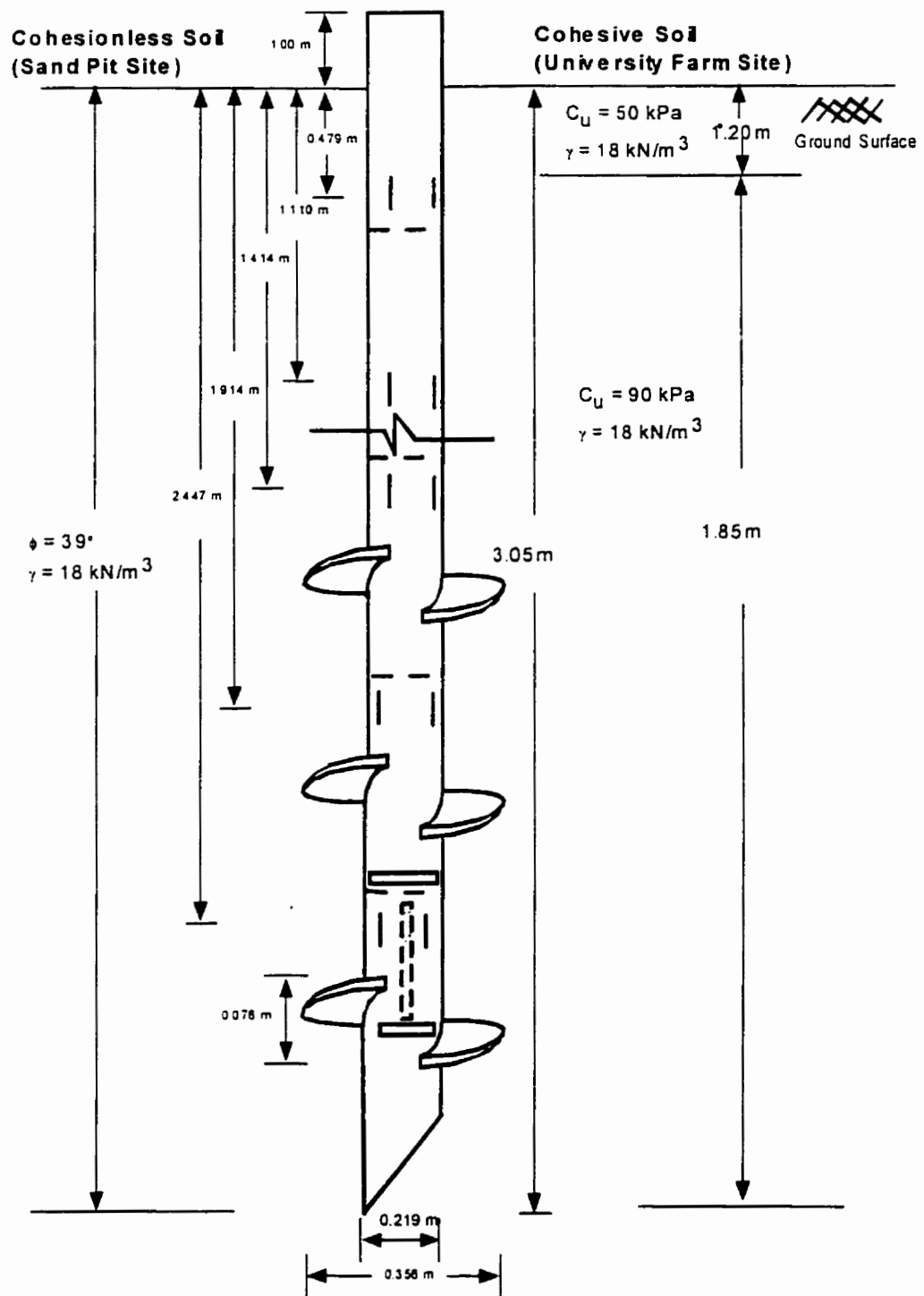


Figure 6.7: Strain Gauge Locations and Soil Strength Versus Depth (CS & TS Tests)

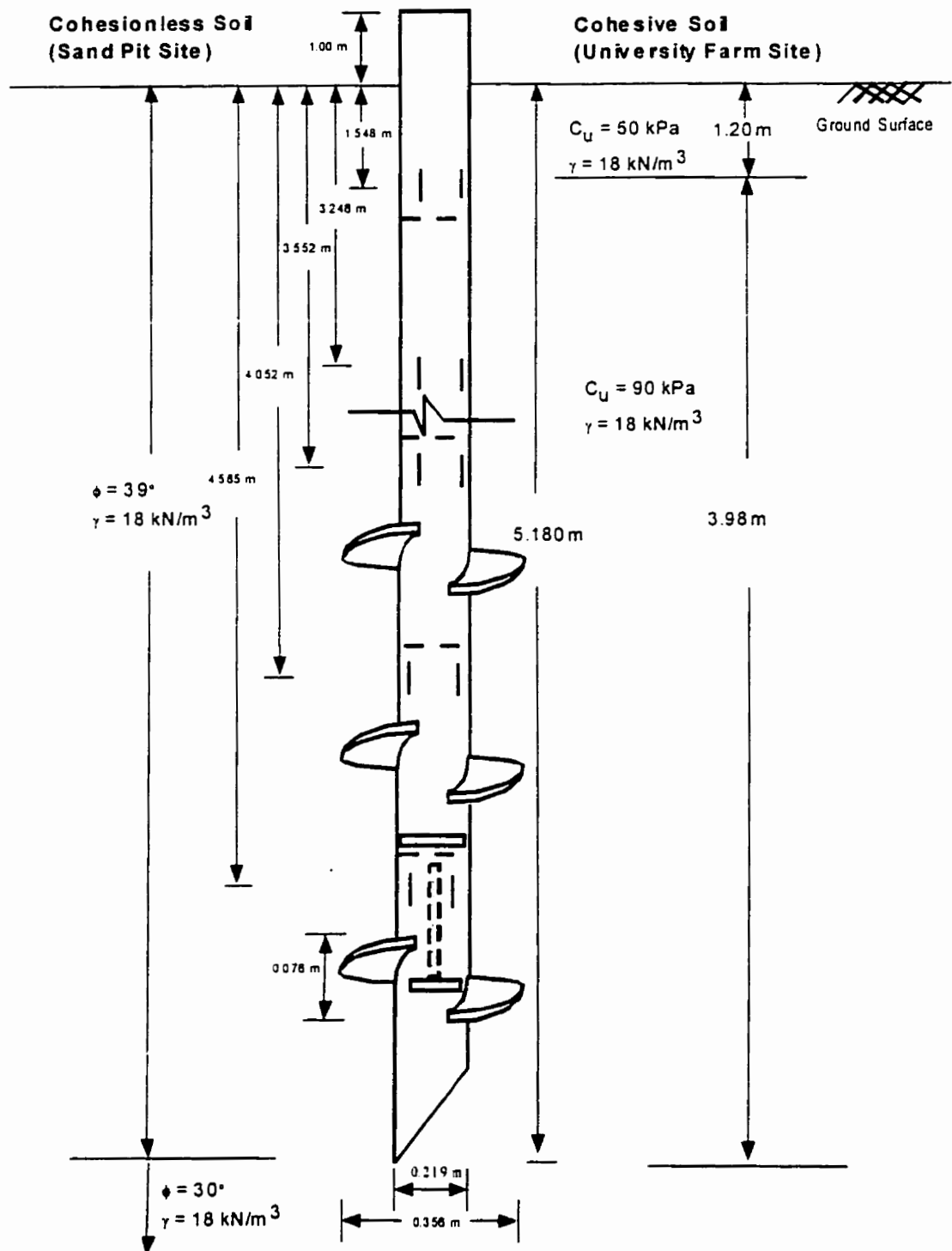


Figure 6.8: Strain Gauge Locations and Soil Strength Versus Depth (CL & TL Tests)

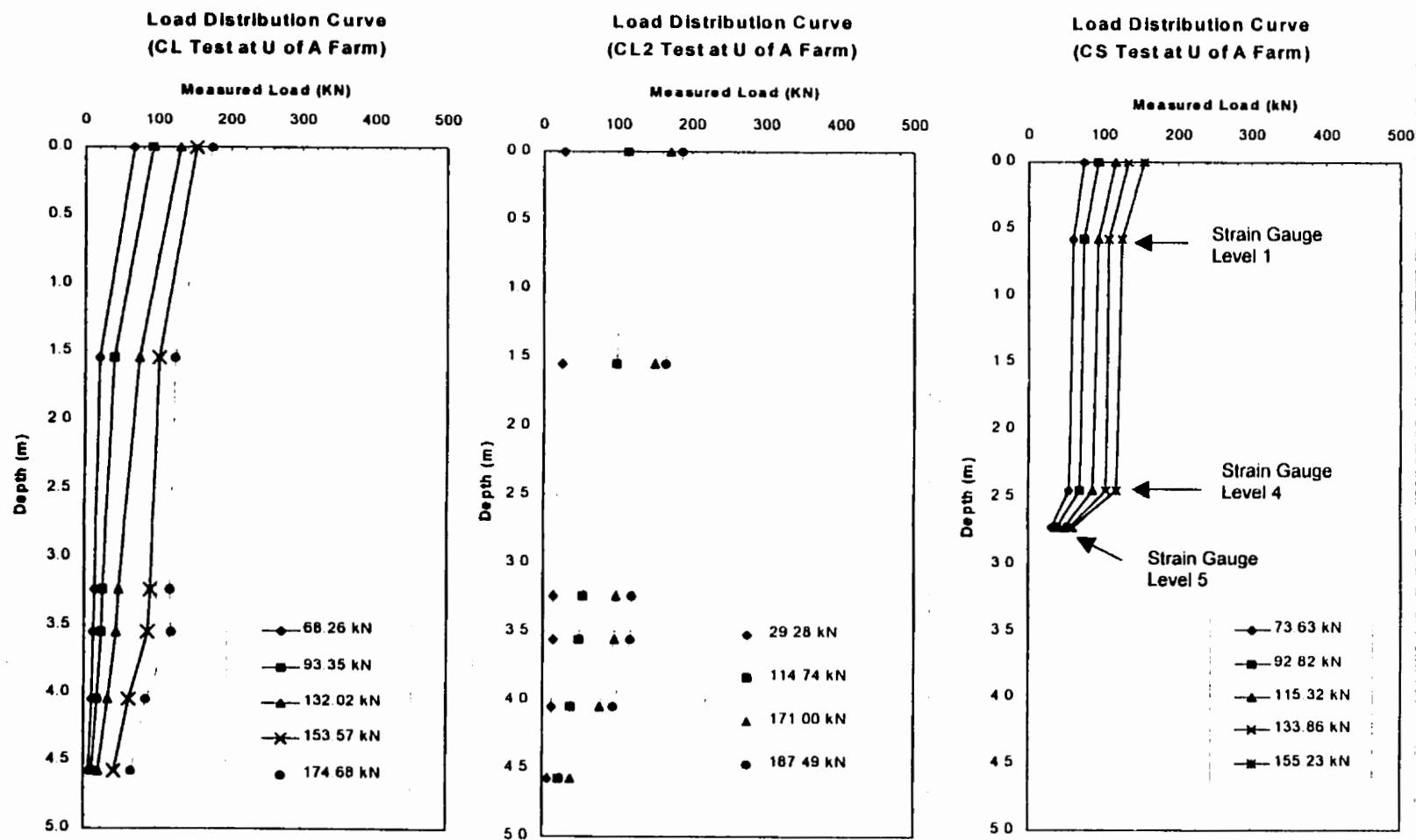


Figure 6.9: Load Distribution Curve for the Compression Tests at the University Farm Site

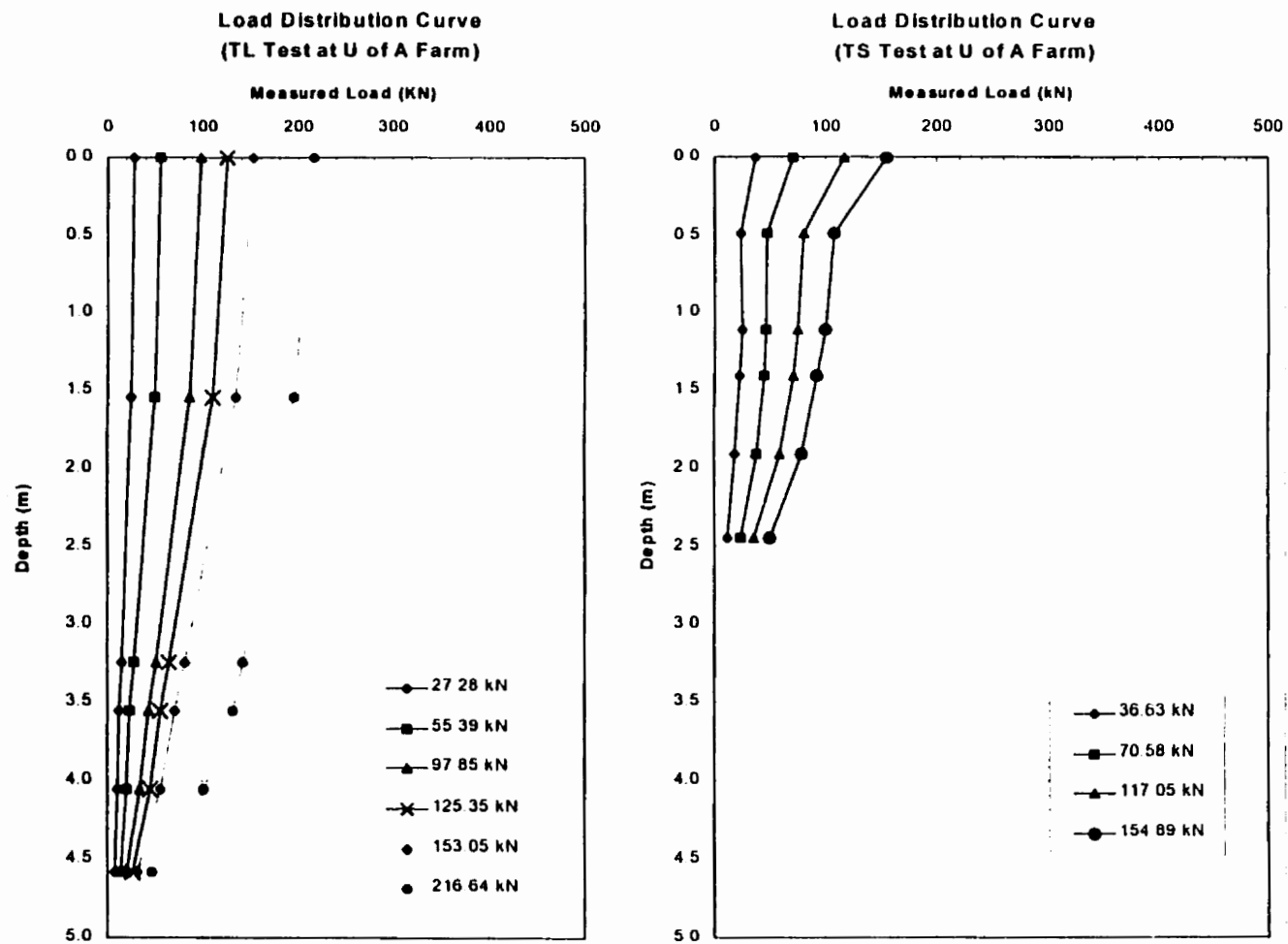


Figure 6.10: Load Distribution Curve for the Tension Test at the University Farm Site

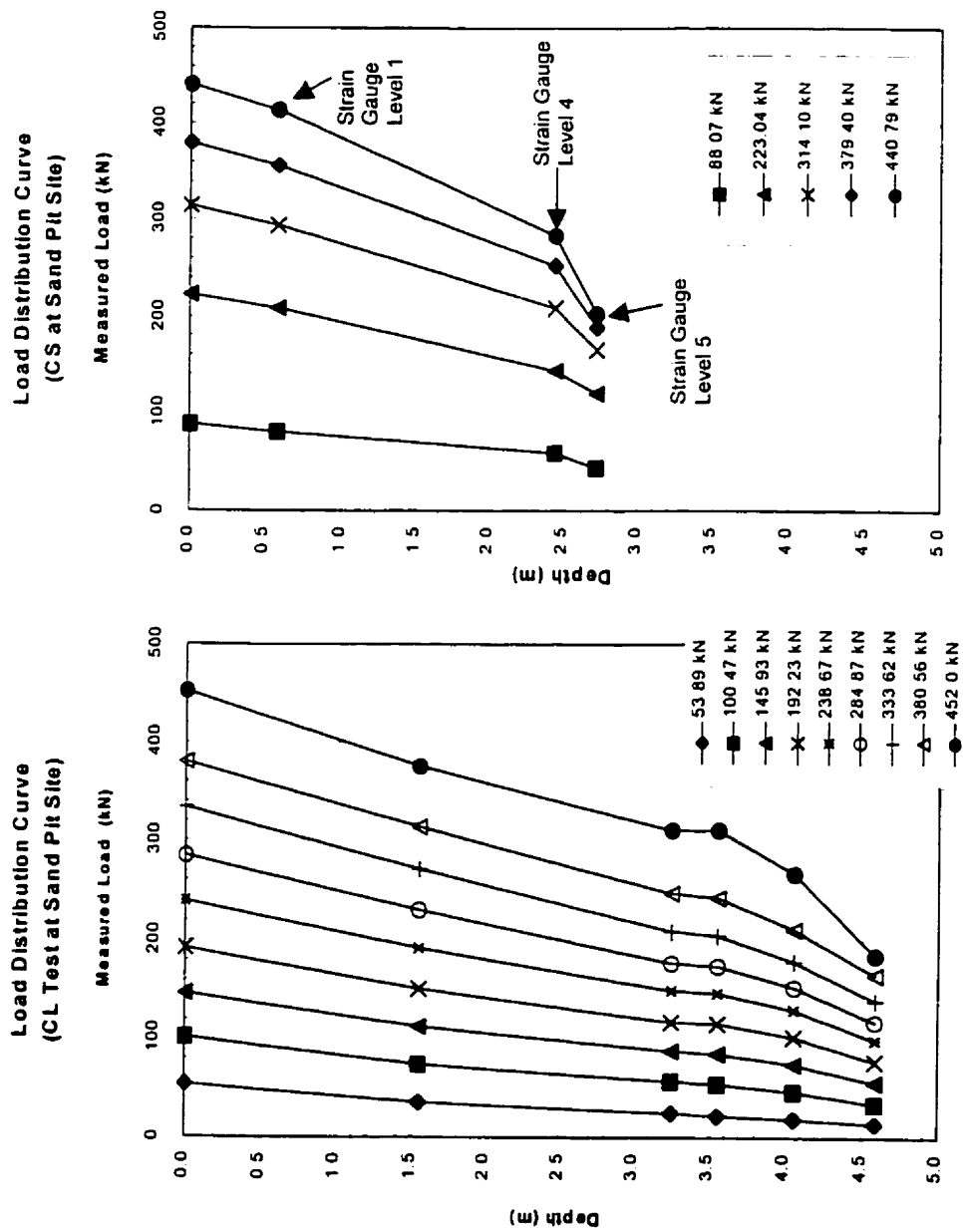


Figure 6.11: Load Distribution Curve for the compression Test at the Sand Pit Site

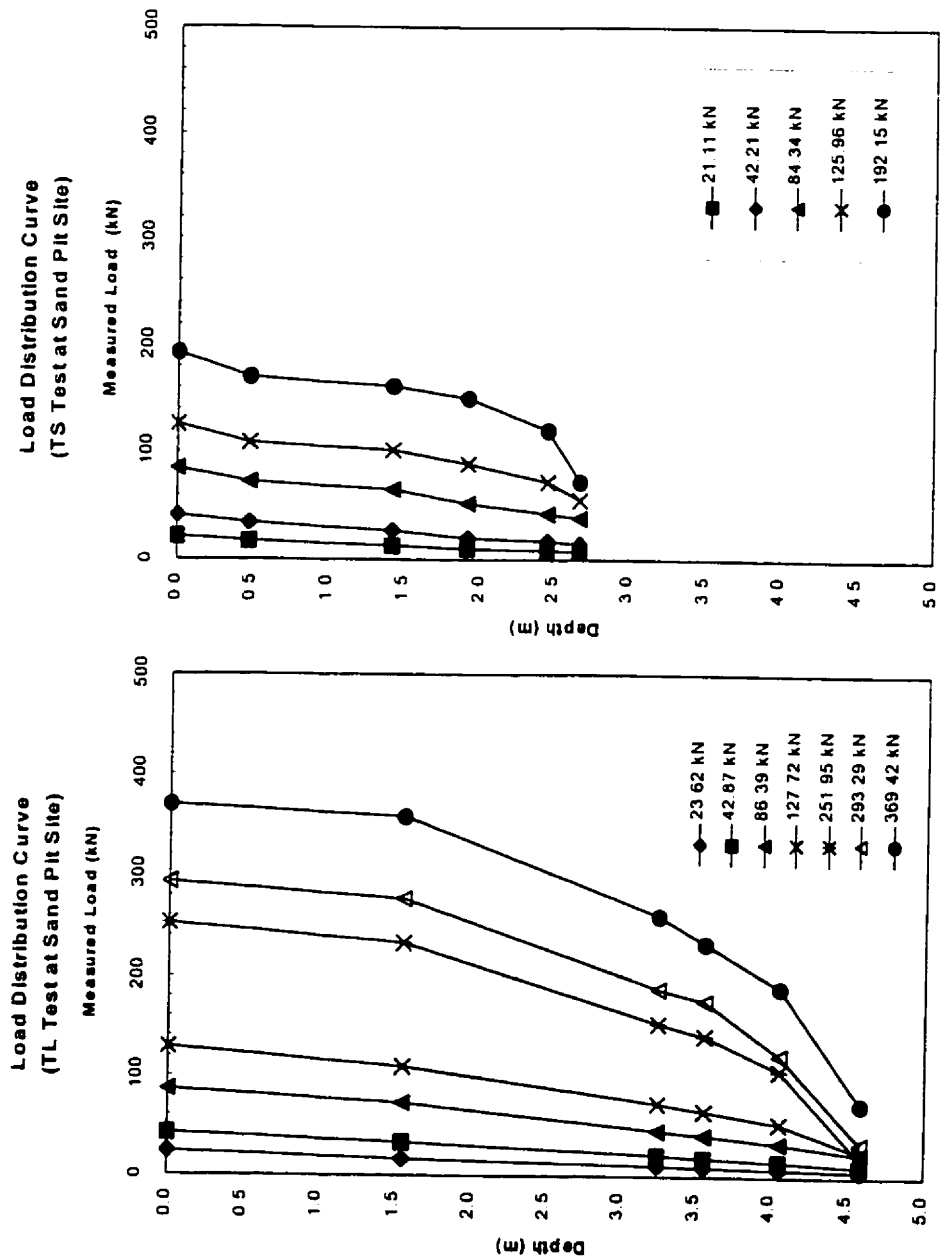


Figure 6.12: Load Distribution Curve for the Tension Test at the Sand Pit Site

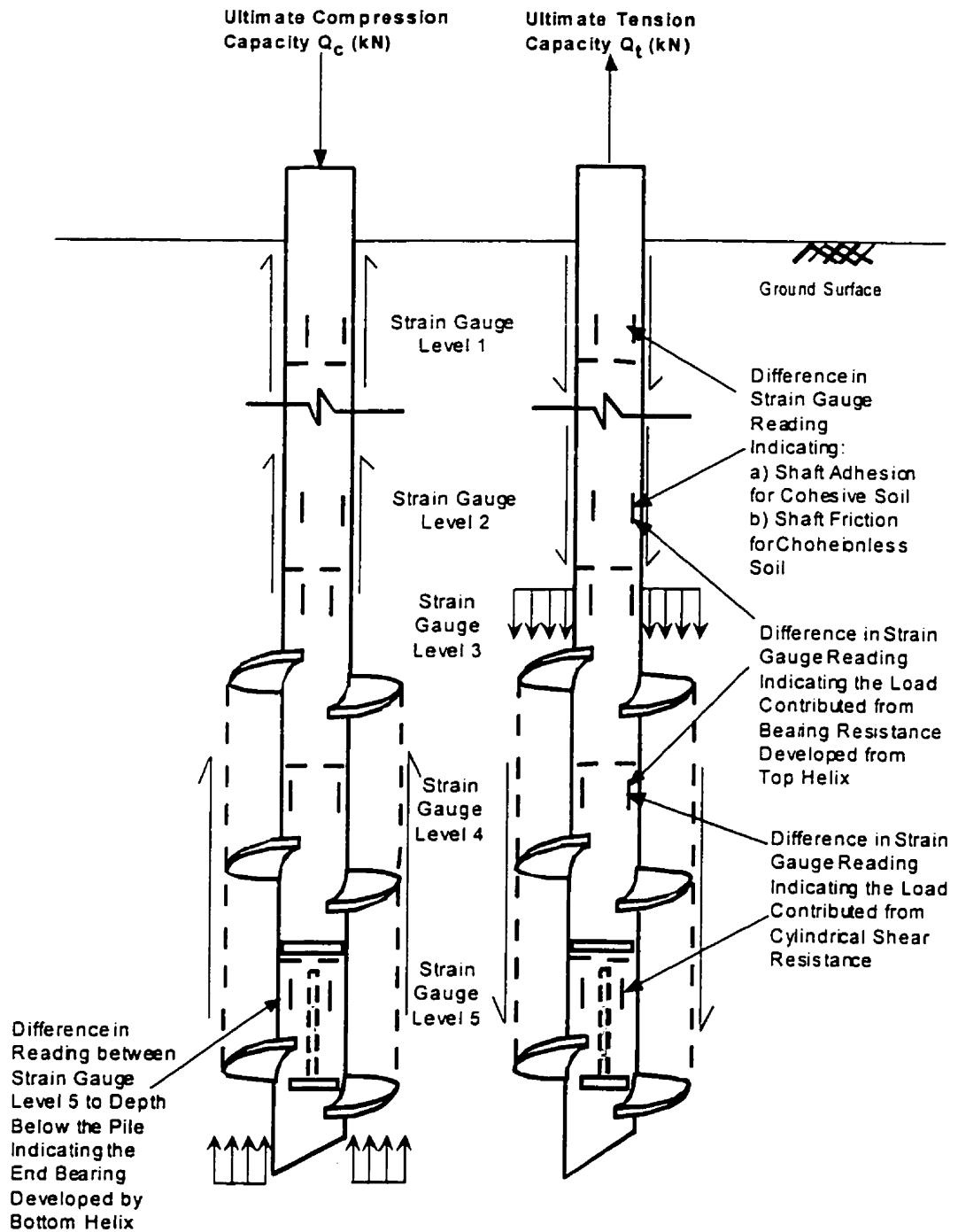


Figure 6.13: Strain Gauge Locations as Indicated in Load Distribution Curves

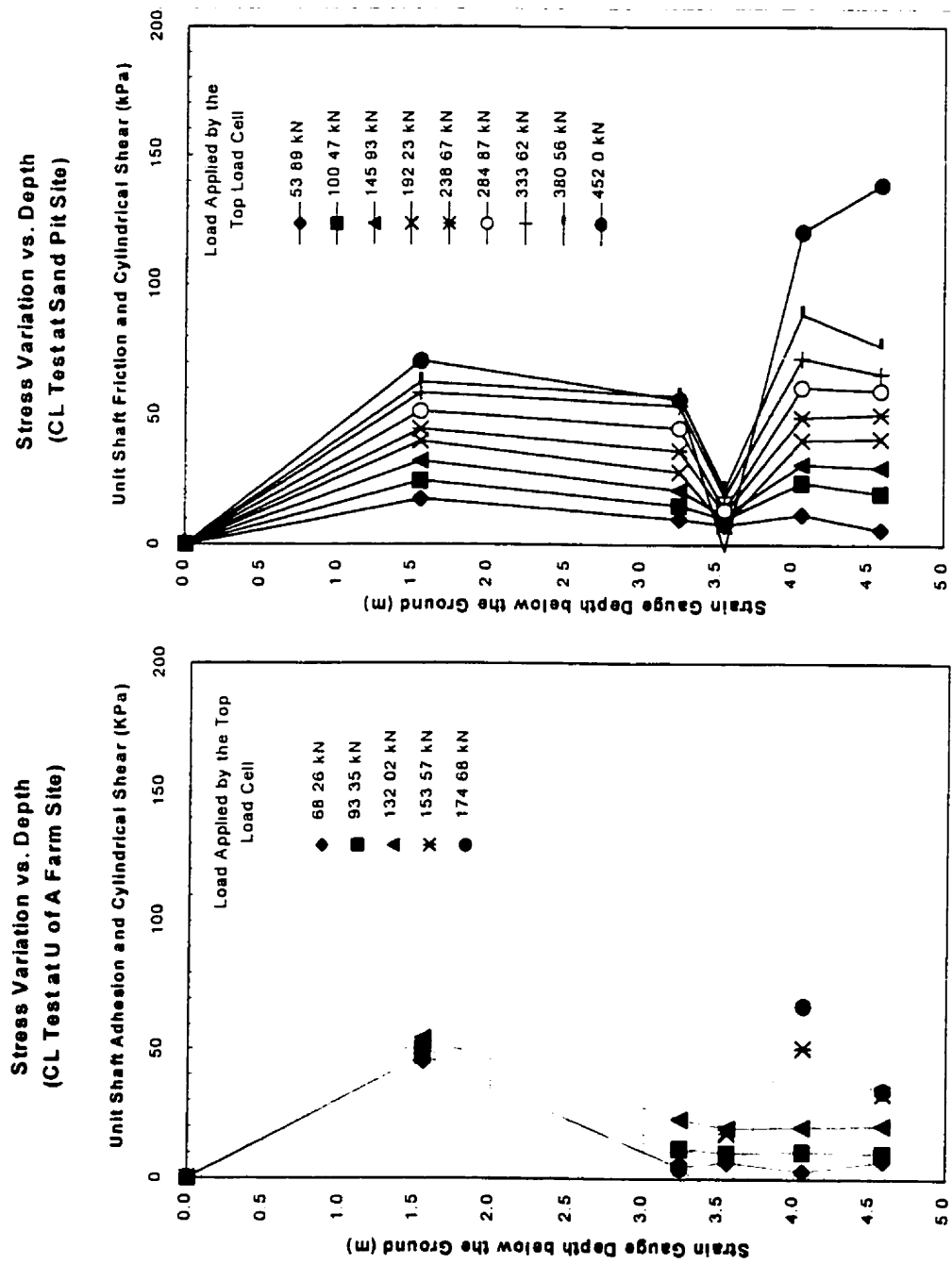
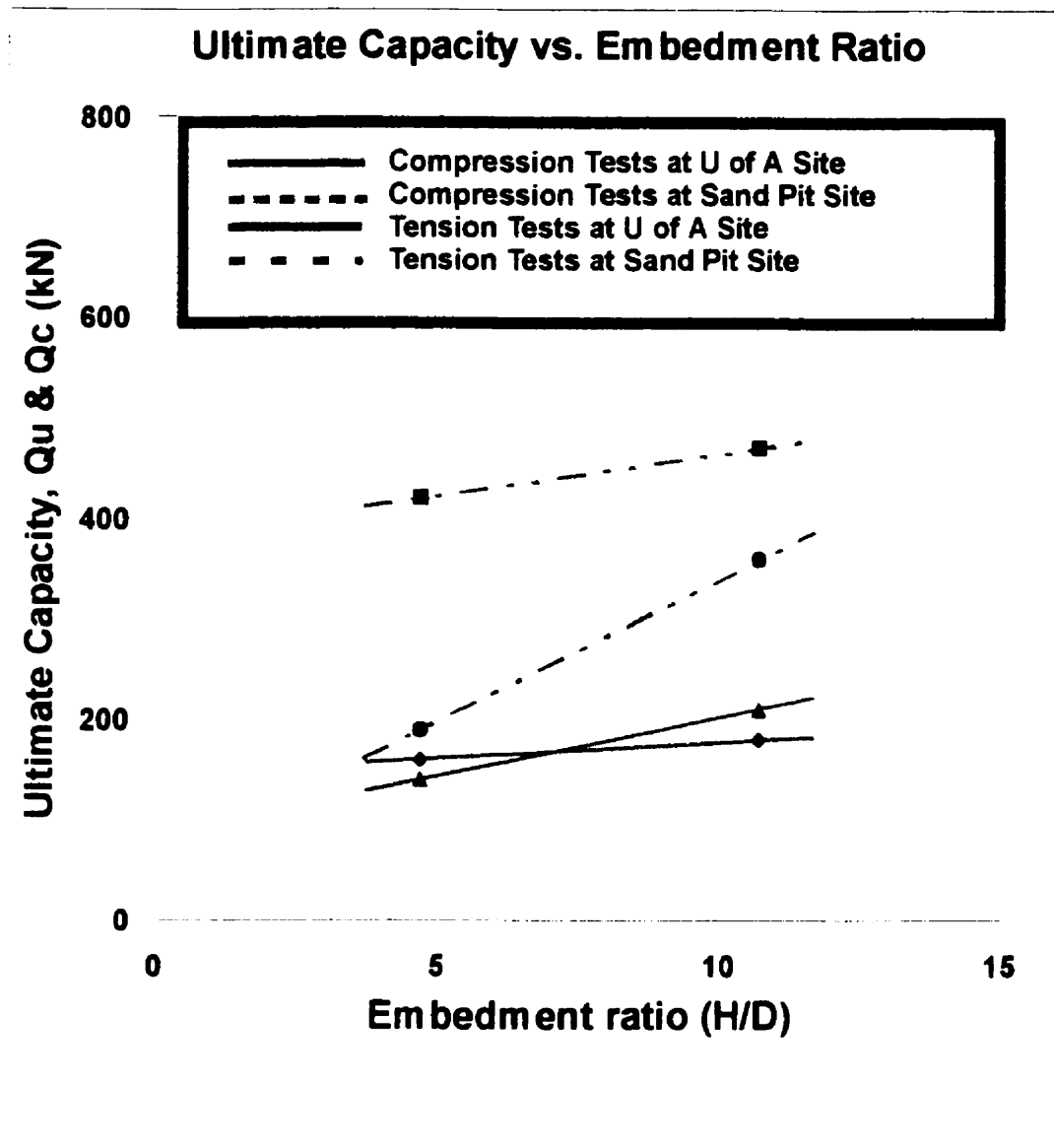
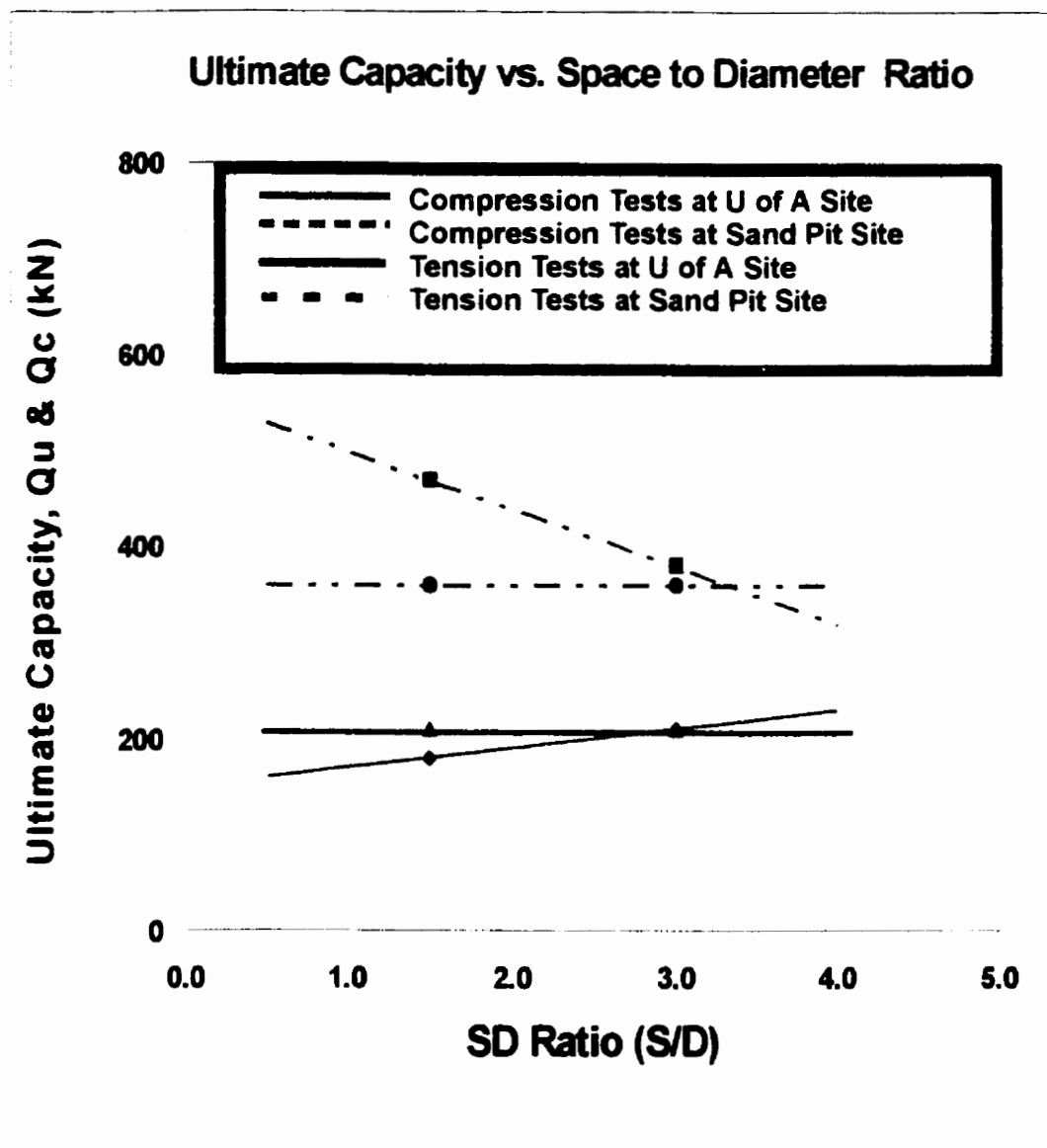


Figure 6.14: Unit Skin Resistance versus Depth Curves Calculated Based on the Strain Gauge Measurements at Indicated Depth



Note: Figure 6.15 is presented for demonstration purposes not for use as a design chart

Figure 6.15: Relationship between the Ultimate Capacity and the Embedment Ratio (H/D)



Note: Figure 6.16 is presented for demonstration purposes not for use as a design chart

Figure 6.16: Relationship between the Ultimate Capacity and the Space to Diameter Ratio (S/D)

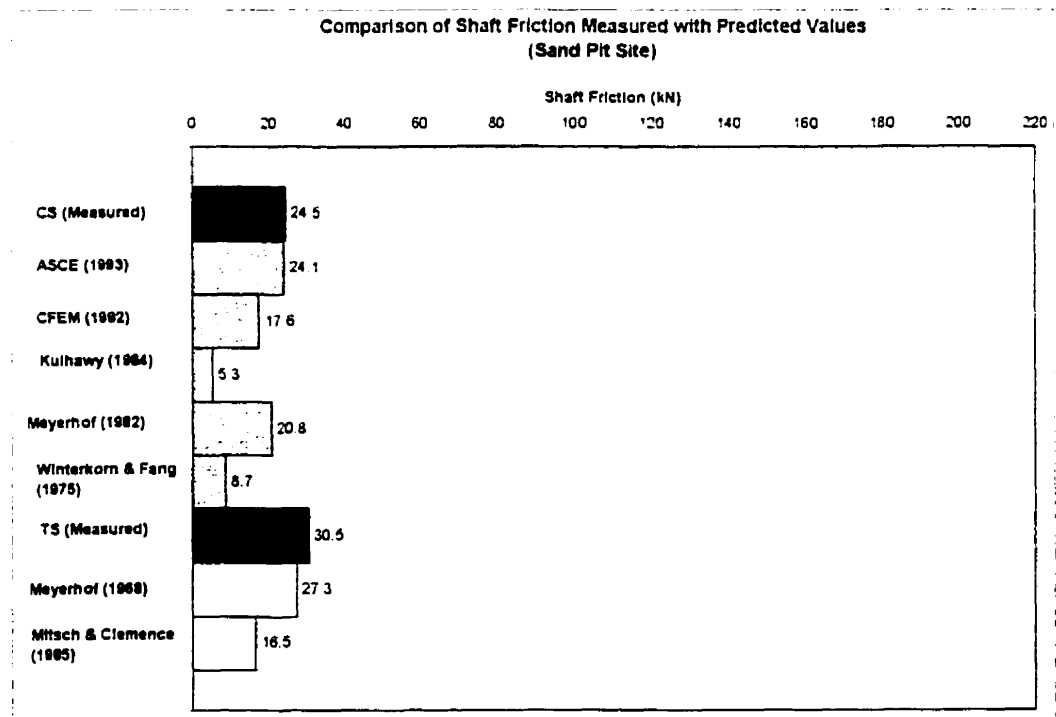
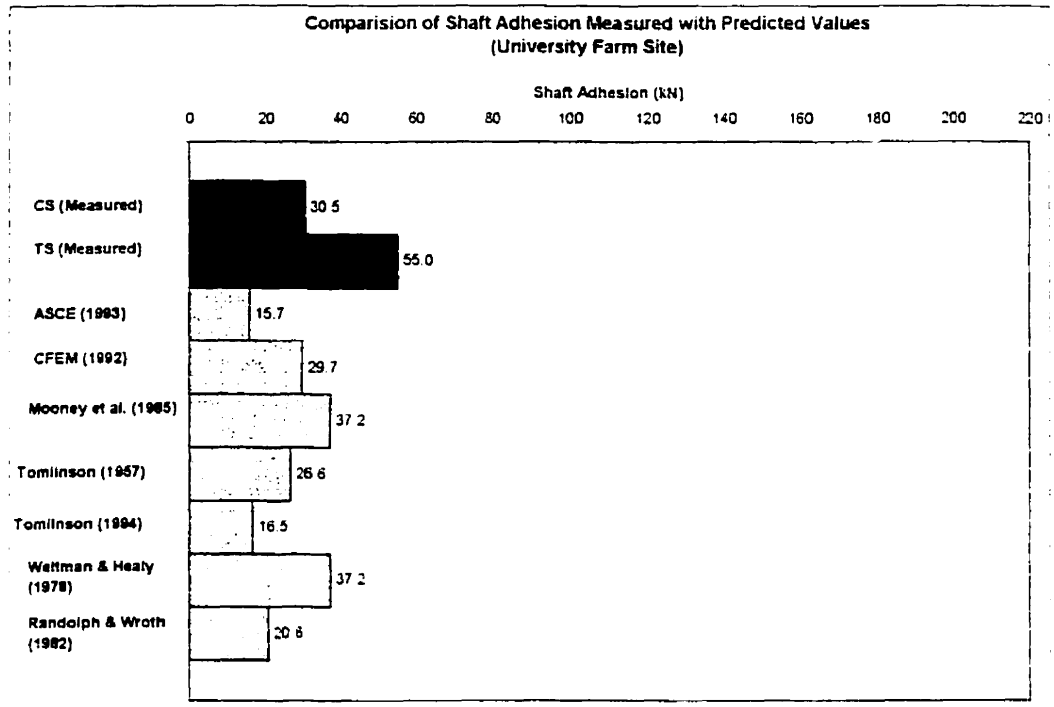


Figure 6.17: Comparison of the Shaft Resistance Measured with the Predicted Values for the CS and TS Tests

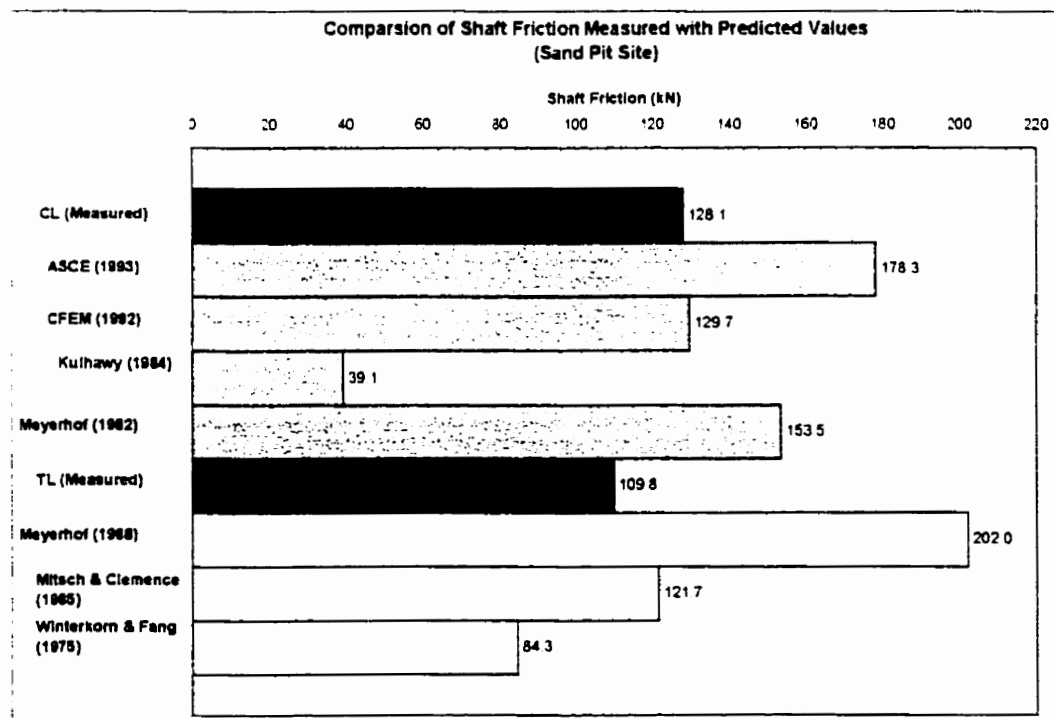
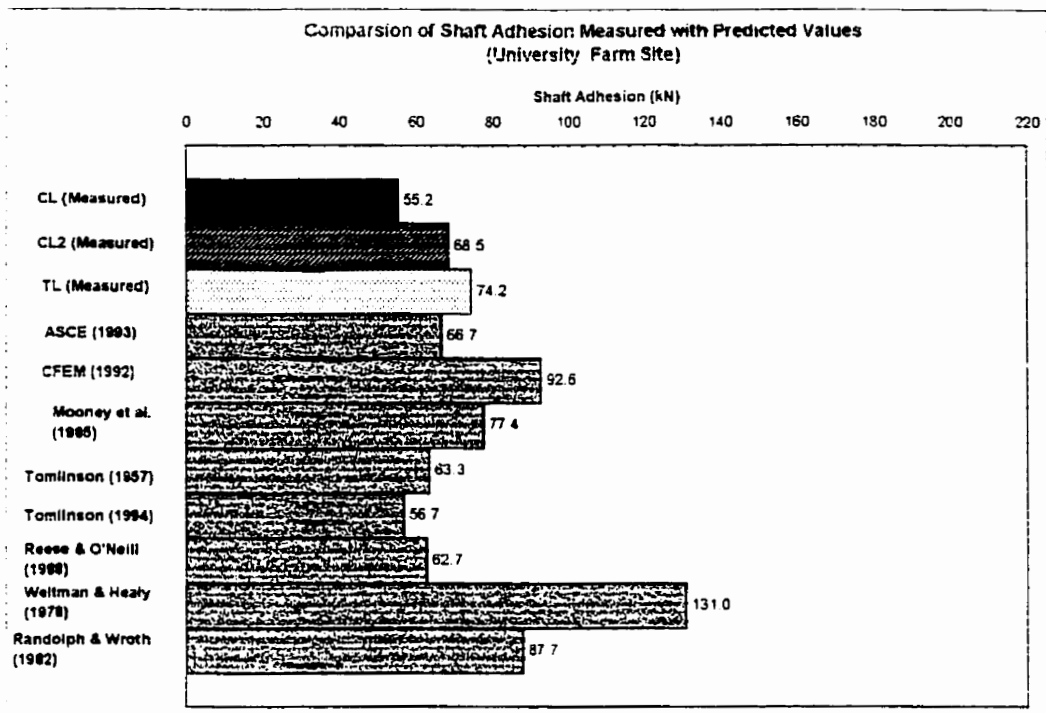


Figure 6.18: Comparison of the Shaft Resistance Measured with the Predicted Values for the CL and TL Tests

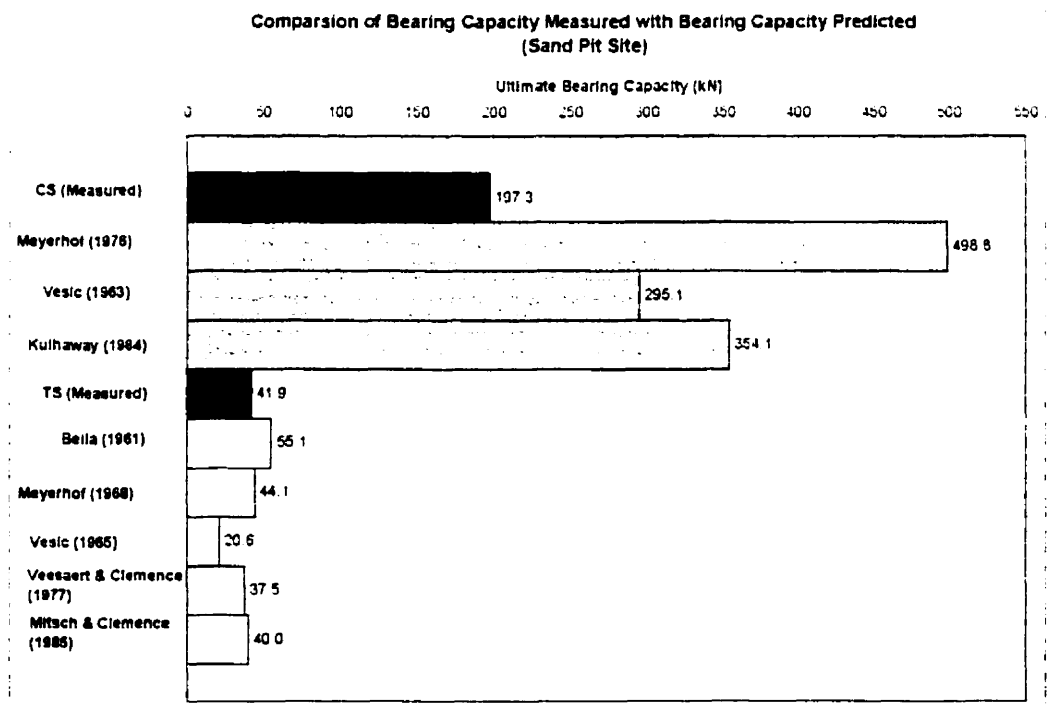
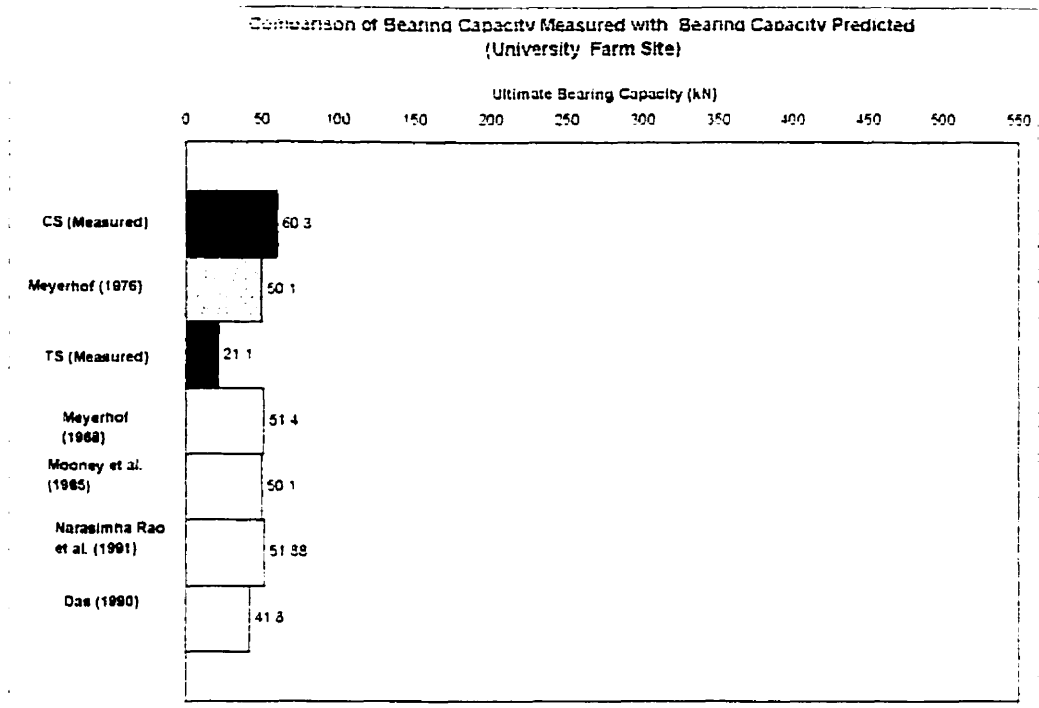


Figure 6.19: Comparison of the Bearing Capacity Measured with the Predicted value for the CS and TS Tests

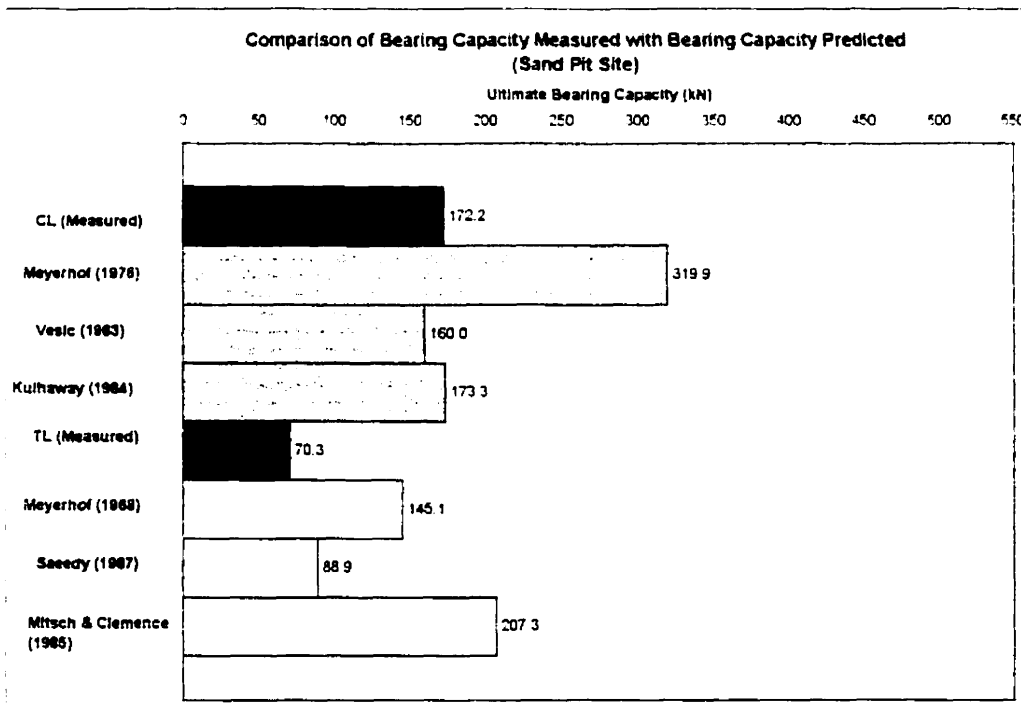
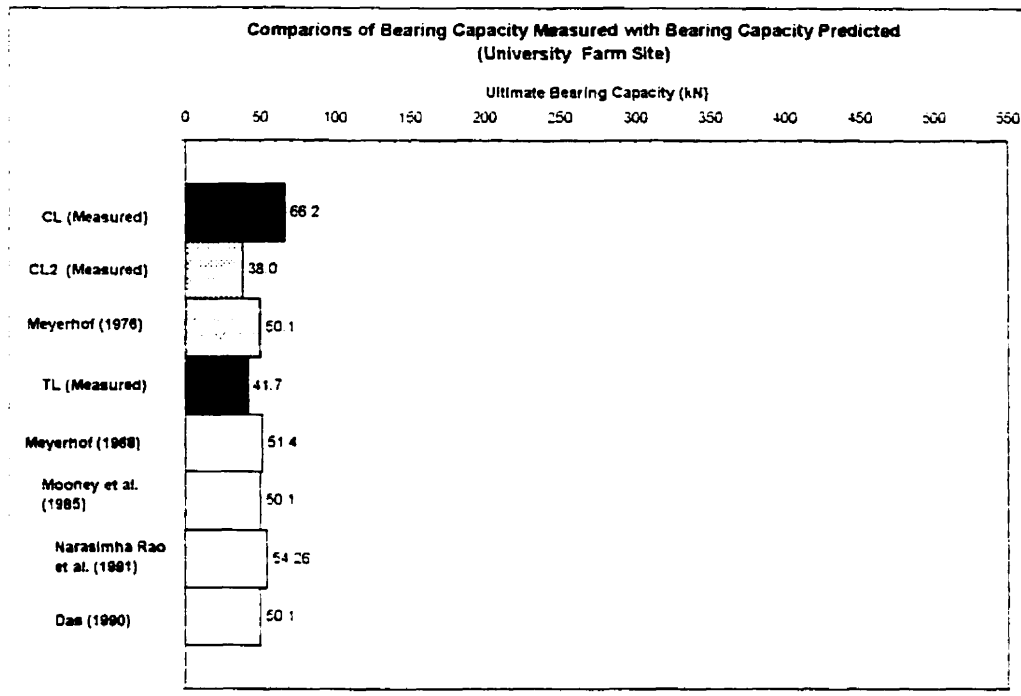


Figure 6.20: Comparison of the Bearing Capacity Measured with the Predicted Values for the CL and TL Tests

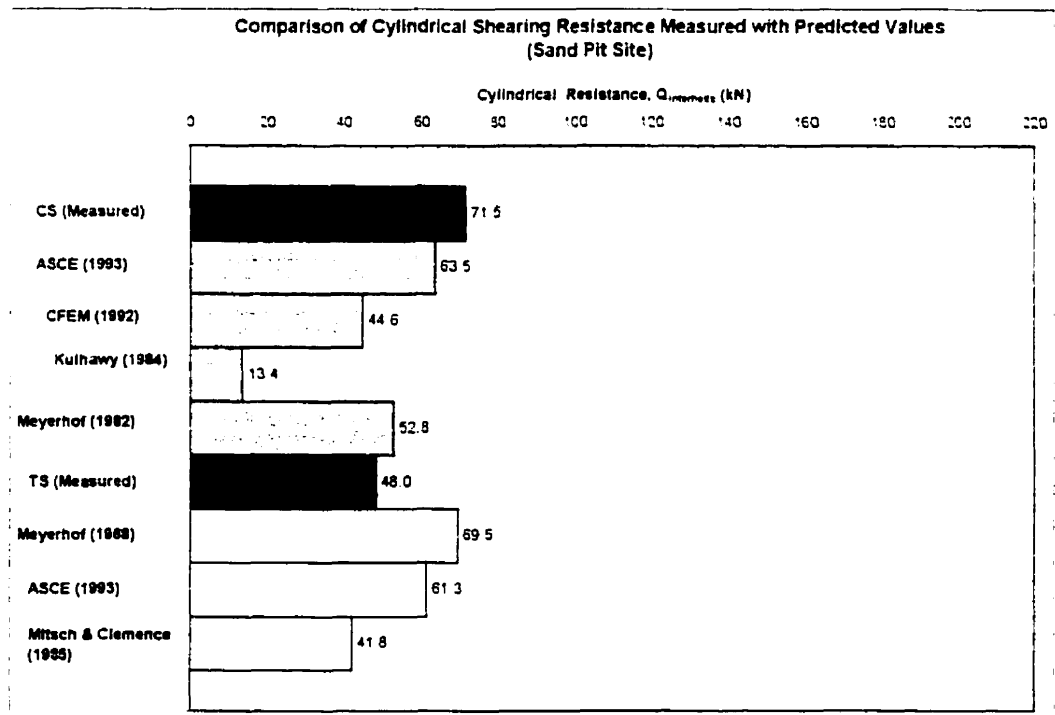
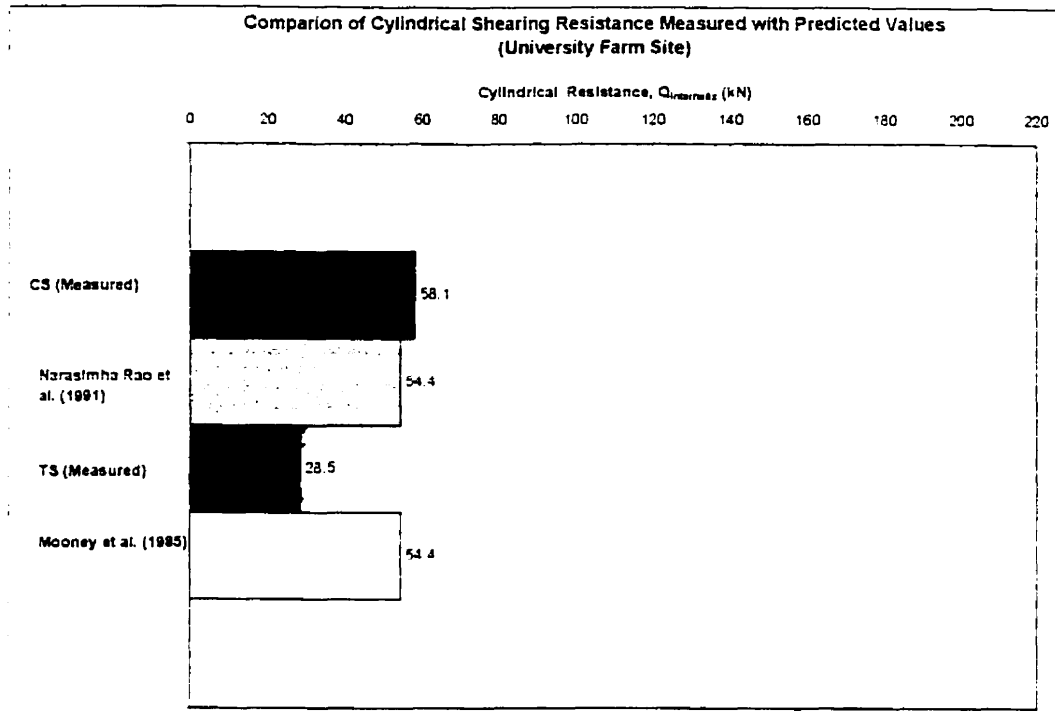


Figure 6.21: Comparison of the Cylindrical Resistance Measured with the Predicted Value for the CS and TS Tests

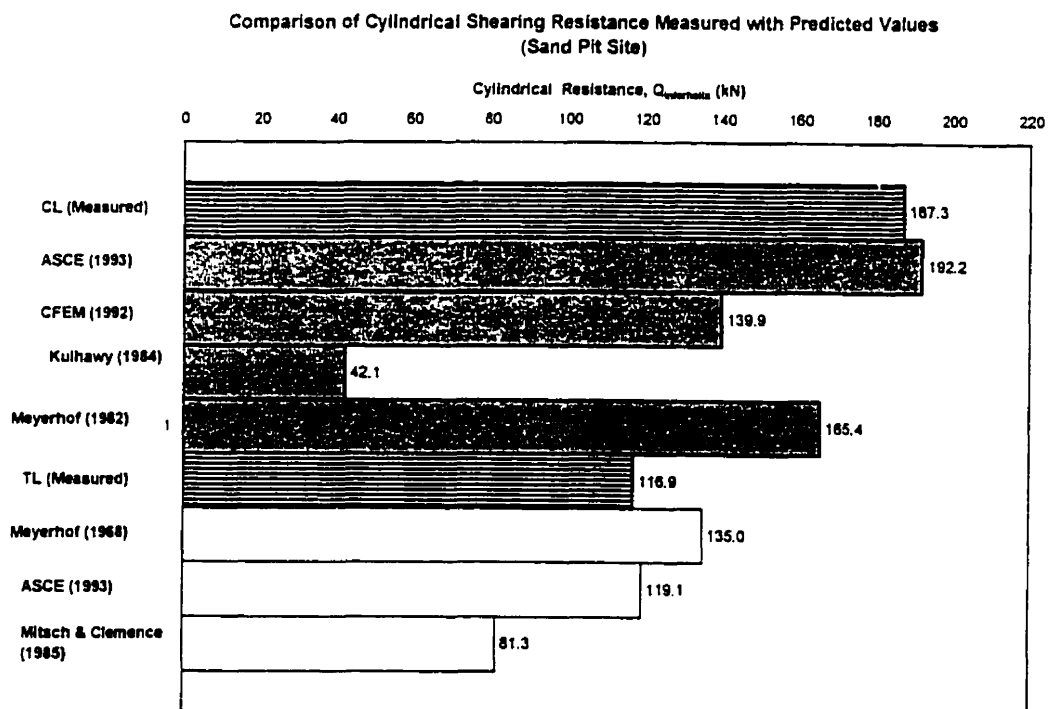
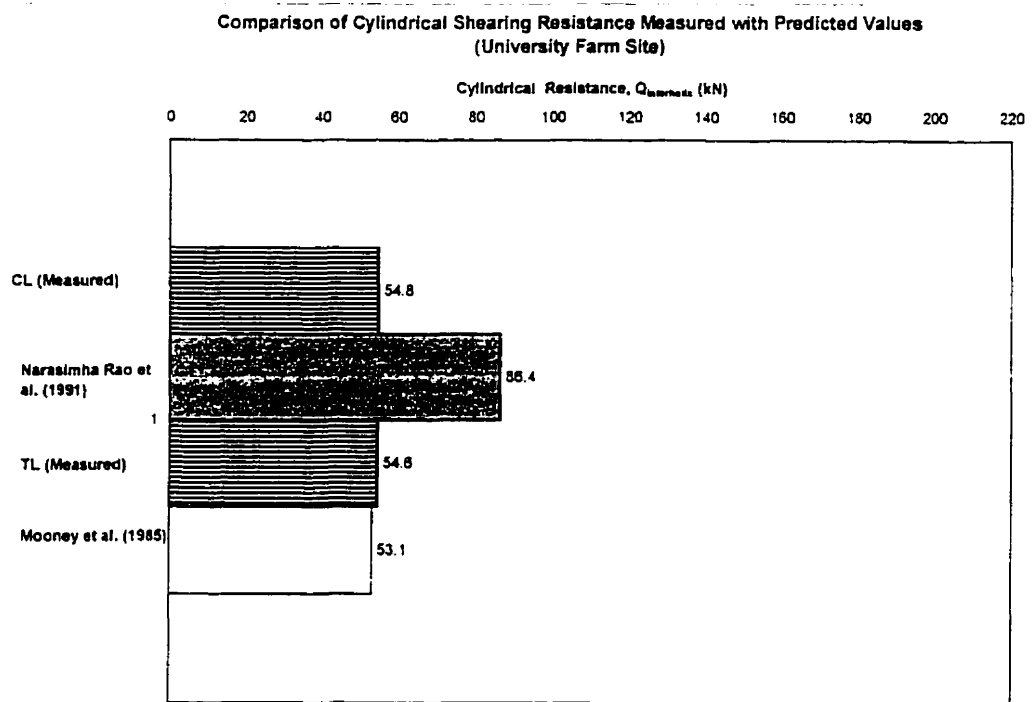


Figure 6.22: Comparison of the Cylindrical Resistance Measured with the Predicted Value for the CL and TL Tests

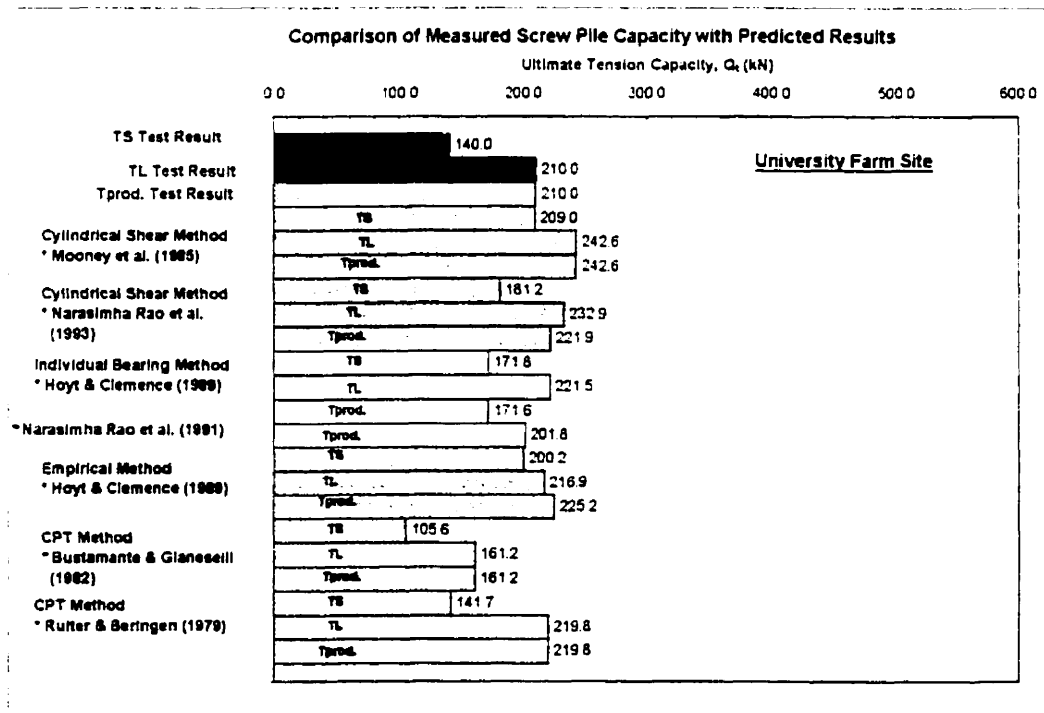
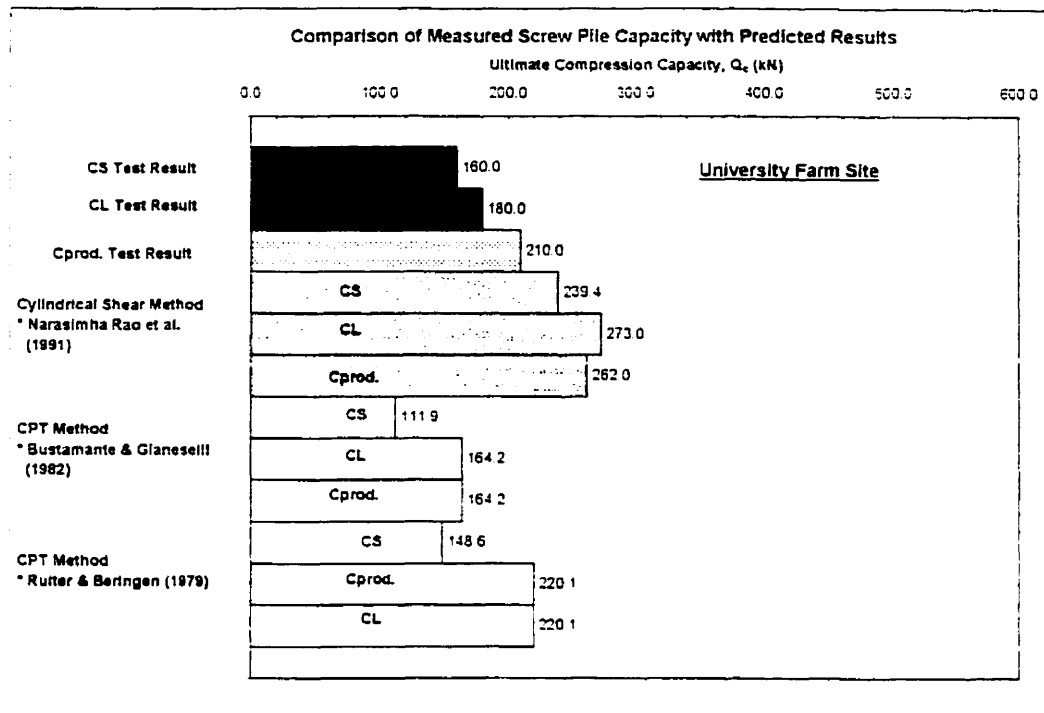


Figure 6.23: Comparison of the Predicted Total Capacity Results with the Measured Capacity Results for Screw Piles Installed at the University Farm Site

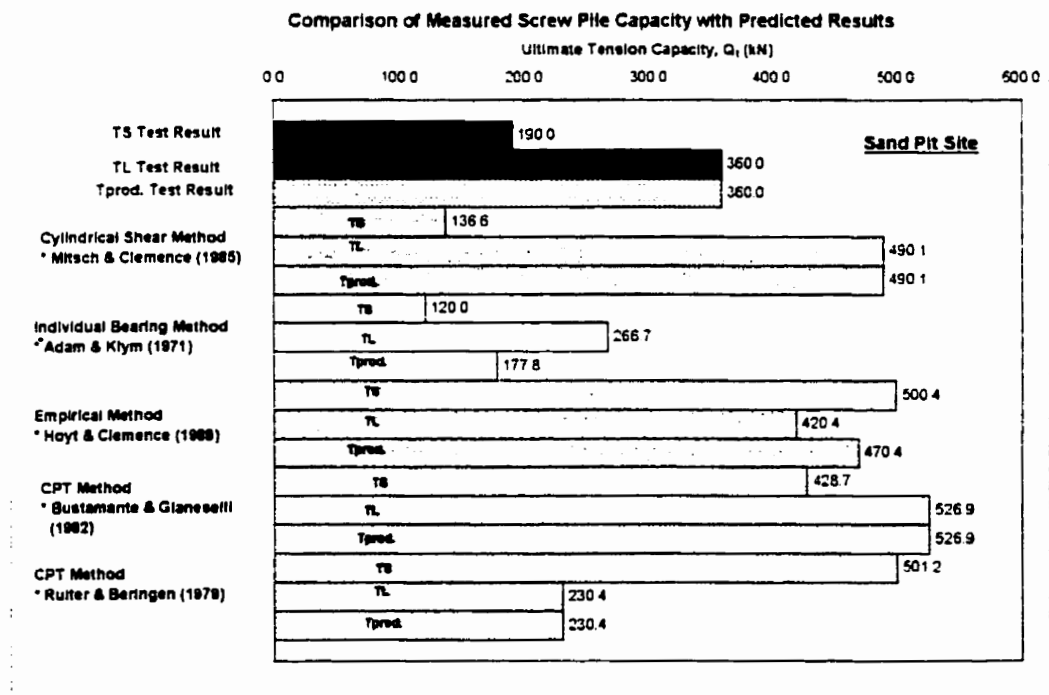
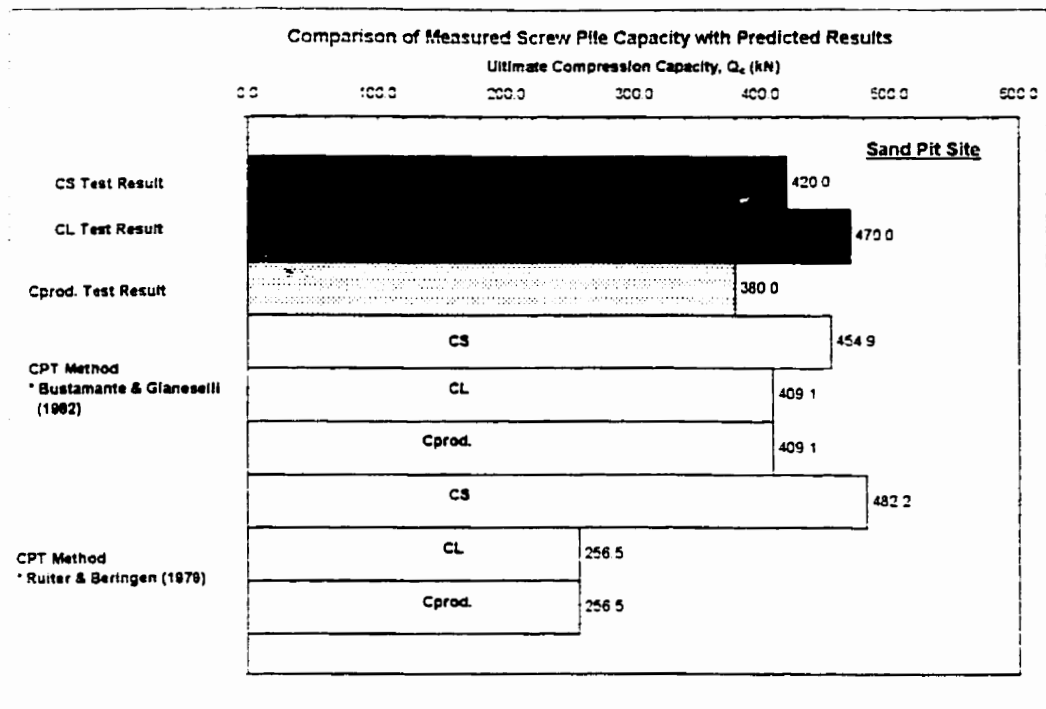


Figure 6.24: Comparison of the Predicted Total Capacity Results with the Measured Capacity Results for Screw Piles Installed at the Sand Pit Site

CHAPTER 7 CONCLUSION AND RECOMMENDATION

7.1 SUMMARY

The purpose of this research program was to study the axial loading behavior of helical piles installed in Alberta soils like the Lake Edmonton Clay and the Sand. With this objective in mind, a study program was carefully planned and carried out.

A detailed review of literature on the subject of the axial capacity of the screw piles narrowed down the study parameters. Piles were then designed and instrumented for the purpose of studying these parameters. For the test sites, namely the University Farm site and the Sand Pit site, site characterization was performed using the standard penetration test (SPT) and the cone penetration test (CPT). Detailed documentation of the geological information is provided in this thesis for future reference. Field pile load tests were carried out using full-scale instrumented multi-helix screw piles at the University Farm site and the Sand Pit site. Total of eighteen pile load tests including the compression, tension and lateral tests were performed at both test sites. Thirteen pile load tests were conducted using fully instrumented research piles and the remaining five pile load tests were carried out using regular production piles. The field pile load tests are carefully documented and presented here. The experimental results obtained from the field pile load tests were used to analyze the load transfer mechanism of the multi-helix screw piles loaded in compression and tension condition. The lateral tests performed are analyzed only in terms of the ultimate lateral capacity of the research piles. The analysis of the lateral loading behavior of the multi-helix screw pile is beyond the scope of this thesis, therefore, the data are summarized and presented for the future study only.

The pile load test results obtained were analyzed for the purpose of developing a more reliable and rational design approach to assist in predicting

the axial capacity of screw piles installed in typical Alberta soils. Based on the observations drawn from the field test results, recommendations for the design of the screw pile installed in the Lake Edmonton Clay and the Sand are provided. Both direct and indirect design approaches are presented in this chapter. However, the guidelines provided here are based on the original framework set by their authors. Only modifications of these methods are suggested based on the field results studied in this program. It is believed that these adjustments can provide better axial capacity prediction for multi-helix screw piles installed in the local soils. Areas that need further study in the future are discussed. It is in the hope that the information synthesized in this research program can provide direction for future research efforts on the capacity of multi-helix screw piles installed in Alberta.

7.2 CONCLUSIONS

The main conclusions that were drawn from this research are summarized below:

1. The load distribution results indicated a general cylindrical shearing surface was formed at failure. Therefore, the total resistance at failure consists three component: the shaft resistance, the cylindrical shearing resistance developed along a cylindrical failure surface connection the top and bottom helices, and the bearing resistance from the bottom helix (compression loading) or from the top helix (tension loading).
2. The shaft resistance generally increases with increase in the embedment depth at both test sites. However, the shaft resistance for a length approximately equal to one helix diameter can not be mobilized at failure. For the compression tests, this inability to mobilize the shaft resistance for a length of $1 \times D$ above the top helix is due to the shadow effect above the top helix. For the tension tests, the ineffective shaft resistance is caused by the general bearing failure above the top helix. Therefore, an effective shaft length ($H_{eff} = H -$

D), where H is the installation depth and D is the diameter of the top helix, should be used to predict the shaft resistance in both cohesive and cohesionless soils.

3. The results obtained at both test sites indicated that the bearing capacity in compression is almost twice the capacity in tension. For the tension tests carried out at the University Farm site, the soil above the top plate is disturbed by the rotary action during the installation of the screw pile and the decrease in undrained shear strength may be the reason that cause the bearing capacities in tension to have a much lower value. At the Sand Pit site, pile installation results loosening of soil within the disturbed zone, which causes the bearing capacity in tension to be lower than that for an undisturbed soil. In the case of compression tests, the soil below the bottom helix is undisturbed; therefore, the bearing capacity for the plate against an undisturbed soil should be higher than the capacity in tension.
4. There is a significant increase in capacity by using multi-helix screw pile instead of single helix screw pile regardless of the pile loading direction.
5. For multi-helix screw piles loaded in compression in the Lake Edmonton clay and the Sand, the bearing resistance developed from the bottom helix and the cylindrical shearing resistance are independent of the embedment depth.
6. For multi-helix screw piles loaded in tension in Lake Edmonton clay and Sand, the bearing resistance from the top helix is dependent on the installation depth. Two types of failure may happen, namely the "shallow" and the "deep" condition failure, and the type of failure depends on the embedment depth (H/D) and surrounding soil strength properties. As a result, the bearing capacity generally increases with the embedment depth (H/D).
7. For multi-helix screw piles loaded in tension in the Lake Edmonton clay and the Sand, the cylindrical shearing resistance does not depend on the installation depth.

8. The ultimate capacities in compression and tension increase with the increase of screw pile embedment ratio (H/D), however the increase is more significant in tension.
9. The compression and tension capacity does not increase with smaller space to diameter ratio (S/D) for screw piles installed at the University Farm site. In stead, the smaller S/D ratio (i.e. $S/D = 1.5$) induced remolding of the surrounding soil and caused reduction of the ultimate compression capacity. For the pullout tests, the space to helix diameter ratio does not effect the total pullout capacity. Therefore, higher capacity can be reached using piles with $S/D = 3.0$ for both the compression and tension tests. However, for the compression tests performed at the Sand Pit site, a 23.7% increase in capacity was observed for the smaller S/D ratio. Therefore, for screw piles installed in the cohesionless soil, significant increase of compression capacity can be achieved by adding an additional helix (i.e. $S/D = 1.5$). Nevertheless, varying the S/D ratio does not effect the total uplift capacity. Based on the experimental results, screw piles with 2 helices ($S/D = 3.0$) performs as well as those with 3 helices ($S/D = 1.5$) in terms of total uplift capacity, therefore, there is no significant benefit of adding a third helix.
10. At the University Farm site, the compression capacity is essentially the same as the pullout capacity. At the Sand Pit site, the compression capacity is significantly larger than the uplift capacity for screw piles with $S/D = 1.5$ installed in shallow depth ($Q_c = 2.2 \times Q_t$). For pile with the same space to diameter ratio installed at a deeper depth, the compression capacity is 1.3 of the ultimate tension capacity. For piles with $S/D = 3.0$ installed in a deep condition, the compression capacity is roughly the same as the tension capacity.
11. The lateral pile load test results has shown no significant increase in lateral capacity due to the increase in shaft wall thickness or the increase in structure stiffness. Hence, the load versus lateral movement response in

lateral loading for these screw piles in these soils is mainly dependent upon the soil characteristics

12. Both indirect and direct methods are used to predict the total axial pile capacity. However, modifications of the original proposed design methods are needed in order to provide better capacity prediction for multi-helix screw piles installed in Alberta soil. In general, for cohesive soil (Lake Edmonton clay), the cylindrical shearing method provides better capacity prediction for multi-helix screw piles with $S/D \leq 3.0$ regardless of loading direction. For screw piles installed in cohesionless soil, the cylindrical shearing method provides good prediction for screw piles with $S/D \leq 2.0$ in compression loading. For a higher space to diameter ratio ($S/D > 2.0$), the individual bearing method provides better capacity estimation than the cylindrical shearing approach. For the tension piles installed in sand, a cylindrical shearing model can be used to provide uplift capacity prediction for screw piles with $S/D < 3.0$.
13. For the direct method, the LCPC CPT method proposed by Bustamante & Giasenelli (1982) can be modified and used to provide capacity approximation for both compression and tension tests.

7.3 DESIGN RECOMMENDATIONS: INDIRECT APPROACHES

7.3.1 Multi-helix Screw Pile

According to the load distribution results obtained from the pile load tests, it can be shown that a cylindrical failure surface was formed at failure for multi-helix screw pile loaded in compression and in tension. Based on the cylindrical shear model, the ultimate capacity is mainly derived from the shaft resistance, the shear resistance along a cylindrical surface connecting the top and bottom helices and bearing resistance below the bottom helix (compression loading) or bearing capacity

above the top helix (uplift loading). Therefore, the total failure resistance can be summarized as follows:

$$Q_u = Q_{shaft} + Q_{helix} + Q_{bearing} \quad \text{Equation 7.1}$$

where

- Q_u = ultimate screw pile capacity
- Q_{shaft} = resistance developed along the steel shaft
- Q_{helix} = shearing resistance mobilized along the cylindrical failure surface
- $Q_{bearing}$ = bearing capacity of the bottom helix in bearing or top helix in uplift

7.3.1.1 In Cohesive Soil ($\phi = 0$ condition)

A model, proposed by Narasimha Rao et al (1993) to predict uplift screw pile capacity in soft clay, is adopted for predicting the ultimate compression capacity for multi-helix screw pile installed in stiff Lake Edmonton clay. The ultimate compression capacity of the helical pile can be given as:

$$Q_c = (\pi D L_c) C_u + A C_u N_c + \pi d H_{eff} \alpha C_u \quad \text{Equation 7.1}$$

where

- Q_c = ultimate compression capacity
- L_c = is the distance between top and bottom helical plates
- H_{eff} = effective length of the shaft ($H - D$)
- α = adhesion factor
- d = shaft diameter
- D = average helix diameter
- A = surface area of the bottom helix plate
- N_c = the bearing capacity factor in compression for cohesive soils
- C_u = undrained shear strength of the soil

The prediction of the bearing resistance developed from the bottom helix is independent of the embedment depth. The bearing capacity factor N_c , proposed

by Meyerhof (1976), provides reasonable predictions for screw piles loaded in compression.

At the University Farm site, there is a 13 to 31 % increase in ultimate compression capacity (Q_c) for screw piles installed in the cohesive soil. The increase in capacity is mainly contributed by the increase in the shaft resistance. For estimation of the shaft adhesion, an effective shaft length H_{eff} is used in the calculation, which the effective shaft length is defined as the embedment length (H) minus the top helix diameter (D). The adhesion developed along the steel shaft is considered in cases where sufficient installation depth (deep pile) is provided. For shallow condition (i.e. embedment ratio $H/D < 3$), the shaft adhesion is considered as insignificant, and thus, the compression capacity equation for helical piles in clay under shallow condition can be given as:

$$Q_c = (\pi DL_c)C_u + AC_uN_c \quad \text{Equation 7.2}$$

For predicting the total uplift capacity, a cylindrical shear model is also adopted and the ultimate tension capacity can be determined using the following equation (Narasimha Rao et al. 1993):

$$Q_t = (\pi DL_c)C_u + A(C_uN_u + \gamma' H) + \pi dH_{eff} \alpha C_u \quad \text{Equation 7.3}$$

where

- Q_t = ultimate screw pile uplift capacity
- γ' = effective unit weight of soil above water table or buoyant weight if below water table
- N_u = uplift bearing capacity factor for cohesive soils
- H = embedment depth

For multi-helix screw pile loaded in tension, the ultimate uplift capacity is dependent upon the embedment depth. At the University of Farm site, the

experimental results had shown a 50% increase in ultimate uplift capacity (Q_t) as the embedment ratio increased from 4.69 to 10.7. The increase in the total uplift capacity is a result of two factors. First, the shaft resistance increases with embedment depth. Secondly, the bearing resistance developed above the top helix is depended on the depth that the screw pile was installed to. The uplift bearing capacity factor, N_u increases with the embedment ratio (H/D) to a limiting value approximately equals to 9. Meyerhof and Adam (1973) provided adjustment to their early work for anchors installed in the stiff clay in the shallow depth. They proposed a simple relationship to evaluate the uplift capacity factor, N_u in relation with the embedment ratio (H/D) as follow:

$$N_u = 1.2 \left(\frac{H}{D} \right) \leq 9 \quad \text{Equation 7.4}$$

Similar to the compression test, for short piles installed at a shallower depth, the term for predicting the shaft adhesion can be neglected since the result is insignificant to the total uplift capacity.

The differences between the modified method, as presented above, and the method proposed by Narasimha Rao et al. (1993) is that the space to diameter ratio (S/D) is not considered here. As discussed in Chapter 6, the decrease in S/D ratio from 3.0 to 1.5 caused remolding of the soil which resulted a decrease in total compression capacity of 17% with a smaller S/D ratio. For the tension tests, the variation of S/D ratio did not effect the ultimate pullout capacity. Therefore, for screw piles installed in Lake Edmonton clay, an S/D ratio equal to 3.0 yields better results.

The cylindrical shearing method discussed above is used to predict the capacity of the screw piles used in this field test program. The results are presented in Table 7.1 and Table 7.2. The parameters used in the calculation are also provided in the tables. As shown by the predicted result, the predictions are within $\pm 10\%$ of the experiment values indicating reasonable agreement.

7.3.1.2 In Cohesionless Soil

An approximation of the ultimate compression capacity of a multi-helix screw pile can be obtained using a cylindrical shearing method as shown in the following formula (Mitsch and Clemence, 1985):

$$Q_c = \gamma' H A N_q + \frac{\pi}{2} D_a \gamma' (H^2_3 - H^2_1) K_s \tan \phi + \frac{P_s}{2} H_{eff}^2 \gamma' K_s \tan \phi \quad \text{Equation 7.5}$$

where

- Q_c = ultimate compression capacity
- γ' = effective unit weight of soil
- K_s = coefficient of lateral earth pressure in compression loading
- ϕ = the soil internal friction angle
- A = area of the bottom helix
- N_q = bearing capacity factor for cohesionless soils
- D_a = average helix diameter
- H = the embedment depth
- H_{eff} = the effective shaft length
- H_1 = depth to top helix
- H_3 = depth to the bottom helix
- P_s = perimeter of the screw pile shaft

For screw piles installed in cohesionless soil at the Sand Pit site, a 12 % increase in total compression capacity was reported as the piles were installed deeper. Similar to the compression tests performed at the University Farm site, the increase in the compression capacity was mainly the result of an increase in shaft resistance. The bearing resistance and the cylindrical shearing resistance do not depend upon the embedment depth.

For the shallow condition (i.e. $H/D < 5$), the ultimate compression capacity of a multi-helix screw pile in sand can be predicted by summing the bearing capacity of the bottom helix and the frictional resistance along the cylinder of soil between the helices without the shaft resistance. Therefore, Equation 7.5 can be expressed as follow:

$$Q_c = \gamma' H A N_q + \frac{\pi}{2} D_a \gamma' (H^2_3 - H^2_1) K_s \tan \phi \quad \text{Equation 7.6}$$

The ultimate compression capacity of a multi-helix screw pile installed in the cohesionless soil is dependent upon the spacing between the helix plates (S/D ratio). The experimental results demonstrated a 24 % increase in the compression capacity with smaller spacing to helix diameter ratio (i.e. $S/D = 1.5$). For the compression tests, a cylindrical failure surface provides a better prediction for screw piles with $S/D \leq 2$ (Mitsch and Clemence, 1995). For higher space to diameter ratios (i.e. $S/D > 2$), bearing failure can occur under each helix without interference with each other, and therefore, the individual bearing method produces better capacity prediction. The method discussed here is summarized in a table format for both the cylindrical shear method and the individual bearing method (see Table 7.3). The methods are then used to predict the compression capacity of the screw piles installed at the Sand Pit site. The comparison of the predicted results using both the cylindrical shear and individual bearing methods are presented in Table 7.4. It can be shown that the cylindrical shear method provided better predictions for multi-helix screw piles with $S/D \leq 2$, and the individual bearing method gave satisfactory estimation result for space to diameter ratios greater than 2.

For the tension tests, a cylindrical shearing method proposed by Mitsch and Clemence (1985) is suggested. The author stated that there are two distinct failure mechanisms for screw pile loaded in tension in the cohesionless soil, namely the shallow or the deep condition. The shallow condition describes the mechanism where a truncated pyramidal shaped failure surface propagates from the top helix to the ground surface. The central angle of the truncated cone is approximately equal to the soil friction angle, ϕ . A cylindrical failure surface is formed below the top helix. For helical piles installed in a much deeper depth, a failure zone develops directly above the top helix. This failure surface is confined by the overburden pressure, and therefore the failure zone does not propagate to the ground surface. Meyerhof and Adam (1968)'s theory stated that there is a

maximum embedment ratio $(H/D)_{cr}$, where the failure mode changes from shallow to deep and this maximum value increases with an increase in the relative density (D_r), and the internal soil friction angle, ϕ , of the sand. The relationship between the critical embedment ratio and the internal soil friction angle is presented in Table 7.5. Therefore, the uplift capacity can be obtained by following formula:

For Multi-helix Screw Pile Installed in Shallow Condition - $H/D < (H/D)_{cr}$

$$Q_t = \gamma' H A F_q + \frac{\pi}{2} D_a \gamma' (H^2_3 - H^2_1) K_u \tan \phi \quad \text{Equation 7.7}$$

For Multi-helix Screw Pile Installed in Deep Condition - $H/D > (H/D)_{cr}$

$$Q_t = \gamma' H A F_q^* + \frac{\pi}{2} D_a \gamma' (H^2_3 - H^2_1) K_u \tan \phi + \frac{P_s}{2} H_{eff}^2 \gamma' K_u \tan \phi \quad \text{Equation 7.8}$$

where

- Q_t = ultimate screw pile uplift capacity
- γ' = effective unit weight of soil
- K_u = coefficient of lateral earth pressure in uplift for sands
- ϕ = friction angle of the soil
- A = area of the top helix
- N_u = uplift capacity factor for cohesionless soils
- H_1 = depth to top helix
- H_3 = depth to the bottom helix
- H_{eff} = effective shaft length
- D_a = average helix diameter
- P_s = perimeter of the screw pile shaft
- F_q = breakout factor for shallow condition
- F_q^* = breakout factor for deep condition

For the shallow condition, the shaft resistance is neglected for the same reason because it does not significantly contribute to the total capacity. For the tension tests, the variation of S/D ratio does not effect the ultimate uplift capacity, therefore, the above stated cylindrical shearing method can be used to predict the uplift capacity of a screw pile with $S/D < 3.0$.

Example calculations using the proposed cylindrical shearing methods for the research and production piles installed in sand are presented in Table 7.5 and Table 7.6. The parameters used in the computation are listed in the tables. The reasons for choosing these parameters are presented in Chapter 6. The predictions are within $\pm 10\%$ of the pile load test results. Therefore, the results demonstrate good agreement with the experimental results.

7.3.2 Single Helix Screw Pile

For a single helix screw pile, the cylindrical shearing resistance connecting the top and the bottom helix for multi-helix piles, does not develop. Therefore, the total resistance is derived from shaft and bearing resistance. Equations used to obtain axial capacity for the multi-helix screw piles should be adjusted to not include the cylindrical component.

7.3.2.1 Single Helix In Cohesive Soil ($\phi = 0$ condition)

Compression

$$Q_c = AC_u N_c + \pi d H_{eff} \alpha C_u \quad \text{Equation 7.9}$$

Tension

$$Q_t = A(C_u N_u + \gamma' H) + \pi d H_{eff} \alpha C_u \quad \text{Equation 7.10}$$

For the compression tests performed by ALMITA Manufacturing Ltd., the new set of field pile load tests focused on studying the effect of varying the pile helix diameter on the ultimate compression capacity of the single helix screw pile. The results indicate that Equation 7.10 reasonably predicts the ultimate compression capacity for pile with helix diameter ranging from 356 mm to 711 mm. Based on the experimental results, recommendations provided by CFEM (1992) for the reduction of the bearing capacity factor, N_c , should be applied with respect to the pile toe diameter (see Section 2.3.1.4).

7.3.2.2 Single Helix In Cohesionless Soil

Compression

$$Q_c = \gamma' H A N_q + \frac{P_s}{2} H_{eff}^2 \gamma' K_s \tan \phi \quad \text{Equation 7.11}$$

Tension

For Single helix Screw Pile Installed in Shallow Condition - $H/D < (H/D)_{cr}$

$$Q_t = \gamma' H A F_q \quad \text{Equation 7.12}$$

For Multi-helix Screw Pile Installed in Deep Condition - $H/D > (H/D)_{cr}$

$$Q_t = \gamma' H A F_q + \frac{P_s}{2} H_{eff}^2 \gamma' K_u \tan \phi \quad \text{Equation 7.13}$$

7.4 DESIGN RECOMMENDATION: DIRECT APPROACH

There are many methods available to predict the pile capacity using CPT data. The European method (de Ruiter and Beringen, 1979) and the LCPC method (Bustamante and Gianeselli, 1982) were used to predict the axial capacity of the screw pile. The LCPC method produced satisfactory predictions for both the University Farm site and the Sand Pit site. The European method provided the best match of results at the University Farm site, but produced a larger discrepancy at the Sand Pit site. Here, only the LCPC method is recommended for the following reasons. First, the method was developed based on a large database with field pile load test data available. Secondly, the method considers wide a range of different piles including the screw type piles. Thirdly, Robertson et al. (1988) used 13 different CPT methods to evaluate 8 full-scale pile load tests performed on six different driven piles. The evaluation showed the best prediction results were provided by the LCPC method, followed by the European method and the method proposed by Schmertmann (1978). Most importantly, the LCPC method provides direct correlation of the pile capacity to the tip resistance q_c without intermediate correlation to determine the soil strength parameters. Robertson and Campanella (1988) provided a flow chart that summarized the LCPC method, and this flow chart is presented in Table 7.7. Based on the experimental test results obtained, the coefficient α and k_c proposed by Bustamante and Gianeselli (1982) are adjusted in order to take into account the more complicated pile geometry and loading directions. The comparison of the modified coefficients used for obtaining the screw pile axial capacity and the original coefficient proposed by the LCPC method is presented in Table 7.9. As shown in Table 7.9, a new coefficient α^* is used for predicting the capacity of the cylindrical shearing resistance. This coefficient is used to recognize the difference between the shaft and cylindrical shear resistance for the piles that have multi-helices. In addition, for the modified method, the loading direction is considered by adjusting the coefficients used in the method. A simplified flow chart for the modified LCPC CPT method is outlined in Table 7.8.

The coefficients used for the method are presented in Table 7.9. The modified method is used to predict the capacities for screw piles installed in the University Farm site and the Sand Pit site, and the results are compared to the predictions using the original proposed method. Figure 7.1 and Figure 7.2 present the comparison of the capacity predictions for both compression and tension tests using both the original and modified LCPC CPT method for piles installed at the University Farm site. Figure 7.3 and Figure 7.4 show the prediction results for the compression tests at the Sand Pit site, and Figure 7.5 present the capacity estimations for the tension tests at the Sand Pit site. The ultimate axial capacities predicted using the modified coefficients are summarized in Table 7.10 in comparison with the prediction results using the original LCPC method and both predictions are compared to the measured experiment results. The modified coefficients produced satisfactory prediction results for both the University Farm site and the Sand Pit site. It is important to note that for the compression tests performed at the Sand Pit site, the coefficient, α , is reduced for the cylindrical failure surface (CFS) for screw piles with larger space to diameter ratio. As discussed previously, for compression tests performed on the production piles ($S/D > 2$), a complete cylindrical failure surface may not formed at failure because the space between the helices is too large. Instead of the cylindrical failure surface, bearing failure may happen under each individual helix. For the same reason, reduction of the cylindrical shear resistance is applied, and the reduced coefficient gave much better predictions for the production piles with $S/D = 3.0$.

For the single helix screw pile, the cylindrical shearing surface does not form, therefore, the ultimate pile capacity can be predicted using the flowchart shown in Table 7.8 and the coefficients in Table 7.9 without the consideration of the resistance from the cylindrical shear surface.

7.5 OTHER FACTORS THAT INFLUENCE THE ULTIMATE CAPACITY

Other factors such as load type, loading condition (long term vs. short term), allowable design load (factor of safety), effects of installation methods, group piles are discussed in Chapter 2, and thus, not discussed in detail here. However, the next two sections were mostly of interest to the sponsor of this program, ALMITA Manufacturing Ltd., therefore, general discussions are provided below.

7.5.1 Compression Capacity Versus Uplift Capacity

At the University Farm site, the compression capacity of the screw piles are not significantly different from the tension capacity regardless of the embedment ratio (H/D) and space to diameter ratio (S/D). At the Sand Pit site, the compression capacity are significantly larger than the uplift capacity at shallow depth ($Q_c = 2.2 \times Q_t$) for piles with $S/D = 1.5$. For pile with the same space to diameter ratio installed at a greater depths, the compression capacity is 1.3 of the ultimate tension capacity. For pile with $S/D = 3.0$ installed in a deep condition, the compression capacity is roughly the same as the tension capacity. According to the experimental results obtained in this program, the results show that a generalized formula as reported by Trofimendkov and Mariupolskii (1965) (i.e. $Q_c = 1.3 \times Q_t$) for piles installed in the Lake Edmonton Clay and the Sand Pit site can not be used indifferently. For stiff clay material such as Lake Edmonton Clay, the compression to tension capacity ratio (Q_c / Q_t) may increases with the increase in soil moisture content as suggested by Narasimha Rao, et al. (1991). However, more testing on screw piles installed in Lake Edmonton clay, should be done in order to verify such suggestion. For the cohesionless soil, the compression capacity can preliminary determined by applied a factor of 1.3 to the ultimate tension capacity for screw piles with $S/D < 2$, and installed into a deep condition (i.e. $H/D > 5$), although this general rule can significantly underestimate the compression capacity installed in very dense sand in shallow depth.

7.5.2 Torque Method

The installation torque is defined as the torque required to install the screw piles to the desired depth. Because torque is always monitored and recorded on a torque chart during the installation process, it is attractive to develop an empirical method that correlates the installation torque directly to the ultimate axial capacity. Hoyt and Clemence (1985) outlined such methods and explained that the torque method is simply analogous to the relationship of pile driving effort to pile capacity. This empirical method is widely used in the industry to predict the uplift capacity of screw anchors because it is simple to use and it provides a procedure to verify if the desired design loads have been reached at a site location. However, as explained by Hoyt and Clemence (1985), although the procedure was used successfully in the construction of thousands of anchors over the past twenty years, the method lacks the support of geotechnical concepts. In addition, the method provides correlations for predicting the pullout capacity but does not include relationships for predicting the compression capacity. The torque method was used to predict the uplift capacity of the screw piles installed in the University Farm site and the Sand Pit site. It provided satisfactory results for piles installed in deep condition ($H/D = 10.7$) and overestimated the results for the shallow condition ($H/D = 4.67$). At the Sand Pit site, a 163% over prediction was reported for the TS test. As noted by Hoyt and Clemence (1985), the anchors used for testing in their test program had an embedment ratio (H/D) varying from 5.1 to 134 and all anchors were analyzed as "deep" anchors. Therefore, adjustment for predicting the uplift capacity of shallow anchors (i.e. $H/D < 5$) should be applied. This empirical method can be used to predict the compression capacity based on the same analogous used for predicting the uplift capacity. However, a larger data base including full scale field pile load test results should be established before providing a more reliable procedure for estimating compression capacity using an empirical approach.

In recent years, some of the larger diameter screw piles are used to provide larger compression capacity for foundation applications. The question of using

these large helix size screw piles is how to determine the required torque to install these piles. Here, a simple chart as shown in Figure 7.6, can be used to predict the required installation torque at the preliminary design stage based on the CPT data. One of the advantages of using CPT data is that the CPT data provides repeatable information about the soil behavior over the profile of interest and classified into different soil type (Robertson, 1990). By plotting the normalized torque against the tip resistance, when the normalized torque is defined as the installation torque divided by the helix diameter (T/D), a preliminary prediction of the installation torque required per m of helix diameter size can be determined according to different soil type. For soils like the Lake Edmonton Clay and the Sand, the installation torque needed to install different helix diameter screw piles are plotted against the average cone tip resistance from CPT. At the University Farm site, for a soil profile which shows an increase in the cone tip resistance with depth, the installation torque generally increases with increase in embedment depth although the increase is not significant after breaking the surface soil crust. The normalized installation torque (T/D) ranges between 3000 to 8000 m kN / m with an average value of approximately 6500 m kN / m. At the Sand Pit site, the cone tip resistance decreases with increase in depth, and the installation torque required was mainly dependent on the torque needed to screw through the sand desiccated soil crust. For the long pile ($H/D = 10.7$), the pile was basically screwed into the ground without applying extra torque after breaking through the surface soil. Consequently, for piles installed in cohesionless material, it is important to determine the installation torque required to break the soil surface instead of studying the influence of increase in pile length on the installation torque.

The relationship between the normalized installation torque and the cone tip resistance should be investigated in detail according to different soil material and helix diameter. In the future, the chart can be completed for different soil types such as the Glacial Till, Lake Edmonton Clay and the Sand, and be used to provide a quick and easy assessment of the installation torque needed to install screw piles with different helix sizes.

7.6 FUTURE RESEARCH

In preparing this thesis, several areas of potential future research were identified and these areas are discussed below:

1. In this study, by adding the second helix, the compression capacity increased significantly. Therefore, by varying the screw pile geometry (i.e. different helix diameter) can help to create a larger resistance surface, thus, help to increase the ultimate pile capacity. However, this effect should be more carefully examined.
2. This thesis only presented the lateral pile load test results not including detailed analysis on the lateral pile load transfer mechanism. Therefore, further study on the lateral load response should be investigated more closely.
3. There are a number of areas that need further researches, such as the design of an inclined screw pile, group piles, and screw piles subjected to vertical or lateral cyclic loading.
4. As discussed in Chapter 3, the till site was cancelled for performing the pile load test. The load-carrying behavior for screw piles installed in Alberta till should be studied because the soil is the parental soil that covers a large portion of Alberta.

7.7 REFERENCE

- Bustamante, M., and Ghaneselli, L. (1982). "Pile Bearing Capacity Prediction by Means of Static Penetrometer CPT"; Proceedings of the 2nd European Symposium on Penetration Testing, ESOPT-II, Amsterdam, 2, pp. 493-500, Balkema Pub., Rotterdam.
- Campanella, R. G., Sy, A. Davies, M. P., and Robertson, P. K. (1989). "Class a Prediction of Driven Pile Behavior"; Predicted and Observed Axial Behavior of Piles. Geotechnical Special Publication No. 23, ASCE New York, pp. 303-317.
- De Ruiter, J., and Beringen, F. L. (1979). "Pile Foundations for Large North Sea Structures"; Marine Geotechnology, 3(3), pp. 267-314.
- Meyerhof, G. G. (1976). "Bearing Capacity and Settlement of Pile Foundations"; Journal of the Geotechnical Engineering Division, Proceedings of the American Society of Civil Engineers, Vol. 102, No. GT3, March 1976, pp. 197-224
- Meyerhof, G. G., and Adams, J. I. (1968). "The Ultimate Uplift Capacity of Foundations"; Canadian Geotechnical Journal, Vol. V, no. 4, pp. 225-244.
- Mitsch, M. P., and Clemence, S. P. (1985). "The Uplift Capacity of Helix Anchors in Sand. Uplift Behavior of Anchor Foundations in Soil"; Proceedings of ASCE, New York, N.Y., pp. 26-47.
- Narasimha Rao, S., Prasad, Y.V.S.N., and Shetty, M. D. (1991). "The Behaviour of Model Screw Piles in Cohesive Soils"; Journal of Soil and Foundations, Japanese Society of Soil Mechanics and Foundation Engineering, Vol, 31, pp. 35-50.
- Narasimha Rao, S., Prasad, Y.V.S.N., and Veeresh, C. (1993). "Behaviour of Embedded Model Screw Anchors in Soft Clays"; Geotechnique, Vol, 43, pp. 605-614.
- Robertson, P. K., and Campanella, R.G. (1988). " Guidelines for Geotechnical Design Using CPT and CPTU"; Soil Mechanics Series No. 120, University of British Columbia.
- Robertson, P. K., Campanella, R. G., Davies, M. P., and Sy, A. (1988). "Axial Capacity of Driven Piles in Deltaic Soils Using CPT"; 1st International Symposium on Penetration Testing, ISOPT-1, Disney World, March, A.A. Balkema.

Robertson, P. K. (1990). "Soil Classification Using the CPT"; Canadian Geotechnical Journal, Ottawa, Vol. 21, no. 1, pp. 151-158.

Schmertmann, J. H. (1978a). "Guidelines for Cone Penetration Test, Performance and Design"; Federal Highway Administration, Report FHWA-TS-78-209, Washington, July 1978, 145 p.

Trofimenkov, J. G., and Mariupolskii, L. G. (1965). "Screw Piles Used for Mast and Tower Foundations"; Proceedings of Sixth International Conference on Soil Mechanics and Foundation Engineering, Montreal, Quebec, Vol. 11, pp. 328-332.

Table 7.1: Example Calculation using the Proposed Cylindrical Shearing Method to Predict the Compression Capacity of Screw Pile Installed in the Lake Edmonton Clay

Cylindrical Shearing Method - Compression Capacity

Clay ($\phi = 0$, method listed below is based on Narasimha Rao et al, 1993 which was proposed to predict uplift pile capacity)

$$Q_c = (\pi DL_c)C_u + A C_u N_c + \pi d H_{\text{eff}} \alpha C_u$$

For Screw Pile with S/D Ratio ≤ 3

		Short Pile	Long Pile	Production Pile	
H	=	1.58 m	3.72 m	3.72 m	embedment depth
D	=	0.36 m	0.36 m	0.36 m	plate diameter
L _c	=	1.07 m	1.07 m	1.07 m	space between top and bottom helix
A	=	0.06 m ²	0.06 m ²	0.06 m ²	surface area of the helix plate = $\pi(D^2 - d^2)/4$
N _c	=	9.00	9.00	9.00	uplift capacity factor
d	=	0.22 m	0.22 m	0.22 m	shaft diameter
H _{eff}	=	1.23 m	3.37 m	3.37 m	effective shaft length = H - D
C _u	=	50.0 kPa		90.0 kPa	Undisturbed Undrained Shear Strength
α	=	0.72		0.30	adhesion factor (after CFEM, 1992 & Mooney et al., 1985)

	Term 1 (πDL_c)C _u (KN)	Term 2 A C _u N _c (KN)	Term 3 $\pi d H_{\text{eff}} \alpha C_u$ (KN)	Q _c (KN)	Q _u (KN)	Difference (KN)
Short Research Pile (CS Test)	64.4	49.9	30.4	145	150	9.56%
Long Research Pile (CL Test)	64.4	49.9	70.0	184	180	2.31%
Production Pile - (Cprod. Test)	107	49.9	40.2	197	210	6.36%

Note:

- * For the long research pile (CL) and short research pile (CS) tests, the undrained shear strength is reduced by 40 % in order to account for the effect of soil disturbuncy caused by adding the third helix.

Table 7.2: Example Calculation using the Proposed Cylindrical Shearing Method to Predict the Uplift Capacity of Screw Pile Installed in the Lake Edmonton Clay

Cylindrical Shearing Method - Tension Capacity

Clay ($\phi = 0$, after Narasimha Rao et al, 1993)

$$Q_t = (\pi DL_c)C_u + A(C_u N_u + \gamma'H) + \pi d H_{eff} \alpha C_u$$

For Screw Pile with $S/D \leq 3$

	<u>Short Pile</u>	<u>Long Pile</u>	<u>Production Pile</u>	
H =	1.58 m	3.72 m	3.72 m	embeddment depth
D =	0.36 m	0.36 m	0.36 m	plate diameter
L_c =	1.07 m	1.07 m	1.07 m	space between 2 helices top and bottom
A =	0.06 m ²	0.06 m ²	0.06 m ²	surface area of the helix plate = $\pi(D^2 - d^2)/4$
N_u =	5.60	9.00	9.00	uplift capacity factor (after Meyerhof, 1973)
d =	0.22 m	0.22 m	0.22 m	shaft diameter
H_{eff} =	1.23 m	3.37 m	3.37 m	effective shaft length = H - D
C_u =	50.0 kPa		90.0 kPa	Undisturbed Undrained Shear Strength
α =	0.72		0.30	adhesion factor (after CFEM, 1992 & Mooney et al., 1985)
		Term 1 (πDL_c)C _u (KN)	Term 2 A(C _u N _u + γ' H) (KN)	Term 3 $\pi d H_{eff} \alpha C_u$ (KN)
Short Research Pile (TS Test)		64.4	35.5	30.4
Long Research Pile (TL Test)		107	54.3	70.0
Production Pile - (Tprod. Test)		107	54.3	70.0

Note:

- For screw pile installed in shallow depth, the fissured undrained shear strength (C_u) is much lower than the intact C_u
In such case, the remolded Cu is assumed to be 60% of the undisturbed undrained shear strength

Table 7.3: The Cylindrical Shearing Method and The Individual Bearing Method Used to Predict the Compression Capacity of Screw Pile Installed in the Sand

*** Cylindrical Shearing Method - Compression Capacity**

Cohesionless Soil (after design procedure proposed by Mitsch & Clemence, 1985)

$$Q_c = \gamma' H A N_q + \frac{1}{2} \pi D_s \gamma' (H_3^2 - H_1^2) K_s \tan \phi + \frac{1}{2} P_s H_{eff}^2 \gamma' K_s \tan \phi \quad \text{For Screw Pile with } S/D \leq 2$$

*** Individual Bearing Method - Compression Capacity**

Cohesionless Soil (after design procedure proposed by Adams and Klym, 1971)

For Screw Pile with } S/D > 2

$$Q_c = \Sigma Q_{bearing} + Q_{shaft}$$

$$Q_c = \gamma' H_1 A N_q + \gamma' H_3 A N_q + \frac{1}{2} P_s H_{eff}^2 \gamma' K_s \tan \phi$$

	<u>Short Pile</u>	<u>Long Pile</u>	<u>Production Pile</u>	
H_1	= 1.58 m	3.722 m	3.722 m	depth to the top helix
H_3	= 2.65 m	4.79 m	4.79 m	depth to the bottom helix
D_s	= 0.36 m	0.36 m	0.36 m	plate diameter
A	= 0.06 m ²	0.06 m ²	0.06 m ²	surface area of the plate anchor = $\pi(D^2 - d^2)/4$
d	= 0.22 m	0.22 m	0.22 m	shaft diameter
H_{eff}	= 1.23 m	3.37 m	3.37 m	effective shaft length = $H - D$
γ'	= 18.0 kN/m ³	18.0 kN/m ³	18.0 kN/m ³	effective unit weight of soil
P_s	= 0.69 m	0.69 m	0.69 m	perimeter of pile shaft
ϕ	=			internal soil friction angle
K_s	=			coefficient of lateral earth pressure in compression for sands
N_q	=			bearing capacity factor

Table 7.4: Compression Capacity Prediction Results using the Proposed Design Methods for Cohesionless Soil

	CS Test $\phi = 39^\circ$		CL Test $\phi = 39^\circ$		
	K_s	N_q	K_s	K_s	N_q
	Ref. 1	Ref. 3	Ref. 2	Ref. 2	Ref. 3
Shaft Resistance	3.195		2.325		
Interhelix Resistance	3.195			2.325	
Bearing Resistance		100			30

References:

- No. 1: ASCE (1993)
 No. 2: CFEM (1992)
 No. 3: Vesic (1963)

Capacity Prediction Results using Cylindrical Shearing Method

	Term1 $\gamma' H A N_q$ (KN)	Term 2 $\frac{1}{2} \pi D_s \gamma' (H^2 - H^2_i) K_s \tan \phi$ (KN)	Term 3 $\frac{1}{2} P_s H_s \pi^2 \gamma' K_s \tan \phi$ (KN)
Short Research Pile (CS Test)	294	117	24.2
Long Research Pile (CL Test)	159	172	132
Production Pile - (Cprod. Test)	159	172	132

(a)	(b)	(c)
(Predicted) (KN)	(Measured) (KN)	Difference
294	220	87%
159	170	-14%
159	180	-21%

Capacity Prediction Results using Individual Bearing Method

	Term1 $\gamma' H_s A N_q$ (KN)	Term 2 $\gamma' H_s A N_q$ (KN)	Term 3 $\frac{1}{2} P_s H_s \pi^2 \gamma' K_s \tan \phi$ (KN)
Production Pile - (Cprod. Test)	124	159	132

(a)	(b)	(c)
(Predicted) (KN)	(Measured) (KN)	Difference
124	1380	9132%

Table 7.5: Proposed Cylindrical Shearing Method to Predict the Uplift Capacity of Screw Pile Installed in Sand

Cylindrical Shearing Method - Tension Capacity

Cohesionless Soil (after design procedure proposed by Mitsch & Clemence, 1985)

Shallow Condition $(H/D < (H/D)_{cr})$

$$Q_t = \gamma' H A F_q + \frac{1}{2} \pi D_s \gamma' (H_s^2 - H_1^2) K_u \tan \phi$$

For Screw Pile with $S/D < 3$

Deep Condition $(H/D > (H/D)_{cr})$

$$Q_t = \gamma' H A F_q^* + \frac{1}{2} \pi D_s \gamma' (H_s^2 - H_1^2) K_u \tan \phi + \frac{1}{2} P_s H_{en}^2 \gamma' K_u \tan \phi$$

Short Pile

Long Pile

Production Pile

H	=	1.58 m	3.72 m	3.72 m	embedment depth
H ₁	=	1.58 m	3.722 m	3.722 m	depth to the top helix
H _s	=	2.65 m	4.79 m	4.79 m	depth to the bottom helix
D _s	=	0.36 m	0.36 m	0.36 m	plate diameter
A	=	0.06 m ²	0.06 m ²	0.06 m ²	surface area of the plate anchor = $\pi(D^2 - d^2)/4$
d	=	0.22 m	0.22 m	0.22 m	shaft diameter
H _{en}	=	1.23 m	3.37 m	3.37 m	effective shaft length = H - D
γ'	=	18 kN/m ³	18 kN/m ³	18 kN/m ³	effective unit weight of soil
P _s	=	0.69 m	0.69 m	0.69 m	perimeter of pile shaft
ϕ	=				internal soil friction angle
K _u	=				coefficient of lateral earth pressure in uplift for sands
F _q	=				breakout factor for shallow condition
F _q [*]	=				breakout factor for deep condition

Soil Friction Angle, ϕ

$(H/D)_{cr}$

(degree)

20	2.5
25	3.0
30	4.0
35	5.0
40	7.0
45	9.0
48	11.0

Table 7.6: Uplift Capacity Prediction Results using the Proposed Design Methods for Cohesionless Soil

	TS Test $\phi = 39^\circ$		TL Test $\phi = 39^\circ$		
	K_u Ref. 1	F_q Ref. 2	K_u Ref. 2	K_u Ref. 2	F_q^* Ref. 3
Shaft Resistance	3.62		2.18		
Interhelix Resistan	3.62			2.18	
Bearing Resistance		22			66

References:

No. 1: Meyerhof and Adam (1968)

No. 2: Mitsch and Clemence (1985)

No. 3: Saeedy (1987)

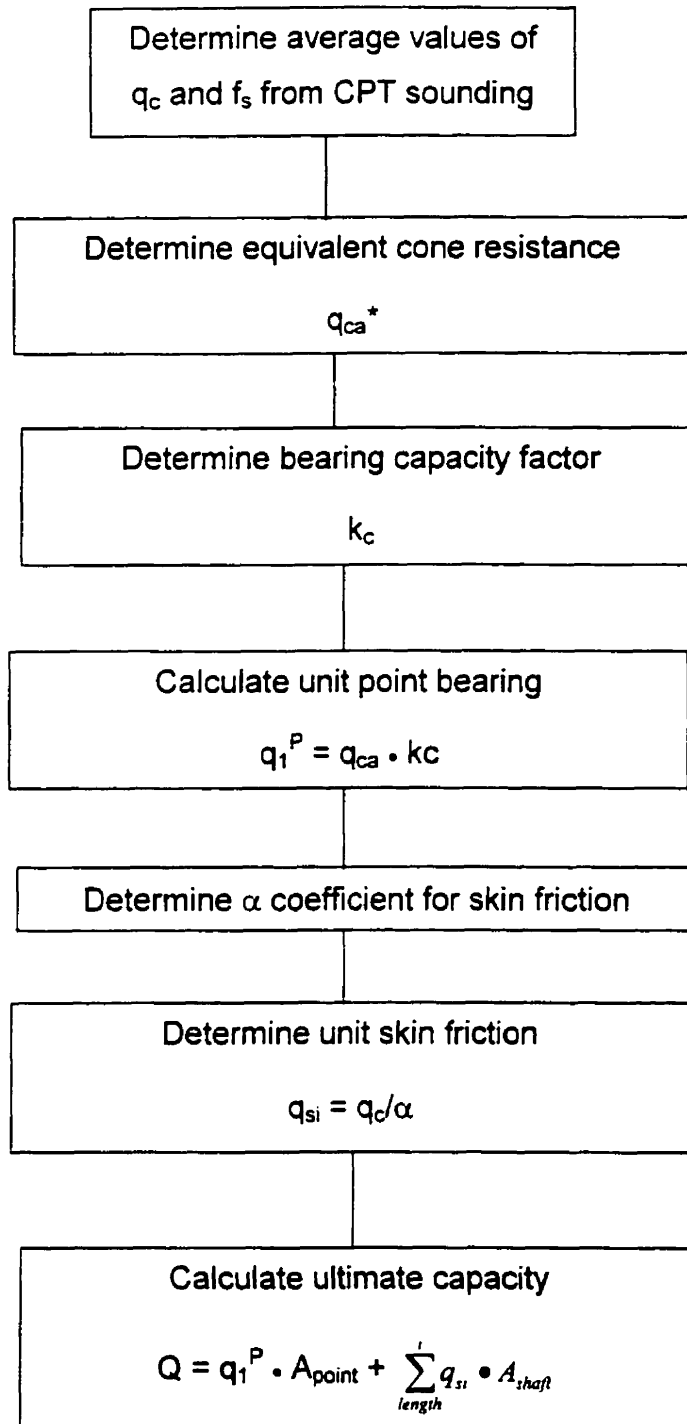
Capacity Prediction Results using Cylindrical Shearing Method

	Term1	Term 2
	$\gamma' H A F_q$ (KN)	$\frac{1}{2} \pi D_s \gamma' (H^2_s - H^2_i) K_u \tan \phi$ (KN)
Short Research Pile (TS Test)	38.7	133

Q_1	Q_2	%
(Predicted)	(Measured)	Difference
(KN)	(KN)	
172	190	9.63

	Term1	Term 2	Term 3
	$\gamma' H A F_q^*$ (KN)	$\frac{1}{2} \pi D_s \gamma' (H^2_s - H^2_i) K_u \tan \phi$ (KN)	$\frac{1}{2} P_s H_s \pi^2 \gamma' K_u \tan \phi$ (KN)
Long Research Pile (TL Test)	87.6	161	124
Production Pile - (Tprod. Test)	87.6	161	124

Q_1	Q_2	%
(Predicted)	(Measured)	Difference
(KN)	(KN)	
373	360	3.37
373	360	3.37



Note: α and k_c dependent upon soil type and pile type.

Table 7.7: Flowchart for the LCPC CPT Method (after Robertson and Campanella, 1988)

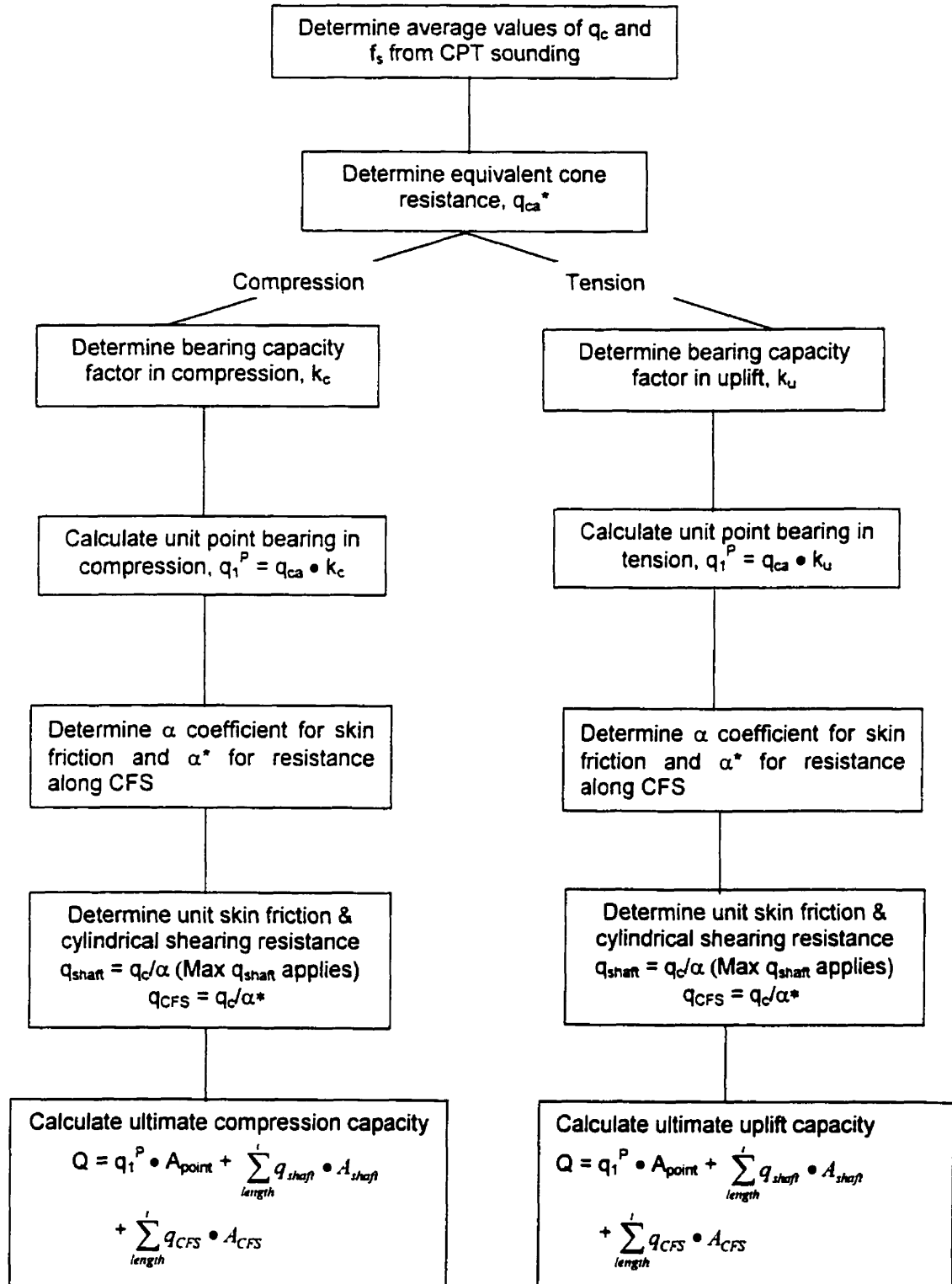


Table 7.8: Flowchart for the Modified LCPC CPT Method (after Robertson and Campanella, 1988)

Table 7.9: Comparison of Original and Modified Coefficients used in CPT Method for the Research Piles (after Bustamante & Giasenelli, 1982)

Nature of Soil	q_{ca} (MPa)	Coefficients (Original)			Coefficients (Modified)							
		Friction Coefficient		Bearing Factors	Friction Coefficient		Bearing Factors	Friction Coefficient		Bearing Factors		
		For both Shaft & CFS			Shaft			Shaft				
		α	Max. Friction (MPa)		α	Max. q_{shaft} (MPa)		α	Max. q_{shaft} (MPa)			
Soft clay and mud	< 1	30	0.015	0.5	20	0.015	20	0.015	20	0.015	20	0.5
Moderately compact clay	1 to 5	40	0.035 (0.08)	0.45	55	0.035 (0.08)	25	55	0.035 (0.08)	25	0.45	
Compact to stiff clay and compact silt	> 5	60	0.035 (0.08)	0.55	60	0.035 (0.08)	60	60	0.035 (0.08)	60	0.55	
Silt and loose sand	≤ 5	60	0.035	0.5	50	0.035	30	50	0.035	30	0.10	
Moderately compact sand and gravel	5 to 12	100	0.08 (0.12)	0.5	100	0.08 (0.12)	70	100	0.08 (0.12)	70	0.10	
Compact to very compact sand and gravel	>12	150	0.12 (0.15)	0.4	150	0.12 (0.15)	150	150	0.12 (0.15)	150	0.15	

Note:

α^* : Friction coefficient applies to the Cylindrical Failure Surface (CFS). No maximum limit of shear resistance assigned for CFS.

Table 7.10: Comparison of Capacity Prediction Results Using the Original and Modified LCPC CPT Method (after Bustamante & Giasenelli, 1982)

See Figure 7.1 to figure 7.5 for comparison of the results presented here		Ultimate Compression Capacity			Ultimate Tension Capacity		
		Q_c			Q_t		
University		CS	CL	Cprod.	TS	TL	Tprod.
Farm Site (UFS)	Bustamante and Giasenelli (1982) - Original	111.9	164.2	164.2	105.6	161.2	161.2
	Bustamante and Giasenelli (1982) - Modified	151.8	189.7	189.7	145.68	197.38	197.38
Sand Pit Site (SPS)	Bustamante and Giasenelli (1982) - Original	454.9	409.1	409.1	428.7	526.9	526.9
	Bustamante and Giasenelli (1982) - Modified	421.8	421.8	394.0	211.67	365.85	365.85
UFS	Bustamante and Giasenelli (1982) - Original	-30.0	-8.8	-21.8	-24.6	-23.2	-23.2
(% Difference)	Bustamante and Giasenelli (1982) - Modified	-5.1	5.4	-9.7	4.1	-6.0	-6.0
SPS	Bustamante and Giasenelli (1982) - Original	8.3	-13.0	7.7	125.6	46.4	46.4
(% Difference)	Bustamante and Giasenelli (1982) - Modified	0.4	-10.3	3.7	11.4	1.6	1.6

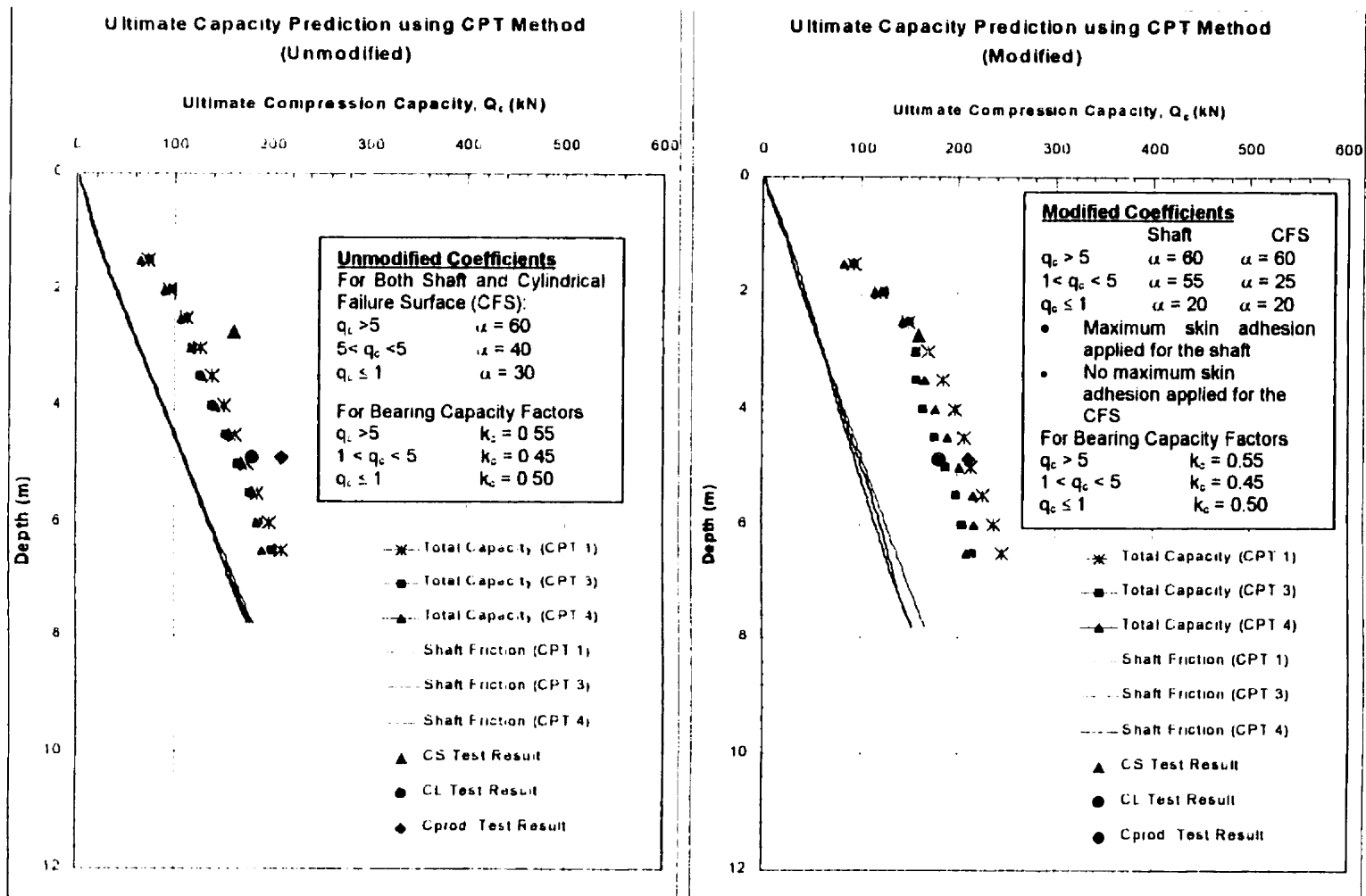


Figure 7. 1: Comparison of the Modified and Unmodified CPT Predictions for the Compression Capacities using Bustamante and Giasenelli (1982) method (the University Farm site)

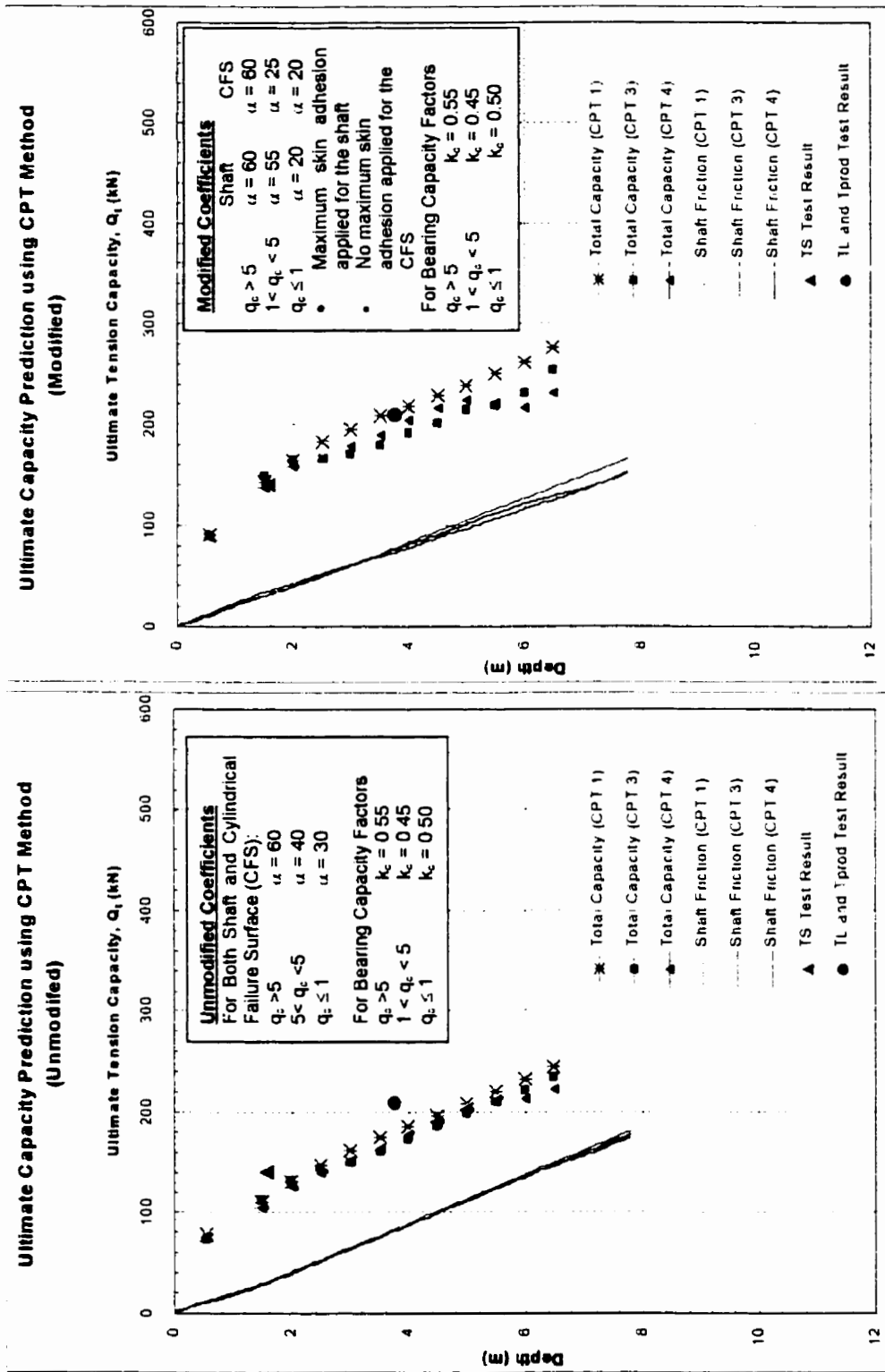


Figure 7.2: Comparison of Modified and Unmodified CPT Predictions for the Tension Capacities using Bustamante and Giasenelli (1982) method (the University Farm Site)

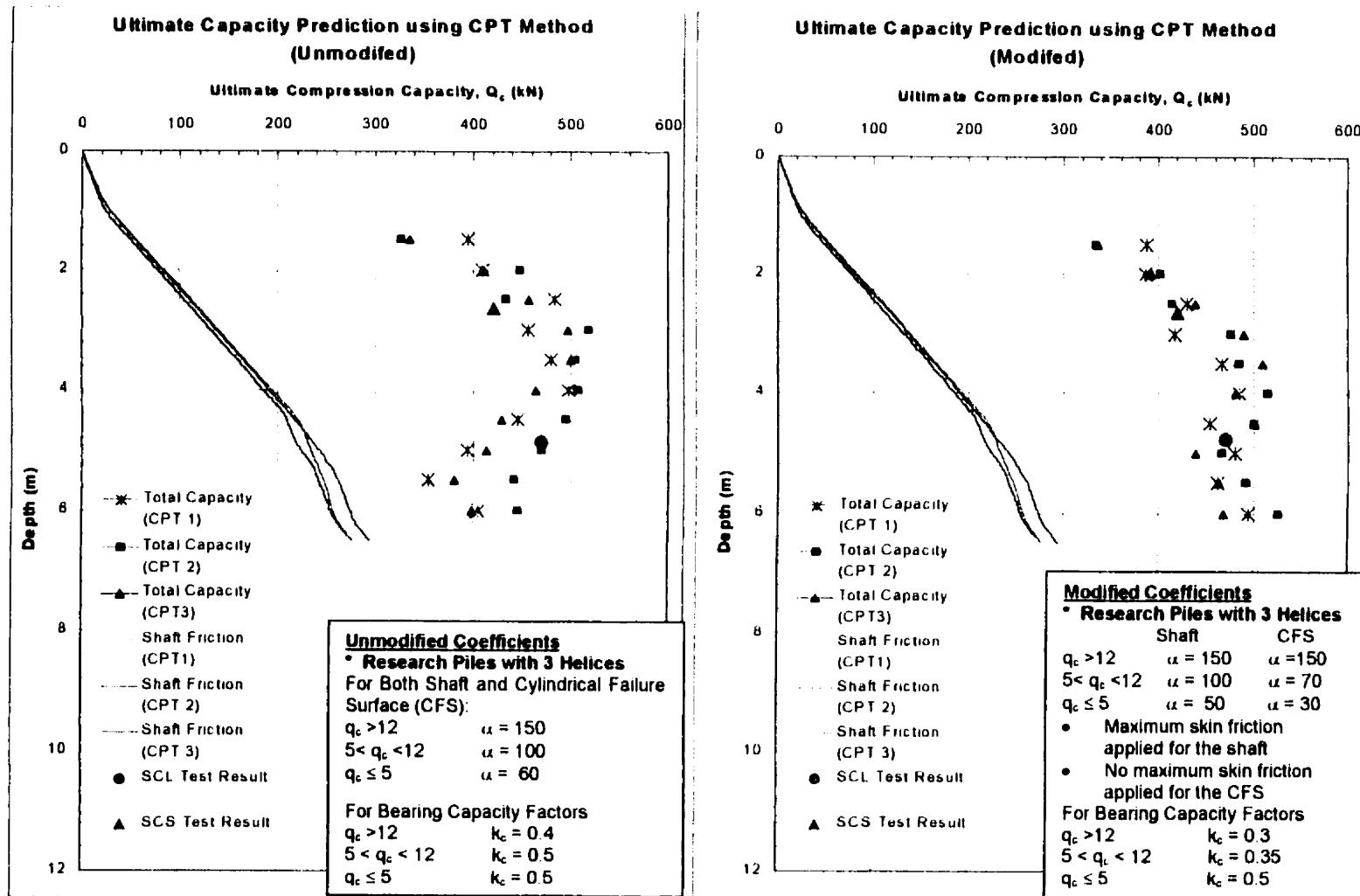


Figure 7.3: Comparison of Modified and Unmodified CPT Predictions for the Compression Capacities using Bustamante and Giasenelli (1982) method for the Research Piles (Sand Pit Site)

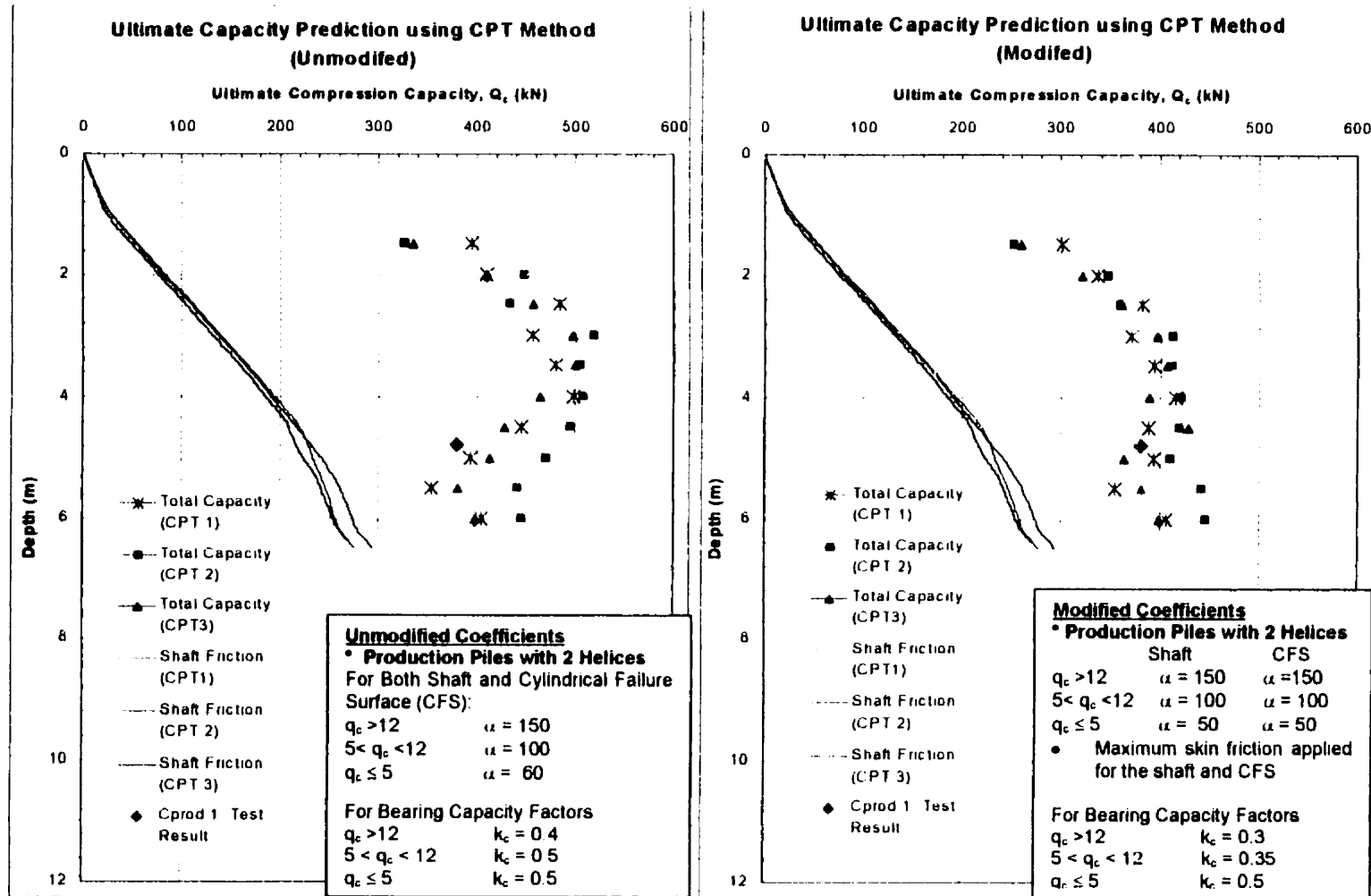


Figure 7.4: Comparison of Modified and Unmodified CPT Predictions for the Compression Capacities using Bustamante and Giasenelli (1982) method for the Production Piles (the Sand Pit Site)

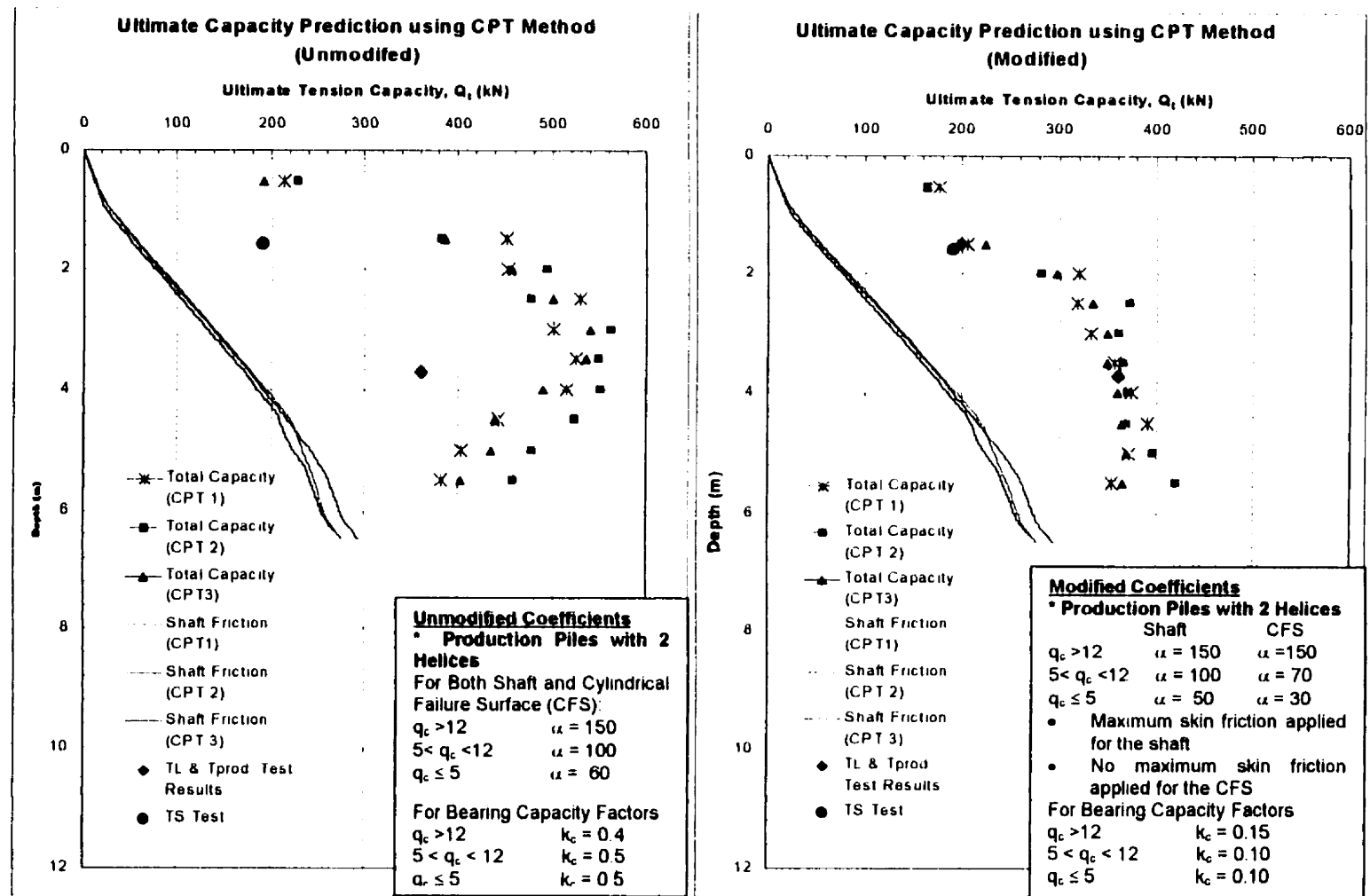


Figure 7.5: Comparison of Modified and Unmodified CPT Predictions for the Tension Capacities using Bustamante and Giasenelli (1982) method (the Sand Pit Site)

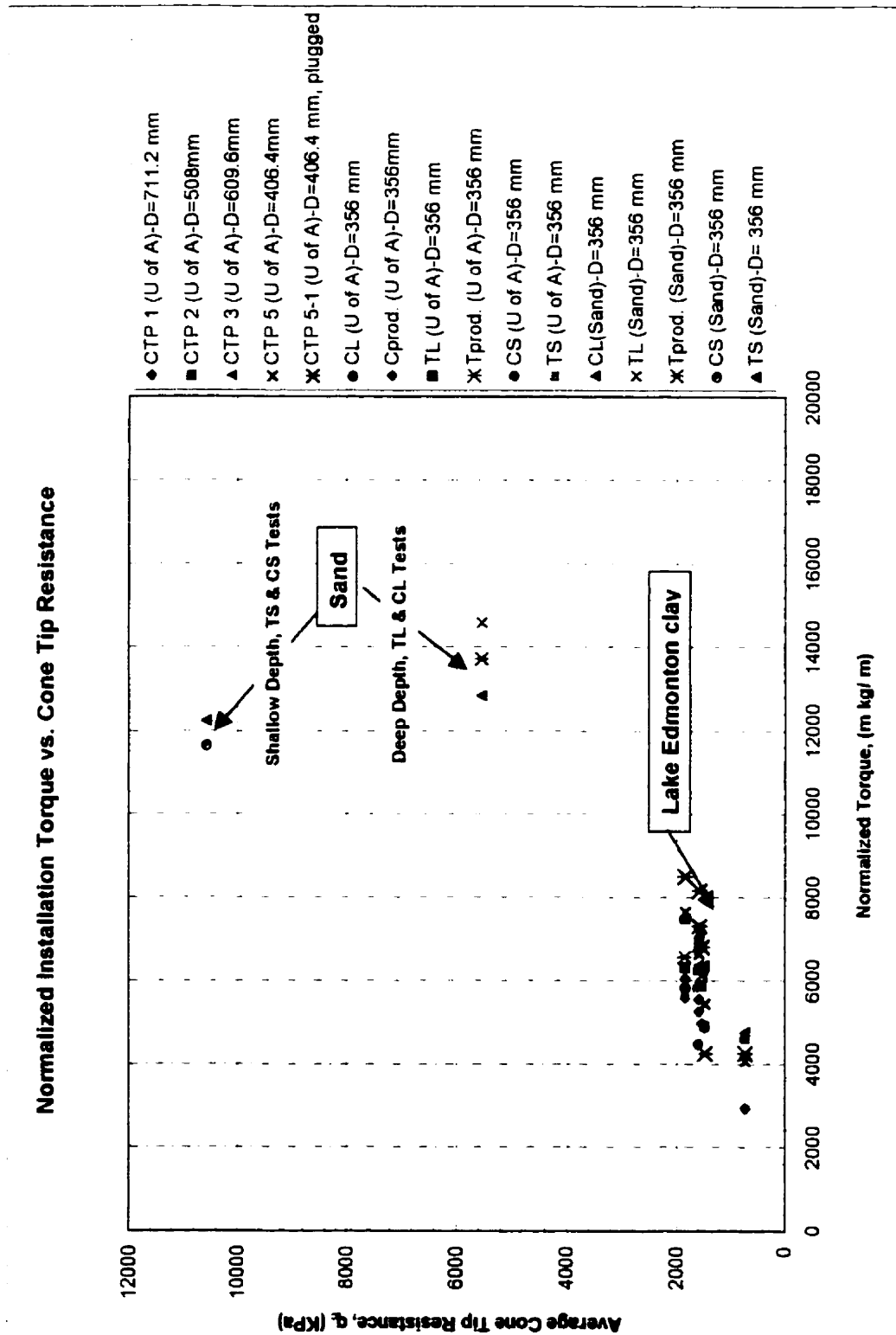


Figure 7.6: The Relationship between the Normalized Installation Torque and the Cone Tip Resistance

Appendix A

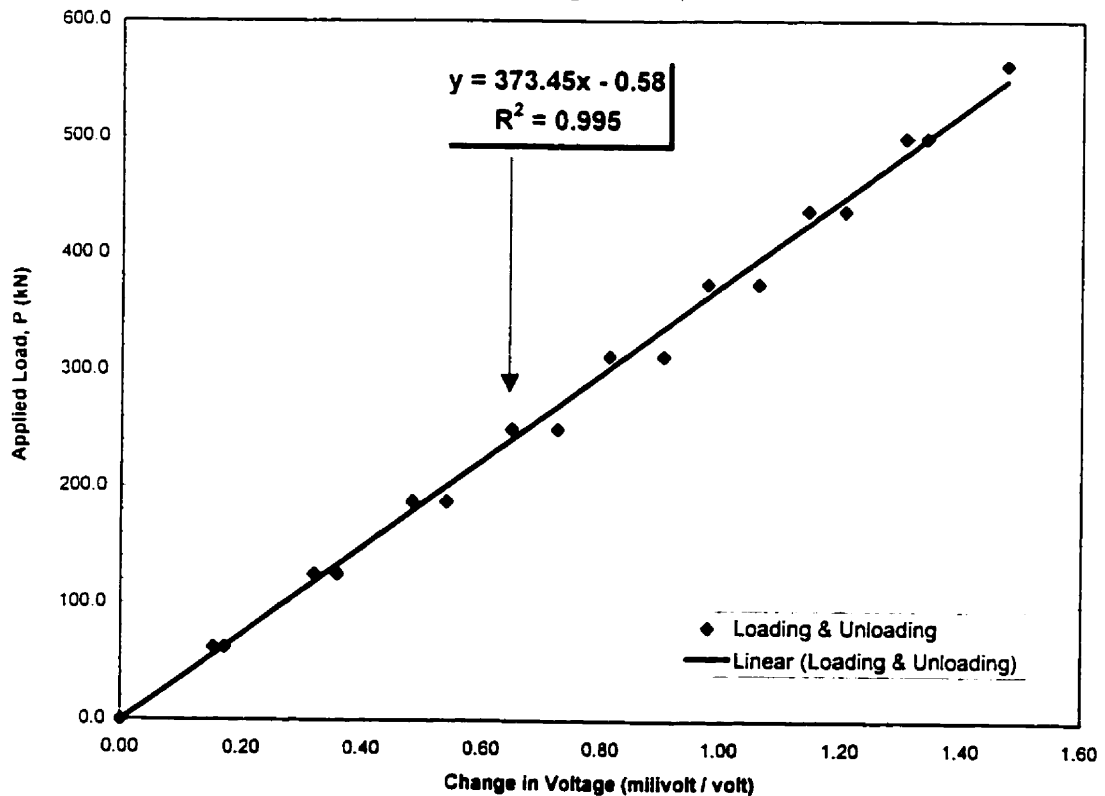
Appendix A contains following information:

- a) Calibration of Strain Gauges and End Load Cells**
- b) Structural Properties the Screw Piles**

CALIBRATION DATA FOR LOAD CELL

Output (millivolts)			Avg. Output V (millivolts)	Change in Voltage (millivolts)			Avg. ΔV (millivolts)	Load P (KN)
-0.501	-0.501	-0.447	-0.483	0.000	0.000	0.000	0.000	0
-0.331	-0.333	-0.33	-0.331	0.152	0.150	0.153	0.152	63
-0.163	-0.166	-0.165	-0.165	0.320	0.317	0.318	0.318	125
-0.001	-0.001	0	-0.001	0.482	0.482	0.483	0.482	188
0.165	0.163	0.166	0.165	0.648	0.646	0.649	0.648	250
0.329	0.329	0.327	0.328	0.812	0.812	0.810	0.811	313
0.492	0.496	0.495	0.494	0.975	0.979	0.978	0.977	375
0.66	0.659	0.66	0.660	1.143	1.142	1.143	1.143	438
0.812	0.825	0.824	0.820	1.295	1.308	1.307	1.303	500
0.99	0.99	0.989	0.990	1.473	1.473	1.472	1.473	563
0.856	0.856	0.856	0.856	1.339	1.339	1.339	1.339	500
0.723	0.719	0.718	0.720	1.206	1.202	1.201	1.203	438
0.58	0.579	0.578	0.579	1.063	1.062	1.061	1.062	375
0.419	0.42	0.421	0.420	0.902	0.903	0.904	0.903	313
0.243	0.24	0.24	0.241	0.726	0.723	0.723	0.724	250
0.056	0.057	0.056	0.056	0.539	0.540	0.539	0.539	188
-0.125	-0.125	-0.126	-0.125	0.358	0.358	0.357	0.358	125
-0.31	-0.313	-0.315	-0.313	0.173	0.170	0.168	0.170	63
-0.503	-0.503	-0.503	-0.503	-0.020	-0.020	-0.020	-0.020	0

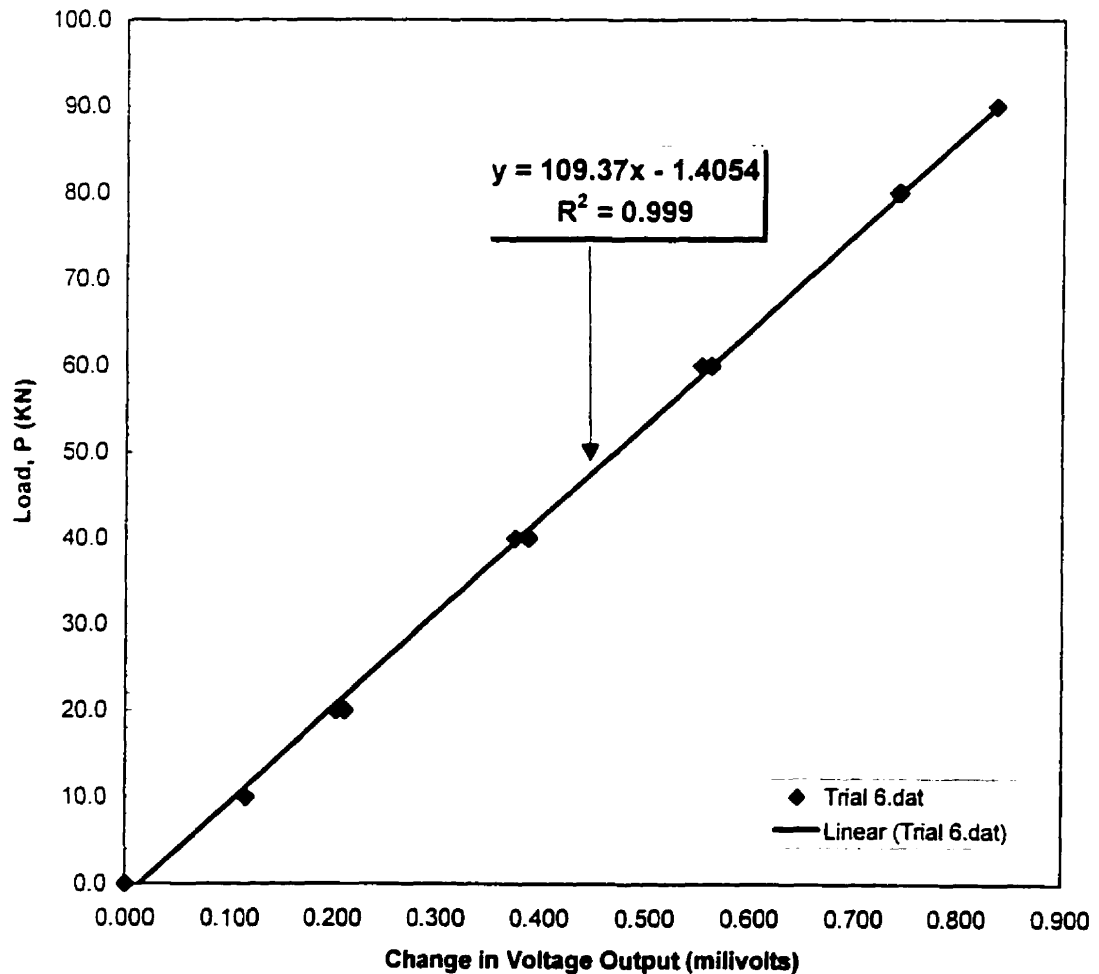
Calibration of Load Cell No. 1 - Max. 600 KN
(Output Range: 2.5 mV)



CALIBRATION DATA FOR END LOAD CELL USED IN COMPRESSION TEST

Output (millivolts)			Avg. Output V (millivolts)	Change in Voltage (millivolts)			Avg. ΔV (millivolts)	Load P (KN)
-0.899	-0.899	-0.899	-0.899	0.000	0.000	0.000	0.000	0
-1.013	-1.014	-1.015	-1.014	0.114	0.115	0.116	0.115	10
-1.111	-1.110	-1.110	-1.110	0.212	0.211	0.211	0.211	20
-1.288	-1.286	-1.288	-1.287	0.389	0.387	0.389	0.388	40
-1.462	-1.460	-1.460	-1.461	0.563	0.561	0.561	0.562	60
-1.642	-1.641	-1.643	-1.642	0.743	0.742	0.744	0.743	80
-1.736	-1.734	-1.734	-1.735	0.837	0.835	0.835	0.836	90
-1.639	-1.640		-1.640	0.740	0.741		0.741	80
-1.450	-1.452	-1.453	-1.452	0.551	0.553	0.554	0.553	60
-1.276	-1.273	-1.274	-1.274	0.377	0.374	0.375	0.375	40
-1.100	-1.102	-1.104	-1.102	0.201	0.203	0.205	0.203	20
-0.899	-0.898	-0.898	-0.898	0.000	-0.001	-0.001	-0.001	0

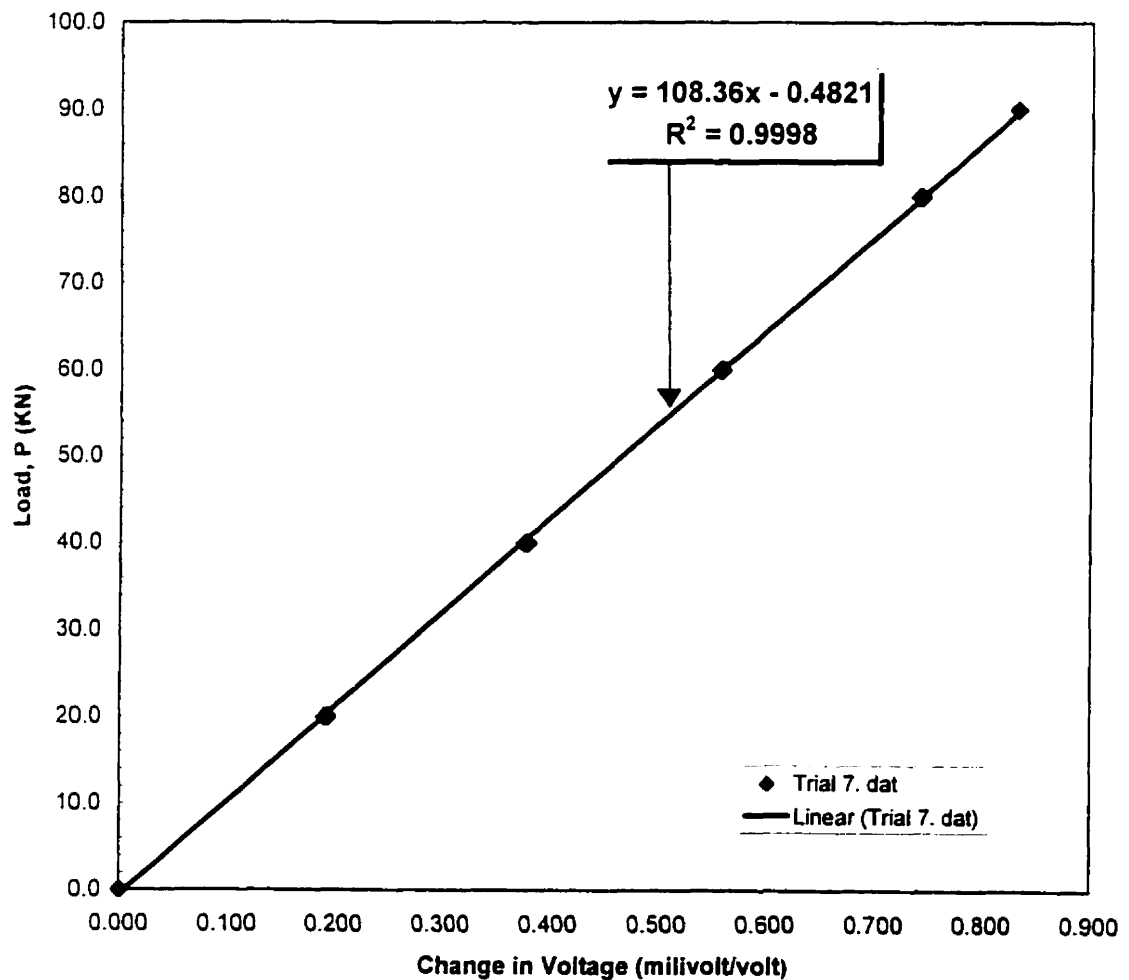
Calibration of Load Cell No. 2 - Max. 100 KN



CALIBRATION DATA FOR END LOAD CELL USED IN COMPRESSION TEST

Output (millivolts)			Avg. Output V (millivolts)	Change in Voltage (millivolts)			Avg. ΔV (millivolts)	Load P (KN)
0.613	-	-	0.613	0.000	0.000	0.000	0.000	0
0.802	0.805	0.803	0.803	0.189	0.192	0.190	0.190	20
0.990	0.990		0.990	0.377	0.377	-	0.377	40
1.171	1.169	1.170	1.170	0.558	0.556	0.557	0.557	60
1.351	1.353	1.354	1.352	0.738	0.740	0.741	0.740	80
1.450	1.442	1.443	1.445	0.837	0.829	0.830	0.832	90
1.354	1.356	1.356	1.355	0.741	0.744	0.743	0.742	80
1.170	1.173	1.173	1.172	0.557	0.560	0.560	0.559	60
0.993	0.993	-	0.993	0.380	0.380	-	0.380	40
0.807	0.806	0.806	0.806	0.194	0.194	0.193	0.193	20
0.612	-	-	0.612	-0.001	-	-	-0.001	0

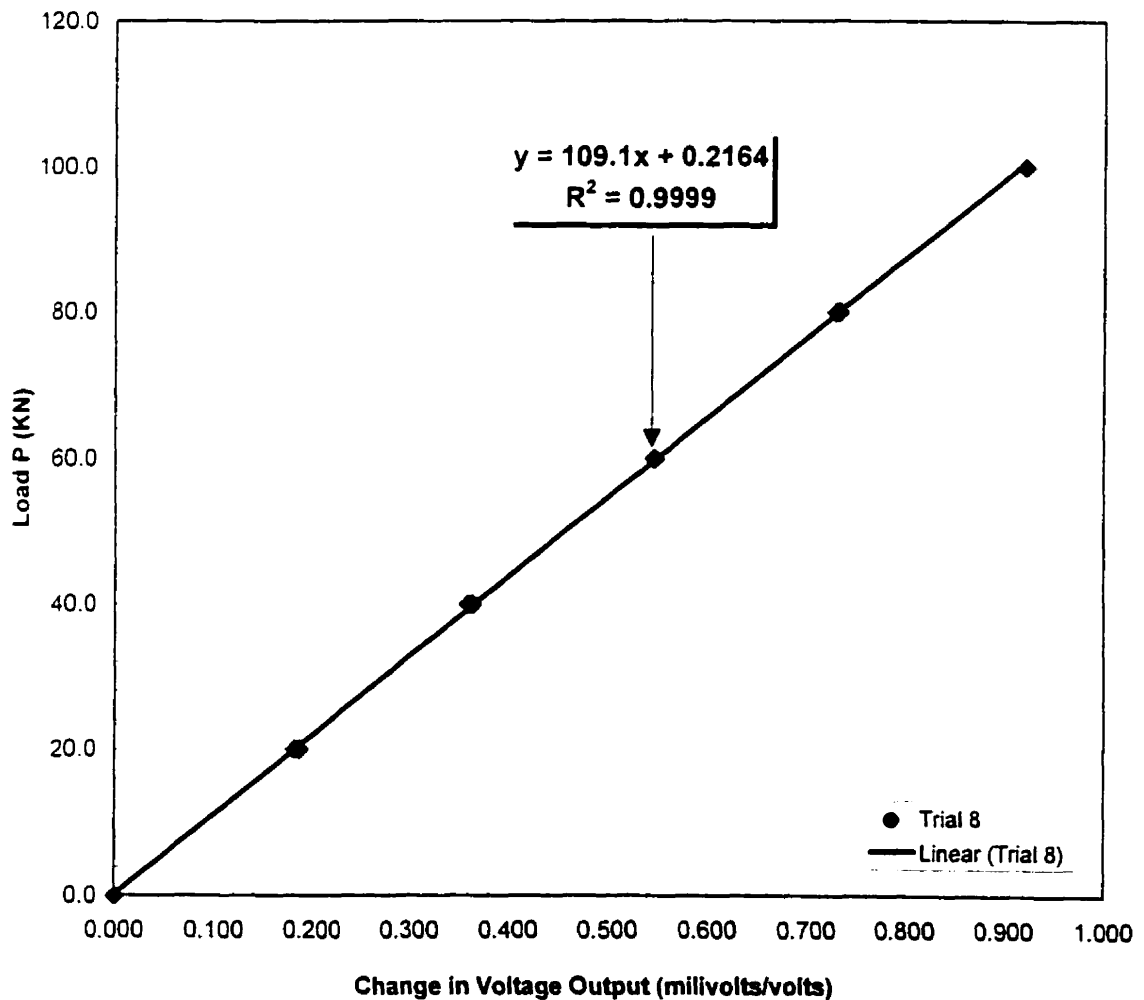
Calibration of Load Cell No. 3 - Max. 100 KN



CALIBRATION DATA FOR END LOAD CELL USED IN COMPRESSION TEST

Output (millivolts)			Avg. Output V (millivolts)	Change in Voltage (millivolts)			Avg. ΔV (millivolts)	Load P (KN)
-0.701	-0.701	-0.701	-0.701	0.000	0.000	0.000	0.000	0
-0.888	-0.888	-0.886	-0.887	0.187	0.187	0.185	0.186	20
-1.065	-1.064	-1.064	-1.064	0.364	0.363	0.363	0.363	40
-1.246	-1.248	-1.248	-1.247	0.545	0.547	0.547	0.546	60
-1.433	-1.435	-1.434	-1.434	0.732	0.734	0.733	0.733	80
-1.619	-1.626	-1.618	-1.621	0.918	0.925	0.917	0.920	100
-1.426	-1.431	-1.433	-1.430	0.725	0.730	0.732	0.729	80
-1.245	-1.246	-1.245	-1.245	0.544	0.545	0.544	0.544	60
-1.059	-1.057	-1.063	-1.060	0.358	0.356	0.362	0.359	40
-0.882	-0.883	-0.881	-0.882	0.181	0.182	0.180	0.181	20
-0.700	-	-	-0.700	-0.001	-	-	-0.001	0

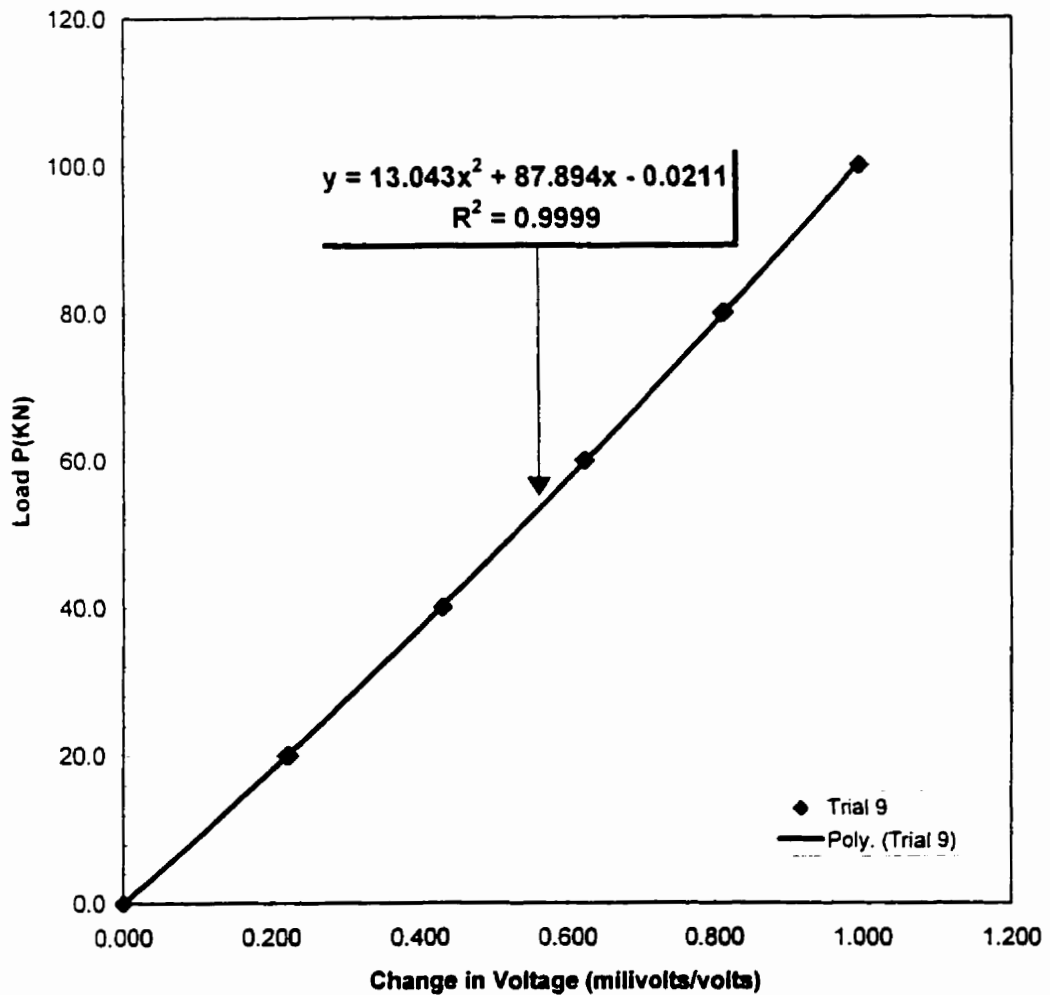
Calibration of Load Cell No. 4 - Max. 100 KN



CALIBRATION DATA FOR END LOAD CELL USED IN COMPRESSION TEST

Output (millivolts)			Avg. Output V (millivolts)	Change in Voltage (millivolts)			Avg. ΔV (millivolts)	Load P (KN)
-0.585	-0.585	-0.588	-0.586	0.000	0.000	0.000	0.000	0
-0.806	-0.808	-0.804	-0.806	0.220	0.222	0.218	0.220	20
-1.016	-1.015	-1.017	-1.016	0.430	0.429	0.431	0.430	40
-1.208	-1.207	-1.207	-1.207	0.622	0.621	0.621	0.621	60
-1.395	-1.394	-1.396	-1.395	0.809	0.808	0.810	0.809	80
-1.579	-1.580	-1.583	-1.581	0.993	0.994	0.997	0.995	100
-1.400	-1.399	-1.397	-1.399	0.814	0.813	0.811	0.813	80
-1.211	-1.210	-1.210	-1.210	0.625	0.624	0.624	0.624	60
-1.017	-1.017	-	-1.017	0.431	0.431	-	0.431	40
-0.810	-0.811	-0.808	-0.810	0.224	0.225	0.222	0.224	20
-0.584	-	-	-0.584	-0.002	-	-	-0.002	0

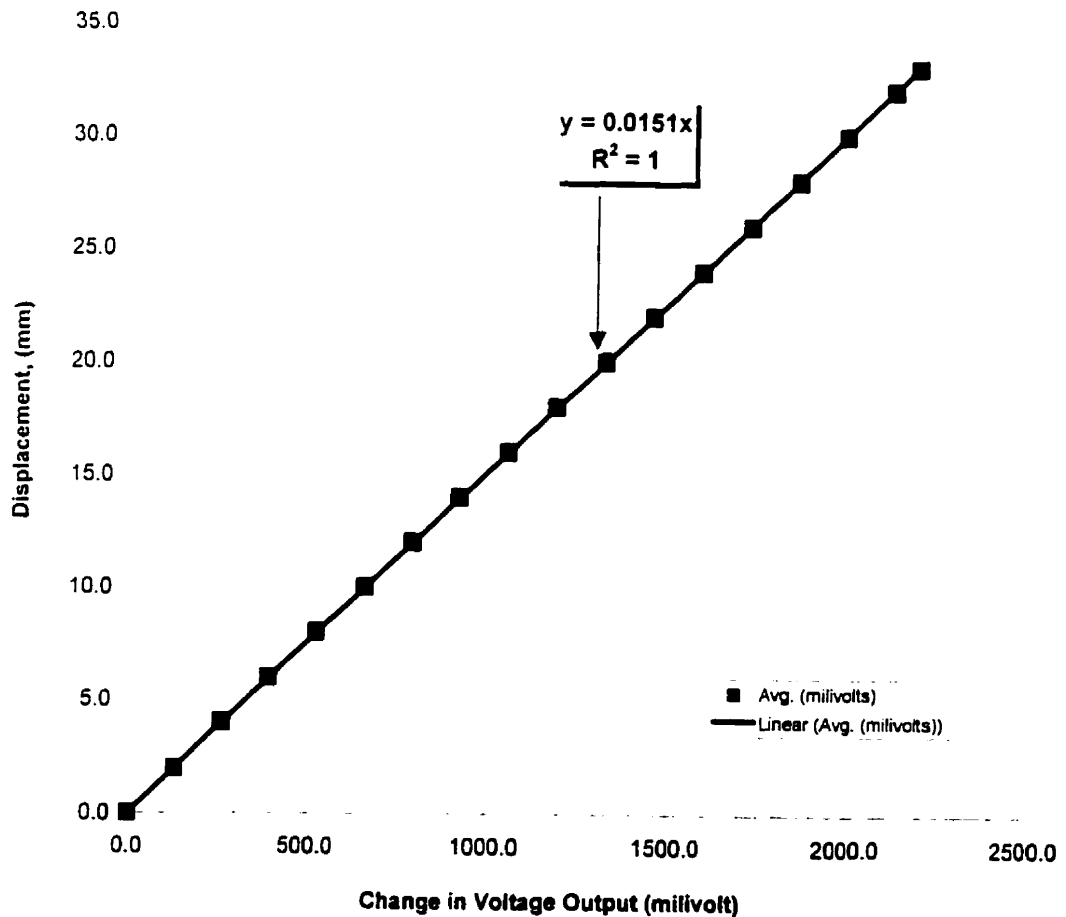
Calibration of Load Cell No. 5 - Max. 100 KN



Transducer No. 1 - Serial Number 8810429

Voltage (millivolts)			Change in Voltage (millivolts)			Avg. (millivolts)	Displacement (mm)
284.370			0.000			0.000	0.0
416.110	415.770	415.770	131.740	131.400	131.400	131.513	2.0
546.840	546.500	546.840	262.470	262.130	262.470	262.357	4.0
677.900	677.570	677.900	393.530	393.200	393.530	393.420	6.0
810.320	809.980	809.980	525.950	525.610	525.610	525.723	8.0
943.740	943.740	-	659.370	659.370	-	659.370	10.0
1075.500	1075.800	1075.800	791.130	791.430	791.430	791.330	12.0
1206.200	1206.500	-	921.830	922.130	-	921.980	14.0
1340.300	1340.600	-	1055.930	1056.230	-	1056.080	16.0
1473.700	1473.100	-	1189.330	1188.730	-	1189.030	18.0
1607.200	1606.500	1606.500	1322.830	1322.130	1322.130	1322.363	20.0
1738.600	1738.900	-	1454.230	1454.530	-	1454.380	22.0
1873.000	1873.000	-	1588.630	1588.630	-	1588.630	24.0
2006.700	2007.100	2006.700	1722.330	1722.730	1722.330	1722.463	26.0
2141.500	2141.500	-	1857.130	1857.130	-	1857.130	28.0
2273.300	2272.900	-	1988.930	1988.530	-	1988.730	30.0
2407.400	2407.000	-	2123.030	2122.630	-	2122.830	32.0
2474.400	2473.700	2474.400	2190.030	2189.330	2190.030	2189.797	33.0

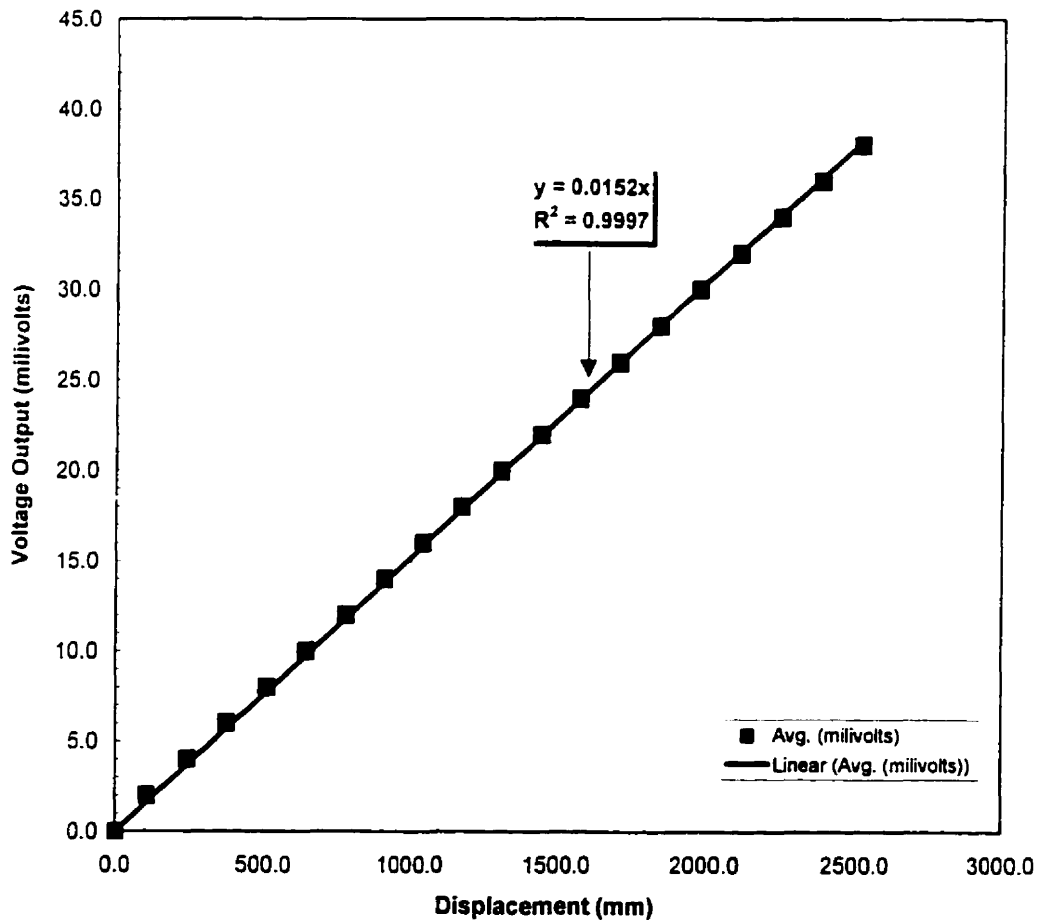
Calibration of Transducer No.1



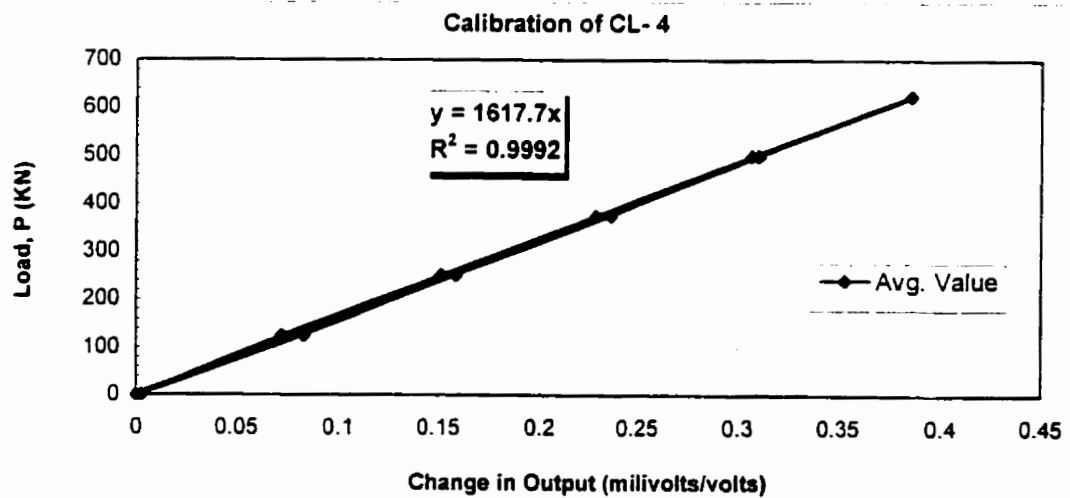
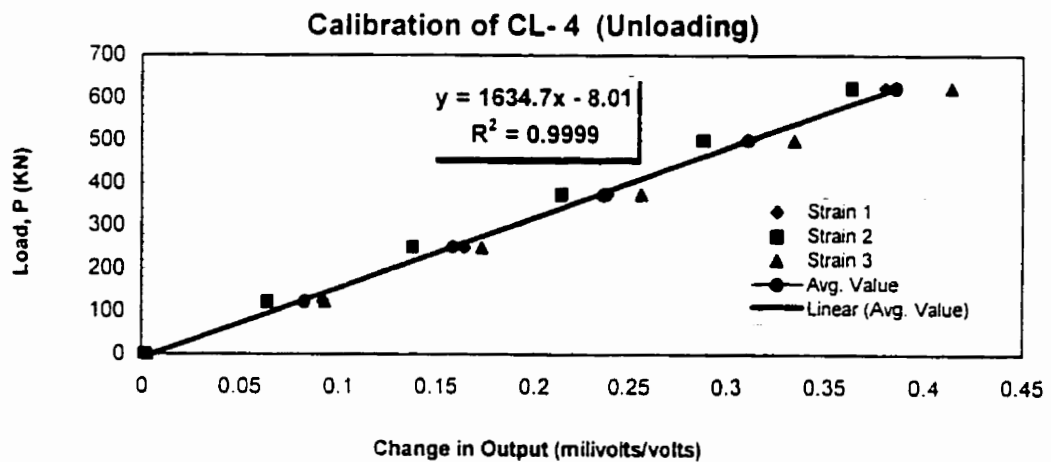
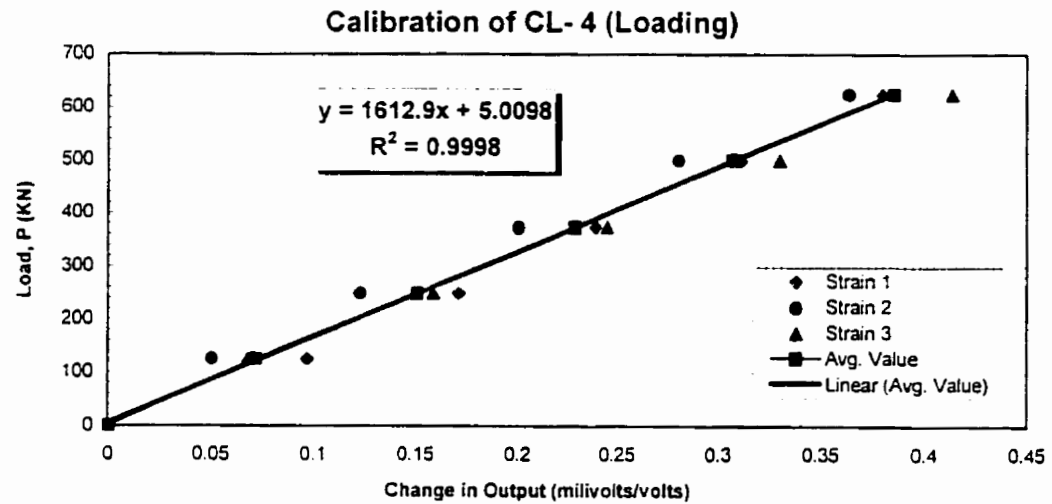
Transducer No. 2 - Serial Number 90490206

Voltage (millivolts)			Change in Voltage (millivolts)			Avg. (millivolts)	Displacement (mm)
6.402	-	-	0.000	-	-	0.000	0.0
113.210	113.210	-	106.808	106.808	-	106.808	2.0
247.310	247.310	-	240.908	240.908	-	240.908	4.0
380.070	379.730	380.060	373.668	373.328	373.658	373.552	6.0
513.150	513.150	-	506.748	506.748	-	506.748	8.0
647.250	647.250	-	640.848	640.848	-	640.848	10.0
782.030	781.690	-	775.628	775.288	-	775.458	12.0
913.090	913.430	913.090	906.688	907.028	906.688	906.802	14.0
1047.200	1047.200	-	1040.798	1040.798	-	1040.798	16.0
1180.600	1180.600	-	1174.198	1174.198	-	1174.198	18.0
1314.700	1314.700	-	1308.298	1308.298	-	1308.298	20.0
1448.500	1448.500	-	1442.098	1442.098	-	1442.098	22.0
1582.200	1581.600	-	1575.798	1575.198	-	1575.498	24.0
1716.000	1715.700	-	1709.598	1709.298	-	1709.448	26.0
1851.100	1851.100	-	1844.698	1844.698	-	1844.698	28.0
1984.200	1983.900	-	1977.798	1977.498	-	1977.648	30.0
2117.600	2117.600	-	2111.198	2111.198	-	2111.198	32.0
2251.400	2251.700	-	2244.998	2245.298	-	2245.148	34.0
2387.500	2387.500	-	2381.098	2381.098	-	2381.098	36.0
2520.900	2520.900	-	2514.498	2514.498	-	2514.498	38.0

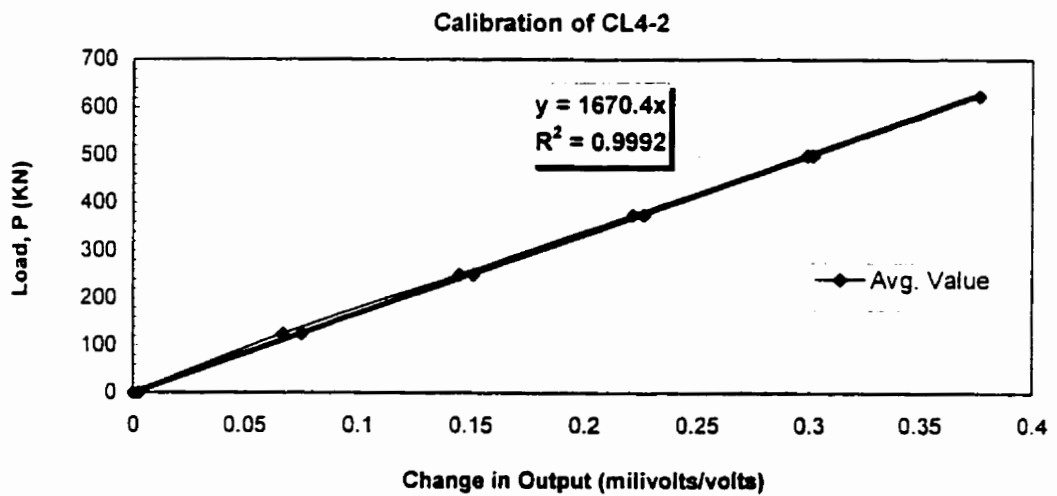
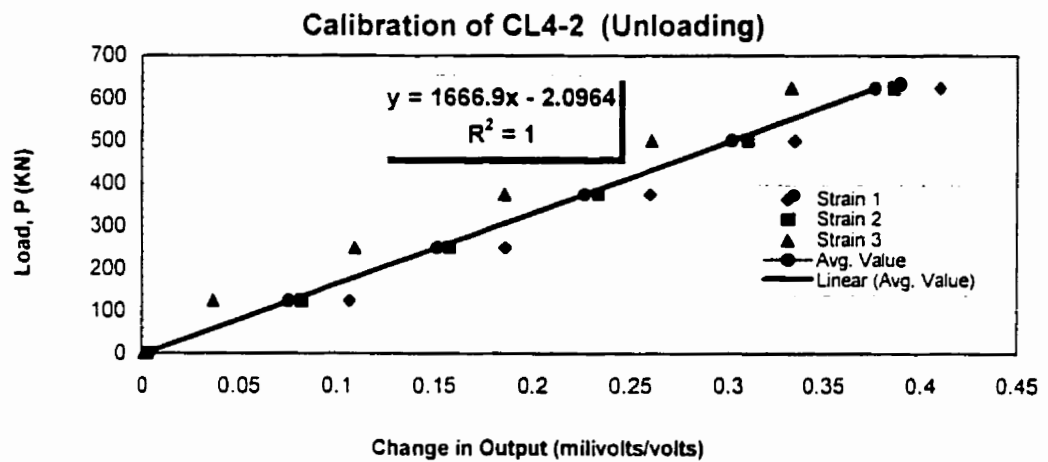
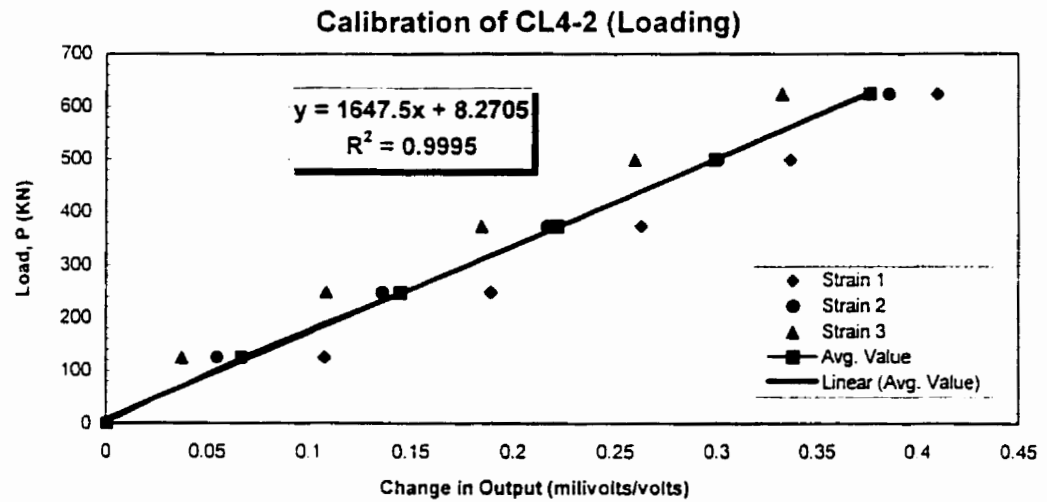
Calibration of Transducer No.2



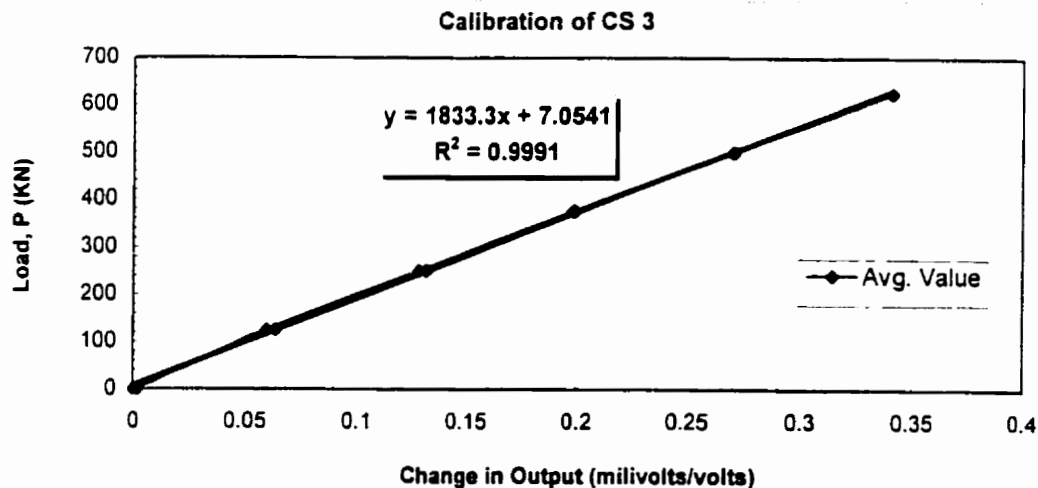
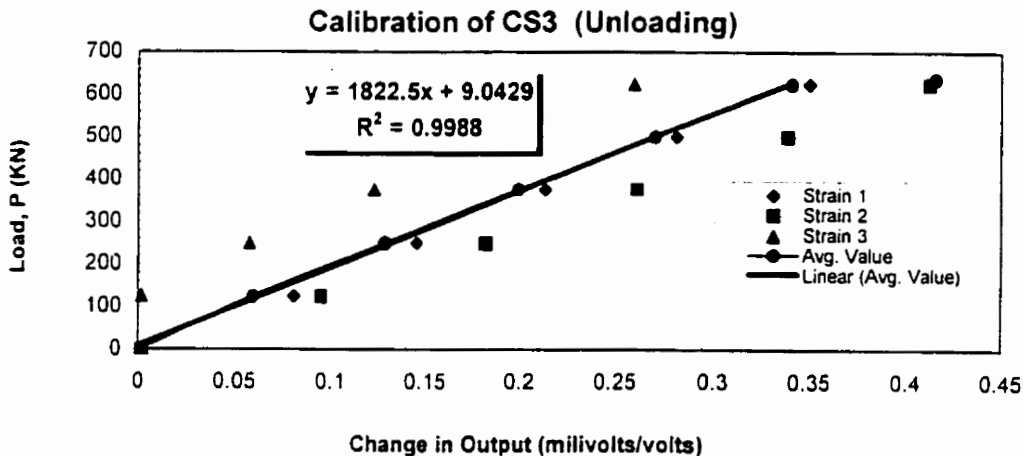
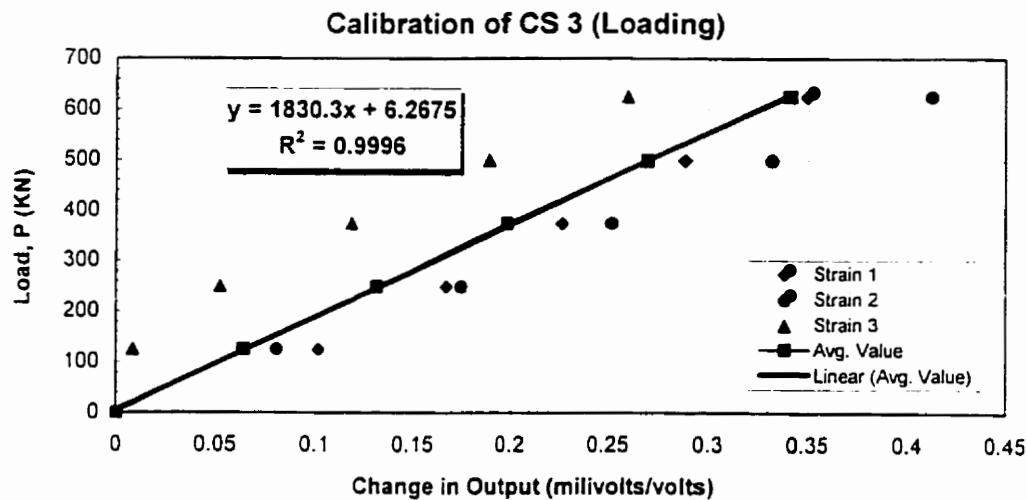
Calibration the Strain Gauge - Section CL-4



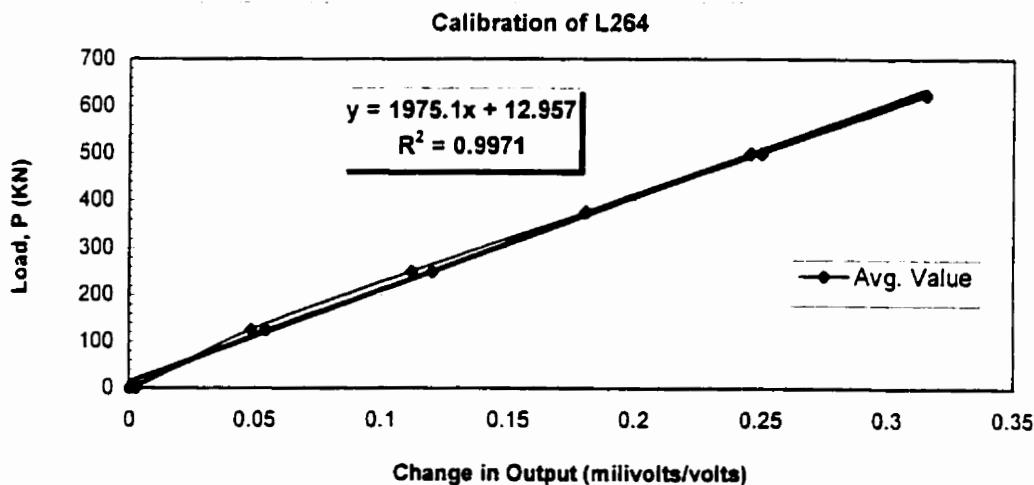
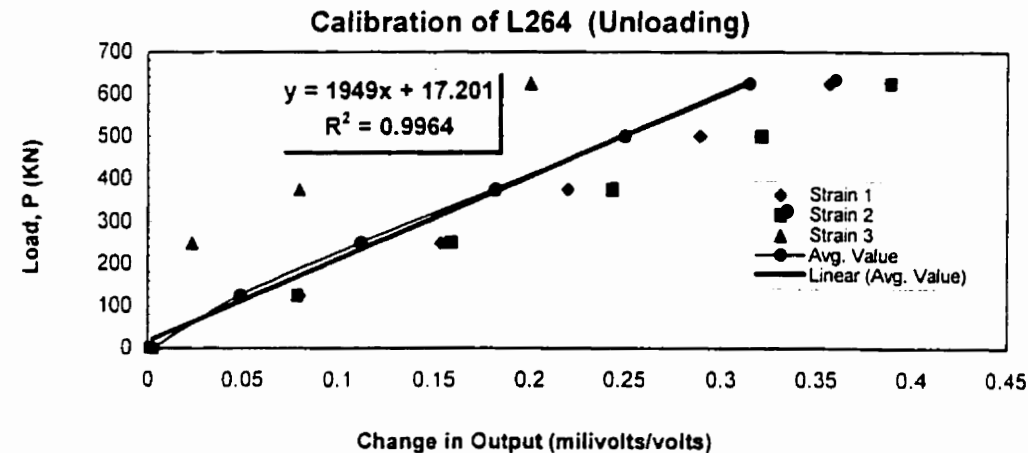
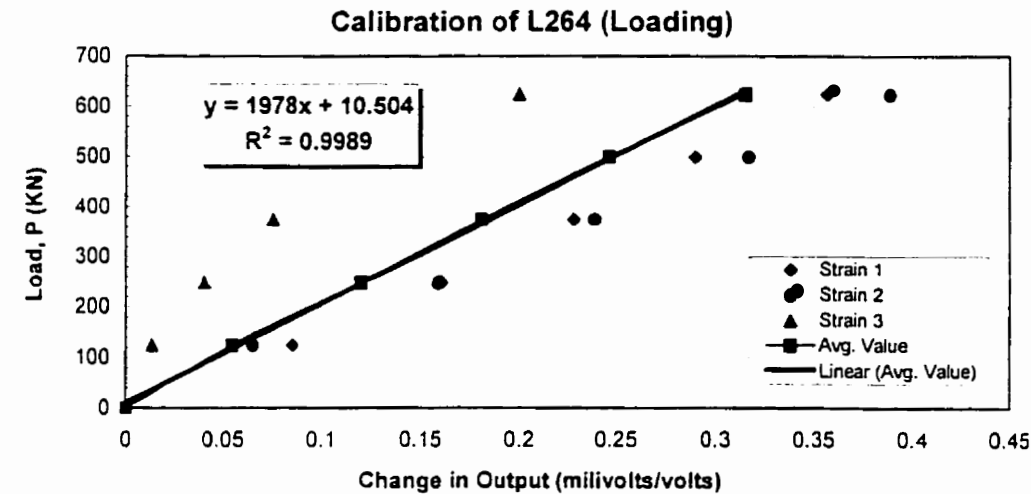
Calibration the Strain Gauge - Section CL4-2



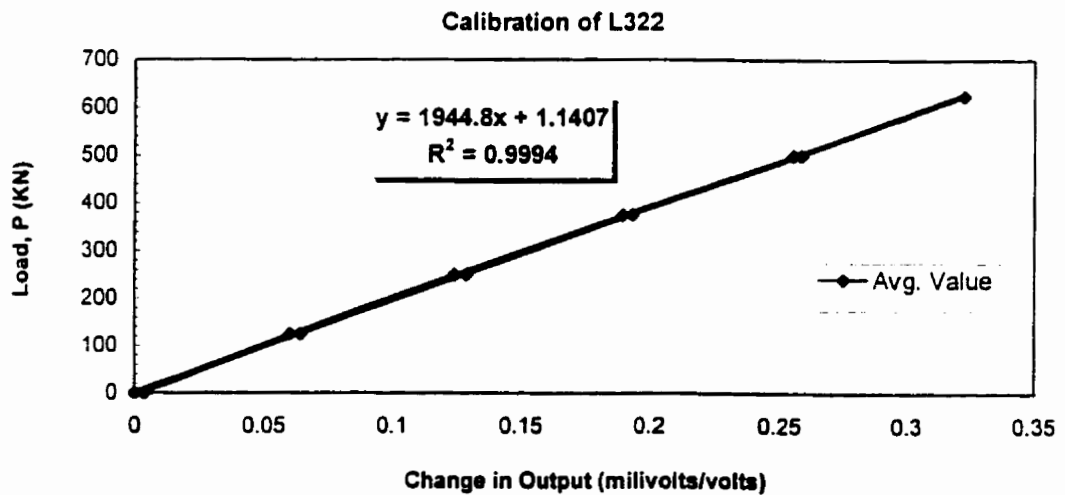
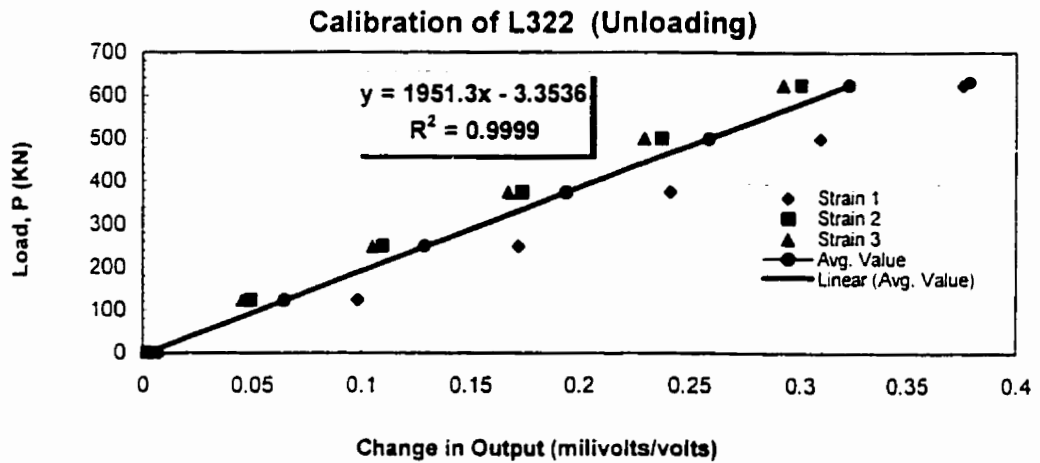
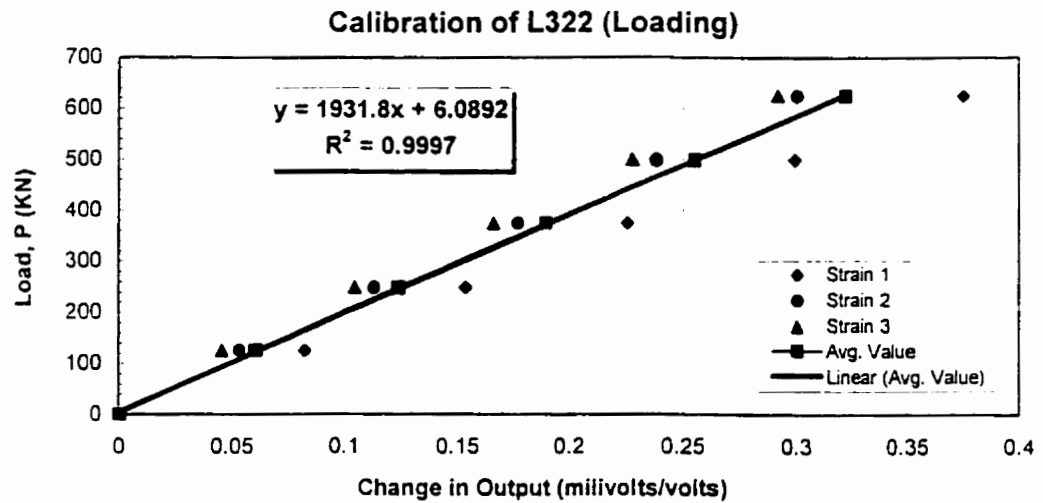
Calibration the Strain Gauge - Section CS 3



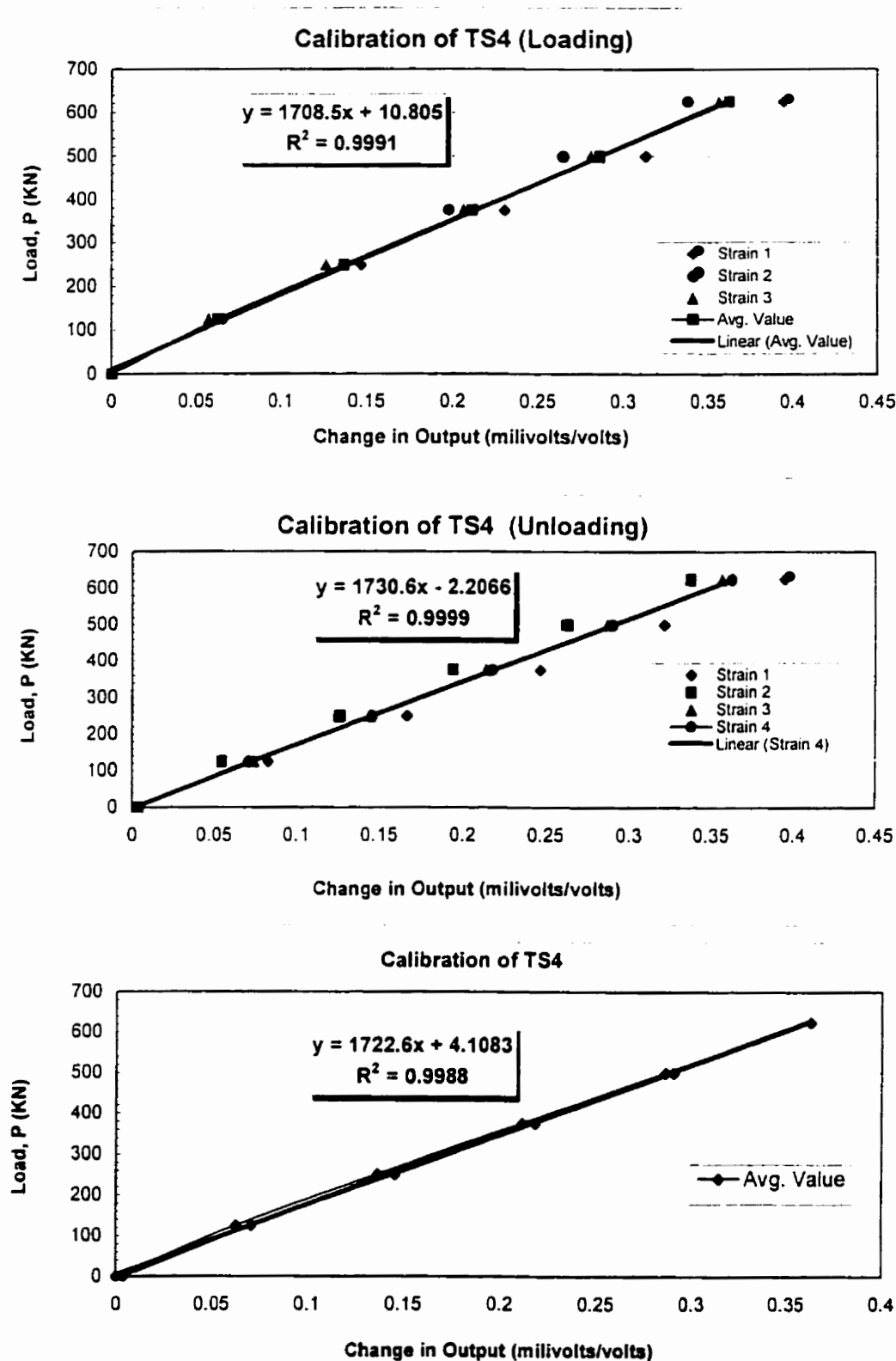
Calibration the Strain Gauge - Section L264



Calibration the Strain Gauge - Section L322



Calibration the Strain Gauge - Section TS 4



MECHANICAL PROPERTY AND CHEMICAL COMPOSITION OF THE PIPE

2⁷/₈" x 0.217" & 3¹/₂" x 0.254" Commercial Pipe

YS	400 – 475 MPa (58000 – 69000 psi)
UTS	525 – 600 MPa (76000 – 87000 psi)
ELONGATION	25 – 35 %

C	0.13 – 0.17	V	0.001 – 0.005
Mn	0.70 – 0.90	Cb	0.030 – 0.035
S	0.002 – 0.010	Mo	0.02 – 0.15
P	0.008 – 0.015	Sn	0.010 – 0.020
Si	0.12 – 0.20	Al	0.030 – 0.060
Cu	0.25 – 0.50	Ti	0.02 – 0.05
Ni	0.10 – 0.30		
Cr	0.10 – 0.20		

All Other Commercial Pipe

YS	425 – 485 MPa (62000 – 70000 psi)
UTS	525 – 600 MPa (65000 – 80000 psi)
ELONGATION	28 – 35 %

C	0.05 – 0.08	V	0.001 – 0.005
Mn	0.80 – 1.10	Cb	0.020 – 0.025
S	0.005 – 0.010	Mo	0.02 – 0.10
P	0.005 – 0.015	Sn	0.010 – 0.020
Si	0.12 – 0.18	Al	0.020 – 0.040
Cu	0.20 – 0.35	Ti	0.00 – 0.05
Ni	0.10 – 0.20		
Cr	0.05 – 0.10		